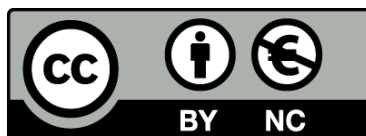UNIVERSITAT DE BARCELONA

Development of a compact NDIR spectometer based on MOEMS components for fruit ripening monitoring

Jordi Fonollosa Magrinyà

DEVELOPMENT OF A COMPACT NDIR SPECTROMETER BASED ON MOEMS COMPONENTS FOR FRUIT RIPENING MONITORING.

Memòria presentada

per optar al títol de

Doctor en Enginyeria i Tecnologies Avançades

per

Jordi Fonollosa Magrinyà

UNIVERSITAT DE BARCELONA

Juny 2009

Departament d'Electrònica

Programa de Doctorat: ENGINYERIA I TECNOLOGIES AVANÇADES

Directors de Tesi: Dr. Santiago Marco Colás i Dr. Mauricio Moreno Sereno

INDEX:

0.- AGRAÏMENTS:

Sens dubte els agraïments és una de les parts més importants de la Tesi, ja que és on queda palès que el treball presentat és fruit de moltes contribucions, ja siguin directes o indirectes. Però també és una de les parts més difícils, ja que a mesura que s'escriuen, esdevenen una mena de repassada de les vivències al voltant de la Tesi, això si les memòries no van encara a temps més remots. I per això, perquè costa refrescar la memòria, no és fàcil ser just i anomenar tothom qui es mereix una menció aquí. Així doncs, serveixi aquest paràgraf per ressaltar la importància dels agraïments i disculpar tots aquells qui no hi figuren però haurien de ser-hi anomenats.

Primer de tot vull agrair al Dr. Santiago Marco i al Dr. Mauricio Moreno per la seva direcció conjunta de la Tesi. Però també pel seu guiatge en el món científic al llarg d'aquests anys. Amb tota seguretat, sense els seus consells aquesta Tesi no hagués estat possible.

Cal destacar les col·laboracions al Centre Nacional de Microelectrònica, liderades pels Dr. Luis Fonseca i Dr. Joaquín Santander, i les estades al Fraunhofer Institute for Physical Measurement Techniques de Freiburg, Alemanya, amb el Dr. Jürgen Wöllenstein i Bernard Halford al capdavant. El resultat d'aquesta Tesi és producte d'aquesta xarxa de col·laboracions. D'altra banda, també he tingut l'oportunitat de fer una estada a Chalmers University of Technology de Göteborg, Suècia, i descobrir el camp dels biosensors. Estic molt agraït a tots aquests centres que m'han brindat la possibilitat de treballar amb ells, descobrir nous equips i metodologies de treball, i sobretot, per la bona acollida que he tingut a tot arreu i l'experiència vital de viure a l'estranger.

També vull anomenar els companys del grup de recerca Xavi, Marta, Ivan, Agustí, Sergi, Fran, Manolo, Alex, Benjamin, Idoya, Aina i Miquel perquè entre tots hem fet un bon grup de treball. I especialment al Rafa Rubio per, en certa manera, deixar un camí marcat en el desenvolupament de la Tesi. I tots aquells com en Mariano P., Nasser D., Josep C., Youcef L., Jordi B., Ivan B., i Romén R. que vam començar junts el llarg i tortuós camí d'una Tesi. I és que ja se sap que compartir cursos de doctorat, DEA, màsters i un llarg etcètera uneix.

Però aquí no hi hagués arribat de cap manera si no hagués tingut un extraordinari recolzament de tots costats. Aquí és on destaca el paper de la meva família, per estar al meu costat sempre, per l'excel·lent educació que m'han proporcionat i per haver-me potenciat el gust per les ciències que ha desembocat en l'escriptura d'una Tesi (potser fins i tot massa, oi?).

I també tenen un paper vital els companys de fatigues d'aquests darrers anys, amb molts dels quals he compartit llargues hores d'estudi, però sobretot amb tots ells un grapat d'experiències personals inoblidables. Els grans moments que hem passat plegats han acabat sent records impagables. Enrere però molt present queda el viatge a Veneçuela amb la Júlia, el

Roger i el Dani; la recurrent visita a la Marta a Menorca (ja en toca una altra!); el partidet de futbol a NY amb el Carles; el becari al sol del Sandro; les excursions nocturnes del Jorge amb l'inseparable iPod; l'escapadeta a Marsella a veure la Laura; compartir l'habitació amb el Martí a es Castell; el bon saber fer del Fortino i el seu poder negociador; les converses (o millor dit lliçons) sobre futbol i més del David; Sant Jaumes, acampades, mones, calçotades, bigcities... de la colla tivissana del Castell. En resum, que em sento ben afortunat d'haver compartit aquest camí amb vosaltres al costat. I ben especialment afortunat em sento de fer camí amb l'Anna, qui amb la seva comprensió i intel·ligència emocional m'ha fet veure una llumeta al final quan el túnel era encara ben fosc.

I finalment a tots aquells que valorin l'esforç que hi ha darrere d'aquest treball i que considerin que contribueix positivament al coneixement. I sobretot, a tots aquells que s'estan barallant amb la seva Tesi avui. Ànim que ja queda menys!

1.- ABSTRACT:

In today's store-houses the ripening of fruit is controlled by managing the ethylene concentration in the ambient atmosphere. Precise and continuous ethylene monitoring is very advantageous since low ethylene concentrations are produced by the fruit itself and are indicative of its ripeness, and on other occasions, ethylene is externally added when ripeness or degreening of the product must be promoted.

In this Thesis an optical multi-channel non-dispersive mid-infrared (NDIR) spectrometer for ethylene measurement is built and characterized for measuring fruit status in apple's store-houses. The corresponding optical components and signal processing electronics have been developed, tested and integrated in a compact measurement system. In addition to the ethylene channel, the spectrometer also features ammonia and ethanol channels to consider their cross-sensitivities, and a reference channel to improve long-term system stability. Moreover, these channels are useful for monitoring a potential malfunction of the cooling system and possible fouling of the fruit. Therefore, the complete system can be considered as a multipurpose instrument for controlled atmosphere management.

In the trend towards miniaturization, a novel detector module containing multiple IR sensor channels is built and characterized. In its final form it contains thermopiles as IR detectors, narrow band filters to select the absorption bands of the target gas, and a four Fresnel lenses fabricated on the same silicon substrate in a combined multi-lens array to increase system sensitivity. In order to reduce the number of photolithographic steps, a new design based on sharing up to sixteen quantization steps by the four lenses is done.

However, it has been found that integration of filters too close to the IR detector may lead to degraded performance due to thermal coupling. To avoid such detrimental effects two possibilities have been considered: set the IR detector in vacuum conditions and increase the solder joint height between the filter and the thermopile.

Specific signal conditioning electronics were designed. They contain an analogue pre-amplification stage based on an instrumentation amplifier, and a digital lock-in amplifier implemented on a commercial microcontroller as a signal recovery system.

The complete spectrometer has been successfully tested in laboratory and field conditions. Assuming that ethylene and ammonia may not appear simultaneously, it has been found an ethylene detection limit of 30ppm, which is low enough to detect when fruit is ripe and prevent it to decline to senescence. The detection limit corresponding to ammonia is 160ppm, which can be used to set an alarm if a leakage from the cooling system occurs.

2.- NDIR SYSTEMS: STATE OF THE ART

2.1.- Miniaturization:

Miniaturization can be considered as a constant technological target during modern and contemporaneous times since the human race has the monotonous tendency towards the fabrication of smaller-scale products fulfilling the promise and industry-defining mantra of "smaller, faster, and cheaper!" Smaller products need less space, are easier to carry and store, and much more convenient to use than bigger and bulky items.

Microelectronics techniques were firstly investigated in the late 1950's with the aim to miniaturize electronics equipment and include increasingly complex electronics functions in a limited space with minimum weight. Since the invention of the integrated circuit in 1959, miniaturization is a continuing trend in the production of technology. The semiconductor industry has improved the productivity of integrated circuits following Moore's Law [1], named after Gordon Moore, who predicted in 1965 that for silicon-based integrated circuits, the number of transistors per square centimeter doubles every 12 months. During the 1960's the doubling time was close to 12 months, and during the 1970's and 1980's it was close to 18 months [2].

Despite multiple complex challenges faced by the microelectronics industry, and the fact that the integration rate has slowed down in recent years, the size and cost of the silicon industry products is still shrinking nowadays. Today devices featuring sizes of 45nm can be manufactured [3].

In the trend towards the integration, systems consisting of microelectronics, microactuators and, in most cases, microsensors have been developed in parallel with microelectronics technology. The integration between micromachines and microelectronics led to the birth of MEMS (Micro-Electrical-Mechanical Systems). There is not a clear definition of MEMS [4]. It can be said that MEMS is the resulting integration of mechanical elements, sensors, actuators, and electronics on a silicon substrate through microfabrication technology. Usually, integrated circuit (IC) techniques are used to fabricate the electronics, and a compatible "micromachining" processes etches away parts of the silicon substrate or adds new structural parts to build mechanical and electromechanical devices [5].

Micromachining can be divided in two large groups of techniques: bulk and surface micromachining. Bulk micromachining forms the desired structures etching through the wafer. Surface micromachining fabricates the devices by depositing thin films on the substrate surface and etching selectively sacrificial layers, typically made of SiO_2 [6]. The high compatibility between the micromachining and microelectronics technologies allowed a rapid growth of

MEMS technology and market [4]. Additionally, since MEMS technology uses batch fabrication processes similar to the used for integrated circuits, high levels of functionality, reliability, and sophistication can be placed on a small silicon chip at a relatively low cost [5]. Other benefits of silicon technology such as the high quality material, extensive process equipment, support services that have been developed over many years by the electronics industry, low voltage operation, and robustness can also be found in MEMS technology [7].

MEMS integration revolutionized almost every product category by bringing together silicon-based microelectronics with micromachining technology and making possible the realization of complete systems-on-a-chip. MEMS allowed the development of smart products featuring more computational abilities together with perception and control capabilities [5].

MEMS are still a growing technology area and they are a key element in several applications and sectors. According to a YOLE market analysis, the global market for MEMS devices and production equipment was US$6.9 billion in 2007, with an 11% market growth, which indicates a healthy industry. The MEMS market sales are expected to reach US$ 13.4 billion in 2012 [8].

For example, pressure and acceleration microsensors are the simplest MEMS devices and are widely used. MEMS pressure sensors are based typically on a flexible diaphragm which is deformed in the presence of a pressure difference. Traditionally the deformation is converted by piezoresistive or capacitive sensors to an electrical signal appearing at the sensor output [9]. Piezoresistive sensors generally consist of a single-degree of freedom system of a mass suspended by several springs; and capacitance sensors measure changes of the capacitance between a proof mass and a fixed conductive electrode separated by a narrow gap [10]. In the 1990's MEMS accelerometers revolutionized automotive airbag system industry, and nowadays, they are widely integrated in airbag systems. MEMS accelerometers are also used to measure vibrations of any machine part. Their information is worth to prevent any deviation from normal operation and enhance machine availability and reduce maintenance costs. They are also integrated in the iPhone (Apple) to change the display accordingly to device orientation.

On the micro-optics side, the field has grown into an important technology in the past two decades. This allowed combining MEMS devices with micro-optics and the acronym MOEMS (Micro-Optical-Electrical-Mechanical Systems) was firstly introduced in the early 1990's to highlight optical MEMS which also include bulk optics. MOEMS can include waveguides, moving mirrors and diffractive gratings. The components of a MOEMS device are compact, low weight and still can be fabricated at low cost using batch processes. MOEMS play an important role in the market since they encountered several applications as switches, filters, splitters, interferometers, deformable micromirrors and telescopic microlens arrays [11].

Miniaturization has extended recently to microfluidics with the aim to develop micro total chemical analysis systems (µTAS). Microfluidics is a powerful field and ready to open

new applications due to its ability to make networks of interconnecting channels. The most basic elements of a microfluidic device are the microchannels and microchambers [12], however more complex devices such as electrically controlled and silicon based micropumps and microvalves have already been reported [13].

2.2.- Applications and examples of MOEMS:

MEMS and MOEMS are already emerging products in several markets such as automotive, aerospace, medical, industrial process control, electronic instrumentation, office equipment, and telecommunications. They can be classified in two main categories: sensors (used to measure parameters of the environment) and actuators (modify this environment). Additionally, sensors can be classified into the families of capacitive, optical and electron tunnelling; and actuators are structured into the families of electrostatic, piezoelectric, thermal and magnetic [14].

MOEMS already found important applications in the market. For example, the Digital Micromirror Device (DMD) [15] has been developed by Texas Instruments and incorporated into Digital Light Processing (DLP) projectors. An optical system illuminates each single DMD, which represents a single pixel in the projected screen. They can be individually switched between two stable tilted states according to the state of a semiconductor memory cell. One state represents full brightness (on) and the other represents full darkness (off). The refresh rate of the DMD state is high enough that the human eye/brain sees an analogue light intensity.

Usually, laser based instruments need complex laser beam manipulations to control laser parameters such as beam's size, phase, and/or structure. Traditional components to perform those manipulations use compound lenses and mirrors, which may introduce misalignment, attenuation, distortion, and light scatter. With the aim to alleviate these challenges and, therefore, enhance the device functionality, arrays of reflective MOEMS elements capable to dynamically focus laser beams have been reported [16].

MOEMS are still under development and new applications are still being proposed. For example, new alternatives based on MOEMS systems for traditionally MEMS based devices such as pressure sensors are being proposed. Pressure sensors using optical sensing have been reported based on Mach-Zehnder [17] and Fabry-Perot [18] interferometries. Optical sensors can reach great accuracy, but can be affected by temperature problems and its calibration can be challenging and expensive.

MOEMS encountered a wide range of applications in the IR spectroscopy since by using them the set-up can be realised in a more efficient way, and the resulting device is much more compact and smaller. IR spectrometers with a scanning micromirror [19] or with a Fabry-

Perot based tunable optical filter [20] instead of an adapted optical set-up detector array have been reported.

Although MOEMS are being used in IR spectroscopy, other techniques are also available for gas measurement purposes.

2.3.- Gas detection techniques:

An enormous effort has been done to develop gas detection techniques to fulfill the rising needs in the progressive industrialization of society through the course of the twentieth century. A wide range of applications are related to gas detection such as environmental and indoor pollution, carbon monoxide poisoning, combustible gas detection and food quality. Nowadays, there are different types of gas sensors techniques currently in large scale use, each with certain advantages and disadvantages [21]. They are based on solid state sensors, electrochemical sensors, catalytic combustion, and IR detection.

Metal oxide sensors (MOX) are one of the most popular technological choices due to their high sensitivity and robustness. They are based on the variation of the sensor conductivity in presence of oxidizing and reducing gases when these gases are adsorbed onto the surface of the semiconductor. However, inaccuracies and inherent characteristics of the MOX sensors themselves have made it difficult to produce fast, reliable, and low-maintenance sensing systems comparable to other micro-sensor technologies that have grown into widespread use commercially. In order to obtain better gas sensors with higher sensitivity and greater selectivity, new materials are being proposed to find more suitable materials with the required surface and bulk properties for use in gas sensors [22].

Nevertheless, nowadays, the selectivity of MOX sensors is still low and they exhibit problems of long-term drift. Due to their lack of specificity and repeatability, their main application has been focused on alarm apparatus and qualitative leak detection [23]. However, the combined response of different MOX sensors can be seen as a 'signature' of each different chemical mixture under test. Therefore, MOX sensors arrays together with the proper data analysis can enhance the applications of MOX techniques [24].

An electrochemical cell sensor is similar to a battery which is exposed to the atmosphere, and a chemical reaction produces an electric current proportional to the target gas concentration. In the 1950's electrochemical cell sensors were used for oxygen monitoring and by the mid 1980's they were ready for measurement of several toxic gases in the permissible exposure limits (PEL). Nowadays, they are being used widely in applications for personal safety and for toxic gases and oxygen detection [23].

While electrochemical sensors are more selective to the target gas than MOX sensors, they still suffer from cross-sensitivities. The type of sensor, the target gas, and the gas concentration affect the degree of selectivity of the electrochemical sensor. Oxygen sensors show good selectivity, are very reliable, and have long life expectancy. However, other electrochemical sensors are subject to interferences from other gases. Additionally, although they usually feature an internal temperature compensation, electrochemical sensors are quite sensitive to temperature [25].

Catalytic sensors (often referred to as pellistors) burn the flammable gas in a controlled manner on a platinum filament and concentration determinations are made by measuring the temperature associated with this. Initially, they were used for gas monitoring in coal mines, but currently they are mainly used for flammable gas detection and they are produced by a large number of manufacturers. Catalytic sensors can be dramatically affected by certain chemicals which can deactivate the sensor and cause the sensor to lose sensitivity and eventually become totally nonresponsive to gases. A very small concentration of some chemicals can totally make the sensor useless. Usually, the exact cause of this poisoning is very difficult to identify but halogen compounds, which are present in fire extinguishers, and Freon which is used in the cooling systems will completely inhibit the sensor. Additionally, the sensor can suffer a dramatic deterioration after a high concentration exposure or an excessive heat [25].

Infrared detection is a non-destructive technique which relies on the ability of certain molecules to absorb IR radiation at wavelengths which are characteristic of the chemical structure of the molecule. The Lambert-Beer equation (Eq. 1) relates the quantity of radiation transmitted (T) to the optical path length (L), the gas concentration (c), and the absorption coefficient (α); which is a specific function of the wavelength (λ) for each gas.

$$T(\lambda) = \exp\left[-\alpha(\lambda).c.L\right] \qquad \text{Eq.1}$$

From an experimental point of view, the gas concentration can be observed by examining the optical absorption in a narrow IR band as it passes through the medium [26]. Figure 1 shows the typical set-up for an IR spectrometer, with the IR emitter, the gas cell, the optical filter to select the absorption band of the target gas, and the IR detector.

IR optical gas analyzers are selective and stable instruments and can be configured for the measurement of several species by selecting different absorption regions. Today, many IR instruments are available for a wide variety of applications. The main advantage of the optical gas sensors is that they are rather immune to false alarms and poisoning since the detectors are not in direct contact with the gas. This also implies easy maintenance and the corresponding friendly use.

Optical gas sensors can be classified depending on the way how the specific wavelength of interest is extracted from the IR source. On one hand, a Dispersive IR (DIR) spectrometer

includes an optical device such as a prism or a diffraction grating to spread the light spectrum and isolate a specific wavelength band. It uses their absorption characteristics to measure ingredients and quantity of a sample [27]. On the other hand, Non-Dispersive IR spectrometer (NDIR) isolates the specific wavelength band of the IR light that corresponds to the absorption spectrum of the target gas using narrowband transmission filters. NDIR technique is much more used than dispersive method.
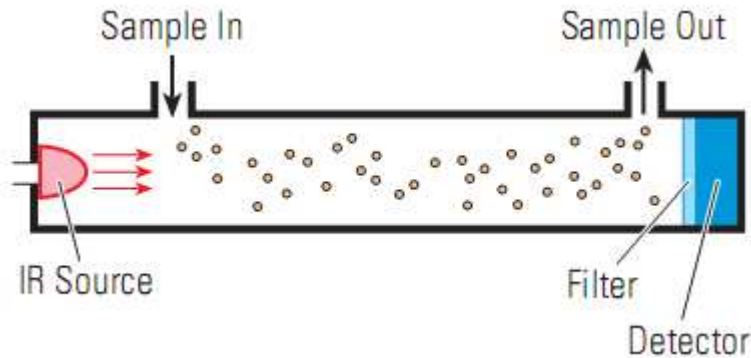

Figure 1: Basic layout of a IR spectrometer [25].

Fourier Transform IR (FTIR) spectroscopy represents another gas detection technique in the IR spectra which is widely used for multi-purpose applications. It is based on Michelson interferometer and a later Fourier Transform to obtain the spectrum. Despite traditional FTIR equipments are designed for laboratory applications, nowadays, portable FTIR can be found in the market (VIR-9000, Jasco Inc.).

Laser based systems can also be found in the market. Usually, in order to eliminate cross sensitivities, the emitting line of the laser is chosen in a region of the near IR where only the target gas absorbs. LaserGas II SP (Norsk Elektro Optikk AS, Norway) is a compact gas monitor based on a tunable diode laser.

Conversely to catalytic sensors, IR gas sensors show excellent performance on poisoning, false alarms, and burn out. Life expectancy of optical sensors is about 10 years, but only 1-5 for catalytic sensors. Additionally, long time exposure to gas changes the characteristic of the solid state and catalytic sensors and leads to permanent damage on these sensors. IR detector overcomes this problem since it is not in contact with the gas [25]. Therefore, in applications where continuous monitoring of chemical species is required and cost is not challenging, infrared instruments are chosen as gas analyzers [26].

Most of the commercial IR instruments for process control or continuous monitoring are based on NDIR architecture. APMA-370 (Horiba Ltd.) is a NDIR device for continuous carbon monoxide measurement to control atmospheric pollution. It features an interference-compensating detector, and a purified reference gas generated by purging the sample through an

oxidation process. It can be configured in four different ranges 0-10/20/50/100ppm, with a repeatability of 1%FS. Gasboard-3100 (Wuhan Cubic Optoelectronics Ltd.) is a NDIR multi-component gas measurement system which can measure carbon monoxide, carbon dioxide, ethylene, and hydrogen in the range 0-100% with a precision of 2%FS, and oxygen in the range of 0-25% with a precision of 3%FS.

Although both presented examples of complete commercial NDIR systems (shown in Figure **2**2) are desktop instruments and relatively big (550x482x221mm and rack type 19 inch 4U respectively), miniaturized NDIR systems can also be found in the market.
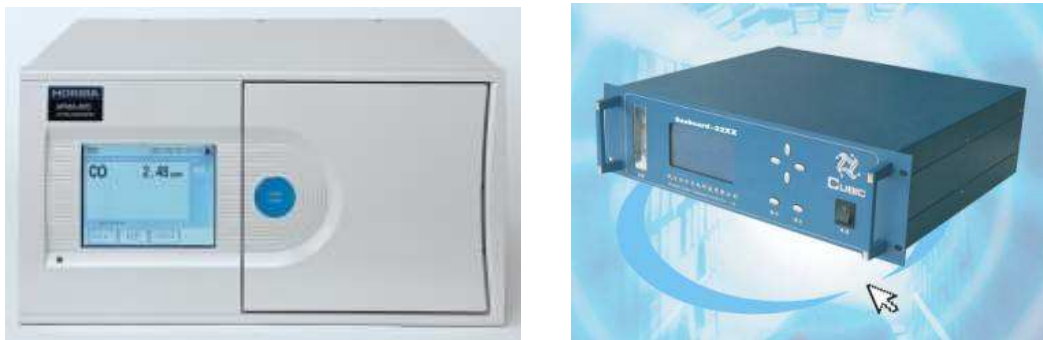

Figure 2: Commercial NDIR complete systems. APMA-370, from Horiba Ltd. (left) and Gasboard-3100, from Wuhan Cubic Optoelectronics Ltd. (right)

Miniaturization is a challenging issue for IR spectrometers since their sensitivity depends on the length of the absorption optical path (Lambert-Beer equation). Therefore, most of the miniaturized spectrometers are based on a high absorbance gases such as carbon dioxide and are only capable to measure relatively high gas concentrations.

Edinburgh Instruments Ltd. offers several NDIR compact systems for carbon dioxide, carbon monoxide, fluorocarbons, and methane detection in different ranges. GasCard II plus (Edinburgh Instruments Ltd.) model is based on a 160x100x40mm board and can be configured for carbon dioxide detection in the range of 0-500ppm with an accuracy of 30ppm. IRceL (City Technology Ltd.) is a miniaturized (16.6mm high and 20.4mm diameter) NDIR gas sensor. It is available for detecting either carbon dioxide (in the range of 0-5% with an accuracy of 0.1%) or hydrocarbons (in the range of 0-100% with an accuracy of 2%). H-550-EV (Environment Leading Technology Ltd.) is a NDIR small (32x12x38mm) sensor module which can detect carbon dioxide in the range of 2000ppm with an accuracy of 30ppm. These three commercial NDIR systems are shown in Figure .

NDIR systems are becoming more and more popular since they encountered several covering areas such as indoor air quality monitoring [28], automotive applications [29], carbon

dioxide detection to prevent greenhouse effect [30], and food status prediction [31], among others.
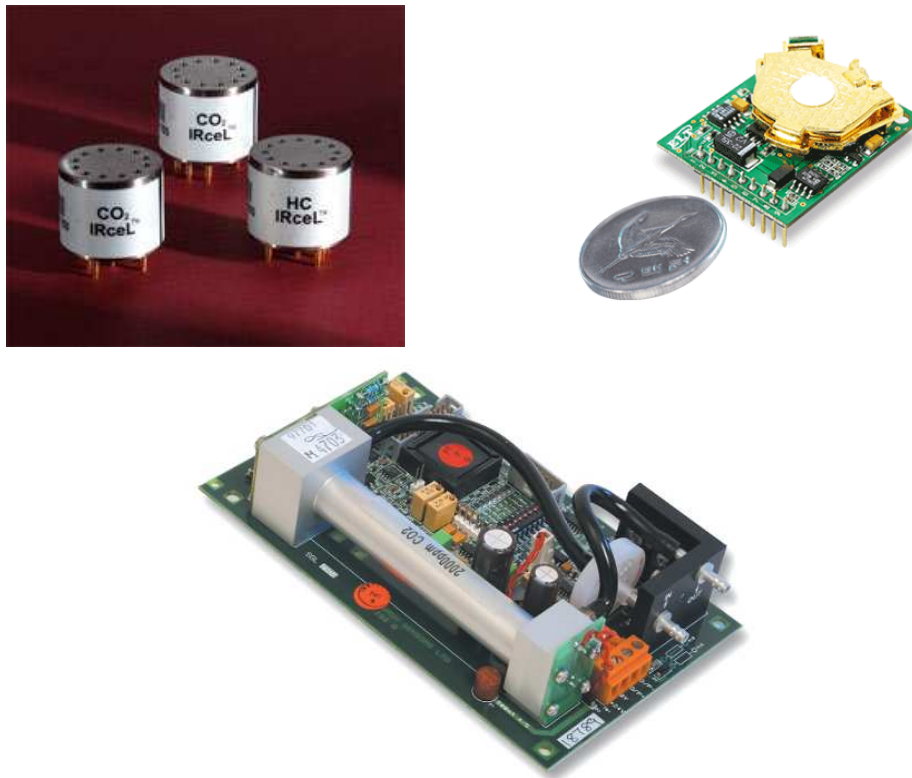

Figure 3: Miniaturized commercial NDIR systems for gas detection. Up left: IRceL (City Technology Ltd.). Up right: H-550-EV (Environment Leading Technology Ltd.). Down: GasCard II plus (Edinburgh Instruments Ltd.)

2.4.- NDIR System components:

Usually, NDIR optical gas sensors consist of an IR emitter, an absorption cell that contains the gas to be measured, and an IR detector where the transmitted radiation is collected. They are considered to be the key components of a NDIR system, together with the optical components present in the system such as the optical filters and any focusing element.

MOEMS open the possibility of combining micro optical elements with micromachining technology and makes it feasible to develop new systems with high volumes and low prices. The set-up of the NDIR spectrometer can be realized in a much more efficient way by using MOEMS and the resulting system is smaller and more compact. Additionally, detector arrays can be replaced by single elements in the adapted optical set-up.

The benefits involved in the use of MOEMS in NDIR systems are already being profited by some commercial devices. For example, miniaturized IR emitters featuring low

thermal-mass filament and ion-beam treated for high emissivity (pulsIR, from Icx Photonics Ltd.) and multi-channel thermopiles IR detectors with optical filters (TPS2534, from Perkin Elmer Ltd.) are MOEMS devices oriented to NDIR systems for gas detection.

a) IR emitters:

Absorption region of common target gases to be detected by means of NDIR spectrometers are in the band 3μm - 10μm wavelength. Therefore, IR emitter must exhibit high IR emission power in this range. Additionally, modulation of this radiation is desirable since synchronous techniques are usually implemented to recover the signal in a lower noise band compared to DC.

The most common form of IR source is a thermal emitter. They produce a spectral irradiance similar to the ideal black-body radiator. Traditional thermal emitters consist of a heated incandescent tungsten filament. However, a protective encapsulation of the heated filament is needed and an external glass is used to cover the emitter. Standard external bulb degrades the emission in the long wavelength region and renders filament thermal emitters unsuitable to detect gases above 5μm wavelength. Nevertheless, tungsten IR emitters with calcium fluoride or zinc selenide windows are already available in the market and enhance the emitter wavelength region (EF-8532, Helioworks Inc.).

Micromachined thermal emitters have been proposed for NDIR systems. On one hand, they need a high operating temperature (up to 2000K) to obtain large radiation power in the mid-IR range. On the other hand their emitting spectrum covers from visible to far infrared. Therefore, they emit a too wide spectrum of light and they are not efficient from a power consumption point of view. Furthermore, the additional emitted radiation degrades system performance since it warms up detectors and electronics elements and generates parasitic components of the detector signal [32].

Despite of mechanical choppers add cost, size, power consumption, and complexity to the optical system and the reliability of the system is degraded, they have been historically used to modulate the radiation emitted by thermal sources. They permit to reach high modulation frequencies. Small time constants are important parameters to directly modulate the IR radiation. Nowadays, thermal emitters permit direct modulation of radiation within the frequency range up to several Hz. However, thermal emitters based on novel materials such as platinum foil are still being proposed to further increase their modulation frequency [33].

Thermal sources normally emit sufficient energy in the 1μm - 5μm wavelength range for the detection of most hydrocarbons, carbon dioxide, and carbon monoxide. Therefore, thermal emitters are widely used since they are a simple and inexpensive light source and offer long life and long-term stability.

Thermal IR emitters have been reported as a key component of a NDIR gas measurement systems such as a carbon dioxide spectrometer [34]. However, miniaturized light bulbs with improved emission and drift and featuring built-in monitoring and self-test are still being proposed [35].

Other IR emitters such as electroluminescent diodes emitting radiation in the mid-IR (Mid-IR LEDs) and VCSEL lasers emitting in the near-IR are used to obtain fast radiation modulation without needing any additional mechanical part. They show limited spectral range and, therefore, the power consumption is improved since all the emitted light is concentrated in the absorption band of the target gas. The emitted wavelength of the Mid-IR LEDs basically depends on the semiconductor materials used, and specific devices can be fabricated for concrete species detection. The absorption of the gases typically is much smaller in the near-IR than in the mid-IR. Figure 4 show the ethylene absorbance, which is three orders of magnitude smaller in the near-IR than in the mid-IR. However, since VCSEL laser encountered several applications in the near-IR they can be tuned in a specific absorption band and used for gas detection. Vertilas GmbH offers different lasers in the range of 1.5μm-2μm for gas detection.
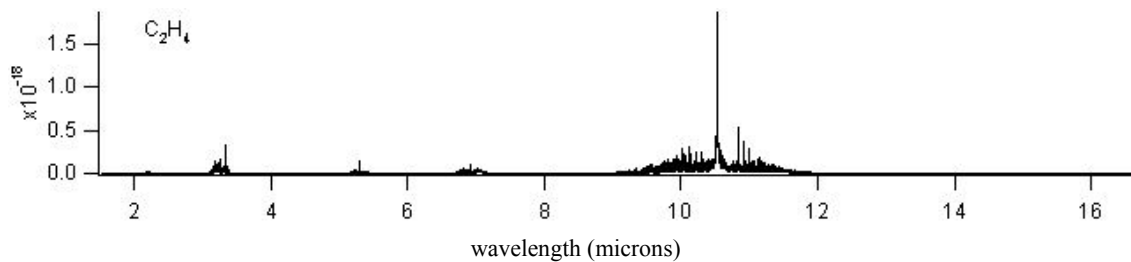

Figure 4: Ethylene absorbance in the IR range (adapted from [36]). Absorbance in the near-IR is much smaller than in the mid-IR

However, NDIR systems based on LEDs and VCSEL lasers need one emitter for each gas to be detected. In addition, they exhibit strong dependency of power and spectrum characteristics on temperature and their price significantly exceed thermal sources costs. Therefore, they are not as used as thermal emitters [33]. Nevertheless, LED sources are used in applications where a low gas concentration must be detected and a high optical power is required. Table 1 shows a comparison between thermal emitters, mid-IR LED, and near-IR lasers.

	Power	Spectrum	Directivity	Cost	Optical filters
Thermal	medium	wide	low	low	needed
Mid-IR LED	medium	narrow	medium-high	low-medium	no needed
Near-IR lasers	medium-high	very narrow	high	medium-high	no needed

Table 1: Comparison between different IR emitters.

b) IR Detectors:

For IR applications, a radiation detector sensitive to a much longer wavelengths range than those of the visible spectrum is needed. An ideal detector should have a flat spectral response curve in all the interesting range. Several sensors types and manufacturers can be found in the market specifically developed for gas sensing monitoring. However, IR detectors can be classified in two main categories regarding its operation principle: quantum detectors and thermal detectors. Figure 1 shows the normalized detectivity characteristics for different types of detectors.
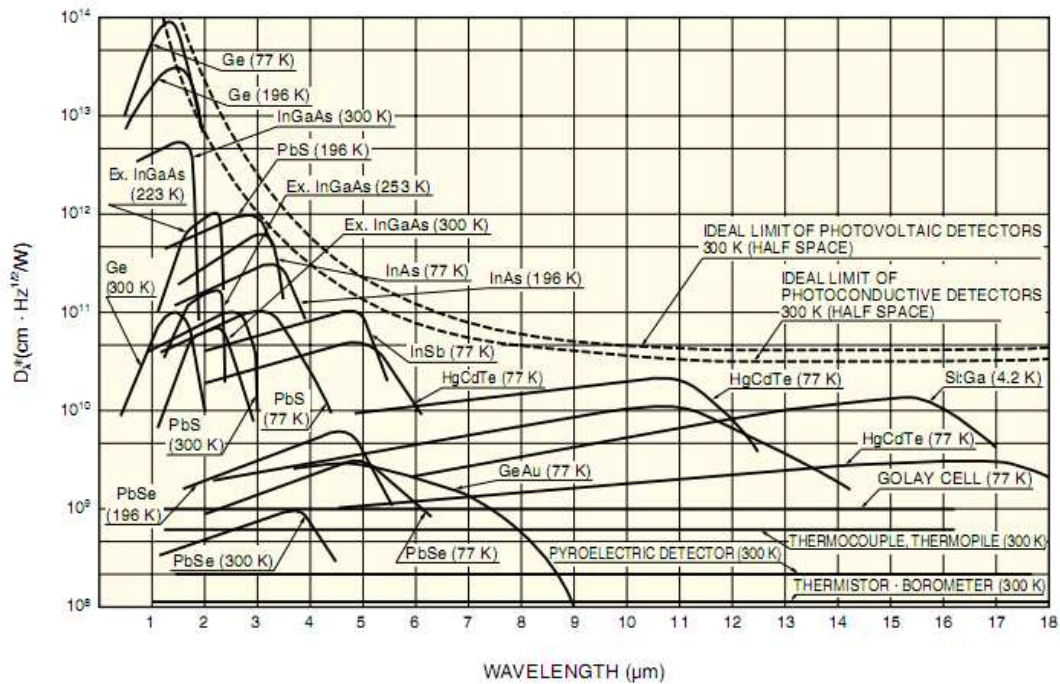

Figure 1: Normalized detectivity characteristics for different type of detectors (from [27]).

Quantum-type detectors are based on photon absorption which directly excites an electron-hole pair in the detector and changes the electrical properties of the detector. An example of quantum detectors is photoconductive detectors. They consist of a high-resistivity semiconductor material, the resistance of which is reduced when it is exposed to IR radiation. A second example is photovoltaic effect based detectors, where the incident radiation causes a current to flow in the p-n junction of a semiconductor.

Quantum-type detectors show excellent detectivity in the IR range and fast response, but they are strongly wavelength dependent (Figure 1) and, additionally, they generally need to be cooled for accurate measurement. Nevertheless, quantum-type detectors (commonly PbS and PbSe) with integrated Peltier cells or thermistors for temperature stabilization can be found in the market and make these detectors are useful for cheap and compact applications. P2038

series from Hamamastu Co. are cooled PbSe detectors in a compact TO-8 package for gas analyzing applications.

In thermal detectors the absorbed photon results in a temperature rise of the detector, which entails an alteration of its electrical properties. Despite of its smaller detectivity compared to quantum detectors (Figure 1), thermal detectors are widely used due to its uncooled operation, their small dependency on the wavelength and flat response [37]. Pyroelectric sensors, bolometers, and thermopiles are the most common thermal detectors.

Bolometers are IR detectors which change their electrical resistance when IR radiation strikes the detector material. Although MOEMS based bolometers have been proposed for gas measurements [38] [39], their main application is related to thermal imaging. They show a very broadband response, but their detectivity is low and they require a tight temperature control of the environment.

Pyroelectric detectors convert the heat collected by the pyroelectric material into static voltage across a crystalline material. However, the signal declines when they are exposed under a constant illumination. Therefore, they must be modulated, which is usually achieved adding an external mechanical chopper. Pyroelectric detectors have been employed for mass production and encountered several applications on intruder alarm systems and automatic light switches due to their capability to detect moving objects.

Thermopiles are simple thermal detectors and show better sensitivity than pyroelectric and bolometer detectors. They consist of two different materials electrically connected at one junction, and shielded and maintained at a standard temperature at the other end. Any radiation incident on the sensitive junction will produce an induced voltage at the reference end. Therefore, the voltage output depends on the temperature difference, but also on the two employed materials.

Modern semiconductor technology allows batch fabrication of thermopiles and makes it possible to produce thermopile sensors consisting of several thermocouples in series in a small area. The resulting sensor is extremely sensitive, with a fast response time due to its smallness, and it is cost effective [40]. These characteristics allowed thermopiles finding several applications in gas measurements such as safety, instrumentation, food processing, air quality control, and environment protection [41].

Unlike to quantum-type detectors, thermopiles show almost constant detectivity over the IR spectrum. Therefore, a thermopile can be combined with the proper optical window to measure any gas. Additionally, long term stability can be improved by the use of a reference channel without absorptions [41] [42]. Therefore, new configurations are proposed with an additional detector with an optical filter at a different wavelength. In this configuration, the reference detector provides a base point value while the active detector is used to provide the

signal and it compensates the changes that occur in the detector's sensitivity with time and any eventual change of intensity of the IR emitter.

Nowadays, silicon based thermopiles are commonly used for IR detection in NDIR spectrometers. TPS-4339 from Perkin Elmer Ltd. is a quad thermopile element in TO-39 housing with four optical windows specifically devoted for gas detection.

c) Optical components:

Non-dispersive infrared (NDIR) gas sensors use one specific detector for each gas to measure. To select the suitable wavelength for each gas, specific optical narrowband filters are needed. They are usually placed directly upon the IR detector set or on a rotative filter roulette. The second architecture is more complex design since additional mechanical parts are needed. However, previous works presented by the same research group where this Thesis is developed involve optical gas systems based on an array of non-specific detectors together with data processing analysis [43], and systems with narrowband but tunable optical filters [44].

A bandpass optical filter usually consists of a number of dielectric layers on a substrate. The thickness, the number and the material of deposited layers on the substrate determine the transmission characteristics of the filter [45] [41]. Usually, silicon is used as a substrate in order to take advantage of its related technologies.

In order to increase the radiation which reaches the sensing element, optimize the sensor signal and improve the global efficiency of the system, some focusing elements can be placed on the detector. It is especially worth when a low signal is expected on the detector or when very low gas concentrations must be detected. However, only a few detector modules are in the market featuring focusing elements, and they are specifically designed for single-channel detectors. Therefore, they are not suitable for multiple gas detection in NDIR systems.

Relatively compact IR detector modules can be found in the market. Several single and multi channel IR detectors featuring optical windows for specific applications are already commercially available. DigiPyro PYD 1988 (Perkin Elmer) is a dual element pyrodetector for motion detection and TS4x200X (Micro-Hybrid Electronic) is a four-channel thermopile for gas sensing.

Some single channel IR detectors featuring focusing elements can also be found in the market such as HTIA-E (Heimann Sensors) and ST-50/R (Dexter Research). ST-50/R detector is assembled with a silicon micromachined diffractive IR lens (A2DIF01, Laser Components) which also acts as a broadband optical filter for bandwidth selection. The corresponding block diagram and the transmission spectra of the integrated lens are shown in Figure 2.

However, no specific narrow optical window is integrated in those detectors and thus the transmitted radiation is determined by the lens. Typically, the lens transmission peaks at 9μm, with an effective operating bandwidth from 7μm to 14μm. Therefore, such a device is not suitable for detection of important gases such as hydrocarbons, carbon dioxide, and carbon monoxide and it cannot be used as a detector module for a NDIR system.
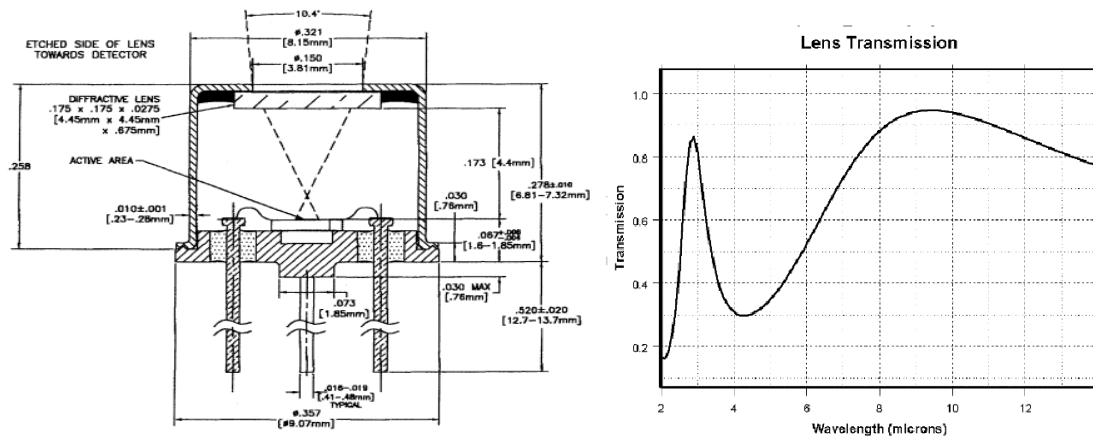

Figure 2: Left: Mounting arrangement of the single channel IR detector ST-50/R (Dexter Resarch) with the silicon micromachined lens. Right: Transmission spectra of the silicon lens (A2DIF01, Laser Components).

d) Absorption cell:

The design of the absorption gas cell is critical since it is where the sample gas interacts with the light and the spectrometer sensitivity depends on the optical path length of the gas cell.

The gas cell design can be relatively simple or much more complicated depending on the requirements of the application such as sensitivity, selectivity, and stability. This is normally done by using a tube that allows light to enter from one end and exit the other, where it meets the detector. There are "inlet" and "outlet" ports that allow the sample gas to circulate through the tube [25].

However, in order to increase the sensor sensitivity, sometimes the path length of the absorption cell is increased. It can be done by a complex design based on a multiple reflections between three concave mirrors which increases optical path length in the gas cell but does not enlarge spectrometer dimensions. This configuration was firstly proposed by White in 1942 [46]. Figure 3 shows the layout of the typical White absorption cell.
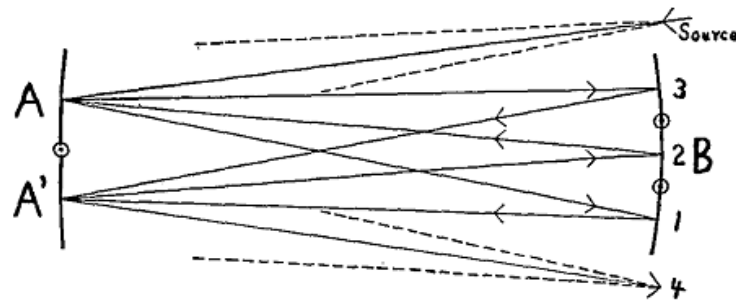
Figure 3: Architecture proposed by White [46] in 1942 to obtain long optical paths.

2.5.- Summary:

In this chapter, the importance of miniaturization and the integration of systems consisting of electronics and sensors have been presented. In this race, silicon technology plays an important role and led to the birth of MEMS and MOEMS, which are holding a large market nowadays.

In particular, an important effort has been done in this trend in the field of gas detection techniques. Several techniques, with different performances, have been proposed for gas detection. The great performance of NDIR spectrometers for long term gas measurements has been highlighted and the state of the art of this technique is presented. Nowadays, compact IR detectors for multi-channel spectrometers based on MOEMS detectors integrated with narrow band pass optical filters for gas detection are already commercially available. However, none of them feature specific optical module to increase the system sensitivity. Only single channel IR detectors can be found in the market with additional focusing elements, but with no narrow optical filters. Therefore, they are not selective for proper gas detection in a NDIR system.

2.6.- References:

[1]   G.E. Moore, "Cramming more components onto integrated circuits (Reprinted from Electronics, pg 114-117, April 19, 1965)," *Proceedings of the Ieee*, vol. 86, (no. 1), pp. 82-85, 1998.

[2]   P.S. Peercy, "The drive to miniaturization," *Nature*, vol. 406, (no. 6799), pp. 1023-1026, 2000.

[3]   T.W. Williams, "EDA to the rescue of the silicon roadmap," *2008 11th EUROMICRO Conference on Digital System Design Architectures, Methods and Tools (DSD)*, pp. xxiv, 2008.

[4]   M.H. Bao and W.Y. Wang, "Future of microelectromechanical systems (MEMS)," *Sensors and Actuators a-Physical*, vol. 56, (no. 1-2), pp. 135-141, 1996.

[5]   MEMSandNanotechnologyClearinghouse, "What is MEMS Technology? http://www.memsnet.org/mems/what-is.html

[6]   P.J. French and P.M. Sarro, "Surface versus bulk micromachining: the contest for suitable applications," *Journal of Micromechanics and Microengineering*, vol. 8, (no. 2), pp. 45-53, 1998.

[7]   T. Rogers, "Microengineering technologies and capabilities," *IEE Colloquium on `Microengineering - the Future!' (Digest No.1993/182)|* pp. 5/1-3|23, 1993.

[8]   J.C. Eloy, "Europe is maintaining its leadership in MEMS," *MST News*, pp. 14-15, 2008.

[9]   W.P. Eaton and J.H. Smith, "Micromachined pressure sensors: Review and recent developments," *Smart Materials & Structures*, vol. 6, (no. 5), pp. 530-539, 1997.

[10]   A. Albarbar, A. Badri, J.K. Sinha, and A. Starr, "Performance evaluation of MEMS accelerometers," *Measurement*, 2008.

[11]   M.E. Motamedi, "MOEMS: Design, technology, and applications," *Journal of Microlithography Microfabrication and Microsystems*, vol. 4, (no. 4), 2005.

[12]   E. Verpoorte and N.F. De Rooij, "Microfluidics meets MEMS," *Proceedings of the Ieee*, vol. 91, (no. 6), pp. 930-953, 2003.

[13]   H. Takao and M. Ishida, "Novel MEMS fluidic integrated circuit technology with 'MOSFET-like microvalve elements'," *Mems/ Nems: Handbook Techniques and Applications Vol 2, Fabrication Techniques*, pp. 111-139, 2006.

[14]   D.J. Bell, T.J. Lu, N.A. Fleck, and S.M. Spearing, "MEMS actuators and sensors: observations on their performance and selection for purpose," *Journal of Micromechanics and Microengineering*, vol. 15, (no. 7), pp. S153-S164, 2005.

[15]   J.B. Sampsell, "Digital Micromirror device and its application to projection displays," *Journal of Vacuum Science & Technology B*, vol. 12, (no. 6), pp. 3242-3246, 1994.

[16]   R. Fayek, "Adaptive MOEMS applications in telemetry and multi-spectral imaging," *2007 International Conference on Microelectronics*, pp. 209-12, 2008.

[17]   B.H.V. Borges, S.K. Manfrin, M.A. Romero, and A.C. Cesar, "Theoretical analysis of silicon-based integrated-optic Mach-Zehnder pressure sensors," *Fiber and Integrated Optics*, vol. 20, (no. 4), pp. 385-401, 2001.

[18]   D.G. Guo, W.J. Wang, and R.M. Lin, "Extrinsic Fabry-Perot pressure sensor using single deeply corrugated diaphragm technique," *Moems and Miniaturized Systems Iv*, vol. 5346, pp. 15-26, 2004.

[19]   T. Otto, R. Saupe, A. Weiss, V. Stock, R. Bruch, and T. Gessner, "Principle and applications of a new MOEMS-spectrometer - art. no. 611409," *MOEMS Display, Imaging, and Miniaturized Microsystems IV*, vol. 6114, pp. 11409-11409, 2006.

[20]   R. Rubio, N. Sabate, C. Calaza, J. Santander, L. Fonseca, I. Gracia, C. Cane, M. Moreno, and S. Marco, "Optical simulation of a MOEMS based tuneable Fabry-Perot interferometer," *Proceedings of the IEEE Sensors 2004, Vols 1-3*, pp. 1324-1327, 2004.

[21]   P.T. Moseley, "Solid state gas sensors," *Measurement Science & Technology*, vol. 8, (no. 3), pp. 223-237, 1997.

[22]   G. Eranna, B.C. Joshi, D.P. Runthala, and R.P. Gupta, "Oxide materials for development of integrated gas sensors - A comprehensive review," *Critical Reviews in Solid State and Materials Sciences*, vol. 29, (no. 3-4), pp. 111-188, 2004.

[23]   SiraTechnology, *Gas Detector Selection and Calibration Guide*: Withrebys publishing, 2005.

[24]   A. Fort, M.B. Serrano-Santos, R. Spinicci, N. Ulivieri, and V. Vignoli, "Electronic noses based on metal oxide gas sensors: the problem of selectivity enhancement," *Proceedings of the 21st IEEE Instrumentation and Measurement Technology Conference (IEEE Cat. No.04CH37510)|* pp. 599-604 Vol.1|2649, 2004.

[25]   J. Chou, *Hazardous Gas Monitors: A Practical Guide to Selection, Operation and Applications*: McGraw-Hill and SciTech Publishing, 2000.

[26]   P.T. Moseley, J.O.W. Norris, and D.E. Williams, *Techniques and mechanisms in gas sensing*, Bristol, England and Philadelphia: Adam Hilger, 1991.

[27]   Hamamatsu, "Characteristics and use of infrared detectors," *Solid State Division*, vol. 12, (no. Technical Information).

[28]   J. Park, H. Cho, and S. Yi, "Self-temperature compensation of NDIR CO2 gas sensor," *Proceedings of the Fourth IASTED International Conference on Circuits, Signals, and Systems*, pp. 220-223, 2006.

[29]   R. Frodl and T. Tille, "A high-precision NDIR CO2 gas sensor for automotive applications," *Ieee Sensors Journal*, vol. 6, (no. 6), pp. 1697-1705, 2006.

[30]   Y.F. Wang, M. Nakayama, M. Yagi, M. Nishikawa, M. Fukunaga, and K. Watanabe, "The NDIR CO2 monitor with smart interface for global networking," *Ieee Transactions on Instrumentation and Measurement*, vol. 54, (no. 4), pp. 1634-1639, 2005.

[31]   W.M. Miller, B. Nelson, R. Richard, and M.A. Ismail, "Review of sensor technologies for realtime process control of ethylene in citrus degreening," *Proceedings of the Florida State Horticultural Society*, vol. 113, pp. 300-303, 2000.

[32]   E. Cozzani, C. Summonte, L. Belsito, G.C. Cardinali, and A. Roncaglia, "Design study of micromachined thermal emitters for NDIR gas sensing in the 9-12 mu m wavelength range," *2007 Ieee Sensors, Vols 1-3*, pp. 181-184, 2007.

[33]   J. Puton, K. Jasek, B. Siodlowski, A. Knap, and K. Wisniewski, "Optimisation of a pulsed IR source for NDIR gas analysers," *Opto-Electronics Review*, vol. 10, (no. 2), pp. 97-103, 2002.

[34]   D. Bauer, M. Heeger, M. Gebhard, and W. Benecke, "Design and fabrication of a thermal infrared emitter," *Sensors and Actuators a-Physical*, vol. 55, (no. 1), pp. 57-63, 1996.

[35]   J. Spannhake, O. Schulz, A. Helwig, G. Miiller, and T. Doll, "Design, development and operational concept of an advanced MEMS IR source for miniaturized gas sensor systems," *2005 IEEE Sensors (IEEE Cat. No.05CH37665C)|* pp. 4 pp.|CD-ROM, 2005.

[36]   "The Hitran Database," in, 2009, Available from Database Provider|.

[37]   M. Noda, "Uncooled thermal infrared sensors: Recent status in microbolometers and their sensing materials," *Sensor Letters*, vol. 3, (no. 3), pp. 194-205, 2005.

[38]   E. Johnson and W. Bodkin, "Gas detection apparatus using a combined infrared source and high temperature bolometer," vol. 6528792, Ion Optics, Inc, 2003.

[39]   H.A. Jones-Bey, "Infrared spectroscopy - MOEMS bolometer may provide cost-effective optical gas sensing," *Laser Focus World*, vol. 37, (no. 12), pp. 44-45, 2001.

[40]   J. Schilz, "Thermoelectric infrared sensors (thermopiles) for remote temperature measurements; pyrometry," *thermophysica minima, Perkin Elmer*, 1999.

[41]   J. Schilz, "Thermopiles for IR absorption gas detection," *thermophysica minima Perkin Elmer*, 2000.

[42]   J. Weathers, S. Ropson, and A.J. Syllaios, "Sensor system for environmental applications," *Intech*, vol. 47, (no. 12), pp. 45-47, 2000.

[43]   R. Rubio, J. Santander, J. Fonollosa, L. Fonseca, I. Gracia, C. Cane, M. Moreno, and S. Marco, "Exploration of the metrological performance of a gas detector based on an array of unspecific infrared filters," *Sensors and Actuators B-Chemical*, vol. 116, (no. 1-2), pp. 183-191, Jul 2006.

[44]   J. Santander, N. Sabate, R. Rubio, C. Calaza, L. Fonseca, I. Gracia, C. Cane, M. Moreno, and S. Marco, "Mirror electrostatic actuation of a medium-infrared tuneable Fabry-Perot interferometer based on a surface micromachining process," *Sensors and Actuators A (Physical)|* vol. 123-124, pp. 584-9, 2005.

[45]   Rancourt, *Optical Thin Films: User Handbook*, 1996.

[46]   J. White, "Long optical paths of large aperture," *Journal of the Optical Society of America*, vol. 32, pp. 4, 1942.

3.- ATMOSPHERE CONTROL FOR FRUIT STORAGE:

3.1.- Motivation:

The key to maintaining good health is combining a daily physical activity with healthy eating plan. Therefore, a balanced diet is crucial for a healthy lifestyle. Mediterranean diet is well-known for being balanced. This diet is characterized by abundant plant foods (fruit, vegetables, breads, other forms of cereals, potatoes, beans, nuts, and seeds), fresh fruit as the typical daily dessert, olive oil as the principal source of fat, dairy products (principally cheese and yogurt), and fish and poultry consumed in low to moderate amounts, zero to four eggs consumed weekly, red meat consumed in low amounts, and wine consumed in low to moderate amounts, normally with meals [1].

Fruit plays an important role in any well-balanced diet. Fresh, canned and frozen fruits provide several benefits to human health since they are rich in fibre, vitamin C and folate. Therefore, an important quantity of fruit is daily needed for a healthy diet. A balanced diet suggests at least 2 serves of fruit daily [2].

Apple is one of the more popular fruit to balance the diet: apple production reached around 60 millions tons in the world in 2000 (being Western European countries the first worldwide producer with 9.6 millions tons) [3].

In particular, Spain is one of the countries where more fruit is consumed per capita. Between 1999 and 2004 the fresh fruit consumption per capita increased to more than 100 kg/capita/year. Oranges, apples, bananas, melons, and pears are the most consumed fruits in Spain. Table 1 shows the total fresh fruit consumption and the more consumed fruit categories during the period 1999-2004 in Spain.

Fruit Consumption (Kg/capita/year)	1999	2000	2001	2002	2003	2004
Total Fresh Fruit	84.5	93.4	95.6	96.5	98.2	101.1
Oranges	20.9	23.0	22.1	23.4	23.4	24.0
Apples	11.2	12.6	13.2	12.7	12.3	12.5
Bananas	7.4	9.4	10.3	10.0	10.1	10.3
Melons	8.0	7.8	8.5	8.0	9.1	9.2
Pears	7.2	7.4	7.9	7.4	7.5	7.8

Table 1: Fresh fruit consumption in Spain. Source: ISAFRUIT [4]

Although orange is by far the most popular fruit in Spain, apple is very consumed in all Europe. For instance, countries where fruit consumption is not so popular such as Germany and Poland, apple is even more consumed. Table 2 and Table 3 show fruit consumption in Germany and Poland respectively.

Fruit Consumption (Kg/capita/year)	1997/98	1998/99	1999/00	2000/01	2001/02	2002/03
Total Fresh Fruit	62.8	60.6	68.4	66.8	62.5	62.4
Apples	18.0	17.7	20.6	19.1	17.5	17.7
Bananas	11.2	10.3	11.0	12.1	11.1	11.1
Oranges	6.4	5.8	6.1	7.0	6.0	6.5

Table 2: Fresh fruit consumption in Germany. Source: ISAFRUIT [4]

Fruit Consumption (Kg/capita/year)	2001	2004	2005
Total Fresh Fruit	37.4	36.6	34.7
Apples	22.1	20.9	20.0
Berries	7.0	6.1	6.6

Table 3: Fresh fruit consumption in Poland. Source: ISAFRUIT [4]

Harvest period depends on the fruit variety, but in the Mediterranean countries, apple usually starts to be harvested in August and it finishes at the end of October. At home most varieties of apple only can be stored for a couple of weeks. However, apple demand is held during all the year.

Quality deterioration during the long-term storage and along the supply chain, price, and fruit availability are factors that affect apple consumption. Figure 1 shows the apple consumption per month in Spain, and Table 4 shows the consumption per trimester of apples in Italy in the period 2000-2005. Both countries present similar behavior: during summer period July-August apple is less consumed, and its popularity is recovered in September, when the fruit is being harvested again.

The apple consumption decay in summer is produced by a lack of good quality fruit since it is complex to store apples during several months and maintain all the quality factors. Therefore, it is important to store the fruit in such a way that the final fruit is in good organoleptic quality and it meets consumer expectations. Organoleptic quality of apple depends on several factors such as firmness, texture, sweetness, tartness, aroma which is mainly comprised by the mixture of volatile compounds produced by apples, and flavour which is a complex combination of taste and odour sensations.
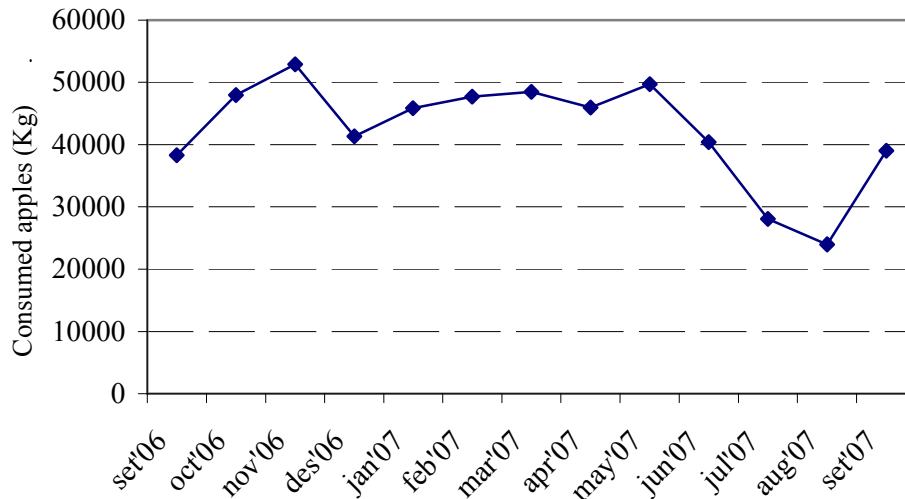
Figure 1: Monthly consumption of apples for a whole year. Source: Ministerio de Medio Ambiente y Medio Rural y Marino [5].

Fruit Consumption (Kg/capita/year)	2001	2002	2003	2004
Jan-Mar	5.13	6.21	5.74	6.09
Apr-Jun	6.05	6.55	6.51	6.26
Jul-Sep	2.97	3.32	3.15	3.56
Oct-Dec	4.71	4.76	4.63	4.76

Table 4: Consumption per trimester of apples in Italy 2000-2005. Source: ISAFRUIT [3]

To assure apple availability during several months, it requires large scale production of apples, huge crop and fruit storing for several months. With that aim, apples are often harvested before the ripeness stage for optimal eating quality is attained, and are stored in controlled atmosphere chambers. With this technique the ripening process is delayed, and storability and transportability are improved [6]. Harvesting mature unripe fruit enhances several fruit quality characteristics such as increased shelf life and a slowed decline in firmness, acidity, and green ground-colour relative to ripe fruit. On the other hand, unripe fruit do not develop typical full-flavour and their taste is strongly impaired [7].

Despite present storage facilities, post-harvest diseases of apple annually cause losses of 5-25 % [3]. The cost of long-term storage is relatively high: in the case of apples stored in controlled atmosphere, this cost amounts to about 40% of the fruit price at the packinghouse gate. In addition, every quantity of fruit lost is expressed in decreased revenue for the farmer and increased costs to the packinghouse. The losses in the case of apples can exceed 14% of total packinghouse revenue from long-term storage [8].

In order to decrease the losses related to long term storage, apple ripening and storage techniques have been deeply studied.

3.2.- Apple ripening and storage techniques:

Fruit is one of the numerous plant species mechanisms for seed dispersal. They are involved in the constant effort to yield subsequent generations of viable and competitive progeny. Therefore, fruit intends to contain mature seeds and also being attractive for optimal seed dispersal. Because of the dual role of fruits as both a unique aspect of plant development and the source of a large portion of the human diet, the molecular basis of development and ripening of fleshy fruits has received considerable scientific attention [9].

Different processes are present during fruit life. They are complex and typically there is an overlap between them. Maturation process starts when the cell growth is near to finish and it ends when the seeds are mature enough to inseminate. Before maturation is finished, ripening begins. The ripening process renders fruit attractive and palatable to a variety of seed-dispersing organisms and typifies fleshy fruits [9]. Color, aroma, taste and flavor characteristics show significant variation during maturation and ripening due to the decisive metabolic change present in these processes. Finally, the fruit declines into senescence.

Fruits can be classified into two major groups based on of the intervention of ethylene during maturation. Non-climacteric fruits are those whose maturation does not depend on ethylene, such as orange, cherry, strawberry and pineapple. Climacteric fruits, such as tomato, avocado, melon, apple, pear, peach and kiwifruit are characterized by an extraordinary increment in ethylene production which accompanies the respiratory peak during ripening [10].

Fruit growth and maturation can only take place properly in the tree. However, although the final result is different, ripening process can occur both in the tree and after harvest. The aim of this chapter is to summarize the ripening process when it takes place out of the tree and introduce the important role of ethylene, which is considered to be a naturally occurring plant hormone, in the fruit metabolism [11].

Ripening is a process of physical, metabolic, and biochemical changes initiated and/or coordinated by ethylene, either on or off the tree, and includes loss of background green color, softening of fruit tissue, and development of characteristic aroma and flavor. Over 300 volatile compounds, including alcohols, aldehydes, carboxylic esters, ketones, and ethers, have been identified in the aroma profile of apples. Some of these compounds are present in very low concentrations but have important contribution to fruit aroma and flavour characteristics (e.g., ethyl-2-methyl butanoate), determine aroma intensity (e.g., trans-2-hexenal), or are related to

aroma quality (e.g., ethanol). Typical flavor and aroma compounds of apples are only produced after ripening has been initiated by ethylene [12].

Ethylene is the simplest organic compound known to affect the physiological processes in plants and is considered to be the ripening hormone. Plant tissue naturally produces ethylene, which triggers several effects at very low concentrations (ppm or less) and regulates many aspects of development and senescence [13]. As part of the normal life of the plant, ethylene production is induced during certain stages of growth, including fruit ripening, leaf abscission and flower senescence [11].

Ethylene is synthesised from the amino acid methionine, which is activated by adenosine triphosphate (ATP) to produce S-adenosylmethionine (SAM). 1-aminocy-clopropane-1-carboxylic acid synthase (ACS) converts SAM to 1-aminocy-clopropane-1-carboxylic acid (ACC), and ethylene is produced from ACC with the aid of ACC oxidase. In climacteric fruits, the regulation of ethylene biosynthesis depends both on the ACC availability and on the capacity of the tissue to convert ACC to ethylene [13].

As soon as ripening begins in a climacteric fruit, the production of ethylene suffers a tremendous burst, which is called climacteric peak. The rate of ethylene production can increase 100-fold in two days. After the climacteric stage the rate of ethylene production declines. The ethylene burst is used to classify apples as either pre-climacteric stage (not yet producing significant quantities of ethylene) or post-climacteric stage (significant production of ethylene) [11]. Additionally, the amount of ethylene and carbon dioxide produced by the fruit can be used to define different stages of ripeness and maturity:

- *Physiologically immature pre-climacteric apples* have low ACC concentration and ACS activity, low ethylene production and fail to ripen normally.
- *Physiologically mature pre-climacteric apples* present increased ACS activity, are accumulating ACC and producing endogenous ethylene. At this stage of maturity, apples can be induced to ripen by exposure to exogenous ethylene and present the greatest postharvest storage life potential.
- *Peak climacteric apples* have reached their maximum respiration rate and ethylene production.
- *Post-climacteric apples* are considered ripe, having moderate ethylene production, low firmness, and a short storage life [12].

Figure 2 shows typical ethylene production and fruit growth during apple lifetime. At the climacteric peak, ethylene burst occurs and fruit growth slows down. In store-houses, ethylene concentration is below 1ppm while fruit is unripe. Then, as fruit ripening begins, the production of ethylene increases dramatically and its concentration continuously rises to values higher than 100ppm. Fruit senescence starts typically 15 days after ethylene burst.

To summarize the ethylene role in the fruit development it can be said that it plays a twofold role: on one hand it can be thought as an indicator that fruit is ripening (low ethylene concentrations are produced by the fruit itself), and on the other hand it is considered as the hormone that triggers the ripening process of fruit [14, 15]. In some occasions ethylene is externally added when ripeness or degreening of the product must be promoted. Therefore, ethylene is commonly used to establish the ripening of fruits [7].
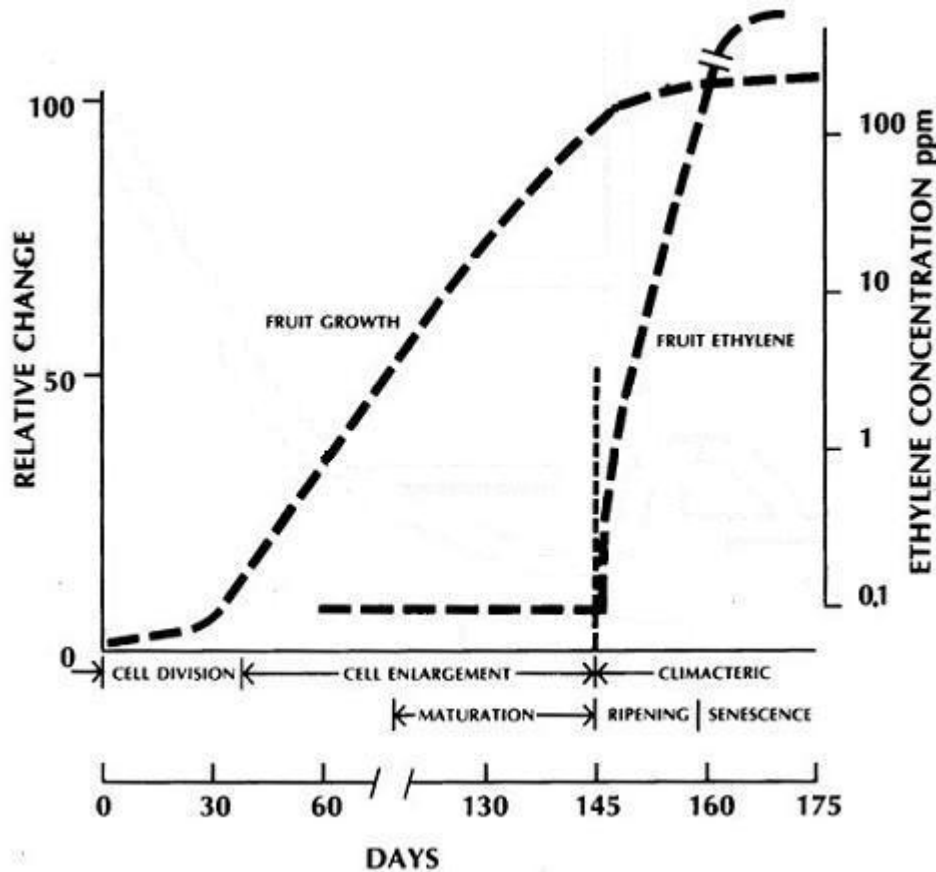
Figure 2: Fruit growth and ethylene concentration during apple lifetime. At the climacteric peak, ethylene concentration increases exponentially and fruit growth slows down. Adapted from [11].

In order to optimize conservation process and extend the postharvest life of crops, modified atmospheres (MA) and controlled atmospheres (CA) are extensively used for fruit storage, transport of crops, and in the packaging of fruits. MA refers to atmospheres with different gas composition than the normal air (21% of oxygen, 78% of nitrogen, 0.03% of carbon dioxide, and traces of other gases) and CA refers to the use of a MA where a strict control during all the period of application is added [16].

The use of MA for the preservation of foodstuffs is as old as it is new and modern. Hermetic storage of grain was practiced in ancient times in underground pits in the dry, subtropical regions of the Middle East, North Africa, India, etc [17].

Nowadays, MA and CA commonly involve atmospheres with low oxygen and/or elevated carbon dioxide concentrations. On one hand, these atmospheres conditions, together with a refrigeration control, provide several beneficial effects to storing fruit such as reducing the respiration rate, control of the synthesis and action of ethylene, delaying ripening and senescence, alleviation of some physiological disorders, control of vitamin losses, and control of some micro-organisms and pests [13].

On the other hand, dramatic effects such as total loss of the product, the initiation and/or aggravation of certain physiological disorders, irregular ripening, increased susceptibility to decay, or development of off-flavors can occur when the fruit is exposed to an atmosphere with oxygen and/or carbon dioxide levels out of the fruit tolerance range [13].

Nowadays, improved CA systems such as rapid CA, which rapidly establish CA conditions in the room compared to the old conventional slow CA, are available for fruit storage. These systems, together with improvements in the structural techniques for the development of sealed storage and CA conditions, feature better fruit preservation.

However, not all the fruit crops are suitable to CA conditions. It is suggested that for the use of CA, the crop should meet the following characteristics [13] :

- Long post-harvest life
- Resistant to chilling injuries
- Large range of non-injurious atmospheres
- Adaptation to a humid atmosphere
- Climacteric fruit: it can be ripened during or after storage
- No negative residual effect of CA
- CA can reduce the production and effects of ethylene.

Apple is characterized by a climacteric respiration, the production and action of ethylene can be controlled by CA, and it features a long post-harvest life and a great tolerance of oxygen and carbon dioxide concentration levels. Additionally, CA allows using lower storage temperatures in some apple cultivars, some physiological disorders are alleviated by CA, and apple can be harvested and stored in bulk. Therefore, apple is a very compatible fruit to CA [13].

CA involves different storage conditions for apples: cold storage (CS) which is the usual procedure during transport and at the retailer vending, low oxygen (LO), and ultra low oxygen (ULO) which are the techniques applied for long duration fruit storage. Table 5 shows typical oxygen and carbon dioxide concentrations, relative humidity, and temperature for CS, LO, and ULO conditions.

	Oxygen concentration	Carbon dioxide concentration	Humidity	Temperature	Pressure
CS	21%	200ppm	(90%, 96%)	0ºC	1atm
LO	(2%, 3%)	(2%, 5%)	(90%, 96%)	(-1ºC, +1ºC)	1atm
ULO	(1%, 1.5%)	(1%, 1.5%)	(93%, 95%)	(0.3ºC, 0.5ºC)	1atm

Table 5: Environment for different CA storage conditions

ULO storage rooms slow down ethylene synthesis and respiration process extending the storage period of 7 to 9 months [3], and have beneficial effects on fruit firmness, titratable acidity and color [18, 19]. On the other hand, the use of unripe fruit and such storage conditions worsen apple's flavor since the production of volatile compounds responsible for the aroma is reduced [20, 21] and fruit taste is strongly impaired [7].

Besides fruit storing in CA, other techniques are used to delay ripening and senescence of several horticultural crops. Ethylene can be eliminated directly from the atmosphere in different ways such as ventilation, cooling, and the use of scrubbers (usually on the basis of potassium permanganate). Inhibitors of ethylene synthesis are also used such as amino-ethoxy-vinyl-glycine (AVG), which inhibits ACC synthase activity, cobalt ions which inhibit ACC oxidase activity, and silver ions which inhibit ethylene binding to receptors. Additionally, silver thiosulphate (STS) is widely used to counteract the effect of ethylene, especially during the postharvest handling of ornamentals. However, techniques based on inhibitors or ethylene action present some negative effects such as possible lack of ripening uniformity, and reduced flavor quality [13].

Despite of different long-term storing techniques are available nowadays, different techniques are being used to assess the quality of the fruit before and after harvest.

3.3.- Fruit status assessing techniques:

The harvest date and well defined storage conditions are crucial parameters for good organoleptic quality of the final fruit, extend the storage time, and minimize fruit losses.

On one hand, if apples are harvested too early, they will not ripen sufficiently when removal from storage and will have low organoleptic quality and they are prone to physiological disorders such as superficial scald. On the other hand, if the apples are harvested too late, they will soften and become mealy and tasteless before marketing [22]. During storage period, controlled atmosphere conditions are used to minimize respiratory activity and fruit quality losses. However, although optimum storage conditions, they can not compensate losses due to the improper timing of harvest.

Therefore, it is essential to harvest the fruit within the optimal harvest period (while the respiratory activity of the fruit is at its minimal) and maintain the proper storing conditions to ensure long term storage of apples with good organoleptic quality of the final fruit.

Different techniques to assess fruit status are used in today's fruit industry. These techniques are very important to obtain the best fruit quality and enhance fruit availability. Additionally, high value information returns to the grower at post-storage stage related to fruit quality since they provide an estimation of the overall sensory evaluation of the fruit [23]. Traditional techniques are widely used, but novel methods, which are no longer biased by human beings and are non destructive, are becoming more popular.

3.3.1.- Pre-harvest techniques:

Traditionally, the days after full bloom and meteorological experience was used to determine optimum date for harvest. These techniques are generally inexpensive and relatively easy to use, but require a relatively long history of meteorological and physiological observations. Additionally, their precision of prediction is poor, which can be even worse during years with atypical weather conditions [22].

Nowadays, methods based on the temporal changes in biochemical and physiological properties during maturation and ripening processes are widely used to determine the best harvest date for eating and/or storing conditions. Several parameters such as fruit firmness, ethylene production, stage of starch transition, skin color, fruit size, components of taste (e.g. sugar content, titratable acidity) and aroma (e.g. esters and alcohols) are considered [22, 24]. In particular, Streif index, which is a combination of firmness, soluble solids content and starch stage, is widely used in the European apple industry to determine the appropriate time to harvest apples assigned to long-term CA storage.

New methods are still being proposed to determinate the optimal harvest dates of apples such as visible/near infrared spectroscopy [22, 25] and spectral transmittance recordings and elastic behavior [26]. These techniques are objective and non-destructive, but their harvest date prediction is only improved for few days compared to Streif index and is still orchard dependent. Firmness is often measured using objective instruments such as penetrometers, which are relatively cheap and easy to handle for field measurements [27]. New non-invasive methods such as resonance frequency [28] and near infrared spectroscopy [29] have been proposed. Soluble solids content (SSC) is commonly measured using refractrometry techniques, which measure the refraction index of the sample. Currently, wavelength or whole-spectra analytical methods are being developed for the non-destructive determination of SSC, acids, starches and overall maturity [28].

3.3.2.- Post-harvest techniques:

After harvest, apples must be stored until they are needed to satisfy market demand. To enhance fruit availability for some months, different equipment to increase or reduce ethylene concentration can be found in the market and are commonly used in today's store houses.

On one hand, ethylene concentration can be increased directly from the use of the archaic steel cylinders containing pressurized ethylene. However, gas generating apparatus based on a catalytic alcohol-ethylene conversion avoids typical unsafe storage and handling problems related to the heavy steel cylinders of pressurized ethylene gas. Additionally, catalytic generators produce small and controlled amounts of ethylene, which makes them the safest commercial form of ethylene production since they cannot produce explosive amounts of ethylene (ethylene becomes inflammable at 27000ppm). Figure 3 (right) shows a catalytic generator to produce ethylene in fruit store-houses (Sure-Ripe Generator, Catalytic Generators LLC, USA).

On the other hand, ethylene can be removed from the store-house atmosphere by using scrubbers. Scrubbers usually feature a fan to draw cold air from the room. Then the air flows through a catalytic layer which is kept hot by an electrical heating element, where the existing ethylene is burnt. Finally, the air cools down while passing through a ceramic heat exchanger and comes back into the room free of ethylene. Figure 3 (left) shows the typical ethylene scrubber bloc diagram. Several companies such as Absoger S.A. (France) and Catalyx technologies llc (USA) are offering ethylene scrubbers.
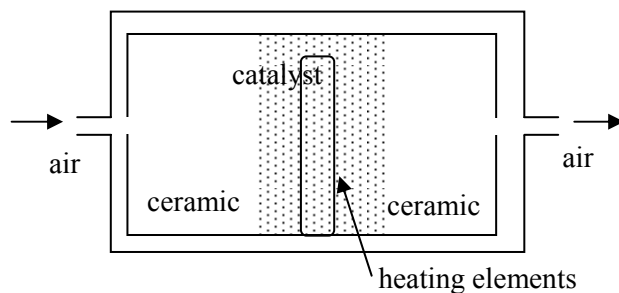

Figure 3: Ethylene concentration can be increased or reduced in today's apple store houses. Right: Catalytic generator to produce ethylene in store-houses (Sure-Ripe Generator, Catalytic Generators LLC, USA). Left: Typical ethylene scrubber bloc diagram. The room air comes in the scrubber, flows through a catalytic layer which is kept hot, cools down while passing through a ceramic heat exchanger, and comes back into the room free of ethylene. (Adapted from Absoger webpage)

Additionally, relatively high ethylene concentration can be reached in storing conditions and threaten fruit conservation process. Apple's ethylene production depends on the harvest date and the storing conditions, but when the ripening process is triggered it can easily reach a

production rate of $150\mu l.kg^{-1}.h^{-1}$ [7]. A 20 foot ISO-Container for fruit transport can be considered to assess the ethylene concentration in transport/storing conditions. A 20 foot ISO-Container is $38m^3$ volume and its maximum allowable payload is 21.5t at $33m^3$. The corresponding free volume when the payload is 80% of the maximum (17.2t) is $11.6m^3$ [30]. Assuming an emission rate of $100\mu l.kg^{-1}.h^{-1}$, the ethylene concentration is increased by 150ppm/h. Figure 3 correlates typical ethylene production with its physiological state and shows that an ethylene concentration above 100ppm will lead to fruit decay into senescence. Fortunately, most of the fresh horticultural crops can tolerate extreme gas concentrations when exposed for very short periods of time.

Despite of ethylene accumulation in conservation or transport chambers threatens the conservation process and different systems which can modify ethylene concentration are present in today's store-houses, none of them is featuring an accurate and specific ethylene measurement to control the ripening process. Most of the today's apple store-houses only continuously monitor oxygen and carbon dioxide concentrations, which do no provide any direct fruit status information. For example, widely used controlled atmosphere systems such as Oxystat 2002 (David Bishop Instruments, England) and GAC 3000 (Fruit Control Equipments, Italy) only provide an infrared sensor to measure carbon dioxide and a thermo paramagnetic or electro chemical sensor for oxygen.

To obtain fruit status information, ethylene is externally measured using portable instruments. GSC560 (Storage Control Systems Inc.) is a hand held sensor based on an electrochemical cell that provides a direct reading of the ethylene concentration in the range of 0-100ppm with a resolution of 0.2ppm (Figure 4, left). However, GSC560 exhibit high cross sensitivities to other gases such as 55% to ethanol. Additionally, a typical disadvantage of electrochemical cells based sensors is their limited lifetime and their gradual decrease of sensitivity that renders calibration obsolete rapidly, making them unpractical for long term fruit monitoring [31].

Ethylene Monitoring and Control System (Geo-centers INC) is a system based on the chemiluminescent reaction of ethylene and is able to detect ethylene in the range of 0-20ppm with an accuracy of 0.5ppm (Figure 4, right). In this technique, a pumping system draws an air sample and injects it into a sample chamber where ozone is used to create chemiluminescent reaction that produces light. Then, a light detector monitors the level produced and measures the ethylene concentration against predetermined light levels associated with certain ethylene concentrations. Ozone is considered a hazardous gas since people can be affected by levels as low as 40 ppb and exposure to ozone and the pollutants that produce it has been linked to premature death, asthma, bronchitis, heart attack, and other cardiovascular problems [32]. Since ozone is used as a reagent, a special care must be considered. Additionally, the whole system is complicated due to the ozone must be generated in situ and the fact that the sample chamber must be held at low pressure (5 - 10 Torr) to enhance the detection limit. These considerations

make chemiluminescent based systems unpractical for an easy, comfortable, and space effective solution and difficult to install in already ongoing store houses.

Figure 4: Commercial systems to measure ethylene. Left: Electrochemical based sensor: GSC560 (Storage Control Systems Inc.). Right: Chemiluminescent based sensor: Ethylene Monitoring and Control System (Geo-centers Inc)

Additionally, portable instruments control ethylene off-line on air samples extracted from the chambers, in a frequency (e.g. weekly) that may be too low to face conservation problems in an efficient way.

Gas chromatograph technique is being used in today's store houses although it is off-line and it is not suitable for a continuous gas monitoring since it requires periodic air samples extracted from the chambers. Important scientific research using gas chromatography techniques to assess apple organoleptic quality after long term storage has been performed by several groups [7] [18] [33] [34]. However, gas chromatography technique is rather used to separate and analyze the components of the fruit aroma than used to monitor ethylene concentration. Nevertheless, more than a measurement technique, gas chromatography itself is considered a technique for separating the different species present in a mixture. This separation comes from the different and characteristic times taken for different species to pass through a chromatographic column. Usually, commercial gas chromatographs are combined with a detector such as flame ionisation, thermal conductivity, electron capture, or mass spectrometry to provide a selective and sensitive instrument for identifying multiple components of a complex mixture [31]. Figure 5 shows the typical block diagram of a gas chromatograph together with mass spectrometer.
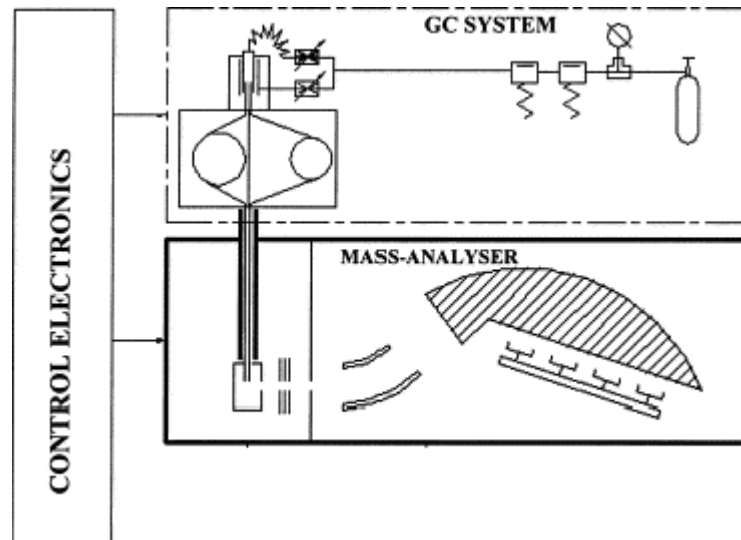
Figure 5: Typical block diagram of a gas chromatograph together with mass spectrometer. Adapted from [35].

Semiconductor sensors have been proposed for continuous monitoring of food quality and safety both along the logistics chain and in the fruit store-houses [36] [37] [38]. The sensor sensitivity can be affected by variations in the oxygen concentration, humidity, and temperature. Nevertheless, algorithms for humidity compensation of the sensor's response have been presented [39]. However, semiconductor sensors still feature problems that make them unsuitable for long term gas measurements such as irreversible changes to its zero gas reading and sensitivity and long recovery time after exposure to high gas concentrations. Therefore, its lifetime is strongly impaired if it is exposed to high gas concentrations or poisoning agents.

To overcome the inconveniences found in current methods to continuously monitor ethylene on today's store houses, and to take advantage of the IR detectors for long term measurements, a multi-channel NDIR spectrometer has been developed along this Thesis.

3.4.- Summary:

The benefits of eating fruit and the position of the apple industry in the market are presented in this chapter. In order to hold apple consumption during all the year, it is important to store the fruit in such a way that the final fruit is in good organoleptic quality and it meets consumer expectations. Therefore, different parameters such as the harvest date and well defined storage conditions are crucial for good quality of the final fruit, extend the storage time, and minimize fruit losses.

The important role of ethylene in apple growth and different fruit storing techniques are presented. On one hand, ethylene is externally added when ripeness or degreening of the product must be promoted; but on the other hand, it can be thought as an indicator that fruit is ripening. Therefore, to enhance fruit availability for some months assuring good quality of the fruit after storage, ethylene control and monitoring is desirable.

Among the techniques proposed for ethylene measurement in today's store houses, IR spectrometer is the desirable since they exhibit extended lifetime, stabilized sensitivity, and better performance for long term measurements.

3.5.- References:

[1]   W.C. Willett, F. Sacks, A. Trichopoulou, G. Drescher, A. Ferroluzzi, E. Helsing, and D. Trichopoulos, "Mediterranean diet pyramid - A cultural model for healthy eating," *American Journal of Clinical Nutrition*, vol. 61, (no. 6), pp. S1402-S1406, 1995.

[2]   S. Natoli, "Balancing your diet," *ABC Health & Wellbeing*, 2007.

[3]   M.H. Jijakli and P. Lepoivre, "State of the art and challenges of post-harvest disease management in apples," *Fruit and Vegetable Diseases*, vol. 1, pp. 59-94, 2004.

[4]   Isafruit. Healty fruit for a healty Europe "http://www.isafruit.org/Portal/objectives.php"

[5]   Ministerio de Medio Ambiente y Medio Rural y Marino, "http://www.mapa.es/es/alimentacion/pags/consumo/ultimdatos.htm#art7,"

[6]   A.A. Kader, "Ethylene-induced senescence and physiological disorders in harvested horticultural crops," *Hortscience*, vol. 20, (no. 1), pp. 54-57, 1985.

[7]   J. Song and F. Bangerth, "The effect of harvest date on aroma compound production from 'Golden Delicious' apple fruit and relationship to respiration and ethylene production," *Postharvest Biology and Technology*, vol. 8, (no. 4), pp. 259-269, Sep 1996.

[8]   G.Y. Din, Z. Zugman, Y. Saks, and M. Kim, "Avoiding economic losses by proper segregation of apples based on maturity indicators prior to storage," *Computers and Electronics in Agriculture*, vol. 39, (no. 3), pp. 193-208, 2003.

[9]   J. Giovannoni, "Molecular biology of fruit maturation and ripening," *Annual Review of Plant Physiology and Plant Molecular Biology*, vol. 52, pp. 725-749, 2001.

[10]   A.L.S. Chaves and P.C. de Mello-Farias, "Ethylene and fruit ripening: From illumination gas to the control of gene expression, more than a century of discoveries," *Genetics and Molecular Biology*, vol. 29, (no. 3), pp. 508-515, 2006.

[11]   E. Kupferman, "The Role of Ethylene in Determining Apple Harvest and Storage Life," *Post Harvest Pomology Newsletter*, vol. 4, (no. 1), 1986.

[12]   J. Dixon and E.W. Hewett, "Factors affecting apple aroma/flavour volatile concentration: a review," *New Zealand Journal of Crop and Horticultural Science*, vol. 28, (no. 3), pp. 155-173, Sep 2000.

[13]   E.M. Yahia, C. Barry-Ryan, and R. Dris, "Treatments and techniques to minimise the postharvest losses of perishable food crops," *Production Practices and Quality Assessment of Food Crops, Vol 4*, vol. 4, pp. 95-133, 2004.

[14]   J.H. Oetiker and S.F. Yang, "The role of ethylene in fruit ripening," in Postharvest Physiology of Fruits, *Acta Horticulturae*, H. Hyodo and A. E. Watada eds., 1995, pp. 167-178.

[15]   M.J.C. Rhodes, "The climacteric and ripening of fruits," *Hulme, a. C. (Edited by). Food Science and Technology, a Series of Monographs. the Biochemistry of Fruits and Their*

Products, Vol. 1. Xviii + 620p. Illus. Academic Press Inc. (Ltd.): London, England; New York, N.Y., U.S.A, pp. 521-533, 1970.

[16] E.M. Yahia, "Modified and controlled atmospheres for tropical fruits," *Stewart Postharvest Review*, vol. 2, (no. 5(Suppl.3)), pp. article 6, 2006.

[17] C. M. and B.-G. R., *Food preservation by modified atmospheres*, 1990.

[18] M.L. Lopez, M.T. Lavilla, I. Recasens, J. Graell, and M. Vendrell, "Changes in aroma quality of 'Golden Delicious' apples after storage at different oxygen and carbon dioxide concentrations," *Journal of the Science of Food and Agriculture*, vol. 80, (no. 3), pp. 311-324, 2000.

[19] A. Brackmann, J. Streif, and F. Bangerth, "Relationship between a reduced aroma production and lipid-metabolism of apples after long-term controlled-atmosphere storage," *Journal of the American Society for Horticultural Science*, vol. 118, (no. 2), pp. 243-247, Mar 1993.

[20] A. Brackmann, J. Streif, and F. Bangerth, "Influence of CA and ULO storage-conditions on quality parameters and ripening of preclimacteric and climacteric harvested apple fruits .2. Effect on ethylene, CO2, aroma, and fatty-acid production," *Gartenbauwissenschaft*, vol. 60, (no. 1), pp. 1-6, 1995.

[21] G.A. Willaert, P.J. Dirinck, H.L. Depooter, and N.N. Schamp, "Objective measurement of aroma quality of golden delicious apples as a function of controlled-atmosphere storage time," *Journal of Agricultural and Food Chemistry*, vol. 31, (no. 4), pp. 809-813, 1983.

[22] A. Peirs, J. Lammertyn, K. Ooms, and B.M. Nicolai, "Prediction of the optimal picking date of different apple cultivars by means of VIS/NIR-spectroscopy," *Postharvest Biology and Technology*, vol. 21, (no. 2), pp. 189-199, 2001.

[23] J.M. DeLong, R.K. Prange, P.A. Harrison, and K.B. McRae, "Comparison of a new apple firmness penetrometer with three standard instruments," *Postharvest Biology and Technology*, vol. 19, (no. 3), pp. 201-209, 2000.

[24] G. Echeverria, M.T. Fuentes, J. Graell, and M.L. Lopez, "Relationships between volatile production, fruit quality and sensory evaluation of Fuji apples stored in different atmospheres by means of multivariate analysis," *Journal of the Science of Food and Agriculture*, vol. 84, (no. 1), pp. 5-20, 2004.

[25] A. Peirs, K. Touchant, A. Schenk, and B. Nicolai, "FT-NIR spectroscopy to evaluate picking date of apples," *Proceedings of the 4th International Conference on Postharvest Science, Vols 1 and 2*, (no. 553), pp. 477-480, 2001.

[26] M. Zude-Sasse, B. Herold, M. Geyer, and S. Huyskens-Keil, "Influence of maturity stage on physical properties in apple," *Proceedings of the 4th International Conference on Postharvest Science, Vols 1 and 2*, (no. 553), pp. 109-110, 2001.

[27] B. Mitcham, M. Cantwell, and A. Kader, "Methods for Determining Quality of Fresh Commodities," in Book Methods for Determining Quality of Fresh Commodities, *Series Methods for Determining Quality of Fresh Commodities*, City, 2003.

[28] M. Zude, B. Herold, J.M. Roger, V. Bellon-Maurel, and S. Landahl, "Non-destructive tests on the prediction of apple fruit flesh firmness and soluble solids content on tree and in shelf life," *Journal of Food Engineering*, vol. 77, (no. 2), pp. 254-260, 2006.

[29] J. Lammertyn, B. Nicolai, K. Ooms, V. De Smedt, and J. De Baerdemaeker, "Non-destructive measurement of acidity, soluble solids, and firmness of Jonagold apples using NIR-spectroscopy," *Transactions of the Asae*, vol. 41, (no. 4), pp. 1089-1094, 1998.

[30] R. Jedermann, R. Schouten, A. Sklorz, W. Lang, and O. Kooten, "Linking keeping quality models and sensor systems to an autonomous," in Book Linking keeping quality models and sensor systems to an autonomous, *Series Linking keeping quality models and sensor systems to an autonomous*, 2006, pp. 3-18.

[31] SiraTechnology, *Gas Detector Selection and Calibration Guide*: Withrebys publishing, 2005.

[32] B. Weinhold, "Ozone nation - EPA standard panned by the people," *Environmental Health Perspectives*, vol. 116, (no. 7), pp. A302-A305, 2008.

[33] A. Plotto, M.R. McDaniel, and J.P. Mattheis, "Characterization of changes in 'Gala' apple aroma during storage using osme analysis, a gas chromatography-olfactometry technique," *Journal of the American Society for Horticultural Science*, vol. 125, (no. 6), pp. 714-722, Nov 2000.

[34] N.A. Mir, R. Perez, P. Schwallier, and R. Beaudry, "Relationship between ethylene response manipulation and volatile production in Jonagold variety apples," *Journal of Agricultural and Food Chemistry*, vol. 47, (no. 7), pp. 2653-2659, Jul 1999.

[35] A.L. Makas and M.L. Troshkov, "Field gas chromatography-mass spectrometry for fast analysis," *Journal of Chromatography B 3rd International Symposium on Separations in the BioSciences: 100 Years of Chromatography*, vol. 800, (no. 1-2), pp. 55-61, 2004.

[36] A. Vergara, E. Llobet, J.L. Ramirez, P. Ivanov, L. Fonseca, S. Zampolli, A. Scorzoni, T. Becker, S. Marco, and J. Woellenstein, "An RFID reader with onboard sensing capability for monitoring fruit quality," *Sensors and Actuators B-Chemical*, vol. 127, pp. 143-149, 2007.

[37] P. Ivanov, E. Llobet, A. Vergara, M. Stankova, X. Vilanova, J. Hubalek, I. Gracia, C. Cane, and X. Correig, "Towards a micro-system for monitoring ethylene in warehouses," *Sensors and Actuators B-Chemical*, vol. 111, pp. 63-70, 2005.

[38] M.D. Balachandran, S. Shrestha, M. Agarwal, Y. Lvov, and K. Varahramyan, "SnO2 capacitive sensor integrated with microstrip patch antenna for passive wireless detection of ethylene gas," *Electronics Letters*, vol. 44, (no. 7), pp. 464-465, 2008.

[39] A. Giberti, M.C. Carotta, V. Guidi, C. Malagù, G. Martinelli, M. Piga, and B. Vendemiati, "Monitoring of ethylene for agro-alimentary applications and compensation of humidity effects," *Sensors and Actuators B: Chemical* vol. 103, (no. 1-2), pp. 272-276, 2004.

4.- THESIS OBJECTIVES

The GoodFood Integrated Project (508774-IP) aims at developing an innovative tool based on micro/nano subsystems for the full safety and quality assurance along the complete food chain in the agrofood industry. The present Thesis has been in the framework of the Workpackage 6 of this Project, the main goal of which is the development of two different approaches for ethylene monitoring at different points of the fruit distribution chain. An infrared spectroscopy based system is targeting the storage application, where the power supply is not considered a problem, and metal oxide gas sensors are more dedicated to monitor the items along transport and vending.

Nowadays, the ripening of fruit is controlled by managing the ethylene concentration in the ambient atmosphere of the apple store-houses. However, ethylene concentration is only measured off-line in a frequency that may be too low to face conservation problems in an efficient way. The task force of this Thesis is the development of a miniaturized optical spectrometer for precise and continuous ethylene detection, which would be very advantageous in this scenario.

Optical components and signal processing electronics must be developed, tested and integrated in a compact NDIR system. The instrument must detect the ethylene burst before the fruit decays into senescence. Cross-sensitivities to other gases which can be present in the ambient such as ammonia, ethanol and acetaldehyde must be considered. With the aim to correct potential cross-sensitivities and to improve the long-term stability, other channels must be included. Additionally, these channels can be used to prevent a possible fouling of the fruit as well. Therefore, the main objective of this Thesis is the development of a stable instrument, and the corresponding components, to continuously assess fruit status in today's store houses.

The development of a novel IR detector module is an important objective of the Thesis. Relatively compact IR detectors can be found in the market nowadays. They can feature optical filters to select the gas absorption bands for NDIR based spectrometers, or focusing elements to improve the global efficiency of the detector.

In the trend towards miniaturization and integration, a novel architecture for a detector oriented to NDIR systems is to develop. The result must be a compact detector comprising a multichannel IR detector array, with the proper optical filters for NDIR gas detection and specific focusing elements. To design the focusing elements, it is important to consider the silicon technology and the related advantages such as batch fabrication processes, reliability, equipment availability, and high levels of functionality. It is important to fabricate the specifically designed for each channel focusing elements in the same batch process.

Once the focusing elements are fabricated, they must be optically tested in order to validate the proposed alternative for the IR detector. Additionally, antireflection coating must be processed in order to increase the system efficiency.

The size of the spectrometer must be reduced as much as possible. Therefore, miniaturization is a constant challenge in the development of the instrument. The gas cell must be relatively small, but without threatening the system sensitivity.

The ethylene concentration level that must be detected by the developed NDIR spectrometer to prevent the fruit to decay into senescence is set to 100ppm. Since a low signal is expected from the IR detector a special effort on the amplification electronics is required. A challenge of this Thesis is to amplify the signal and reduce the noise considering analog and digital techniques. Digital lock-in must be considered as a signal recovery system in order to shift the signal to a low-noise region. Different simulations to determine the lock-in architecture and parameters such as reference frequency, order of the filter and sample and cutoff frequencies must be performed.

After the complete instrument assembly, a system calibration is required to test the detection limit and the possible cross-sensitivities. Different data analysis alternatives can provide different results. Therefore, it is necessary to explore the obtained data to build the optimum calibration model.

5.- INFRARED SPECTROMETER:

To ensure a good organoleptic quality of the final fruit, the quality and safety of the fruit should be continuously monitored and controlled during storage. This will enable producers, logistics groups and customers to trace their goods at any time and consumers will be protected against frauds as well as from the consummation of unsafe food.

Therefore, precise and continuous ethylene detection would be very advantageous to assess fruit ripening and prevent the fruit to decline into senescence. An enhanced storage period can be assessed by a good fruit quality control. Better fruit quality and wider range availability will lead to higher fruit consumption and to increased health and wellbeing.

Infrared (IR) spectrometers are widely used to measure continuous emissions and ambient air quality monitoring, process control and personal and plant safety. They are highly selective instruments, and they are stable and rather immune to false alarms and poisoning since the detectors are not in direct contact with the gas [1]. Therefore, IR spectrometers are suitable for long term monitoring species with absorption in the IR range.

The aim of this Thesis is to present an IR spectrometer that is able to monitor apple's quality while it is being stored in the controlled atmosphere chambers and assures a good quality for the final fruit. This chapter introduces the developed spectrometer, detailing its components such as the novel detector architecture and the system electronics, the spectrometer calibration, and the performed measurements. Nevertheless, for more technical details the reader is referred to the enclosed Journal papers by means of the following nomenclature:

P#1: *Exploration of the metrological performance of a gas detector based on an array of unspecific infrared filters*. Page 64

P#2: *Design and fabrication of silicon-based mid infrared multi-lenses for gas sensing applications*. Page 73

P#3: *Limits to the integration of filters and lenses on thermoelectric IR detectors by flip-chip techniques*. Page 83

P#4: *A compact optical multichannel system for ethylene monitoring*. Page 92

P#5: *Ethylene optical spectrometer for apple ripening monitoring in controlled atmosphere store-houses*. Page 100

5.1.- Complete System description:

Infrared optical gas analyzers are selective and stable instruments based on the attenuation of the incident radiation at specific absorption bands (Lambert-Beer equation). The amount of light absorbed by the gas determines the gas concentration. The maximum sensor sensitivity corresponds to the maximum absorbance. Therefore, to optimize ethylene detection, filter window selection was made considering the most prominent absorption band for ethylene. The selected optical filter is a 10.6μm central wavelength (CWL) with a bandwidth (BW) of 4% of the CWL. The complete ethylene spectrum and the corresponding selected window are shown in Figure 1.
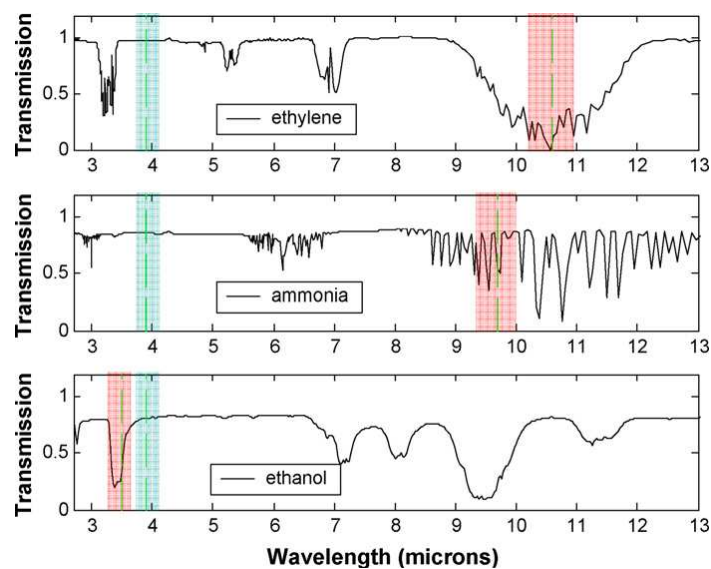
Figure 1 Ethylene (above), ammonia (middle) and ethanol (lower) transmission spectrums, with the corresponding selected windows, and the reference window. Adapted from [2].

Over 300 volatile compounds have been identified in the aroma profile of apples [3] and typical flavor compounds of apples are produced when ripening is initiated, but they are of a very low concentration and it can be assumed that they do not interfere to ethylene measurement. However, other gases such as ethanol, acetaldehyde and ammonia can also be present in the store house and exhibit significant absorption in the 10.6μm region. Therefore, they must be considered for possible cross sensitivities of the IR optical measurement of ethylene and a multichannel spectrometer is then a must.

On one hand, gases produced by the fruit itself can be present in a high concentration in the storage rooms. For example, exposing apples to low oxygen conditions consistently enhances acetaldehyde and ethanol concentrations, which can greatly exceed concentrations of several hundred of ppm. However, when the atmosphere is set to air conditions, ethanol and acetaldehyde concentrations decrease to initial values [3, 4].

On the other hand, external gases can also affect ethylene measurement. Ammonia is increasingly the coolant of choice for food cooling systems instead of substances with high ozone layer endangering potential [5] and it can interfere in the ethylene measurement if a leakage occurs. Besides the importance of the ammonia channel to reject potential interferences on the ethylene measurement, this channel acquires importance since ammonia can poison and damage apples and produce necrotic lesions [6]. Additionally, due to the environmental relevance and toxic potential of ammonia, this channel is also useful to fulfill the claimed instructions by the legislators in order to minimize the potential hazard of ammonia for humans and the environment. Different regulations apply on the safety requirements of cooling devices that use ammonia on the setting of safe concentration limits and on the equipment to monitor ammonia. If the concentration level exceeds 200ppm, the ventilation system must be switched on and a pre-alarm must be signaled. If the leakage persists and a concentration of 1000ppm is reached, the main alarm must be set and the cooling system must be stopped [5].

A four-channel NDIR spectrometer has been developed to measure ethylene, considering ammonia and ethanol cross sensitivities and featuring a reference channel to improve the long term stability of the system.

Ethanol absorption region is selected considering the most prominent absorption band (3.4μm CWL and 4% BW). Since the most important absorption band for ammonia overlaps the region chosen for ethylene absorption, ammonia channel is set on another absorption band (9.7μm CWL and 4% BW) which is far from the ethylene channel. The reference channel is set in a region were no absorptions are expected (3.9μm CWL and 2% BW). Figure 1 shows ethylene, ammonia, and ethanol IR spectrums with the corresponding windows and the reference window.

As fruit ripening begins, the production of ethylene increases dramatically and ethylene concentration rises to values higher than 100ppm. The ethylene burst that comes together with the climacteric transition can be used to determine the fruit status. Therefore, the ethylene detection limit of the developed spectrometer must be below 100ppm. On the other hand, spectrometer must detect ammonia concentration levels which are set by the legislators when it is used in the cooling system. Table 1 show gas detection limits respectively. The environment details for different CA storage conditions are shown in Table 5 (chapter 3). Additionally, spectrometer must be insensitive to potential cross-sensitivities from other gases such as ethanol.

Gas	Required detection limit
Ethylene	100ppm
Ammonia	200ppm

Table 1: Required detection limits for ethylene and ammonia. A concentration of 100ppm of ethylene occurs when fruit ripening begins. At a concentration level of 200ppm of ammonia the ventilation system must be switched on.

The developed spectrometer is composed of an IR emitter, a multi-path gas cell (White cell), an IR detector module, a low noise analogue amplification stage, and a digital lock-in.

Since the IR detector signal is expected to be low and noisy, it is convenient to use lock-in techniques to recover the system signal [7]. In that scenario, signal must be modulated. The emitter can be directly electrically modulated. However, due to the observed large thermal capacity, it is convenient to use an external mechanical chopper. Therefore, a microcontroller based lock-in amplifier is used as a signal recovery system and a mechanical chopper to modulate the IR radiation. Figure 1 (P#5) shows a block diagram of the developed multichannel IR spectrometer, and a picture of the system detailing its optical setup is shown in Figure 2.
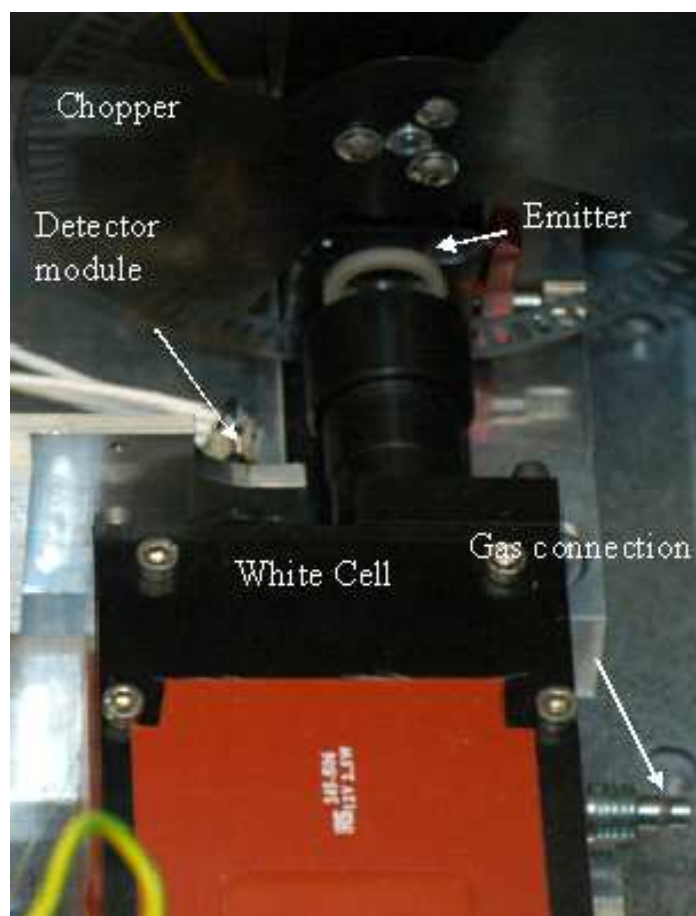
Figure 2: Optical system, with miniaturized White Cell, IR emitter, IR detector module, and optical chopper

5.2.- Spectrometer components:

a) Infrared emitter and coupling optics:

Several companies such as Ion Optics Inc. (USA), Laser Components GmbH (Germany), and Scitec Instruments Ltd (England) provide IR emitters. However, these emitters exhibit moderate emission compared to an ideal black-body radiator, especially at longer wavelengths, which are particularly critical in the application since they correspond to ethylene and ammonia absorption regions. A novel type of micromachined thermal IR emitter has been developed in Fraunhofer Institute for Physical Measurement Techniques (Freiburg, Germany) with increased IR emission efficiency [8] [9].

The use of 3D structured macroporous silicon gives a higher black-body-like emission compared to the commercially available emitters at longer mid infrared wavelengths. Figure 3 (left) (P#4) shows a SEM-picture of the IR emitter structure based on regular ordered macropore array. The device is heated using a thin film Pt-heater structured onto the backside of the substrate. It features an advantageous emission in the interesting 10μm band. Figure 3 (right) (P#4) shows the emission spectrum of the developed IR emitter compared to a black-body radiator and two commercial devices.

The IR emitter was housed in a TO8 package, featuring special longer pins (3mm) to achieve better thermal decoupling from the round baseplate of socket. Figure 3 shows an image of the developed IR emitter in its TO8 package (left) and when it is placed in the corresponding support for the optical system assembly (right). More technical details about the IR emitter can be found in the enclosed paper P#4 and in the related works [8] [9].
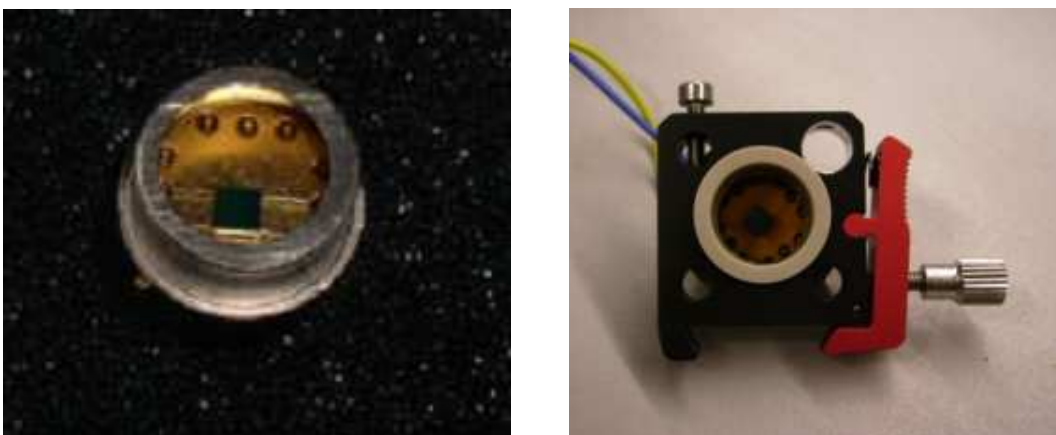
Figure 3: Developed IR emitter. In its TO8 package (left) and on the support for the optical system assembly (right)

The IR emitter was developed with a close collaboration concerning the geometrical issues for the further optical assembly. With that aim, coupling optic elements have been designed, considering several aspects:

- Collection of the source radiation within an angle as wide as possible
- The output aperture of the coupling optics has to meet the one of the White cell
- Sufficient quality of imaging (small spot size) at the input focus of the White cell
- Compact set-up of the optics, suitable for the dimensions of the 1.6m-White cell

An antireflection coated ZnSe lens was designed and added between the emitter and the optical input of the gas cell to increase the radiation captured by the White cell and increase the system sensitivity. The captured half angle of the emitter radiation increases from 7º to 18.4º when the lens is added. The complete optical assembly including the IR emitter and the ZnSe lens, the White cell, and the IR detector is shown in Figure 4.
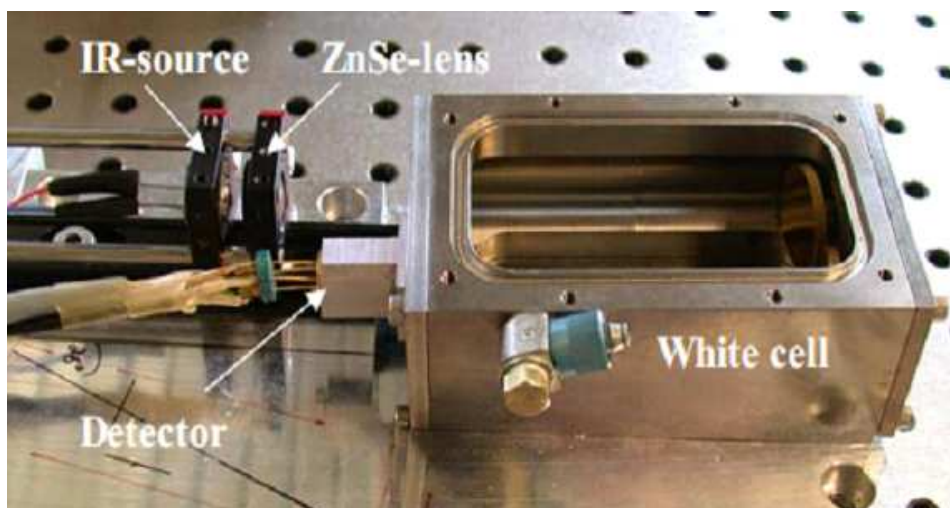
Figure 4: Complete optical setup showing the IR emitter, the ZnSe lens, the White cell, and the IR detector.

Since the designed signal recovery system is a lock-in amplifier, the input signal must be modulated. In some cases, the IR radiation is directly modulated by switching the IR emitter. However, a large time constant of the IR emitter was empirically observed, which limit the modulation frequency. For this reason the IR emitter operates in continuous mode, and an optical chopper modulates the emitted radiation at 1Hz, which is the optimum frequency compatible with the time response of the detector.

A two slot chopper blade (MC1F2, Thorlabs Ltd, UK) featuring additional speed control was used for modulating the IR beam (Figure 5). The microcontroller synchronizes the speed of the chopper with the reference for the signal recovery.

Figure 5: Slot blade for modulating the IR beam. 10.5cm diameter.

b) Gas cell:

In order to increase the optical path length yet maintaining the small physical dimensions of the gas sample chamber, a multiple reflections White cell was developed in Fraunhofer Institute for Physical Measurement Techniques (Freiburg, Germany). Nevertheless, the White cell output was designed in close collaboration since its geometry and optical parameters directly affect the global optical assembly and the lens focal length design.

The body of the cell is machined in aluminum and employs three concave mirrors achieving an optical path length of 1.6m after 19 reflections within a volume of 11x5x6cm^3. The mirrors are suitable gold-coated plane-concave glass lenses. An exploded view of the schematic setup of the White cell is shown in Figure 6. More technical details and a picture showing the internal part (Figure 2 P#4) of the gas cell can be found in P#4.
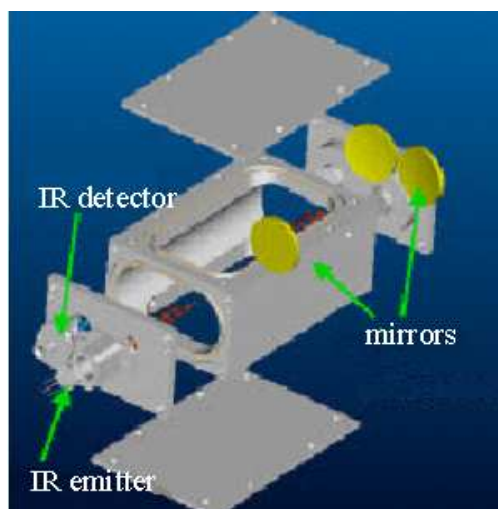
Figure 6: Exploded view of the schematic setup of the White

c) Detector module:

A novel highly-integrated compact detection module comprising thermopiles, optical filters, and focusing elements is proposed to measure the remaining radiation after gas absorption. Unlike commercial IR detectors, the developed multi-channel detector features both optical filters and focusing elements. More details of the design and fabrication of the detector can be found in P#2, P#3, P#4, and P#5. The general block diagram of the detector module and the final device are presented in Figure 4 (P#4) and Figure 12 (P#2) respectively.

Micromachined thermopiles based on CMOS processing and bulk micromachining are chosen as infrared detectors since they exhibit good performance in terms of reproducibility, accuracy, low cost, sensitivity and rapid response [10]. Additionally, thermopiles do not need power to be operated, offer a wide spectral response, can be fabricated in silicon technology, and an array of them can be easily integrated with a low foot-print in a single chip.

The fabricated thermopiles consist of a series of thermocouples made of n-doped polysilicon and aluminum that are placed in a thin and free-standing silicon nitride membrane. The silicon rim of the structure acts as a heat sink. A doped silicon slab added under the nitride membrane converts the IR radiation into thermal energy, thus acting as an absorber and heat spreader. The thermal resistance membrane isolates thermally hot and cold junctions and allows developing temperature difference when IR radiation reaches the absorber [11]. Figure 2 (P#3) shows the schematic of the micromachined thermopile.

Substrate chips ($6.1x6.1mm^2$ size) with four micromachined thermopiles in a 2x2 arrays, featuring a size compatible with a TO8 package, have been fabricated. Each thermopile features 32 thermocouples and absorber and membrane sizes are $350x350\mu m^2$ and $1300x1300\mu m^2$ respectively. Thermopile array was fabricated at Centre Nacional de Microelectrònica (IMB-CNM-CSIC, Barcelona, Spain).

The optical filters were assembled by flip-chip technique on top of the thermopiles at Centre Nacional de Microelectrònica (IMB-CNM-CSIC, Barcelona, Spain). Flip-chip is based on a solder paste, which needs bump pads in bottom and top devices (the thermopile array and filters). The bump pads are made of three stack metal layer (Ti/Ni/Au), which are sputtered sequentially onto the wafers and patterned after standard photolithographic steps. Ni assures the bond with the solder paste, Ti acts as an adhesion promoter, and Au provides oxidation protection. The fabricated chip with the thermopile array and the bump pads for the flip-chip is shown in Figure 3 (P#3).

The design and fabrication of a multi-lens array as a focusing unit to be integrated in the IR detector is an important task developed along this Thesis. The purpose of the lens array is to collect as much radiation as possible from the absorption cell and divide the total transmitted IR radiation into four parts and focus each one of them into the corresponding absorber element of

the four thermopile array. Diffractive lenses are compatible with the planar nature of silicon microtechnology. Additionally, silicon is transparent in the IR range of interest. Therefore, silicon is a suitable material as lens substrate and typical advantages of silicon technologies such as reliability, mass production, and equipment availability can be made with diffractive lenses. Due to technological constraints of silicon planar microtechnology, it is necessary to reproduce the theoretical ring profile as a discrete number of flat steps. The design and fabrication of the lens array is deeply detailed in P#2.

Some single lenses were fabricated for several focal lengths and wavelengths using two different designs: binary lenses, which only need one photolithographic mask, and eight levels lenses, which can be fabricated using three photolithographic masks. The first option is cost-effective, but the second one provides more efficient lenses. The profile of a binary and an eight levels lenses are shown in Figure 4 and Figure 5 (P#2) respectively.

The lens efficiency as a function of the minimum feature size, the number of levels, and the wavelength is presented in Figure 3 (P#2). Lens measurements such as focal length, spot size, and radiation pattern are shown in Figure 6, 7, 8 and Table 1 (P#2). They show promising results and validate the eight levels lens design.

For the final detector, four lenses working at different wavelengths are required. The proposed device consist of a lens array composed of four sectors, each of them featuring a portion of a Fresnel Lens optimized for the wavelength matching the corresponding filter.

12 different photolithographic masks would be needed to reproduce a 4 Fresnel Lenses array, with a binary combination of 3 masks for each sublens. However, a new approach to design the four lenses array in a single chip based on the shared use of four photolithographic masks is proposed. Lens efficiency calculations (Table 2 P#2) show that the proposed approach is a cost effective alternative and assures optical transmission efficiencies over 85% in the worst case.

Lens parameters such as diameter, focal length, and center position must be designed after geometrical considerations and assuming that the IR beam comes out of the White cell forming a cone of 8º half angle. Figure 7 shows the White cell output and the relative position to the detector unit, and the geometrical parameters used to design the lens array with the best optical performance.

The diameter of the fabricated FL array is D=10mm, and the half angle of the IR beam is α=8º. The distance from the White Cell output focus to the FL placement, A, is designed to collect as much radiation as possible. Equation 1 determines A with that purpose:

$$A = \frac{D}{2\tan(\alpha)} = 35.6mm \qquad\qquad (1)$$

The distance from the thermopiles to the lens array is 8.7mm in the case of the developed detector module. Additionally, the obliqueness of the incoming light and the thickness of the optical filters also affect the design of the distance from the focus point to the image plane. With a non infinite A, B no longer equals the focal length. The added through-the-filters optical path also changes B in a factor that will depend on the thickness of the filters and their effective refraction index at the operating wavelengths. The filter thickness is d=0.55mm, and its effective refraction index n=3.3.

Another parameter which must be considered for the FL design is the position of the thermopiles absorbers (Figure 8). Since they are not in the center of the chip, the center of each FL must be calculated as well. The equation system presented is coupled, but it can be solved numerically, resulting a focal length of f=6.7mm for all the sublenses.
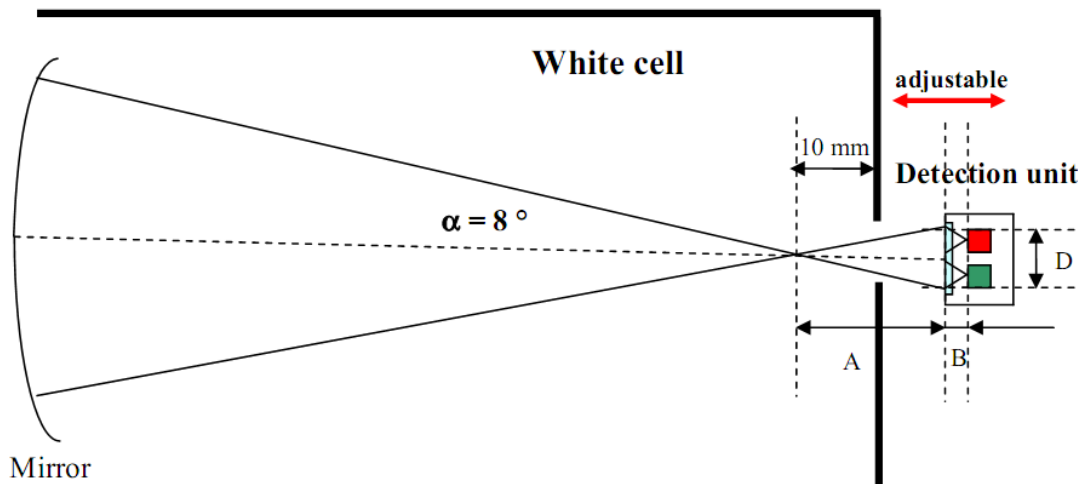
Figure 7: White cell output and relative position to the detector unit.
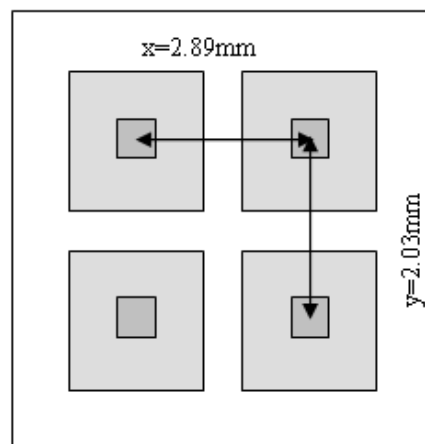
Figure 8: Thermopiles geometry, showing the placement of the absorbers.

A specific four 6.7mm focal length lens array for the required system application was fabricated. Figure 10 (P#2) shows the central region of each single lens of the four FL array.

To attach the lens array easily to the TO8 lid package it is convenient to design a round shaped chip. In order to do so, a 'through the wafer' deep silicon etch mask has been processed. After the etching, only three small silicon arms connect the bulk of the wafer to the lens array, which can be easily detached by applying a gentle pressure. Figure 9 shows the details of the supporting arms and Figure 9 (P#2) shows the fabricated Fresnel lens array using four photolithographic masks.
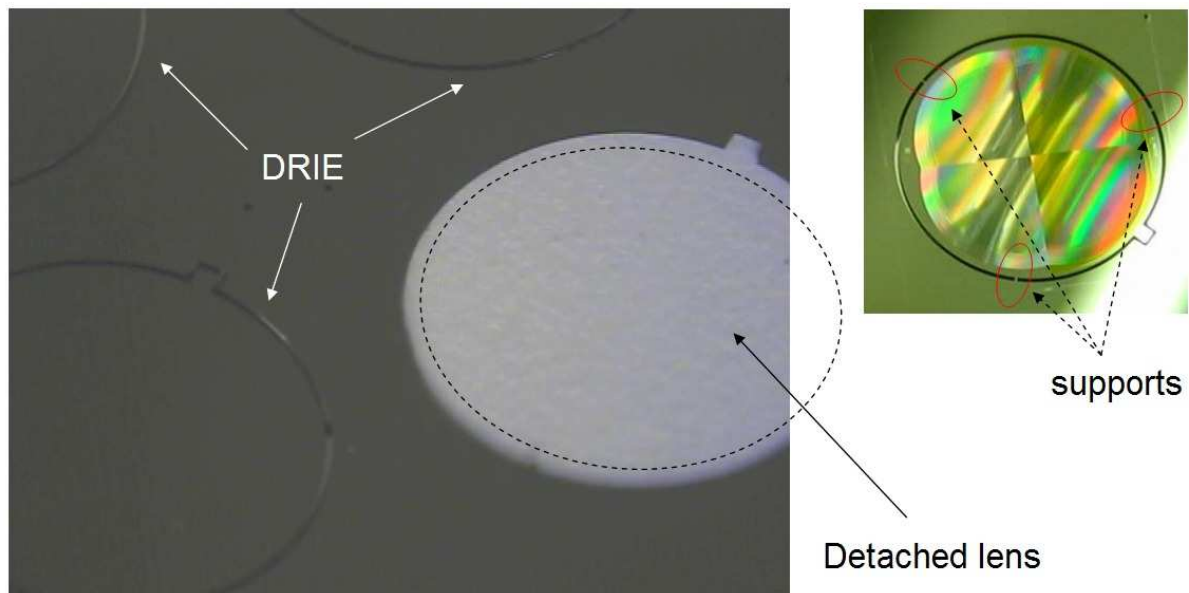
Figure 9: Details of the supporting arms of the detachable 10mm diameter four-lens array after the Deep RIE.

To prevent reflection losses at the lens surfaces, zinc sulphide 1193nm thickness antireflection λ/4 layers were been post-processed on both sides of some multi-lens arrays. The coated FL has been optically tested and exhibit better efficiency compared to uncoated lenses and only small shifts in the focal length have been observed (Table 4 P#2). More technical details of the antireflection coating can be found in P#2.

However, the thickness of the AR coating is very critical for the shorter wavelengths since a small variation of the layer thickness may shift the curve (presented in Figure 11 P#2) and decrease the effect of the ZnS layer for those wavelengths. Additionally, the ZnS layer exhibits adherence problems on the non-structured side of the FL chip and it starts peeling off after some time.

Two different methods have been proposed to overcome the adherence problems. On one hand, patterning a periodic subwavelength structure acting as AR layer on the non-structured side of the FL will avoid depositing a ZnS layer on that side, but will require the use

of a technological technique able to define submicron features. On the other hand, structuring the rear side of the FL chip with some stripes (much larger than the interesting wavelengths to avoid diffraction effects which may interfere with the FL operation) is considered as well in order to solve the adherence problems.

The focal length measurement of the fabricated device has an error smaller than 5% (see Table 3 P#2), the measured spot diameter at the focal plane (Figure 8 P#2) is smaller than the thermopile absorber size ($350x350\mu m^2$), the antireflection coating increases the transmitted radiation (Table 4 P#2) and improves the lens efficiency, and the method to assemble the lens array with the detector lid secures the proper alignment lens-detector. These results validate the new approach based on sharing the photolithographic levels among the different sublenses and confirm that the fabricated devices are suitable for the detection module.

However, it has been found that integration of filters too close to the IR detector lead to degraded performance due to thermal coupling, caused by radiation absorption in the filter and a later heat transfer to the thermopile. To avoid such detrimental effects, which dramatically worsen the required selectivity of a NDIR system and increase considerably the time response of the IR detector; two different alternatives have been proposed: set the device in vacuum conditions or increase the solder joint height. More details of the thermal coupling are given in P#3. In the meanwhile, a four-channel commercial thermopile (HTS-Q21, Heimann Sensor GmbH, Germany) with similar optical filters on the package lid, but with no optical module, has been used to overcome the problem and for gas measurements.

d) Analog pre-amplification:

The output thermopile voltage is in the range of tens of microvolt. The aim of the pre-amplification stage is to expand the low thermopile voltage range to the analog-digital converter input range of the microcontroller (0-0.6V). Since the detector unit is a four-channel device, the pre-amplification stage is four fold.

Due to a high analog gain is desired for all the channels, amplification architecture choice is crucial. With the purpose to choose an analog amplifier featuring excellent noise performance, a comparison between several amplifiers (those commonly readily available) is done in terms of the total amplifier noise, which is assumed to be flicker noise at low frequencies (from 0.1Hz to 10Hz) superposed to white noise (considering a bandwidth of 10Hz).The noise analysis comparison is performed considering a non-inverting amplifier configuration with a gain of 1000 (resistors $R_1=100K\Omega$ and $R_2=100\Omega$) and the equivalent thermopile circuit with a nominal resistance of $R_{th}=100K\Omega$.

Thermopile resistor values (which are typically several tens of hundreds of ohms) allow assuming that R_{th} is much larger than $R_1||R_2$. In these conditions, the inner amplifier noise

expression referred to the input terminals (RTI) can be simplified to Equation 2, where v_n is the amplifier thermal voltage noise, $v_{1/f}$ is the 1/f voltage noise, i_n is the current thermal noise, and $i_{1/f}$ is the 1/f current noise [7]:

$$vn_{RTI} = \left[v_n{}^2 + v_{1/f}{}^2 + (i_n \cdot Rth)^2 + (i_{1/f} \cdot Rth)^2 \right]^{1/2} \qquad (2)$$

Table 2 shows important noise parameters, chip sizes, and corner frequency for different amplifiers. Table 3 shows the corresponding induced noise contributions assuming R_{th}=88KΩ, which is the Heimann Sensors thermopile resistance, and a 10Hz bandwidth to calculate 1/f noise contributions.

To assess the noise level introduced by the amplifier it is convenient to compare it to the inner thermal noise of the thermopile. Equation 3 shows the thermal noise of a resistor R. For the Heimann Sensors thermopile (88KΩ) the corresponding thermal noise is 0.97µVpp, at 300K and considering a bandwidth of BW=10Hz.

$$v_R = \sqrt{4 K_B T R BW}; \qquad (3)$$

Among the compared amplifiers MAX4475, AMP01, and AD8626 noises still are considerably under the inner thermal noise of the thermopile. Therefore, the amplification stage will only exhibit a slight difference in terms of the total noise when any of these three amplifiers is used.

Selecting an amplifier with the lowest corner frequency is important to reduce the 1/f noise. AMP01 exhibits the lowest corner frequency (8Hz), and the thermal noise introduced by the thermopile is more than twice the noise from the amplifier. The only drawback for the AMP01 is its size: the bigger dimensions for AMP01 force to place the amplifier further from the thermopiles than smaller amplifiers, and additional noise can be picked up on the signal. However, since AMP01 features instrumentation amplifier architecture the common mode disturbances at the input terminals will be cancelled and the effect of being placed further from the thermopiles will be reduced. This makes AMP01 the best voltage amplifier choice for the application.

Each pre-amplification channel is based on one AMP01 instrumentation amplifier and a follow up filter stage to reduce the noise and avoid aliasing before the lock-in routine. Instrumentation amplifiers are designed with the required gain to expand the thermopile voltage to 0-0.6V (10^4V/V for reference and ethylene channels, and 6.10^3V/V for ethanol and ammonia channels). The pre-filter stage features a 4th order unity gain low pass filter, implemented using Sallen-Key architecture, with a cut-off frequency of 2.5Hz. Figure 10 shows the implemented low-pass filter circuit schematic and Figure 11 shows the simulation result in the frequency domain.

Amplifier parameters	AD8628	AMP01	MAX4475	AD620	LTC1050	LT1037	AD820	AD797
Manufacturer	Analog Devices	Analog Devices	Maxim	Analog Devices	Linear Technology	Linear Technology	Analog Devices	Analog Devices
Type	Operation Amplifier	Instrumentation Amplifier	Operation Amplifier	Instrumentation Amplifier	Chopper Amplifier	Operation Amplifier	Operation Amplifier	Operation Amplifier
ev_n (nV/√Hz)	22	5	4.5	9	NS	2.5	16	0.9
$v_{1/f}$ (µVpp)	0.5 0.16[1]	0.12	0.26	0.28	1.6	0.06	2	0.05
ei_n (fA/√Hz)	5[2]	150	0.5	100	1.8[2]	400 1500[2]	0.8	2000
$i_{1/f}$ (pApp)	NS	2	NS	10	0[3]	NS	0.018	NS
Corner frequency	NS	8Hz	1KHz	20Hz	NS	NS	20Hz	100Hz
Chip dimensions	2.9x2.8mm^2	13x10mm^2	3x3mm^2	5x6mm^2	5x4mm^2	5x4mm^2	5x6mm^2	5x6mm^2

Table 2: Important noise parameters for several amplifiers.

v_n (G=1000, f_0=1KHz); $v_{1/f}$ (G=1000, 0.1Hz-10Hz); ei_n (G=1000, f_0=1KHz); $i_{1/f}$ (G=1000, 0.1Hz-10Hz)

0.1Hz-1Hz[1]; 10Hz[2]; no 1/f noise for chopper amplifiers[3].

NS: No specified.

Noise contributions	AD8628	AMP01	MAX4475	AD620	LTC1050	LT1037	AD820	AD797
Voltage induced noise (µVpp)	0.75	0.17	0.28	0.36	1.6	0.09	2.04	0.05
Current induced noise (µVpp)	0.01	0.38	0.001	0.91	0.004	0.89	0.002	4.45
Inner amplifier noise (µVpp)	**0.75**	**0.42**	**0.28**	**0.98**	**1.60**	**0.89**	**2.04**	**4.45**

Table 3: Noise contributions for different amplifiers.
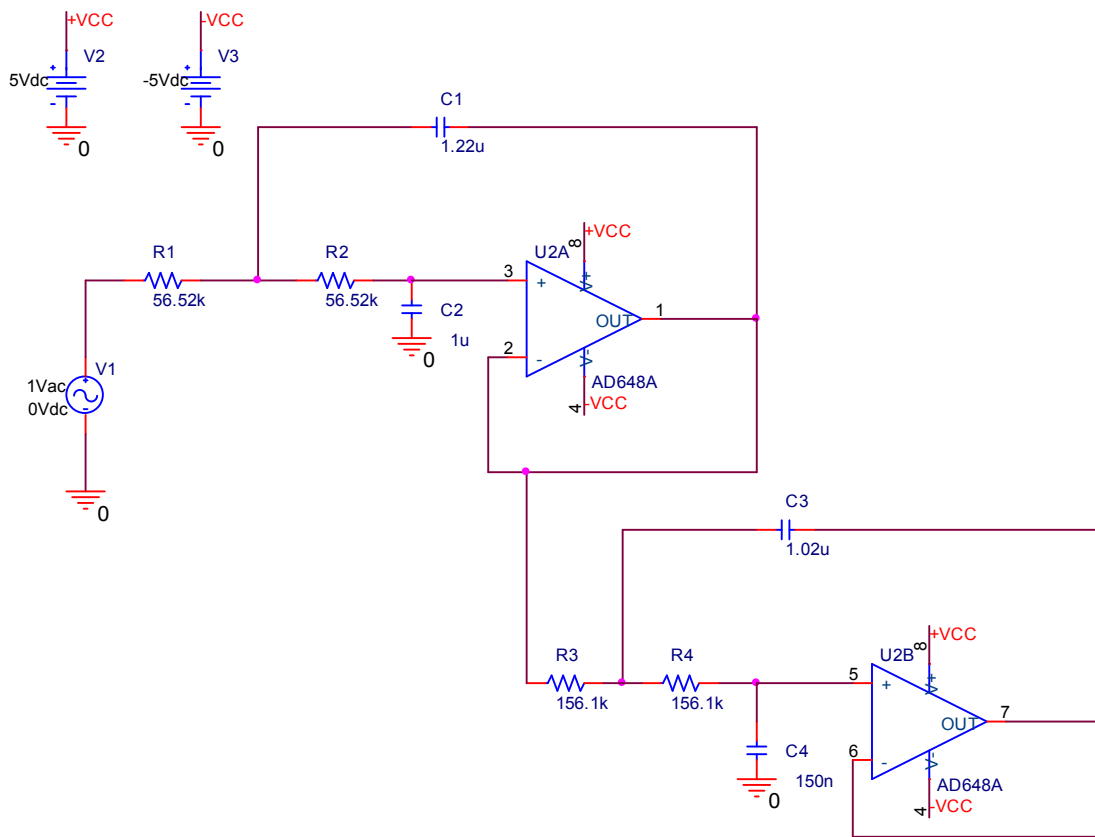
Figure 10: Schematic of the implemented low-pass filter.
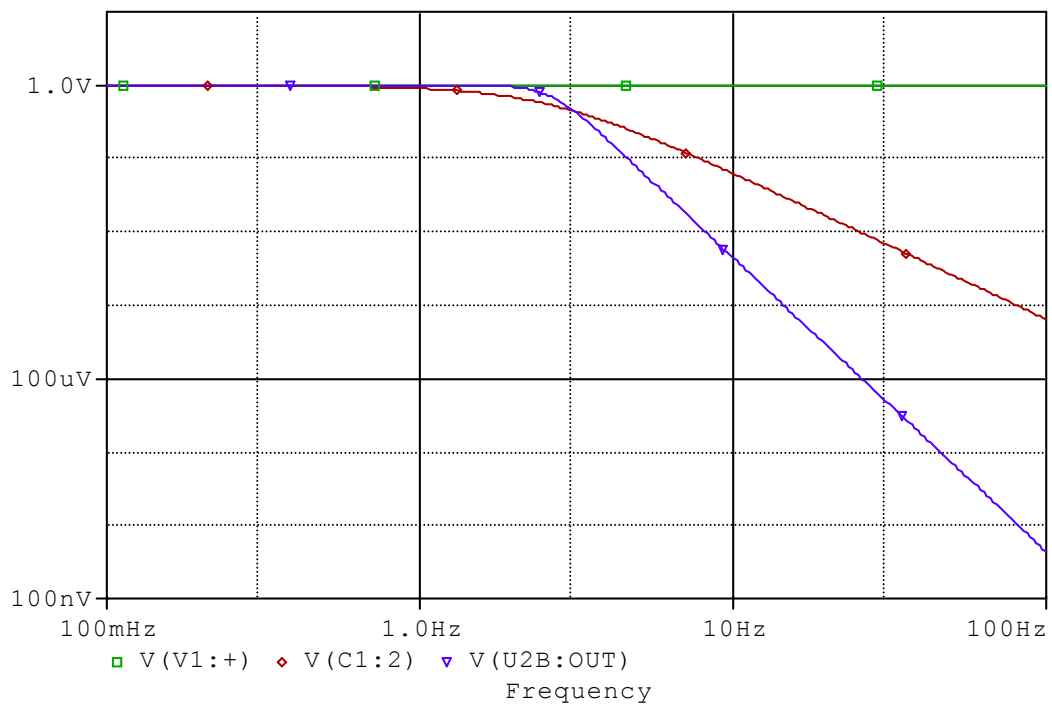
Figure 11: Low-pass filter response, in the frequency domain.

The board design has been carried out trying to maximally reduce noise. Additionally, to avoid drift and additional noise from the power supply, positive (MC7808) and negative (MC7908) voltage regulators were included. To reduce the external interference, the board is placed inside of a metallic box. The fabricated board is presented in Figure 12.

Figure 12: Analog pre-amplifier, featuring an instrumentation amplifier and a low-pass filter for each channel. The board is placed inside of a metallic box to reduce external interferences.

e) Digital lock-in:

Lock-in amplifiers are widely used as signal recovery systems since they are characterized by a wide dynamic range which gives the ability to measure signals accompanied by relatively high levels of noise and interference. A lock-in amplifier behaves like a bandpass filter centered on a reference frequency. Signal modulation (at reference frequency) is convenient to shift the signal to a lower noise band. In practice, the modulation frequency is usually made as high as possible to facilitate separation of the chopped output voltage from noise components [7].

A digital implementation of the lock-in opens the possibility to enhance the carrier frequency range to arbitrarily low values, the implementation of the low pass digital filter cut-off frequency to both shorter and longer values, the rejection of unwanted DC components, and reduced drift [12]. Additionally, higher order digital filter may be more easily implemented since it depends solely on the processor computing power, in comparison to analog filters which require more hardware components (and board space) as the filter order increases.

The selected lock-in architecture is a dual-phase lock-in amplifier, which is not sensitive to phase shifts between the reference and input signal but it requires more computation time. The implemented digital lock-in amplifier is based on a MSP430F4270 microcontroller (Texas Instruments, USA). Input signals are multiplexed every 15min, which is considered to be a short

time compared to the expected concentration variations in the fruit store-houses. More details of the developed digital lock-in can be found in P#5, where the corresponding block diagram (Figure 2, P#5) and the measured BW (Figure 3, P#5) are also shown. The board featuring both microcontrollers is shown in Figure 13.

Figure 13: Board featuring both microcontrollers for lock-in routines.

5.3.- Results

Spectrometer calibration to ethylene and ammonia concentrations, including their mixtures, has been performed in laboratory conditions. A picture of the laboratory setup is shown in Figure 14. 21 different concentration values (presented in Figure 4 P#5) were used to test the developed spectrometer, but using commercial IR detectors (HTS-Q21, Heimann Sensors). It can be assumed that only one of the species is in a high concentration level and the other gases are in residual concentration levels which do not affect spectrometer measurements. In that scenario, prediction errors become much smaller reaching a root mean square error of 15 ppm for ethylene and 80 ppm for ammonia.

Experimental results show that the developed spectrometer is suitable for detecting that fruit is ripe and preventing it to decline to senescence (typically when ethylene concentration is over 100 ppm). Additionally, the spectrometer is also able to detect ammonia over 160 ppm if a leakage from the cooling system occurs. System detection limits are close to gas mixing station errors, which may point to the idea that the spectrometer is measuring gas station variance in fact.

Laboratory tests give promising results concerning ethylene and ammonia detection. However, in order to assess the spectrometer performance in real storage conditions, field test were carried out in IRTA-Lleida, where usually ripening tests of fruit in typical fruit storage conditions have been performed. Field tests show that designed spectrometer is suitable as gas alarm for the proposed application.

A detailed explanation of the laboratory and field measurements and the system calibration is presented in P#5, and Table 4 shows the main spectrometer specifications.

Further improvements are envisaged. At this point standard commercial detectors are used in the system because of problems of thermal coupling between optical filters and thermopiles of our initial detector design. However, once these problems are solved the performance of the original detector looks promising since it features the integration of Fresnel lenses for improved optical throughput.
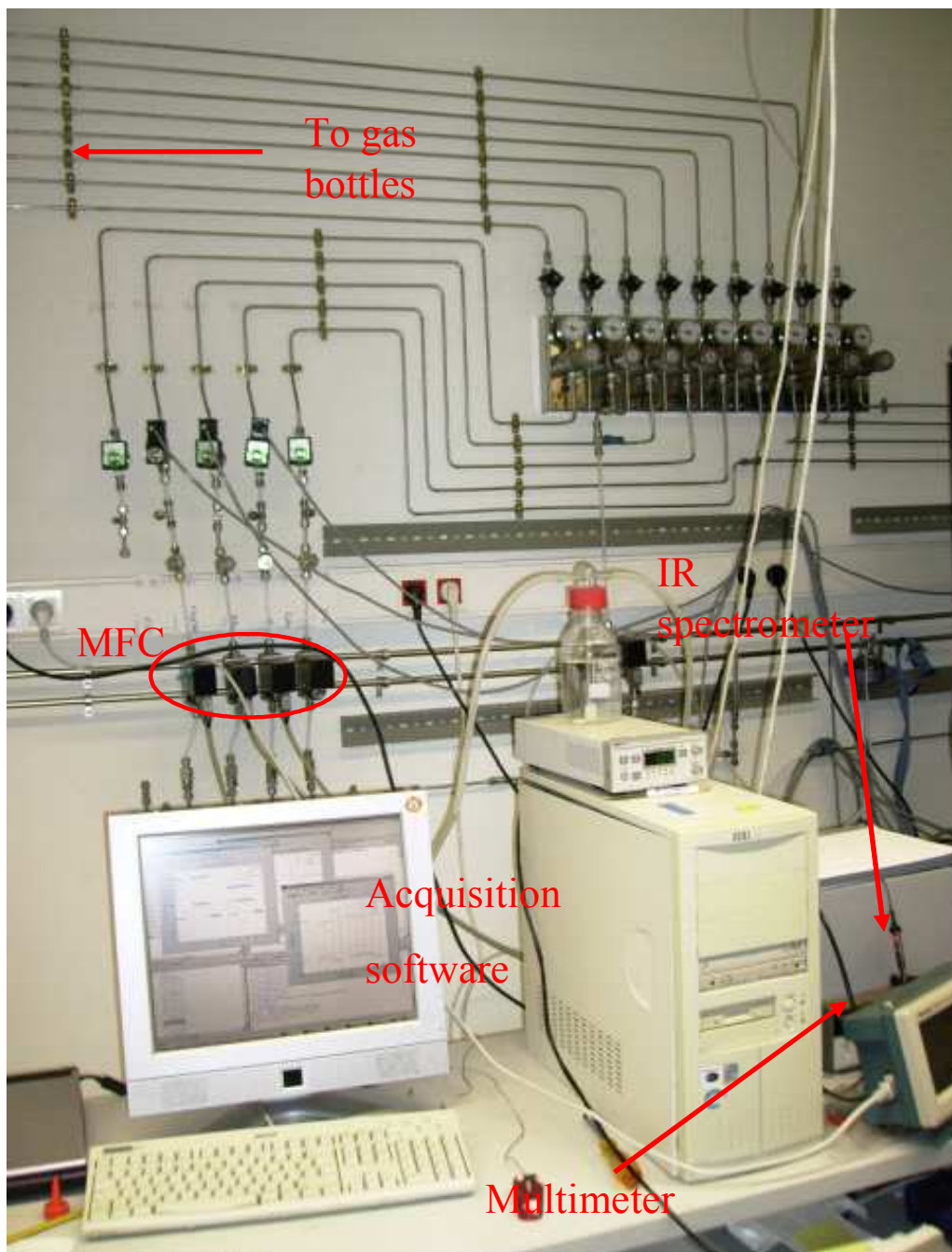
Figure 14: Laboratory setup used to perform spectrometer calibration. The IR spectrometer, the data acquisition system, the mass flow controllers (MFC), and gas connections are shown.

Power	24W
Size	330mm x 230mm x 180mm (L,W,H)
Time response	15min
Selected absorption bands	ethylene: 10.6μm
	ammonia: 9.7μm
	ethanol: 3.4μm
	reference: 3.9μm
Accuracy	ethylene: 15ppm
	ammonia 80ppm
Detection limit	ethylene: 30ppm (95% of confidence)
	ammonia 160ppm (95% of confidence)
Measurement ranges	ethylene: 0-2000ppm
	ammonia 0-1750ppm

Table 4: Spectrometer specifications

5.4.- Summary

In this chapter the developed spectrometer to monitor apple's quality while it is being stored in the controlled atmosphere chambers is presented. However, more details and technical information can be found in the enclosed Journal papers.

The spectrometer is based on NDIR architecture and comprises an IR emitter, a White cell, a novel and compact four-channel IR detector, and system electronics. The IR detector features four optical filters to select the absorption bands for ethylene, ammonia, and ethanol, and an additional reference channel. Focusing elements based on a Fresnel lens array are fabricated to improve system sensitivity and are placed on the lid of the detector. The lens array is fabricated on the same silicon substrate using available silicon technologies and following a new design based on four photolithographic masks which is cost effective and assures optical transmission efficiencies over 85%. Signal recovery system is based on a low noise instrumentation amplifier and a digital lock-in, which is implemented in a general purpose microprocessor.

The integration of optical filters too close to the detector leads to degraded performance. It is suggested to set in vacuum conditions the detector or increase the solder joint. However, in the meantime, a commercial detector is used to test the complete system. Laboratory and field test show that the developed spectrometer is able to detect the ethylene burst that comes together with the fruit climacteric transition, and therefore, it can be used to determine fruit status and prevent fruit to decline into senescence. Additionally, ammonia leakage from the cooling system can be detected as well and avoid fruit deterioration and poisoning.

5.5.- References

[1]   SiraTechnology, *Gas Detector Selection and Calibration Guide*: Withrebys publishing, 2005.

[2]   National Institute of Standards and Technology (NIST), *The NIST Chemistry WebBook*, 2005.

[3]   J. Dixon and E.W. Hewett, "Factors affecting apple aroma/flavour volatile concentration: a review," *New Zealand Journal of Crop and Horticultural Science*, vol. 28, (no. 3), pp. 155-173, Sep 2000.

[4]   M. Knee and S.G.S. Hatfield, "The metabolism of alcohols by apple fruit tissue," *Journal of the Science of Food and Agriculture*, vol. 32, (no. 6), pp. 593-600, 1981.

[5]   A. Jerger, H. Kohler, F. Becker, H.B. Keller, and R. Seifert, "New applications of tin oxide gas sensors II. Intelligent sensor system for reliable monitoring of ammonia leakages," *Sensors and Actuators B-Chemical*, vol. 81, (no. 2-3), pp. 301-307, 2002.

[6]   H. Griffiths "Effects of Air Pollution on Agricultural Crops," *Factsheet*, vol. 85-002, 2003.

[7]   M.L. Meade, *Lock-in Amplifiers: principles and applications*, London: Peter Peregrinus Ltd., 1983.

[8]   W. Konz, J. Hildenbrand, M. Bauersfeld, S. Hartwig, A. Lambrecht, V. Lehmann, and J. Wollenstein, "Micromachined IR-source with excellent blackbody like behaviour," *Smart Sensors, Actuators, and Mems Ii*, vol. 5836, pp. 540-548, 2005.

[9]   S. Hartwig, J. Hildenbrand, M. Moreno, J. Fonollosa, L. Fonseca, J. Santander, R. Rubio, C. Cane, A. Lambrecht, and J. Wollenstein, "A highly sensitive IR-optical sensor for ethylene-monitoring," *Smart Sensors, Actuators, and Mems Ii*, vol. 5836, pp. 452-460, 2005.

[10]   L. Fonseca, E. Cabruja, C. Calaza, R. Rubio, J. Santander, E. Figueras, I. Gracia, C. Cane, M. Moreno, and S. Marco, "Feasibility of a flip-chip approach to integrate an IR filter and an IR detector in a future gas detection cell," *Microsystem Technologies-Micro-and Nanosystems-Information Storage and Processing Systems*, vol. 10, (no. 5), pp. 382-386, 2004.

[11]   L. Fonseca, F. Perez-Murano, C. Calaza, R. Rubio, J. Santander, E. Figueras, I. Gracia, C. Cane, M. Moreno, and S. Marco, "AFM thermal imaging as an optimization tool for a bulk micromachined thermopile," *Sensors and Actuators a-Physical*, vol. 115, (no. 2-3), pp. 440-446, 2004.

[12]   L.A. Barragan, J.I. Artigas, R. Alonso, and F. Villuendas, "A modular, low-cost, digital signal processor-based lock-in card for measuring optical attenuation," *Review of Scientific Instruments*, vol. 72, (no. 1), pp. 247-251, 2001.

6.- PUBLISHED JOURNAL PAPERS:

The developed infrared system is reported in five different Journal papers, where the reader can find specific technical details concerning the spectrometer architecture, its components and calibration, and the performed tests.

A short introduction detailing the main contribution of each paper to the final spectrometer is presented before the compilation of the Journal papers:

6.1.- R. Rubio, J. Santander, J. Fonollosa, L. Fonseca, I. Gracia, C. Cane, M. Moreno, and S. Marco, "**Exploration of the metrological performance of a gas detector based on an array of unspecific infrared filters**," *Sensors and Actuators B-Chemical*, vol. 116, (no. 1-2), pp. 183-191, Jul 2006

Traditionally, NDIR systems are based on a setup composed by an infrared source that illuminates the gas to be detected, a fixed set of narrow bandpass optical filters typically in roulette, and an IR detector. The filters placed before the infrared detector select the band where the absorption lines of the target substance are placed. This system architecture is highly selective, can be configured for the measurement of several species by using different optical filters, the resulting system is immune to false alarms and poisoning, and, additionally, long term stability can be improved by the use of a reference band without absorptions.

In this paper, a novel architecture of NDIR system with wide bandpass optical filters is presented. Therefore, the optical filters are not substance oriented and the output of the system is a voltage pattern. After multivariate regression techniques, the system output can be used to predict gas concentrations and gives the architecture for a general purpose spectrometer.

This new configuration opens the possibility to detect any gas with absorption bands in the IR with a moderate number of optical filters. However, the gases to detect are well-defined for fruit status monitoring in today's store houses. Therefore, for this application traditional narrow optical filters can be used and, additionally, cross-sensitivities are reduced with this filters selection.

6.2.- J. Fonollosa, R. Rubio, S. Hartwig, S. Marco, J. Santander, L. Fonseca, J. Wöllenstein, and M. Moreno, "**Design and fabrication of silicon-based mid infrared multi-lenses for gas sensing applications**" *Sensors and Actuators B: Chemical* vol. 132, no. 2, pp. 498-507, 2008

In this work the development of a novel architecture of an IR detector specifically designed for a NDIR system is presented. The resulting device is a highly-integrated compact

detection module comprising a 2x2 thermopile array, flip-chipped optical filters for wavelength selection, and focusing elements in the lid of the TO-8 package to optimize system detectivity.

Diffractive Fresnel lens approach is chosen as a focusing element since they are compatible with silicon microtechnology. Therefore, they benefit from the typical advantages of silicon technology such as reliability, mass production, and equipment availability. The fabrication of four lenses on the same silicon substrate in a combined multi-lens is presented. In order to reduce the number of photolithographic steps, a new design based on four photolithographic masks and sharing up to sixteen quantization steps by the four lenses is done.

The test of the multi-lens array shows a promising performance and the resulting device is successfully assembled on the detector lid securing the proper alignment. Therefore, the fabricated device is suitable for being the IR detector module of a NDIR spectrometer. Thus, an important system sensitivity increase is expected since more radiation is focused on the sensitive area of the IR detector.

6.3.- J. Fonollosa, M. Carmona, J. Santander, L. Fonseca, M. Moreno, and S. Marco, "**Limits to the integration of filters and lenses on thermoelectric IR detectors by flip-chip techniques**," *Sensors and Actuators: A Physical*, vol. 149, (no. 1), pp. 65-73, 2009.

The performance of the IR detector module presented in the previous paper in the trend towards miniaturization is studied in this work. An important feature of such module is the assembly by flip-chip techniques of the IR filters on top of the thermopiles.

In order to determine the effect of the attached optical filters above the thermopiles, IR measurements have been performed in air conditions using thermopiles with and without flip-chipped narrow optical filters. It is shown that, in air conditions, flip-chipped optical filters on the thermopile array cause a response much larger and slower than when the filters are far from the detector. This behavior is explained by a thermal coupling between the detector and the filters when the integration of filters is too close to the IR detector.

To avoid such detrimental effects a possibility is to set the device in vacuum conditions, obtaining an improved output response and avoiding the influence of the filters. Therefore, the packaging solution should be able to guarantee complete sealing conditions during the lifetime of the component, which are not easily achieved. Another proposed way is to increase the solder joint height. Beyond a certain height, the filter is considered to be isolated from the thermopile.

Due to the reported thermal coupling, the required selectivity for the proposed NDIR system is strongly impaired. Therefore, the fabricated IR module is not suitable for gas detection as a component of a traditional NDIR spectrometer.

6.4.- J. Hildenbrand, J. Wollenstein, S. Hartwig, A. Eberhardt, B. Halford, M. Moreno, J. Fonollosa, L. Fonseca, J. Santander, R. Rubio, I. Gracia, and C. Cane, "**A compact optical multichannel system for ethylene monitoring**," *Microsystem Technologies-Micro-and Nanosystems-Information Storage and Processing Systems,* vol. 14, no. 4-5, pp. 637-644, 2008

A multi-channel NDIR spectrometer for ethylene measurement in today's store houses is built and characterized. The instrument contains additional channels to reject potential cross-interferences like ammonia and ethanol and a reference channel to improve long term stability. Additionally, these channels are useful for monitoring a potential malfunction of the cooling system and possible fouling of the fruit respectively.

The corresponding optical components and signal processing electronics are developed, tested and integrated in a compact measurement system. The main optical components, their integration of the optical system, as well as a description of the developed electronics and the first results of gas measurements are described in this paper.

A prototype of the proposed NDIR architecture is built using developed components such as the IR-emitter and the gas cell, and commercial ones such as the IR detector and the digital lock-in. Preliminary simple ethylene measurements are performed with the presented spectrometer, showing a detection limit better than 20ppm. Such a result validates the presented system architecture and the overall approach to measure ethylene in the today's store-houses.

6.5.- J. Fonollosa, B. Halford, L. Fonseca, J. Santander, S. Udina, M. Moreno, J. Hildenbrand, J. Wollenstein, and S. Marco, "**Ethylene optical spectrometer for apple ripening monitoring in controlled atmosphere store-houses**," *Sensors and Actuators B: Chemical*, vol. 136, (no. 2), pp. 546-554, 2009.

In this paper, an improved version of the IR spectrometer for ethylene gas measurements in fruit store-houses is reported. Presented spectrometer features significant differences in comparison with already presented previous version such as it is calibrated for both ethylene and ammonia, a new assembly of the optical components is presented, it features a pre-amplification stage based on an instrumentation amplifier and a specifically developed digital lock-in amplifier, and a multi-variable regression model is built for the gas calibrations.

A four-channel commercial thermopile, with similar optical filters than the developed IR detector module but on the package lid, and without Fresnel lenses, is used to overcome the thermal coupling problem and test the system selectivity. Spectrometer calibration to ethylene and ammonia concentrations, including their mixtures, has been performed in laboratory conditions. A calibration Partial Least Square model is presented in this work and the resulting root mean square error for ethylene and ammonia prediction are 95ppm and 120ppm respectively.

A new algorithm for error reduction in PLS output space has been proposed, assuming that both gases may not appear simultaneously. Ethylene detection limit (30ppm) is suitable for detecting that fruit is ripe and preventing it to decline to senescence (typically when ethylene concentration is over 100ppm). Additionally, the spectrometer is also able to detect ammonia over 160ppm if a leakage from the cooling system occurs. Therefore, it is shown that the fabricated spectrometer is suitable for ethylene monitoring in the today's store houses to asses fruit status and to set an alarm if an ammonia leakage occurs.

ELSEVIER

Exploration of the metrological performance of a gas detector based on an array of unspecific infrared filters

R. Rubio [a],*, J. Santander [a], J. Fonollosa [b], L. Fonseca, I. Gràcia [a],
C. Cané [a], M. Moreno [b], S. Marco [b]

[a] *Centro Nacional de Microelectrónica (IMB-CSIC), Spain*
[b] *Departament d'Electrònica, Universitat de Barcelona, Spain*

Abstract

The feasibility of a non-dispersive infrared (NDIR) gas detection system based on an array on non-specific detectors is studied in this work. The measurement system, that is intended to be low cost and of reduced dimension, is aimed to the simultaneous quantitative detection of different gases with IR absorption bands in the region of the 1000–4000 cm^{-1}. The detector is a single module that has been already fabricated. It is composed by an array of broadband infrared filters and a matching array of thermopile detectors joint together by means of flip chip. The elements of the filter array are not tuned for the specific measurement of any gas, in opposition to traditional NDIR setups, making necessary the use of multivariate regression techniques (Partial least squares) to predict the gases concentration. A preliminary evaluation of the metrological characteristics of the complete NDIR system is carried out using a realistic model of the system. Two arrays sizes, 3×3 and 4×4 elements, are studied for the discrimination of a mixture composed by methane, carbon monoxide and carbon dioxide at different concentrations. Prediction errors about tens of ppm are found for an optical path length of 10 cm. In traditional NDIR systems infrared source aging is compensated by means of a reference channel where no absorptions bands are present. Instead, in this in this work these effects are removed using a digital component correction technique.
© 2006 Elsevier B.V. All rights reserved.

Keywords: NDIR; Optical gas detection; Thermopile; Thin films filters; Flip chip; Component correction; Drift

1. Introduction

Analytical methods based on infrared spectroscopy are highly selective methods that make the estimation of an analyte in a complex matrix possible. There are four types of instruments for infrared spectroscopy measurements available: dispersive grating spectrophotometers for qualitative measurements, Fourier transform instruments for both qualitative and quantitative measurements, non-dispersive photometers for quantitative determination of organic species in the atmosphere and reflectance photometers for analysis of solids. The size and the price of this kind of instruments are their main drawbacks.

Non-dispersive infrared (NDIR) gas detection systems are based on the detection of the absorption of radiation by analytes at certain wavelengths [1]. Although the relationship between the optical absorption and the gas concentration shows a non-linear behaviour (Lambert-Beer law), optical measurements are, in general, more reliable than solid state gas sensors.

A typical NDIR measurement setup is composed by an infrared source that illuminates the gas to be detected. In most cases these devices use a fixed set of multilayer filters, or filter roulette, limiting the number of simultaneous gases that can be detected. Those filters placed before the infrared detector select the band where the absorption lines of the target substance are placed. The main advantages of this system are high selectivity, the ability to be configured for the measurement of several species by using different selective filters and the immunity to false alarms and poisoning since the detectors are not in direct contact with the gas. In addition, long term stability is improved by the use of a reference band without absorptions. Using this reference band, effects of the infrared source aging can be corrected.

This NDIR measurement method based on the use of selective filters has been already used in commercial devices. Previ-

* Corresponding author. Tel.: +34 935947700; fax: +34 935801496.
E-mail address: rafael.rubio@cnm.es (R. Rubio).

ous attempts to build a NDIR micro spectrometer by the use of MEMS structures have been done only recently [2]. Other proposal is based on the use of a Fabry Perot micro spectrometer built using surface micro-machined polysilicon mirrors that are actuated electro statically [3,4]. Tuneable infrared laser differential absorption spectroscopy has been used for years, although recently quantum cascade lasers have been introduced [5]. Also, the dependence of the emission spectra of the IR source on the temperature has been proposed, in this way modulating the temperature of the IR source different emission spectra are achieved and hence acting like a spectrometer [6].

Our goal is to develop a low cost and reduced dimension NDIR analyzer that may be of use for the large number of analytes with absorption bands in the mid infrared. To do so, we propose a *non-selective* optical detection system based on a broadband filter array. Instead of using one selective filter per substance we use an array of filters with different transmittance spectra that cover the interest region (1000–$4000\,cm^{-1}$). As a result of this, a voltage pattern is obtained as the output of the system and multivariate regression techniques should be used to predict the gas concentration.

A model of the system is built to evaluate the ability to discriminate and quantify different mixtures of gases, despite having non-selective sensors. The simulation uses real measured characteristics of all the system elements. To simulate the infrared gas spectrum HITRAN database is used [7]. To illustrate this concept, we prove in this work the feasibility of an array of broadband filters in combination with multivariate regression techniques for the simultaneous detection of three gases (CO, CO_2 and CH_4). Note that although these three gases are used in this work, the scope of applications of these systems is broader and the choice of these gases is due to the fact that their infrared absorbances are well known and available at the HITRAN database, and because of their practical engineering interest.

In the following sections, we will first introduce the measurement system making a short description of all the elements and how they have been modelled. Then, a synthetic experiment will be described, followed by multivariate regression leading to an estimation of the expected accuracy for this system.

A potential drawback of this system is the absence of a reference band to correct source aging or obscuration due to dirtiness. The last section of the paper shows that component correction is an effective way to compensate source drift [8].

2. NDIR system model description

A sketch of the measurement system structure is shown in Fig. 1. The radiation produced by the infrared source passes through a gas chamber and reaches the detector array. Each filter weights in different manner different parts of the spectrum and consequently the thermopile array generates a voltage pattern. This voltage pattern will be subsequently processed to finally estimate the gas concentration by suitable multivariate calibration methods.
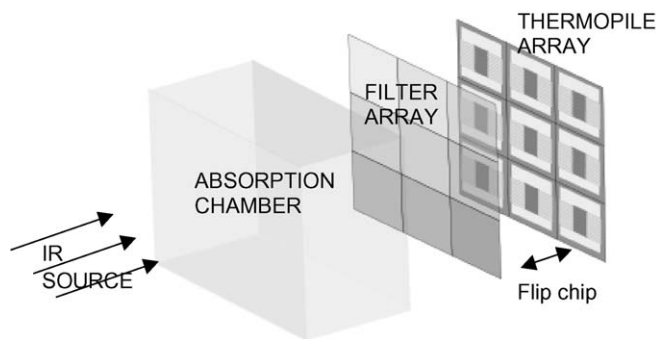
Fig. 1. Gas detection system architecture.

2.1. Infrared radiation source

The radiation source is a commercial device (refelctIR-P1C Ion Optics Waltham, USA). The radiation spectra produced by this device is considered proportional to that of an ideal blackbody heated at the same temperature ($850\,°C$). The spectral irradiance of the source is calculated from Plank's Law [1] using uniform values for the temperature T ($850\,°C$) and the source emissivity ε (0.7). The effective emitting area used is $2\,mm^2$.

The full angle for 50% of peak power of the IR source, provided by the manufacturer ($\theta_{1/2} = 30°$), allows us to calculate the directivity parameter of the source n assuming a Lambertian distribution: in our case the obtained directivity is 4.8.

$$n = \frac{-\ln 2}{\ln(\cos\theta_{1/2})} \tag{1}$$

2.2. Power transmission

Two zinc selenide lenses, placed in both extremes of the absorption chamber, are used in order to enhance the power transmission. The model considers the dispersion losses between the source and the entrance of the chamber assuming that once inside, the light is only influenced by the gas absorption. The power losses due to the lenses transmission are considered using the transmittances values provided by the manufacturer ($T = 0.9$).

The fraction of the emitted power Φ_E arriving to the entrance of the chamber Φ_D, after a certain optical path length L (distance between the IR emitter and the first lens), is obtained from the partial integration over the solid angle sustained by the lenses respect to the source. We assume that the source is in the focal length of the lens.

This fraction is:

$$\frac{\Phi_D}{\Phi_E} = 1 - \cos^{n+1}\left(\arctan\left(\frac{r}{L}\right)\right) \tag{2}$$

where r is the radius of the first lens ($r = 1.27\,cm$) of the system and n the directivity parameter of the source. The last lens of the optical system, located between the gas chamber and the detector filters, is devoted to focus the beam to the sensing area of the array. To calculate the fraction of optical power that arrives to each element of the array, we integrate over the portion of solid angle of the beam captured by the corresponding sensitive area.
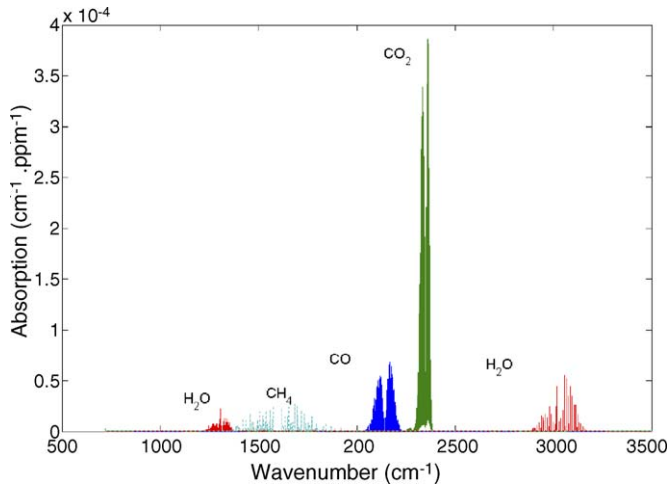
Fig. 2. HITRAN database absorbances for CO, CO_2 and CH_4.

2.3. Gas absorption

Gas absorption is calculated using Lambert-Beer law. According to this law, the transmittance of a medium for a particular wave number ν can be expressed as:

$$T(\nu) = e^{-a(\nu)cL} \qquad (3)$$

with $a(\nu)$ being the absorption index of the gas at a particular frequency, c the gas concentration, and L the absorption optical path that is 10 cm in the considered case. As it has been mentioned the transmittance is non-linear with the gas concentration, however this effect is only observed for large values of the exponent.

The absorption index $a(\nu)$ for the gases to detect is computed using the data provided by the HITRAN database [9]. This database includes the values of the intensities and widths of the individual absorption lines associated to the different vibration modes of the gas molecules. The absorbances of the three simulated gases can be seen in Fig. 2.

2.4. Filter array

Two arrays sizes were fabricated. The single detector size is of 620 μm × 620 μm for the 3 × 3 array and 450 μm × 450 μm for the 4 × 4 array. In both cases the size of the whole array is 2100 μm × 2100 μm. A filter array is built over a silicon substrate by the combination of thin films (silicon oxide and polysilicon) with different refractive index, acting as a Fabry-Perot structure composed by two mirrors. Transitions peaks are located in the interest region (1000–4000 cm^{-1}) delimited by an additional band pass filter (Calcium Fluoride window 1000–5000 cm^{-1}) placed in the IR source housing which is also considered in the simulation. The stacked composition of the filter is described in Table 1.

The thickness of the SiO_2 film between the polysilicon mirrors determines the number and position of peaks in the transmittance spectra. This thickness is linearly increased from 1 to 8 μm for the array elements. An additional SiO_2 film is used to optically separate the polysilicon from the silicon substrate.

Table 1
Filter layer structure

Layer	Index	Thickness (μm)
Polysilicon (upper mirror)	3.433	0.2
SiO_2	1.411	1–8
Polysilicon (lower mirror)	3.433	0.2
SiO_2	1.411	1
Silicon substrate	3.433	500

Measured transmittances for a 3 × 3 array are shown in Fig. 3. The spectra of the different filters were obtained using an IR-Plan Spectra Tech (Stamford, USA) microscope that allows focusing on each array element. Fig. 4 shows a fabricated device.

2.5. Thermopile array

Thermopiles are thermal radiation detectors based on the Seebeck effect [10]. They consist of the serial combination of several thermocouples that transform the temperature difference between a cold and a hot junction into a voltage output. In a previous work, the design and fabrication by bulk micro-machining processes using aluminium and n-doped polysilicon for the thermocouples of a individual thermopile detector was described [11,12].

Now we propose the design and fabrication of a thermopile array built on a single membrane following the same principles and without increasing the number of technological steps. Each individual thermopile sensor structure is sketched in Fig. 5.

The integration of thermopile arrays has been considered by a number of authors. For instance, Oliver and Wise [13], report the integration of a 1024 element array. Thermopile arrays with higher number of elements have been previously reported but usual applications of these kind of devices is thermal imaging. For gas sensing applications, there is no need to go to very high number of IR detectors, since probably the increase of array elements does not increase the information obtained due to the redundancies of the broadband filters. IR detectors need a minimum size to achieve the necessary sensitivity. Replication of these elements beyond the sizes considered in this work makes difficult to concentrate the incoming radiation into the detector elements.

The whole matrix is built on a single silicon oxide/silicon nitride square membrane (2.1 mm × 2.1 mm) defined by anisotropic wet etching of bulk silicon. To ensure the existence of hot and cold junctions for each detector we define in the same process absorbers and ribs on the insulating membrane. These structures, which are 6 μm thick, are defined by boron heavy doping that renders them unaffected by the anisotropic etching. The ribs, which are 120 μm wide, crisscross the membrane contacting the silicon bulk and thus acting as a heat sink. Absorbers are located in the centre of each individual membrane defined by the ribs intersection. In this way, being doped and isolated, they are efficiently heated up by the absorption of the incoming radiation while the ribs remain at ambient temperature.

A fabricated 4 × 4 thermopile array can be seen in Fig. 6. The number of thermocouples is always the maximum allowed for
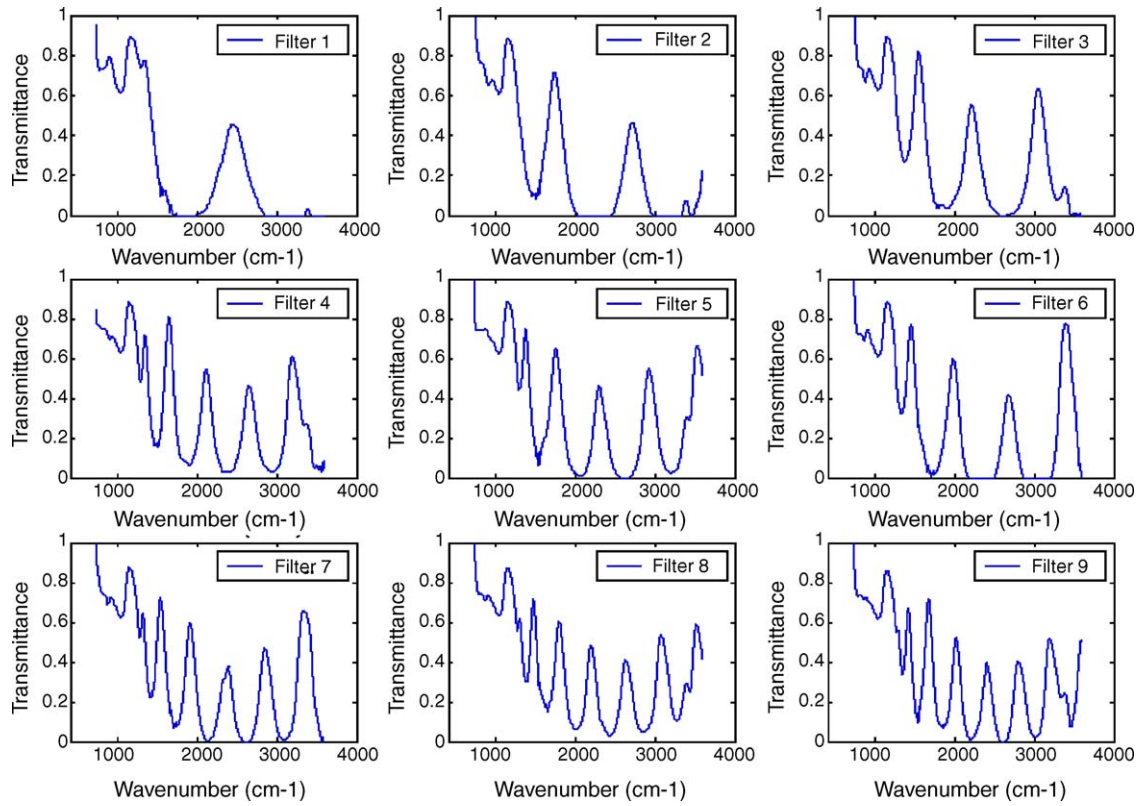
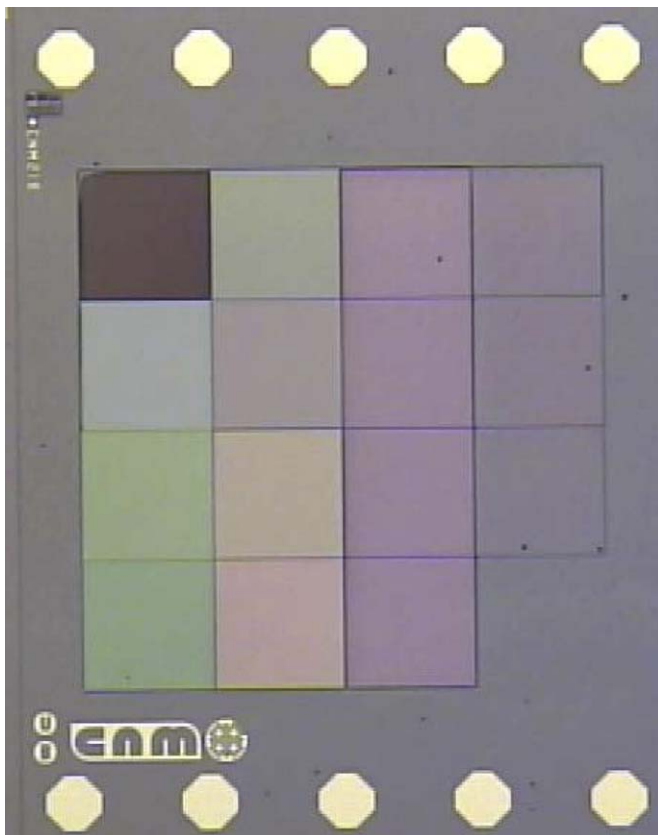Fig. 3. Measured transmittance of the *non-selective* filter array (3 × 3).

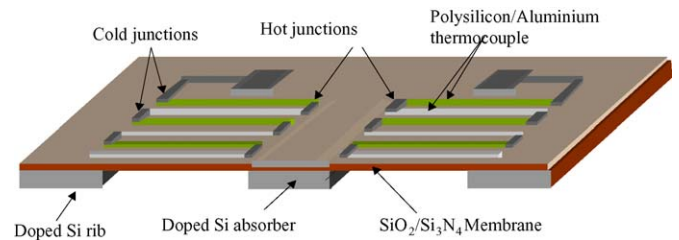Fig. 4. Optical image of the fabricated 4 × 4 elements filter array.

Fig. 5. Scheme of a single thermopile detector.

the given size of the absorber. This size is optimized to reduce the thermal loses. Table 2 summarizes these parameters for the two array sizes.

The measured device parameters, responsivity (R) and noise equivalent power (NEP) are used in the model. NEP is calculated from the devices resistance assuming that the most important contribution to the thermopile noise voltage is the thermal noise.

Empirical measurements have shown that the absorption of IR radiation is not absolutely uniform for different wavelengths due to the multilayer present on the thermopile membrane.

Table 2
Parameters of the fabricated devices

Design parameters			Measured parameters	
Array size	Thermocouples	Absorber size (μm)	R (V/W)	NEP (nW)
3 × 3	48	150 × 470	17.0 ± 0.4	0.95 ± 0.01
4 × 4	32	150 × 310	13.6 ± 0.2	0.87 ± 0.02
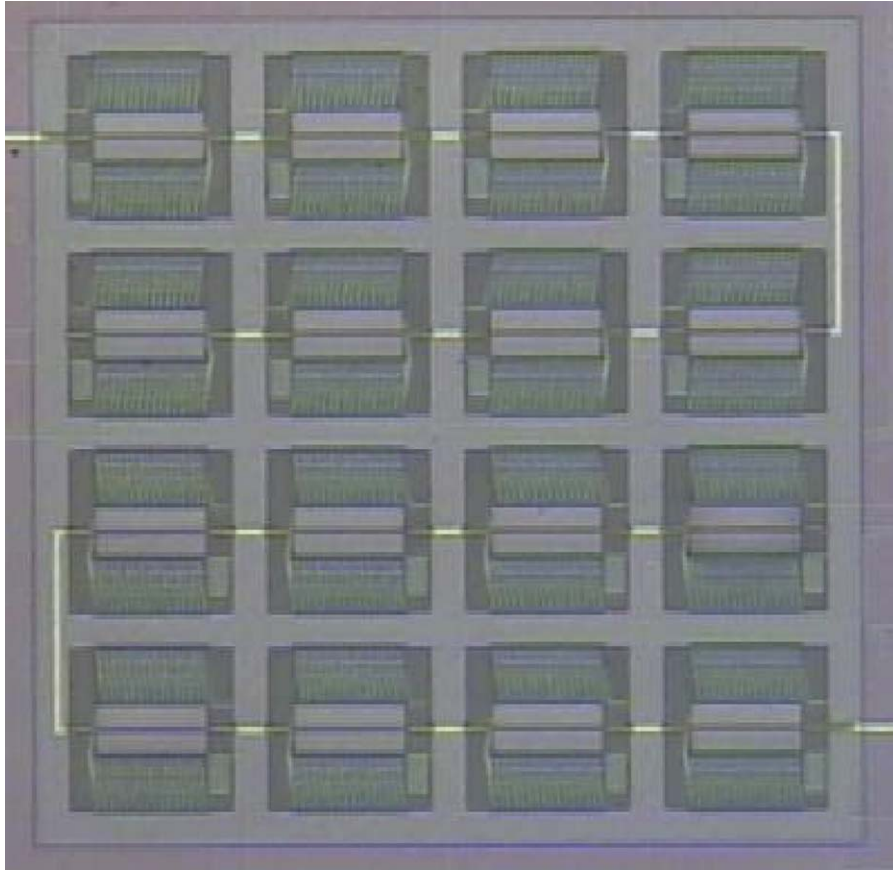
Fig. 6. Optical image of the fabricated 4×4 thermopile array.

The way the absorber element absorbs the radiation is taken into account using the measured absorption spectra. The same microscopy technique used in the measurement of the filter elements was used to obtain the reflectance and the transmittance spectrum. The absorbance spectra are obtained as the difference of the transmitted and reflected radiation.

2.6. Measurement method

The output voltages (9 or 16 channels depending on the array size) analyzed by the NDIR instrument have been obtained from a system simulation, using the different analytical models described before for each of the elements. The integration time for the measure of each channel is 1 s and the length of the optical path considered is 10 cm.

Combinations of the simulated gases (CO, CO_2 and methane) for concentrations in the 0–1000 ppm range are studied. Humidity and temperature changes are not taken into account in this first preliminary study.

3. Signal and data processing

Fig. 7(a) shows the different voltage responses variations produced for each gas at a concentration of 1000 ppm. Each array element has a different response for each gas shaping a distinc- tive voltage pattern. Carbon dioxide shows the highest responses of the threes substances and the typical voltage variations are around tens of micro volts. Also the PCA plot of the responses for simulations of the three gases (not mixture) for concentra- tions of 0, 500 and 1000 ppm (Fig. 8(a)) shows how different directions corresponding to the variation of each gas can be observed.

Calibration set is done taking five samples for each possible mixture of the three gases at four different concentrations (0, 100, 500 and 1000 ppm). Therefore, 320 data points ($4^3 = 64$ combinations and 5 points for each mixture $64.5 = 320$) are used. Reduction of this number of calibration points will be subject of a further study. Measurement errors have been evaluated using the root mean square error for prediction (RMSEP) definition:

$$\text{RMSEP} = \sqrt{\frac{\sum_{i=1}^{n}(\hat{y}_i - y_i)^2}{n}} \qquad (4)$$

where y_i is the real concentration, $\hat{y}_i$ the predicted concentra- tion and n the number of samples.

Instead of using the voltage output, we prefer a logarithmic transformation of the output. The rationale behind this trans- formation is to make variations of the source into an additive perturbation. This choice will become more evident in the Sec- tion 4 concerning drift compensation.
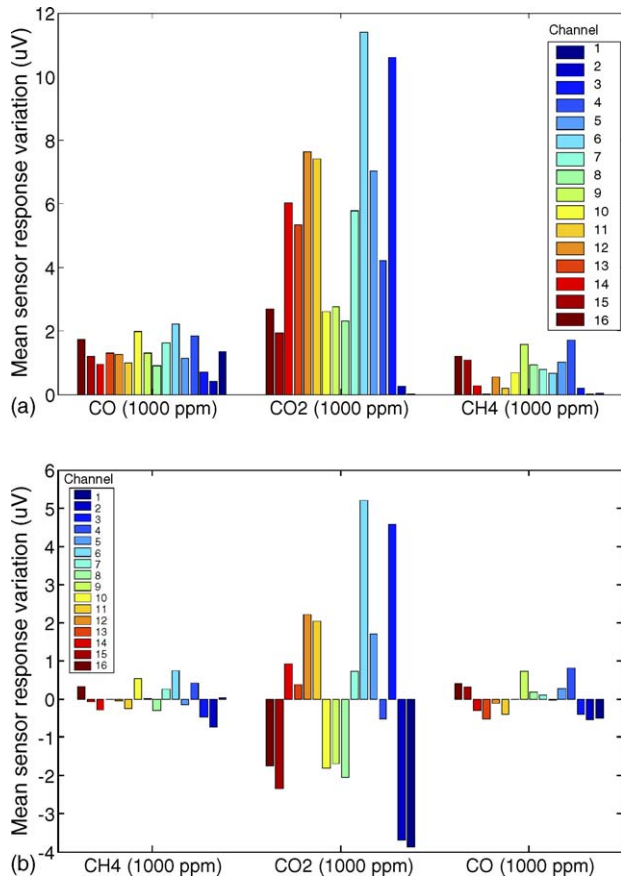
Fig. 7. (a) Variation of the responses of the array elements for the different gases. (b) Variation of responses for the gases with component correction.

Expression (5) shows how the effect of the variation of the infrared source is multiplicative:

$$V_{Thermopile} = P_{source} TR \qquad (5)$$

The output voltage of each element of the array $V_{Thermopile}$ is the product of the power emitted by the source P_{source}, the transmittance of the whole system T, including the optical elements and the gas transmittance, and the responsivity R of the thermopiles.

A model for each gas is built using Partial Least Square algorithm. Cross validation using two random subsets with the same number of samples is carried out to determine the complexity of the PLS model, this is, the number of latent variables.

Fig. 9 shows the results of the complexity optimisation of the models for a 4×4 array. CO and methane models require four latent variables while CO_2 requires a more complex model with six latent variables. CO_2 also shows the higher RMSEP for the calibration set. The high number of latent variables required for the three gases shows the non-linearity behaviour of the absorption process of the mixture since the expected number of latent variables is three (assuming perfect linearity). Regression models for 3×3 arrays need the same number of latent variables.

Once the model is built, a validation set is used to evaluate the model. This set is formed by 100 data points obtained setting the concentration of the mixture in a random way. Table 3 shows
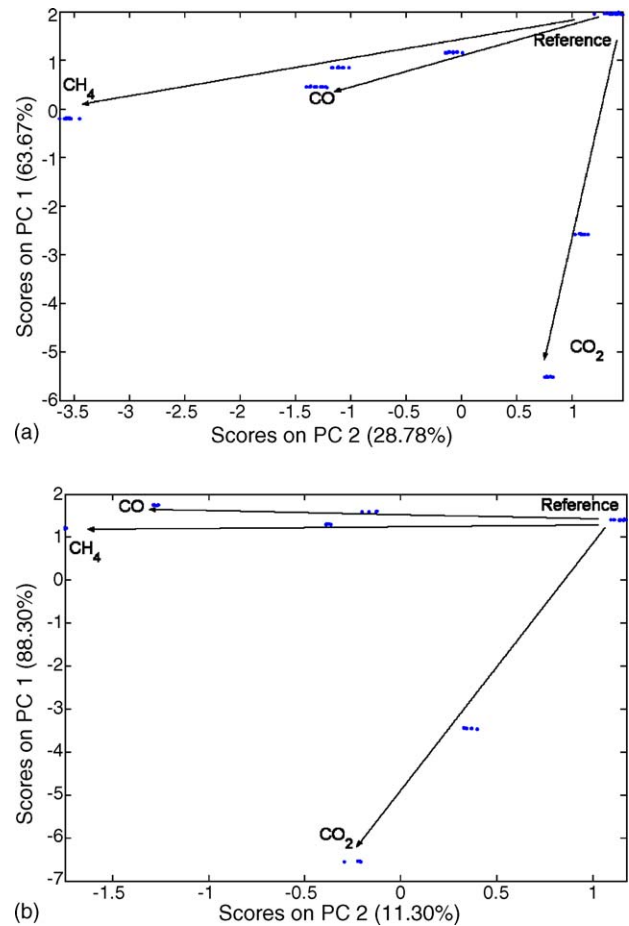
Fig. 8. (a) PCA plot of the no IR aged data. (b) PCA plot of IR aged data with component correction.
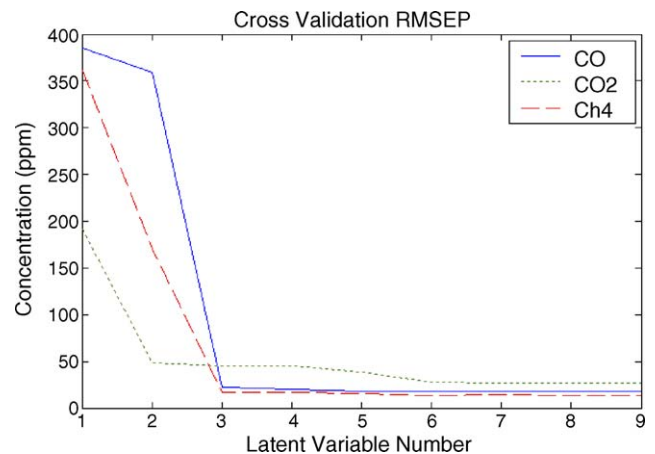
Fig. 9. Evolution of the RMSEP for the different number of latent variables.

Table 3
RMSEP for the validation set

Array size	RMSEP (ppm)			Latent variables		
	CO	CO_2	CH_4	CO	CO_2	CH_4
3×3	15	26	13	3	6	3
4×4	13	18	8	3	6	3

the obtained results for the validation set. A slightly increase of the RMSEP from those calculated for the calibration set is obtained shows the prediction behaviour for the different substances. Results in Table 3 show that the errors are lower for the 4×4 array, compared to the 3×3 array. This is more clear for CO_2 and CH_4, while is only slightly better for CO: these results are in the same range of errors that the obtained before for tuneable IR detectors [3].

Slight non-lineal effects of the response can be observed especially in the case of the CO_2. This could be related to the fact that CO_2 has the highest responses showing a more non-linear behaviour. The small values of the prediction error prove the feasibility to recover the real concentrations of the three gases using an array on non-selective filters.

4. Infrared source aging correction

As we said before, traditional NDIR instruments use a reference band without absorptions to eliminate the influence of the aging of the infrared source. This effect will be simulated like a homogeneous decrease of the power emitted for all wavelengths. In our case instead of using a reference band we use a component correction technique in order to remove this effect [8]. The idea is basically to make sensor patterns orthogonal to the drift direction.

First the loadings, p, and weights, w, correlated to the infrared source aging are calculated using the PLS regression algorithm. A set of 100 simulated data with a reference gas with a gradual decrease of the power emitted from the IR source from 100 to 80% is used. The variation of response caused by a source working at the 80% of the initial power emission is shown in Fig. 10. This is the pattern indicating the drift direction in the input space. A regression model with only one latent variable is enough to explain the drift direction due to the aging in the input space.

Then the response vectors matrix X is projected along this axis. This is done using the previous calculated loading and
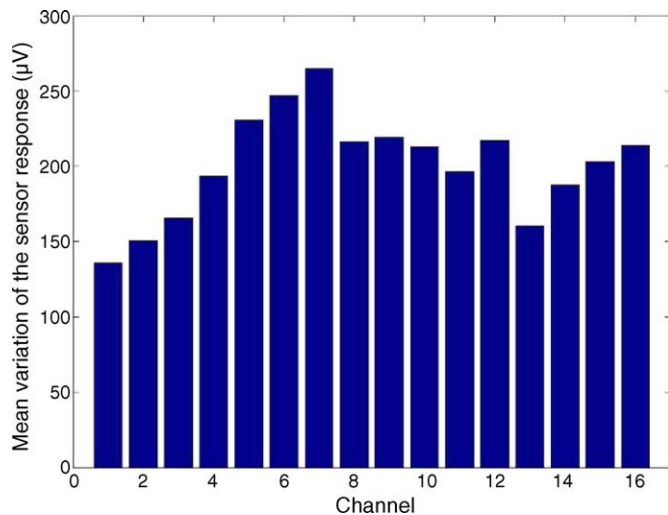
Fig. 10. Pattern of responses for an IR source emitting at the 80% of the full power, indicating the drift direction.
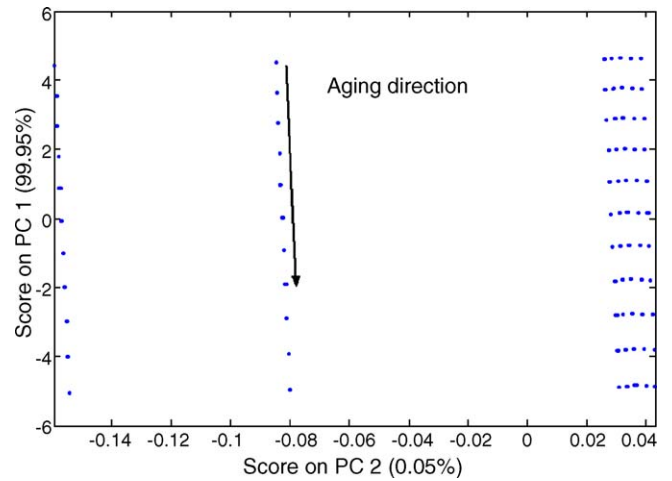
Fig. 11. PCA plot of the IR aged data.

weight:

$$t_{new} = Xw(p^T w)^{-1} \qquad (6)$$

The component-corrected matrix is calculated as:

$$X_{corrected} = X - t_{new} p^t \qquad (7)$$

In this way we project the data into the space that is orthogonal to the direction of the aging of the IR source.

We can see the effect of the drift in a data set of different concentrations (0, 500 and 1000 ppm) of the pure gases in the PCA plot in Fig. 11. The drift due to the aging effect has a clear direction that is the same for all the samples.

Fig. 7(b) shows the new gas characteristic patterns after component correction. They may be compared to the original ones in Fig. 7(a). New patterns orthogonal to the drift direction are shown in Fig. 10. Fig. 8(b) shows the variation of responses and the PCA plot of the dataset affected of the IR source aging with component correction. We can see how this technique not only removes the effect of the aging but also keeps basically the original information. We still have different voltage patterns, modified by the component correction, and different directions for each gas variation in the PCA plot can be observed.

The same calibration model explained in the last section is used with a validation set of 100 randomly distributed points with IR source powers between the 100% and the 80%, of the nominal one. The RMSEP obtained for the different array sizes with and without the component corrections can be seen in Table 4. Results of the regression without the component

Table 4
RMSEP for the validation set with aging effects

Array size	Component correction	RMSEP (ppm)		
		CO	CO_2	CH_4
3×3	No	6×10^3	1.6×10^5	1.2×10^5
3×3	Yes	15	26	14
4×4	No	2.2×10^4	1.1×10^4	5.3×10^5
4×4	Yes	14	18	10

correction show extremely high prediction errors. These results show how a variation of the source emitted power makes the gas prediction impossible without a new calibration. However, component correction completely eliminates the influence of the IR source aging in the prediction errors as it can be noted in the low increase of the prediction errors, avoiding the need of recalibration. Tables 3 and 4 show that the error values are basically the same after component correction when compared with the original errors with the source at 100% power. These results show that in this case component correction does not lead to a degradation of the system accuracy.

5. Conclusions

The simulation shows the feasibility of measuring gas concentrations in the infrared by using a set of non-selective filters. The advantage of this configuration is that in principle it should be possible to approach the measurement of any gas with absorption bands in the infrared, with a moderate number of filters. In this work this have been tested by system modelling for the prediction of concentrations for mixtures of CO, CO_2 and methane in the range of 0–1000 ppm. Measurement errors have been found in the range of tens of ppm. A larger optical path would be required to reduce this value.

An important point is the significant decrease of the RMSEP was obtained by increasing the number of detectors in the array. However, we believe that this increase will saturate fast if the total array size keeps constant since the detectivity of the individual detectors will decrease with the number of elements in the array.

Component correction techniques have been successfully used to reduce the effect of the IR source aging, keeping system accuracy unaffected. Thus, no reference band filter has to be used to eliminate the age effects of the infrared source, in our proposed configuration.

Future work involves the test of the system to validate the results of the present model.

Acknowledgment

References

[1] Infrared Methods for Gaseous Measurements, New York, Marcel Dekker, Inc., 1985.

[2] G. Lammel, S. Schweizer, S. Schiesser, P. Renaud, Tunable optical filter of porous silicon as key component for a MEMS spectrometer, J. Microelectromech. Syst. 11 (2002) 815–828.

[3] C. Calaza, E. Meca, S. Marco, M. Moreno, J. Samitier, L. Fonseca, I. Gracia, C. Cane, Assessment of the final metrological characteristics of a MOEMS-based NDIR spectrometer through system modeling and data processing, IEEE Sens. J. 3 (2003) 587–594.

[4] C. Calaza, L. Fonseca, M. Moreno, S. Marco, C. Cane, I. Gracia, A surface micromachining process for the development of a medium-infrared tuneable Fabry-Perot interferometer, Sens. Actuators A: Phys. 113 (2004) 39–47.

[5] R.E. Baren, M.E. Parrish, K.H. Shafer, C.N. Harward, S. Quan, D.D. Nelson, J.B. McManus, M.S. Zahniser, Quad quantum cascade laser spectrometer with dual gas cells for the simultaneous analysis of mainstream and sidestream cigarette smoke, Spectrochim. Acta Part A: Mol. Biomol. Spectrosc. 60 (2004) 3437–3447.

[6] D.A. Andrews, T.A. King, Gas analysis using an infrared source with temporally varying temperature, Meas. Sci. Technol. 12 (2001) 1263–1269.

[7] The HITRAN database: High-Resolution, Transmission Molecular Absorption Database.

[8] T. Artursson, T. Eklov, I. Lundstrom, P. Martensson, M. Sjostrom, M. Holmberg, Drift correction for gas sensors using multivariate methods, J. Chemom. 14 (2000) 711–723.

[9] L.S. Rothman, A. Barbe, D.C. Benner, L.R. Brown, C. Camy-Peyret, M.R. Carleer, K. Chance, C. Clerbaux, V. Dana, V.M. Devi, A. Fayt, J.M. Flaud, R.R. Gamache, A. Goldman, D. Jacquemart, K.W. Jucks, W.J. Lafferty, J.Y. Mandin, S.T. Massie, V. Nemtchinov, D.A. Newnham, A. Perrin, C.P. Rinsland, J. Schroeder, K.M. Smith, M.A.H. Smith, K. Tang, R.A. Toth, J. Vander Auwera, P. Varanasi, K. Yoshino, The HITRAN molecular spectroscopic database: edition of 2000 including updates through 2001, J. Quant. Spectrosc. Radiat. Transfer 82 (2003) 5–44.

[10] J. Muller, U. Dillner, Thermal microsensors: their bases, principles and applications—special issue, Sens. Mater. 8 (1996) U4–U6.

[11] C. Calaza, L. Fonseca, M. Moreno, S. Marco, C. Cane, I. Gracia, Design and fabrication of CMOS compatible thermoelectric IR sensors for gas analysing system, Actas de la conferencia de Dispositivos Electrónicos (2001) 45–49.

[12] C. Calaza, M. Moreno, S. Marco, L. Fonseca, C. Cane, I. Gracia, J.Y. Fourniols, G. Soto-Romero, F. Bony, Design, fabrication and characterisation of CMOS compatible thermoelectric IR sensors for a gas analysis application, presented at IRS2, Erfut, Germany, 2002.

[13] A.D. Oliver, K.D. Wise, A 1024-element bulk-micromachined thermopile infrared imaging array, Sens. Actuators A: Phys. 73 (1999) 222–231.

Biographies

R. Rubio was born in Madrid, Spain on August 14, 1978. He received his BS degree in physics from the University of Barcelona in 2001. In 2002, he joined the Microelectronics National Center, where he is pursuing his PhD. His main research activities are related not only to the infra-red sensing technologies but also with the pattern recognition techniques.

J. Santander was born in Terrassa, Spain, in 1966. He received the BS and PhD degrees in physics from the Autonomous University of Barcelona, Spain, in 1989 and 1996, respectively. He is currently working at the Microelectronics National Center in Barcelona, as responsible for the electrical characterization laboratory, developing solutions for the electrical parametric characterization of different microelectronic technologies (CMOS, MCM, sensors, microsystems) using mainly test structures. His main research areas are related to microsystems and gas sensing applications.

J. Fonollosa was born in Barcelona, in 1980. He received a degree in physics from University of Barcelona in 2002. He started his PhD studies in 2004. His research is focused on low-voltage amplification and on diffractive lenses design.

L. Fonseca was born in Barcelona, Spain, on February 17, 1966. He received his BS and PhD degrees in physics from the Autonomous University of Barcelona in 1988 and 1992, respectively. In 1989, he joined the National Center of Microelectronics as a Post-graduate student, working till 1992 on the growth and characterization of thin dielectric films for VLSI and ULSI applications. After this first research period, he has worked as Process Engineer, currently leading the diffusion and deposition areas of the CNM production facilities.

This technological background has allowed him to undertake research tasks in the general field of MEMS fabrication, and lately in gas sensing applications.

I. Gràcia received the PhD degree in physics in 1993 from the Autonomous University of Barcelona, Spain, working on chemical sensors. She joined the National Microelectronics Center (CNM) working on photolithography. She is currently working in the Microsystems department in the gas sensing field.

C. Cané received the BSc degree in telecommunications engineering in 1986 and the PhD degree in 1989 from the Universitat Politécnica de Catalunya in Barcelona, Spain. Since 1990, he is a permanent researcher at the National Microelectronics Center (CNM) in Barcelona. He is currently working in the fields of sensors and microsystems and their compatibility with standard CMOS technologies.

M. Moreno was born in Barcelona, Spain. He received the degree in physics in 1989 from the University of Barcelona (UB), and the PhD degree in sciences in 1995 from the Polytechnic University of Catalonia (UPC), Spain. He has been Associate Professor in the Electronics Department, UB, since 1997. He is involved in the design and test of infra-red thermopile detectors and the test of integrated optical devices in silicon technology for DWDM applications. Other fields of interest include arrays of CMOS integrated photodetectors for imaging, rangefinders, and CMOS optical receivers for fiber optical communications.

S. Marco is Associate Professor at the Departament d'Electronica of Universitat de Barcelona since 1995. He received the degree in physics from the Universitat de Barcelona in 1988. In 1993, he received his PhD (honor award) degree from the Departament de Fi'sica Aplicada i Electrònica, Universitat de Barcelona, for the development of a novel silicon sensor for in vivo measurements of the blood pressure. In 1994, he was visiting professor at the Universita di Roma 'Tor Vergata' working in Data Processing for Artificial Olfaction. He has published about 40 papers in scientific journals and books, as well as more than 80 conference papers. His current research interests are two-fold: chemical instrumentation based on intelligent signal processing and microsystem modeling.

Design and fabrication of silicon-based mid infrared multi-lenses for gas sensing applications

J. Fonollosa [a,*], R. Rubio [b], S. Hartwig [c], S. Marco [a], J. Santander [b],
L. Fonseca [b,1], J. Wöllenstein [c,2], M. Moreno [a]

[a] *Department of Electronics, Barcelona University, Barcelona, Spain*
[b] *Centro Nacional de Microelectrónica, CNM-IMB (CSIC), Barcelona, Spain*
[c] *Fraunhofer Insitute for Physical Measurement Techniques, Freiburg, Germany*

Abstract

To improve the sensitivity of a non-dispersive infrared optical gas sensor, diffractive Fresnel lenses have been designed, fabricated with silicon microtechnologies, and tested. The target gases (for fruit storage applications) determine the wavelengths for the lens design: 10.6 μm, 9.7 μm, 3.5 μm, and 3.9 μm for ethylene, ammonia, ethanol, and the reference band, respectively. Four lenses are fabricated on the same silicon substrate in a combined multi-lens. In order to reduce the number of photolithographic steps, a new design based on sharing up to sixteen quantization steps by the four lenses is done. Due to the high reflection losses at the silicon–air surfaces, some multi-lenses have been coated with zinc sulphide antireflection layers. The difference between the measured and the target focal length is smaller than 5%. Alignment fixtures have been fabricated to assemble the Fresnel lenses chip on the detector lid in the correct orientation.
© 2007 Elsevier B.V. All rights reserved.

Keywords: Fresnel lenses; Optical gas sensor; Microoptics; Silicon technology; Ethylene; Non-dispersive infrared gas sensor

1. Introduction

In recent years, microsystems technologies have played a central role in spectrometry with the aim of taking advantages of the integration possibilities [1]. Several examples of integration of radiation detectors in microsystem technology can be found in spectroscopy instruments [2–4]. In particular, the use of micromachined thermopile detectors is widespread for infrared (IR) spectrometry for gas detection [5].

Traditional solid state gas sensors are limited by a short lifetime, cross sensitivity to other gases, risk of fatal errors when overexposed in high gas concentrations, and output dependency of environmental conditions [6].

Infrared optical gas sensors are selective and stable instruments based on the attenuation of the incident radiation at specific absorption bands. The Lambert-Beer equation relates the quantity of radiation absorbed to the optical path length, the gas concentration, and the absorption coefficient; which is a specific function of the wavelength for each gas.

Usually, optical gas sensors consist of an IR-emitter, an absorption cell that contains the gas to be measured, and an IR-detector where the transmitted radiation is collected. Non-dispersive infrared (NDIR) gas sensors use one specific detector for each gas to measure. Therefore, to select the suitable wavelength for each gas, a specific optical filter must be placed upon the IR-detector set.

IR thermal emitters have also been proposed as a component of a NDIR system, using a combination of surface and bulk micromachining for its fabrication [7,8]. New materials are still proposed in literature in order to increase thermopiles sensitivity and extend their operation in harsh environments [9]. Currently, multi-channel IR thermopile detector featuring integrated optical filters for gas sensing exist in the market [10].

Since NDIR systems typically exhibit lower sensitivity than other technologies, low gas concentrations might be undetectable in these systems. In order to focus the maximum radiation onto the detector, i.e. to increase the sensor signal, and

* Corresponding author. Tel.: +34 93 403 9146.
E-mail addresses: jfonollosa@el.ub.es (J. Fonollosa), luis.fonseca@cnm.es (L. Fonseca), juergen.woellenstein@ipm.fraunhofer.de (J. Wöllenstein).
[1] Tel.: +34 93 594 7700.
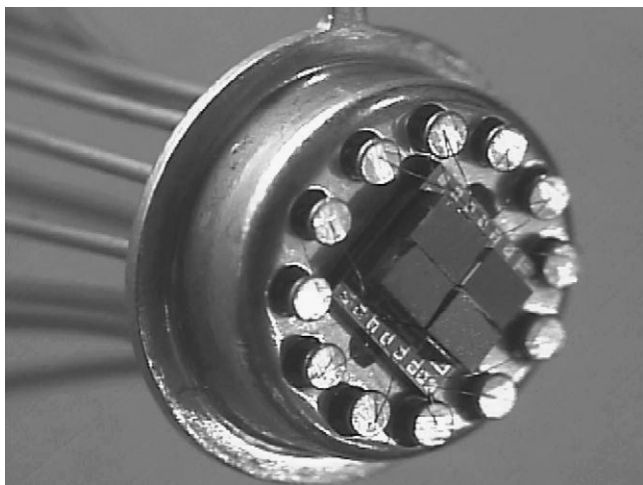[2] Tel.: +49 761 8857 134.

Fig. 1. Fabricated module with optical filters above the thermopile array.

improve the global efficiency of the system, a focusing module to optimize the optical part will be desirable.

The authors already presented a multi-channel NDIR system, where a thermal emitter [11] and a bulk micromachined four-fold thermopile array [12] were used. The corresponding optical filter has been attached above each thermopile using flip-chip techniques [13]. Fig. 1 shows the optical filters above the thermopiles. The goal of the designed optical module in this work is to optimize the detection unit and increase the sensitivity of the whole system.

Diffractive lenses are compatible with the planar nature of silicon microtechnology and silicon is transparent in the IR range of interest. Since silicon is a suitable material to be used as a lens substrate, typical advantages of silicon technology such as reliability, mass production, and equipment availability can be made compatible with a diffractive lens. Diffractive lenses are thinner (less radiation is absorbed in the substrate) and lighter (less material is needed) than refractive lenses.

Single-channel silicon-based thermopile with integrated diffractive lens can be found in the market (HTIA-E from Heimann Sensors, ST-60 from Dexter Research). However, no optical filter is integrated in those detectors and thus the transmitted radiation is determined by the lens. Typically, the lens transmission peaks at 9 μm, with an effective operating bandwidth from 7 μm to 14 μm. Therefore, such a device cannot be used as a detector module for a NDIR system. Moreover, we are interested in a four-channel thermopile. As far as the authors' knowledge, no lens array has been integrated in a multi-channel detector unit with thermopiles and optical filters previously.

In this work we propose a multi-lens array to be assembled in a multi-channel IR-detector to optimize its detectivity. The aim of this work is to continue the proposed assembly in the literature building a compact multi-channel detection unit with the IR-detectors, the optical filters, and the corresponding lenses for each channel.

The present work is included in the development of compact ethylene-monitoring systems to control fruit status in today's store-houses. Low ethylene concentrations are produced by the fruit itself and are indicative of its ripeness [14]. On other occa-

sions ethylene is externally added when ripeness or degreening of the product must be promoted. Anyway, other gas species might be present in the store-house atmosphere and could interfere with the sensor response. For instance, ethanol is produced as a result of fruit stress and ammonia may present due to a leakage from the cooling system. A multi-channel device is then a must for such applications.

In Section 2 we present a study of Fresnel lenses (FL) efficiency, as a function of the technological constrains and the maximum number of topographic steps. The design, fabrication and test of a single FL and of a four lens array are presented, respectively, in Sections 3 and 4. In Section 5 we introduce antireflection coating, and in Section 6 the final device integration.

2. Study of Fresnel lenses efficiency

Diffractive silicon-based FL approach is chosen to be placed at the top of the detector package. A FL consists of a series of concentric rings with a given tapered shape, whose width decreases with the distance to the center. Each ring is ideally shaped in such a way that all the lens points introduce a change of the optical path that produces a constructive interference at the lens focal point.

The topographical lens design depends on the wavelength of the radiation it should focus, λ, the difference between the refraction index of the chosen material and of the medium, Δn, the distance to the center, r, and the required focal length f. Eq. (1) relates the ideal phase shift introduced at each point as a function of these parameters and an arbitrary phase φ_0 [15]. The lens profile is defined by the etched depth, d, in each point (Eq. (2)) and the radius of the Nth ring (Eq. (3))

$$\varphi(r) = \text{mod}\left[\frac{2\pi}{\lambda}(\sqrt{f^2 + r^2} - f) - \varphi_0, 2\pi\right] \quad (1)$$

$$d(r) = \frac{\phi(r)}{2\pi}\frac{\lambda}{\Delta n} \quad (2)$$

$$R_N = \left[N\lambda f\left(2 + \frac{N\lambda}{f}\right)\right]^{1/2} \quad (3)$$

The chosen wavelengths for the gases of interest determine the FL design. The multi-lens design is carried out for 10.6 μm, 9.7 μm, 3.5 μm, and 3.9 μm wavelengths, which, respectively, correspond to ethylene, ammonia, ethanol absorption bands, and the reference band. Two other parameters that complete the FL design are the lens diameter and the focal length, which are both defined by the detector package geometry.
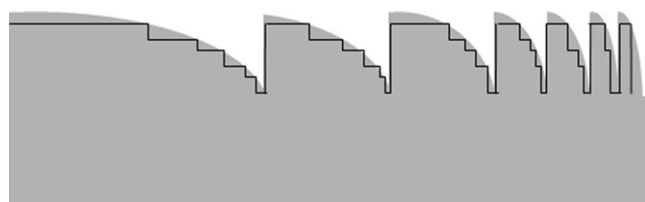

Fig. 2. Ideal FL profile, and the corresponding quantized profile.

Due to technological constraints of silicon planar microtechnology, it is necessary to reproduce the theoretical ring profile as a discrete number of flat steps. The Reactive Ion Etching (RIE) technique has been chosen to etch the needed profile. In Fig. 2 the ideal profile and the corresponding quantized profile of a FL are shown.

The lens efficiency can be evaluated as a function of the designed lens profile [15–17]. The higher the number of steps, the higher the efficiency. However, technological constraints when using contact photolithography tools limit the minimum feature size to 2–3 μm. This implies that for the more demanding topographically designs (the grating period is smaller for shorter wavelengths and focal lengths) the outer rings cannot meet this criterion, the number of steps must be reduced for them, and the lens efficiency will decrease somewhat. In this case, the global lens efficiency can be calculated as the weighting sum of the present efficiencies along the lens. In Eq. (4) the total lens efficiency is computed, where γ_L is the part of the total area where L quantization steps are used [15].

$$\eta_{\text{total}} = \sum_{i=L\ \min}^{i=L\ \max} \eta_{L,i}\gamma_{L,i} \tag{4}$$

The complex amplitude transmittance $g(x,y)$ has radial symmetry and is periodic in r^2. The intensity of the diffracted wave is given by the complex modulus of the Fourier coefficients of $g(r^2)$. The Fourier coefficients A_n of $g(r^2)$ are computed in Eq. (5) [17]. For multilevel phase lenses, the complex amplitude transmittance can be expressed as the sum of the contribution of each step. The Fourier coefficients for a lens with L equally distributed steps can be expressed as shown in Eq. (6). The corresponding efficiency of the diffracted wave in the first focal plane can be calculated from Eq. (6) and is presented in Eq. (7).

$$A_n = \frac{1}{\lambda f}\int_0^{\lambda f} g(r^2)\exp(-2\pi i n r^2)d(r^2) \tag{5}$$

$$A_n = \sum_{k=0}^{K=L-1}\left[\int_{\lambda f K/L}^{\lambda f(K+1)/L}\exp\left(\frac{-2\pi i k}{L}-2\pi i n r^2\right)\frac{d(r^2)}{\lambda f}\right] \tag{6}$$

$$\eta_L = |A_{-1}|^2 = \left[\frac{\sin(\pi/L)}{\pi/L}\right]^2 \tag{7}$$

3. Single Fresnel lens

3.1. Design

The fabrication of the desired staircase lens profile would in principle require the combination of photolithographic processes for spatially defining each step and RIE processes to give each step its proper depth. As it has been said, the more numerous the steps, the more efficient the lens will be. However, cost and process complexity limit the number of photolithographic
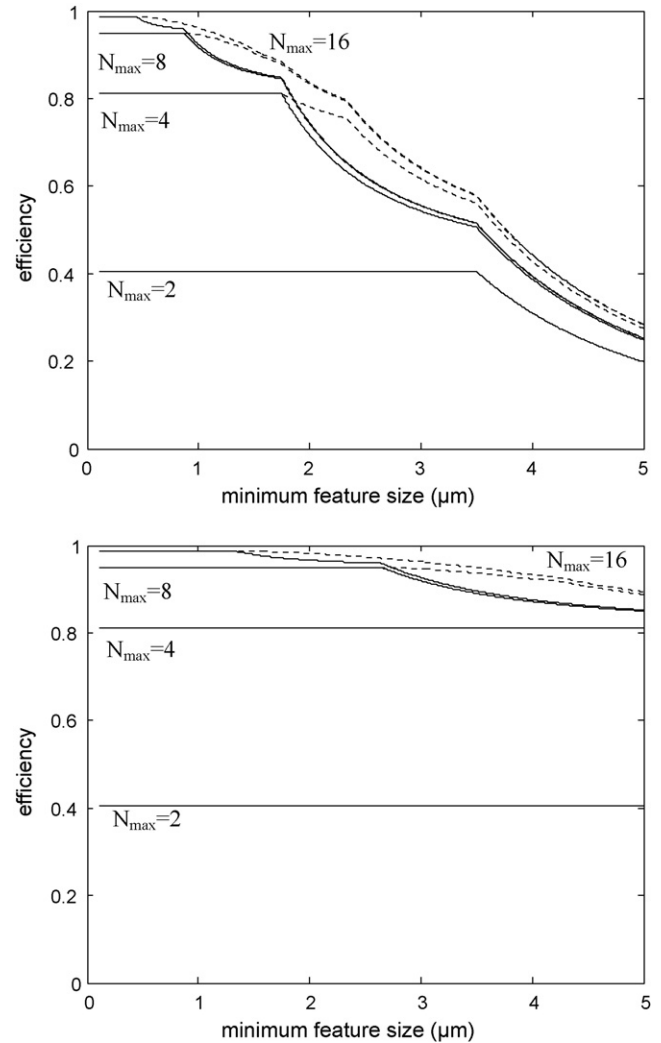
Fig. 3. Calculated lens efficiency for the most costly alternative (dashed line) and for the binary combination of levels (solid line). $f = 4$ mm, $D = 4$ mm, and $l = 3.5\ \mu$m (top) and $l = 10.6\ \mu$m (bottom).

masks which can be used. A cost effective way to face this situation is to binary combine m photolithographic levels, choosing for each one the proper etch depth to achieve a total of $N = 2^m$ quantization steps evenly distributed in depth for each ring.

The more costly and optically efficient and flexible alternative one can think uses as many flat steps as possible along the lens surface within the dimensional constrains of each ring. Less photolithographic masks are needed for the alternative based on a binary combination of photolithographic levels, but the lens efficiency is earlier affected when the technological constrains force to reduce the number of steps. From Eq. (7), the efficiency loss for both approaches as a function of the minimum feature size and the maximum number of steps can be simulated (Fig. 3). Since the grating period is larger as the wavelength and the focal length increase (Eq. (3)), the technological constrains become more critical for shorter wavelength (Fig. 3).

As shown in Fig. 3, the lens efficiency is only slightly worse when the lens profile is reproduced by the binary combination of steps, which has significantly less complexity design and cost

fabrication. Therefore, this alternative is chosen to reproduce the FL profile [18].

3.2. Fabrication

As first prototypes, several binary FL of different topological complexity have been fabricated. Two level FL (also known as binary FL, not to be confused with the approach of binary combining the photolithographical masks), using only one photolithographic mask, and eight level FL, using up to three photolithographic masks, have been designed, fabricated, and tested.

For a binary FL (BFL), the etching depth, d, equals d_π (Eq. (8)). Therefore, the required etching depth for a BFL at 10.6 μm wavelength can be calculated for a silicon substrate ($n = 3.42$) $d_\pi = 2.2$ μm. The proper photolithographic mask has been designed for BFL for 10.6 μm wavelength; 4 mm, 1 cm, 2 cm, 5 cm, and 10 cm focal length; and 4 mm and 8 mm diameter.

$$d_\pi = \frac{\lambda}{2\,\Delta n} \tag{8}$$

In addition, some 4 mm diameter, 4 mm and 1 cm focal length and 3.5 μm and 10.6 μm wavelength FLs have been designed and fabricated in silicon using three photolithographic mask levels. An eight steps quantization profile can be achieved in this way. However, photolithographical constrains limit the clearance between features and the step number must be reduced to four or even two in the outer regions of the more demanding designs.

3.3. Test of the single Fresnel lenses

Using a confocal microscope the corresponding profiles have been measured, showing that with the proper etch associated to each mask level (d, 2d, 4d etch depths) up to eight evenly spaced steps are obtained with the three photolithographic masks. The measured profiles of a 10.6 μm wavelength and 1 cm focal length BFL and a 10.6 μm wavelength and 4 mm focal length eight levels FL are, respectively, presented in Figs. 4 and 5.

In order to test the fabricated lenses, the focal length and the pattern radiation in some planes have been measured. The experimental set-up is based on an IR parallel beam (from a Quantum Cascade Laser with an emission line at 10.3 μm),
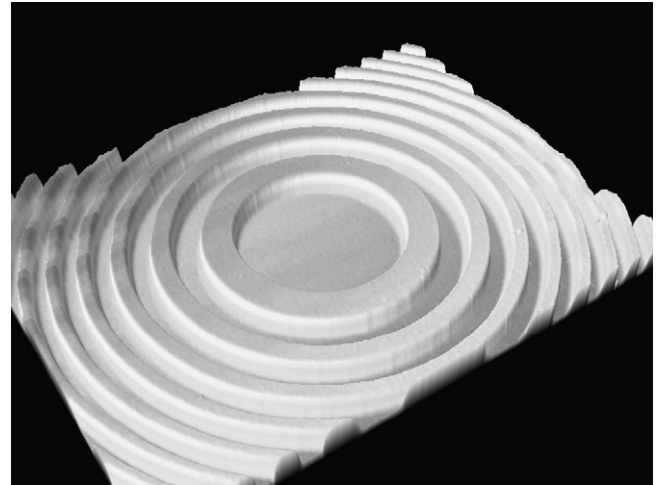
Fig. 4. Measured BFL profile using a confocal microscope.

which impinges on the FL, and then on an IR pyrodetector, with a limited sensitive area. Therefore, the focal length is determined when the detector response is maximum. Table 1 shows the measured and the designed focal lengths.

In Fig. 6, the pyrodetector response for a BFL and for an eight levels FL, for different focal lengths, are presented versus the distance to the focal plane. The maximum acquired value corresponds to the focal plane, and it gradually decreases when the analyzed plane is further off the focal plane. The lens transmittance increases when going from two to eight quantization steps of the lens profile.

The spot size is defined as the region where the irradiance of the beam, on either side of the optical axis, has decreased $1/e^2$ of its value at the center of the beam [19]. Slightly shifting in a controlled way the IR-detector through the plane, the pattern radiation can be measured (as shown in Fig. 7 for one single lens) and spot sizes in the vicinity of 100 μm estimated.

Since the measured spot size at the focal plane is smaller than our typical thermopile absorber size (350 μm × 350 μm) the quality of the tested FL is enough to focus all the IR radiation on the absorber and maximize the thermopile response. The tolerance of the lens-detector assembly is given by the region where the spot size is smaller than the absorber size. Fig. 8 shows that the focus depth is quite sharp, thus the lens position respect the detector must be highly controlled. Anyway, in real working conditions, the IR thermal emitter spot might be

Table 1
Measured focal lengths compared to the design values for single lenses of different complexity

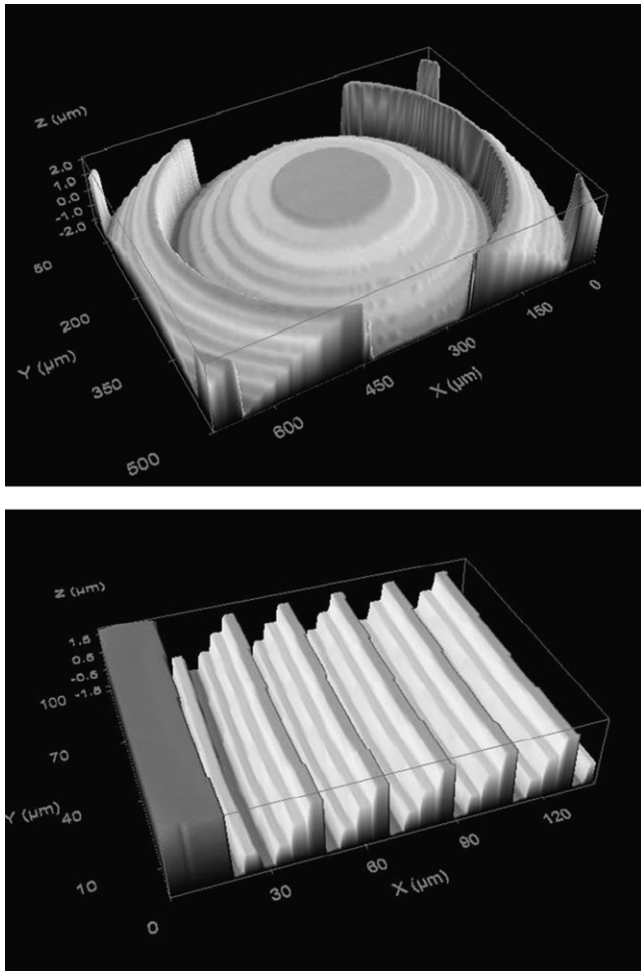| $\lambda = 10.6$ μm	Binary		8-FL
f_{design} (mm)	$D = 4$ mm, $f_{measured}$ (mm)	$D = 8$ mm, $f_{measured}$ (mm)	$D = 4$ mm, $f_{measured}$ (mm)
4	3.9	4.4	3.9
10	10.1	9.6	10.3
20	20.0	19.8	
50	48.5	49.5	
100	99.5	97.5	

Fig. 5. Measured eight level lens profile in the central region (top) and in the outer region (bottom), where spatial resolution of the photolithographical process limits the maximum number of topographical steps available.

much larger than the test laser and might entail a not so critical assembly.

4. Four-lens array

4.1. Design

For our gas sensing application, four FLs working at different wavelengths are needed. Since each FL needs a specific set of etching depths (wavelength dependent), 12 different photolithographic masks would be needed to reproduce a FL multi-lens, with a binary combination of 3 masks for each sublens.

In order to save some photolithographic processes and to assemble the four required lenses in the same substrate, a new design based on using a binary combination of 4 masks for all the lenses is considered. The four corresponding silicon etches have been designed for the 10.6 μm wavelength FL, reaching a depth up to 3.75 μm. Hence the available levels for the others FLs are fixed and they have been used as the best approximation to reproduce the ideal profile of each lens. This approach secures at least 6 or 8 levels for the shorter wavelength lenses.
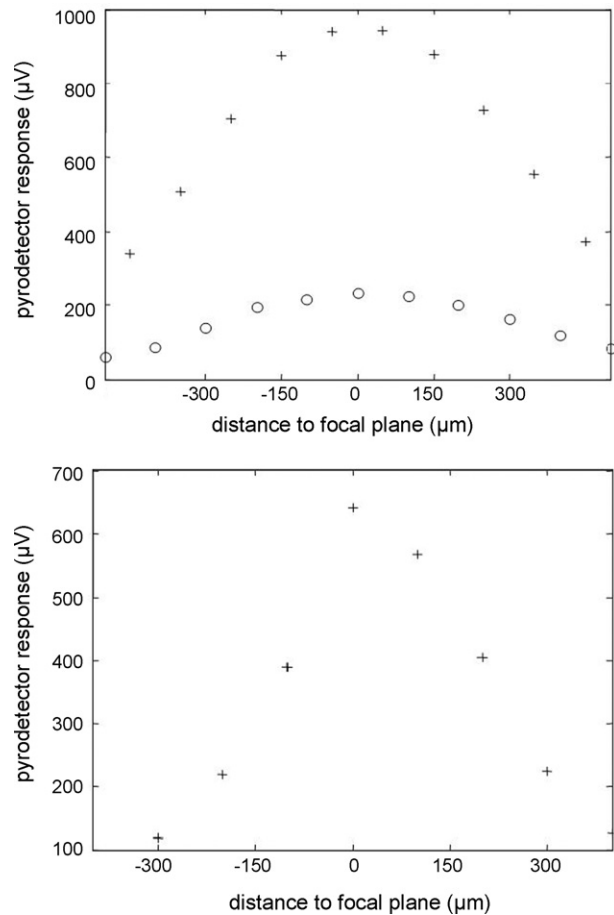
Fig. 6. Pyrodetector response for a $D = 4$ mm and $l = 10.6$ mm FL. Top: $f = 1$ cm BFL (circle) and eight levels FL (cross). Bottom: $f = 4$ mm eight levels FL.

A comparison of the lens efficiency, when three photolithographic masks are devoted specifically for each lens (twelve in total) and when four photolithographic masks are devoted for all the four lenses is shown in Table 2. Since the levels of the resulting FL are not evenly distributed, the lens efficiency must
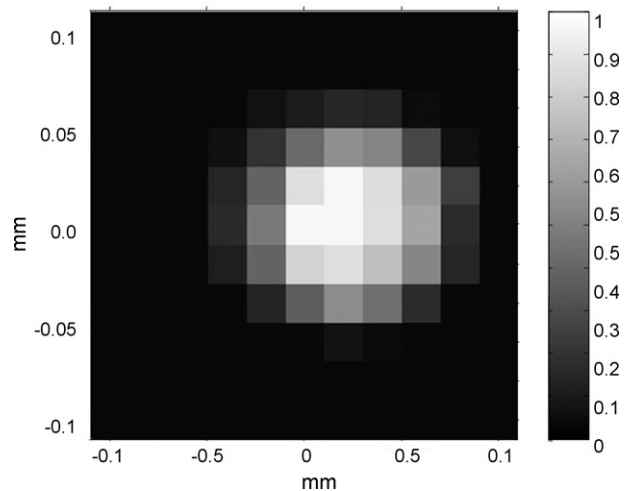
Fig. 7. Measured radiation pattern for an eight level FL at the focal plane. $D = 4$ mm, $f = 4$ mm, $l = 10.6$ μm. Normalized data, linear gray-level coding.
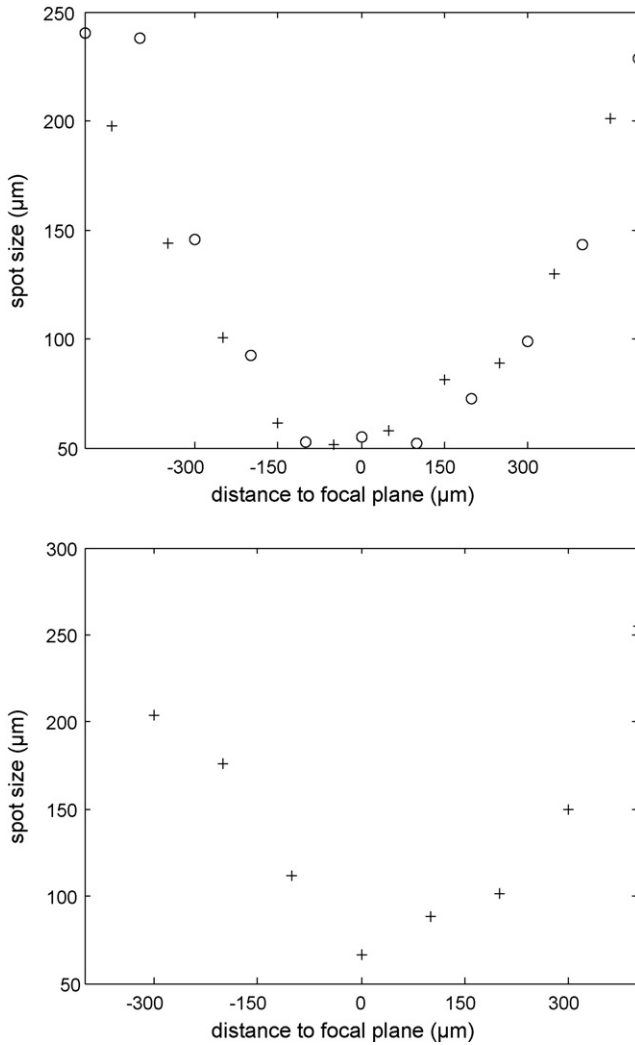
Fig. 8. Estimated spot size (radius) for a $D = 4$ mm and $l = 10.6$ mm FL. Top: $f = 1$ cm BFL (circle) and eight levels FL (cross). Bottom: $f = 4$ mm eight levels FL.

be computed from Eq. (5). Table 2 shows that the lens efficiency does not decrease dramatically when four photolithographic masks are shared by all sublenses.

4.2. Fabrication

A batch of multi-lenses following the new described design, limiting the feature size to 1.2 μm, has been fabricated. Fig. 9 shows an image of the substrate with the four FL and Fig. 10 shows the central region of the corresponding FL. To alleviate to

Table 2
Theoretical FL efficiency. $f = 6.7$ mm, 1.2 μm minimum feature size, and $D = 4$ mm

	3 masks devoted for each lens	4 masks devoted for all the lenses
$\lambda = 10.6$ μm	0.950	0.987
$\lambda = 9.7$ μm	0.950	0.987
$\lambda = 3.9$ μm	0.950	0.891
$\lambda = 3.5$ μm	0.950	0.863
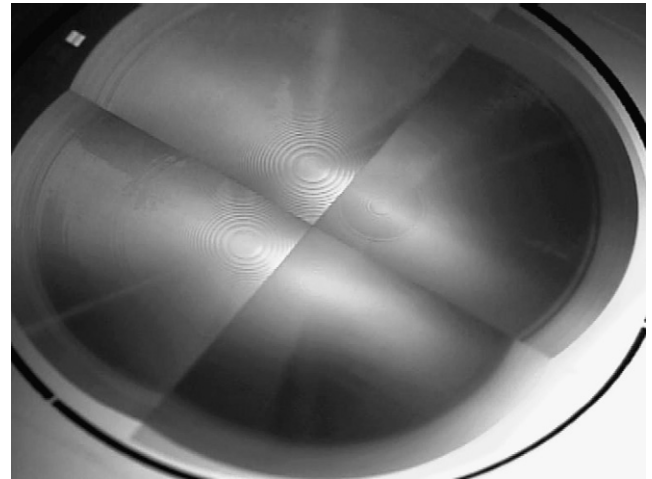
Fig. 9. Fabricated 4 FL-array using 4 photolithographic masks.

some extent the photolithograpical constrains, a stepper has been used for the multi-lens fabrication instead of a contact aligner. A minimum feature around 1 μm is assumed.

4.3. Test

The focal length of each lens of the fabricated multi-lens array has been measured. With that purpose, an IR-emitter with the appropriate optical filter to select the desired wavelength and a liquid nitrogen cooled IR-detector have been used. Table 3 shows that the fabricated FL-array is suitable for the detector module since the measured focal lengths for the four lenses are homogeneous and the error respect the target focal length is less than 0.3 mm.

5. Antireflection coatings

Reflection losses at the surfaces of the FL worsen the lens efficiency. Reflection is from the front side as well as the back side. Eq. (9) shows the combined reflection coefficient for this case as a function of the refraction indexes of the medium and the substrate. The high refractive index of silicon ($n_{\text{silicon}} = 3.42$, at 10 μm wavelength) implies a radiation loss of 46%.

$$R_{\text{total}} = \frac{2R}{1+R} = \frac{(n_{\text{silicon}} - n_{\text{air}})^2}{n_{\text{silicon}}^2 + n_{\text{air}}^2} = 0.46 \tag{9}$$

Antireflection (AR) coatings have been used to reduce the effect of the reflection losses. Typical silicon related materials such as SiO_2 or Si_3N_4 are not good candidates for the whole wavelength region of interest because they exhibit important absorption lines

Table 3
Measured focal length for each lens of the multi-lens array

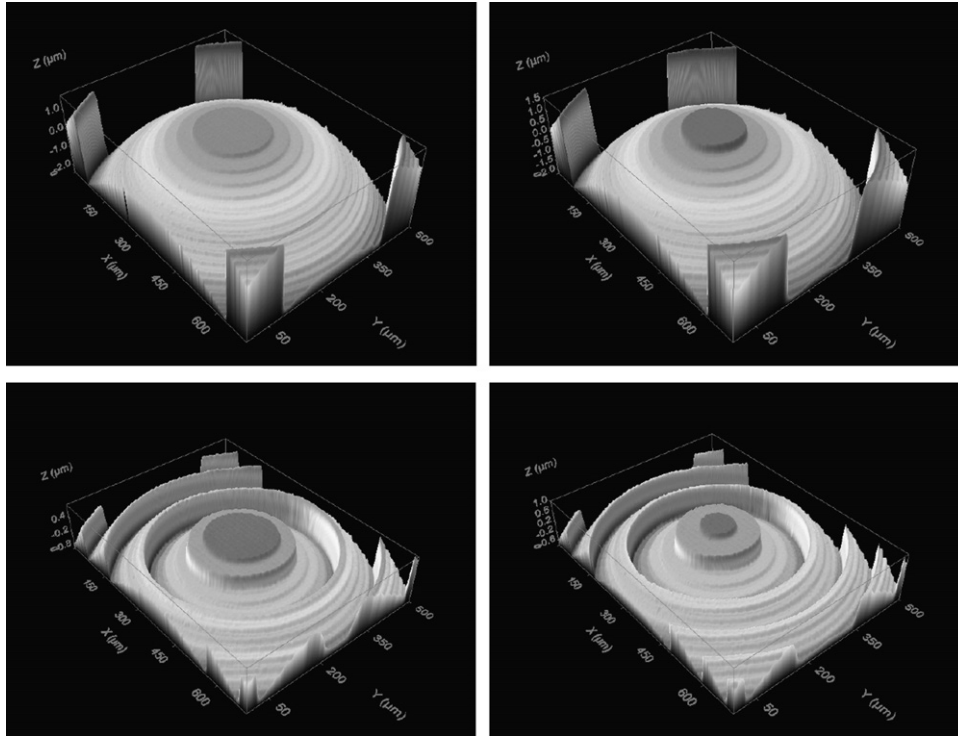|	f_{design} (mm)	f_{measured} (mm)
$\lambda = 10.6$ μm	6.7	6.41
$\lambda = 9.7$ μm	6.7	6.39
$\lambda = 3.9$ μm	6.7	6.47
$\lambda = 3.5$ μm	6.7	6.50

Fig. 10. Measured lens profile of each single lens of the FL-array, in the corresponding central region. $f = 6.7$ mm, $D = 4$ mm. $\lambda = 10.6$ μm (top, right), 9.7 μm (top, left), 3.9 μm (bottom, right), and 3.5 μm (bottom, left).

around 10 μm, thus rendering the lenses opaque at that particular wavelength. ZnS ($n = 2.22$), ZnSe ($n = 2.4$), CdTe ($n = 2.7$), and Ge ($n = 4$) can be considered transparent in the IR region of interest. The optimal refraction index for the AR coating is the geometric mean of the refraction index of both mediums (Eq. (10))

$$n_{AR} = \sqrt{n_{silicon} n_{air}} = 1.85 \qquad (10)$$

From the proposed materials, the refraction index of zinc sulphide (ZnS) is the closest to the optimal value and has been chosen for the AR coating. The thickness of the AR coating can be obtained from the one quarter wave layer (Eq. (11))

$$d_{AR} = \frac{\lambda}{4 n_{AR}} = 1193 \, \text{nm} \qquad (11)$$

The proposed AR layer has been simulated when coated on one side and on both sides of the FL (Fig. 11). The material absorption was neglected due to the small thickness of the layer. From the previous simulation, a 1193 nm thickness ZnS layer can be used as AR coating since the reflection losses decrease from 46% to 6%, 17%, 8%, and 6% for 3.5 μm, 3.9 μm, 9.7 μm, and 10.6 μm wavelengths, respectively, when coated on both sides of the FL.

The required AR layer has been post-processed on both sides of some multi-lens arrays. The coated FL has been optically tested with the described set-up for the uncoated multi-lens array. Table 4 shows the measured focal length for a double side AR coated multi-lens array and the measured gain of radiation for each lens when the AR layers were coated. Since only small shifts in the focal length (less than 0.15 mm) have been observed

and all the lenses exhibit an improvement of the transmitted radiation when coated with the proper AR layer on both sides, the fabricated device is suitable to be integrated with the detector module.

The maximum gain introduced by each lens is the ratio between its area and the absorber area of the thermopile. For the fabricated device, the maximum gain is expected to reach a factor of 140.

As can be observed in the simulation presented in Fig. 11, the thickness of the AR coating is very critical for the shorter wavelengths since a small variation of the layer thickness may
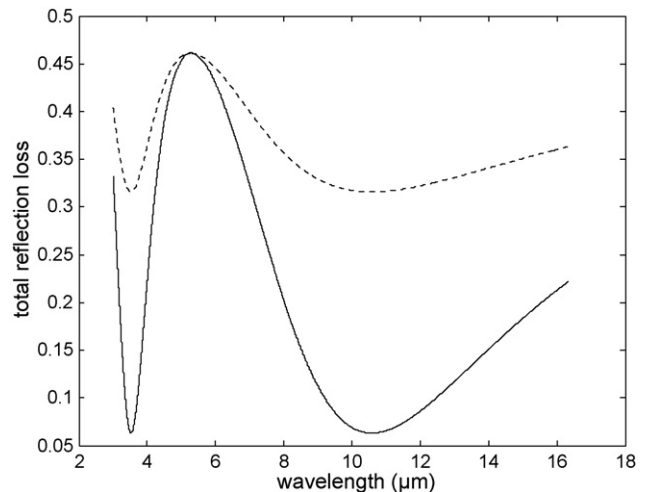

Fig. 11. Simulated reflection losses when the proposed AR layer is coated on one side (dotted line) and on both sides (solid line).

Table 4
Measured focal length for a double-side AR coated multi-lens array and the corresponding transmission improvement when the AR layer is present

	Reflection losses without AR (%)	Reflection losses with AR (%)	Theoretical radiation gain	Measured radiation gain	f_{design} (mm)	$f_{measured}$ (mm)
$\lambda = 10.6\,\mu m$	46	6	1.74	1.82	6.7	6.38
$\lambda = 9.7\,\mu m$	46	8	1.70	1.7	6.7	6.26
$\lambda = 3.9\,\mu m$	46	17	1.54	1.99	6.7	6.33
$\lambda = 3.5\,\mu m$	46	6	1.74	1.36	6.7	6.48

shift the curve and decrease the effect of the ZnS layer for those wavelengths. This effect can be observed to some extent in the results of Table 4, where the measured transmission levels for the shorter wavelength pair are further from the theoretical value than for the longer one pair. Additionally, the ZnS layer exhibits adherence problems on the non-structured side of the FL chip and it starts peeling off after some time. Structuring the rear side of the FL chip with some stripes (much larger than the interesting wavelengths to avoid diffraction effects which may interfere with the FL operation) is considered in order to solve the adherence problems. Patterning a periodic subwavelength structure acting as AR layer on the non-structured side of the FL will avoid depositing a ZnS layer on that side, but will require a photolithographic technique, such as Electron Beam Lithography, able to define submicron features [20].

6. Detector module integration

The light has to reach each thermopile absorber after coming out from the gas cell and after being focused by the corresponding lens. The thermopile absorber size is just 350 µm × 350 µm so alignment may be crucial. Fortunately, the gas cell output is not working as a point source since the output is more than 1 mm wide, but nevertheless a proper alignment of the detector

Fig. 12. FL-array, properly aligned and attached to the detector lid of a TO8 package.
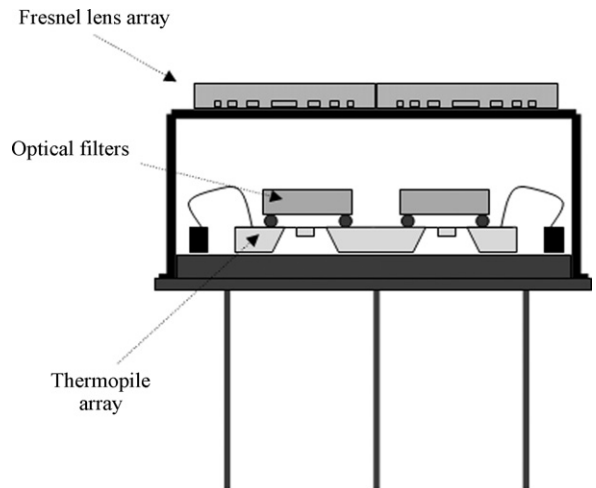

Fig. 13. Proposed detector module architecture showing the different element arrangement.

module has to be addressed. The way to achieve this goal is to assume that the thermopile detector is well centered in the bottom platform, the multi-lens array is well centered in the lid and both elements are correctly oriented. To secure this situation, alignment accessories have been designed and fabricated for the mounting module. Fig. 12 shows the final fabricated device, attached and properly aligned to the detector lid and Fig. 13 the scheme of the compact detection unit. Further tests are underway to confirm the gain in sensitivity in all channels of the detector due to the Fresnel multi-lens addition.

7. Conclusions

A compact detection unit, with the four-channel thermopiles, the optical filters and the corresponding lens for each channel has been successfully assembled and tested at component level.

Some single lenses (binary and up to eight levels) were designed, fabricated and successfully tested as first prototypes of the final multi-lens array.

A new approach based on the use of four photolithographic masks to design a four lens-array has been presented. The theoretical study shows that the lenses efficiency does not decrease dramatically when this approach is used instead of using twelve photolithographic masks.

The focal length measurement of the fabricated device has an error smaller than 5%, and the measured spot size at the focal plane is smaller than the typical thermopile absorber size. The proposed AR coating increases the transmitted radiation and

improves the lens efficiency. And finally, the method to assemble the lens array with the detector lid secures the proper alignment lens-detector. Therefore, the fabricated devices are suitable for the detection module.

A significant increase of the sensor sensitivity is expected when the lens is added in the NDIR system. Future work includes the complete sensor tests, working in real gas conditions.

Acknowledgements

References

[1] R.F. Wolffenbuttel, State-of-the-art in integrated optical microspectrometers, IEEE Trans. Instrum. Meas. 53 (2004) 197–202.

[2] G. Lammel, S. Schweizer, S. Schiesser, P. Renaud, Tunable optical filter of porous silicon as key component for a MEMS spectrometer, J. Microelectromech. Syst. 11 (2002) 815–828.

[3] H. Sagberg, M. Lacolle, I.R. Johansen, O. Lovhaugen, R. Belikov, O. Solgaard, A.S. Sudbo, Micromechanical gratings for visible and near-infrared spectroscopy, IEEE J. Sel. Top. Quantum Electron. 10 (2004) 604–613.

[4] R.F. Wolffenbuttel, MEMS-based optical mini- and microspectrometers for the visible and infrared spectral range, J. Micromech. Microeng. 15 (2005), Sp. Iss. S145–S152.

[5] J. Muller, U. Dillner, Thermal microsensors: their bases, principles and applications, Sens. Mater. 8 (1996) U4–U6.

[6] Sira Technology, Gas Detector Selection and Calibration Guide, Withrebys Publishing, London, 2005.

[7] D. Bauer, M. Heeger, M. Gebhard, W. Benecke, Design and fabrication of a thermal infrared emitter, Sens. Actuators, A, Phys. 55 (1996) 57–63.

[8] J. Spannhake, O. Schulz, A. Helwig, G. Müller, Design, development and operational concept of an advanced MEMS IR source for miniaturized gas sensor systems, in: The 4th IEEE Conference on Sensors, Irvine, CA, USA, Oct. 31–Nov. 3, 2005.

[9] A. Balducci, A. D'Amico, C. Di Natale, M. Marinelli, E. Milani, M.E. Morgada, G. Pucella, G. Rodriguez, A. Tucciarone, G. Verona-Rinati, High performance CVD-diamond-based thermocouple for gas sensing, Sens. Actuators, B, Chem. 111 (2005) 102–105.

[10] J. Schilz, Applications of thermoelectric infrared sensors (thermopiles): gas detection by infrared absorption; NDIR, Thermophysica minima PerkinElmer Optoelectronics, 2000.

[11] W. Konz, J. Hildenbrand, M. Bauersfeld, S. Hartwig, V. Lehmann, J. Wöllenstein, Micromachined IR-source with excellent blackbody like behaviour, Smart Sensors, Actuators, and MEMS II, Proc. SPIE 5836 (2005) 540–548.

[12] L. Fonseca, F. Perez-Murano, C. Calaza, R. Rubio, J. Santander, E. Figueras, I. Gracia, C. Cane, M. Moreno, S. Marco, AFM thermal imaging as an optimization tool for a bulk micromachined thermopile, Sens. Actuators, A, Phys. 115 (2004) 440–446.

[13] L. Fonseca, E. Cabruja, C. Calaza, R. Rubio, J. Santander, E. Figueras, I. Gracia, C. Cane, M. Moreno, S. Marco, Feasibility of a flip-chip approach to integrate an IR filter and an IR detector in a future gas detection cell, Microsyst. Technol. 10 (2004) 382–386.

[14] J. Oetiker, S.F. Yang, The role of ethylene in fruit ripening, Acta Hort. (ISHS) 398 (1995) 167–178.

[15] U. Levy, D. Mendlovic, E. Marom, Efficiency analysis of diffractive lenses, Opt. Soc. Am. 18 (2000) 86–93.

[16] M. Kuittinen, H.P. Herzig, Encoding of efficient diffractive microlenses, Opt. Lett. 20 (1995) 2156–2158.

[17] J. Jahns, S. Walker, Two-dimensional array of diffractive microlenses fabricated by thin film deposition, Appl. Opt. 29 (1990) 931–936.

[18] J. Fonollosa, R. Rubio, J. Hildenbrand, M. Moreno, S. Marco, J. Santander, L. Fonseca, S. Hartwing, J. Woellenstein, Fresnel Lenses: study and fabrication in silicon technology for medium-IR applications, Proc. SPIE (2006) 61860R-1–61860R-11.

[19] F.L. Pedrotti, L.S. Pedrotti, Introduction to Optics, Prentice-Hall International Editions, United States of America, 1987, p. 166.

[20] D. O'Shea, T. Suleski, A. Kathman, D. Prather, Diffractive Optics: Design, Fabrication and Test, SPIE PRESS, Washington, 2004, p. 54.

Biographies

J. Fonollosa was born in Barcelona, in 1980. He received his BS in physics and his BS in electronic engineering from the University of Barcelona in 2002 and 2007, respectively. He started his PhD studies in 2004 in the University of Barcelona. His main research areas are related to diffractive lenses design and synchronous detection for gas sensing applications.

R. Rubio was born in Madrid, Spain on August 14, 1978. He received his BS degree in physics from the University of Barcelona in 2001. In 2002, he joined the Microelectronics National Center, where he received his PhD in 2007. His main research activities are related to the infra-red sensing technologies and pattern recognition techniques.

S. Hartwig studied environment engineering at the University of Applied Science Jena. Since 2002, she works at the Fraunhofer Institute for Physical Measurement (IPM).

S. Marco is associate professor at the Departament d'Electronica of Universitat de Barcelona since 1995. He received the degree in physics from the Universitat de Barcelona in 1988. In 1993, he received his PhD (honor award) degree from the Departament de Física Aplicada i Electrònica, Universitat de Barcelona, for the development of a novel silicon sensor for in vivo measurements of the blood pressure. In 1994, he was visiting professor at the Universita di Roma 'Tor Vergata' working in Data Processing for Artificial Olfaction. He has published about 40 papers in scientific journals and books, as well as more than 80 conference papers. His current research interests are twofold: chemical instrumentation based on intelligent signal processing and microsystem modeling.

J. Santander was born in Terrassa, Spain, in 1966. He received the BS and PhD degrees in physics from the Autonomous University of Barcelona, Spain, in 1989 and 1996, respectively. He is currently working at the Microelectronics National Center in Barcelona, as responsible for the electrical characterization laboratory, developing solutions for the electrical parametric characterization of different microelectronic technologies (CMOS, MCM, sensors, microsystems) using mainly test structures. His main research areas are related to microsystems, gas sensing applications and micro fuel cells.

Luis Fonseca was born in Barcelona, Spain, in 1966. He received his BS and PhD degrees in physics from the Autonomous University of Barcelona in 1988 and 1992, respectively. In 1989 he joined the National Center of Microelectronics as a post-graduate student, working till 1992 on the growth and characterization of thin dielectric films for VLSI and ULSI applications. After this first research period he worked as a process engineer, leading the diffusion and deposition areas of the CNM production facilities. In 2001 he joined the Microsystem group as a full senior researcher being his actual research area focused on technological developments for gas sensing and more specifically on optical gas sensing.

J. Wöllenstein received his diploma and later his PhD in electrical engineering from the University of Kassel, Germany. In 1994, he joined the Fraunhofer Institute of Physical Measurement Technique, Freiburg, Germany, where he is engaged in development of optical and semiconductor gas sensors and microsystems.

Mauricio Moreno was born in Barcelona, Spain. He received the degree in physics in 1989 from the University of Barcelona (UB), and the PhD degree in sciences in 1995 from the Polytechnic University of Catalonia (UPC), Spain. He has been associate professor in the Electronics Department, UB, since 1997. He is involved in the design and test of optical evanescent biosensors (gratings and surface plasmon resonance) optical waveguides for biological applications. Other fields of interest include arrays of CMOS integrated photodetectors for imaging and rangefinders.

Limits to the integration of filters and lenses on thermoelectric IR detectors by flip-chip techniques

J. Fonollosa [a,c,*], M. Carmona [c], J. Santander [b], L. Fonseca [b], M. Moreno [a], S. Marco [a,c]

[a] *Departament d'Electrònica, Universitat de Barcelona, Martí i Franquès 1, 08028 Barcelona, Spain*
[b] *Centre Nacional de Microelectrònica, Campus UAB, 08193 Bellaterra, Spain*
[c] *Artificial Olfaction Lab, Institute of Bioengineering of Catalonia, Baldiri i Rexach 13, 08028 Barcelona, Spain*

ARTICLE INFO

ABSTRACT

In the trend towards miniaturization, a detector module containing multiple IR sensor channels is being built and characterized. In its final form it contains thermopiles, narrow band filters and Fresnel lenses. An important feature of such module is the assembly by flip-chip of the IR filters on top of the thermopiles. The performance of the filter-thermopile ensemble has been assessed by physical simulation and experiments and it has been optimized by the use of an empirically validated model. It has been found that integration of filters (or lenses) too close to the IR detector may lead to degraded performance due to thermal coupling. The impact and extent of this degradation has been thoroughly explored, being the main parameter the distance between the IR sensor and the filter. To avoid such detrimental effects a possibility is to set the device in vacuum conditions, obtaining an improved output response and avoiding the influence of the filters. Another way is to increase the solder joint height. Beyond a certain height, the filter is considered to be isolated from the thermopile.

© 2008 Elsevier B.V. All rights reserved.

1. Introduction

Cointegration of optics with microelectronics circuits is playing a central role in spectrometry since silicon process compatible technologies provide low-cost batch fabrication of small, lightweight, and intelligent optoelectronic system-on-a-chip [1,2]. Several examples of integration of radiation detectors with optical microsystems featuring capability for spectral analysis can be found in spectroscopy instruments [3–9].

Optical gas sensors are based on the radiation attenuation produced by the specific absorption spectrum of each gas. Non-dispersive infrared (NDIR) gas sensors devote one channel for each gas to measure and usually an additional reference channel. In a NDIR approach the required gas selectivity comes from the presence of proper elements filtering the broad spectrum radiation of a thermal source around wavelengths that correspond to the gases of interest.

Thermal infrared detectors are in many cases based on thermopiles. They consist of the serial combination of several thermocouples that transform the temperature difference between a cold and a hot junction into a voltage output. In particular, the use

of micromachined thermopile detectors is widespread for infrared spectrometry for gas detection [10].

Filters are the optical gas sensor components that ensure the selectivity of the sensor. They are multilayer thin-film devices formed by a stack of several high and low index of refraction layers. Wavelength selection is based on constructive/destructive light interference phenomena. Highly selective interferometric filters are formed by tens of these layers.

Integrated multi-thermopile arrays with specific optical filters to select the desired wavelength for each channel are already commercially available (*Heimann Sensors*, *Dexter Research*, *Perkin Elmer*).

Aiming to optimize the sensitivity of the gas sensor and going further with the detector module integration, the authors presented a NDIR compact 4-channel detection unit consisting of a bulk micromachined fourfold thermopile array, the specific optical filters, and a multi-lens array [11]. The corresponding optical filter was attached above each thermopile using flip-chip techniques. The flip-chip approach is a promising way to integrate a stack of two optical devices. It provides the necessary optical alignment and it has been proved compatible to the handling of fragile micromachined devices, such as micromachined thermopiles [12].

In this work, empirical testing, as well as physical simulation, shows the existence of limits for the dense integration of those optical elements. The constraints for the integration of the thermopile array with the corresponding optical filters are presented.

---

* Corresponding author at: Departament d'Electrònica, Universitat de Barcelona, Martí i Franquès 1, 08028 Barcelona, Spain. Tel.: +34 93 403 9146.
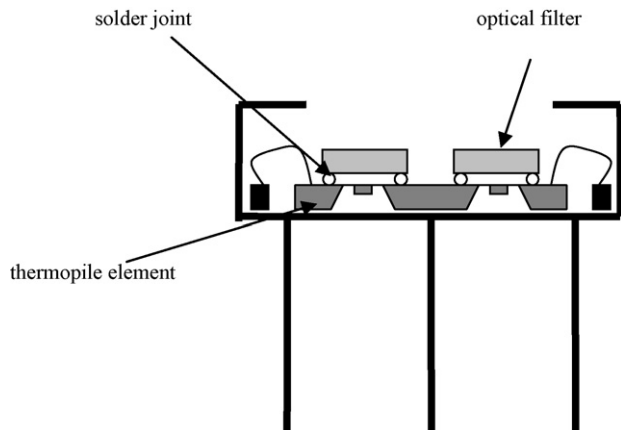*E-mail address:* jfonollosa@el.ub.es (J. Fonollosa).

Fig. 1. Schematics of the detection unit in a TO8 package, with thermopile elements, optical filters, and solder joints.

In particular, the time response of the detector is analyzed and suggestions are given to prevent detrimental effects.

2. Device description

The detector unit consists of a substrate chip with an array of thermopile elements that is attached to the base of the package. For wavelength selection the appropriate optical filters are flip-chipped onto the thermopile elements. Fig. 1 shows a schematic of the detector unit in a TO8 package.

Micromachined thermopiles based on CMOS processing and bulk micromachining are chosen as infrared detectors since they offer adequate reproducibility, accuracy, sensitivity and rapid response [13]. The authors already presented a bulk micromachined thermopile [14], where the device architecture can be found in detail. Fig. 2 shows a schematic of the described thermopile.

Substrate chips (6.1 mm × 6.1 mm size) with four micromachined thermopiles in a 2 × 2 arrays, featuring a size compatible with a TO8 package, have been fabricated. Each thermopile features 32 thermocouples and the absorber and membrane sizes are 150 μm × 150 μm and 1300 μm × 1300 μm, respectively. Fig. 3 shows a fabricated chip with four thermopiles.

Filter selection was made considering the target gases: Infrasil (a type of fused quartz registered by Heraeus Quarzglas) substrate and 3.4 μm central wavelength (CWL) for hydrocarbons; germanium substrate and 9.7 μm CWL for ammonia; 3.9 μm CWL for reference band; and 10.6 μm CWL for ethylene. Filters wafers were successfully diced and conditioned to be attached to the thermopile substrate.

Aluminium pads are not directly solderable, therefore a wettable metal (a Ti/Ni/Au stack) has to be defined on top of the connecting pads. When performing the flip-chip procedure, cylinders of solder paste (Sn/Pb 63–37% in our case) are deposited on each bump pad
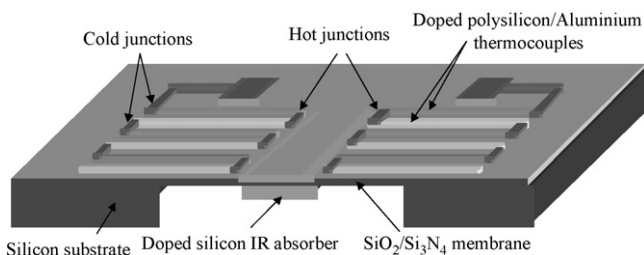

Fig. 2. Schematics of a micromachined CMOS-compatible thermopile.
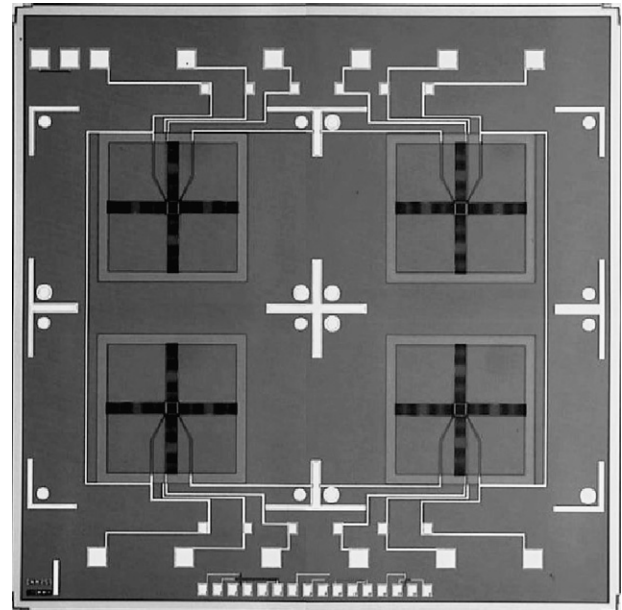

Fig. 3. Fabricated substrate chip (6.1 mm × 6.1 mm size) with a 2 × 2 thermopile array.

of the substrate wafer by dispensing the paste through the round holes of a metal stencil mask that has been defined in accordance with the bump pad distribution on the thermopiles and the filters. Afterwards, a pick-and-place machine takes the chips to be mounted on top and arranges them so that the bumped solder pads of the substrate face their corresponding pad on the chip.

Once the chips are placed onto the substrate, the wafers undergo a short inert thermal process using a standard reflow ramp procedure that reaches a maximum temperature of 220 °C. The solder paste melts and partially dissolves the wettable metal forming a strong contact between the pads on the substrate and the ones on the flipped chips. Therefore, in the current set-up and after the flip-chip procedure, optical filters and thermopile elements are successfully assembled through 60 μm solder joints.

Once the filters dies are in place, the thermopile wafer must be diced in order to single out the covered arrays that are the core of the infrared detector. The last step is to wire bond the detector units in their final TO8 packaging. In Fig. 4 the optical filters attached to the substrate wafer (left) and the final detector with the corresponding wire bonding (right) are shown.

3. Empirical device characterization

In order to determine the effect of the attached optical filters above the thermopiles, IR measurements have been performed using thermopiles with and without flip-chipped optical filters, in air and in vacuum conditions.

The optical bench consists of an IR emitter (ORIEL, 80007) and the corresponding lens (ZnSe) to collimate the radiation, an optical shutter, and a calcium fluoride windowed chamber with a wall bushing that allows measuring voltage signals from outside while the device is in vacuum conditions. Calcium fluoride IR spectrum decays to 60% at 10 μm wavelength, therefore thermopile measurements have been focused on the shorter CWL optical filters. Fig. 5 shows the optical bench. The chamber with one of the thermopile arrays is detailed in Fig. 6.

A fourfold thermopile array without flip-chipped optical filters was set in the optical bench and the corresponding voltage was measured: firstly without any optical filter, and secondly inserting a
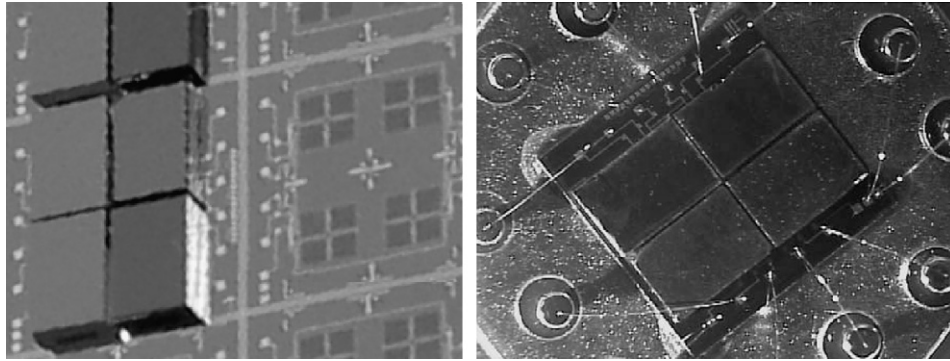
Fig. 4. Optical filters attached to the substrate using flip-chip techniques (left) and final device in the TO8 packaging (right).
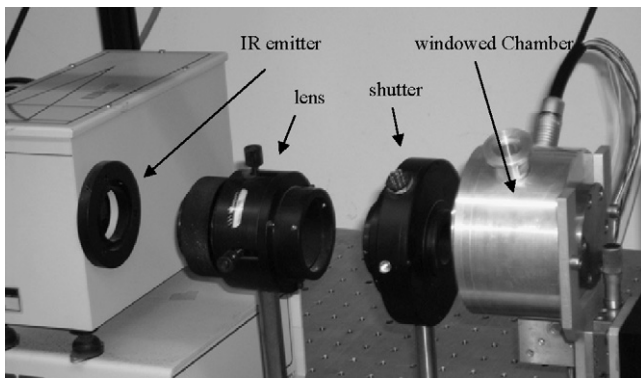

Fig. 5. Optical bench with the IR emitter, lens, shutter, and the vacuum chamber.

3.95 μm CWL optical filter in front of the shutter. This configuration assures that no thermal coupling is present between the filters and the thermopiles. The step response of the system was measured switching the shutter and an estimation of the time constant was obtained fitting the signal to a first order system response. Fig. 7 shows the measured thermopile output without optical filter, and with a 3.95 μm CWL optical filter in front of the shutter. Table 1 presents the corresponding estimated parameters from the fitting in both conditions.

In order to assess the effect of the flip-chipped filters, the same measurements have been performed using a fourfold thermopile array with flip-chipped optical filters and measuring the voltage corresponding to the thermopile with the 3.95 μm CWL filter (Fig. 8 and Table 2).

Fig. 6. Vacuum chamber, with a bushing wall to measure thermopile output voltage from outside, and a calcium fluoride window.

Tables 1 and 2 and Fig. 7 show that inserting a narrow band filter close or far from the thermopile decreases the signal level since the radiation reaching the thermopile is severely reduced. When inserting the filter far from the detector the time response is not significantly different from the one attained when no filter is in place. On the other hand, Fig. 8 shows that flip-chipped optical filters on the thermopile array cause a response that is larger and much slower. However, it is remarkable that an initial 20 mV fast voltage step is similar regarding time response to the one obtained for a far located filter.
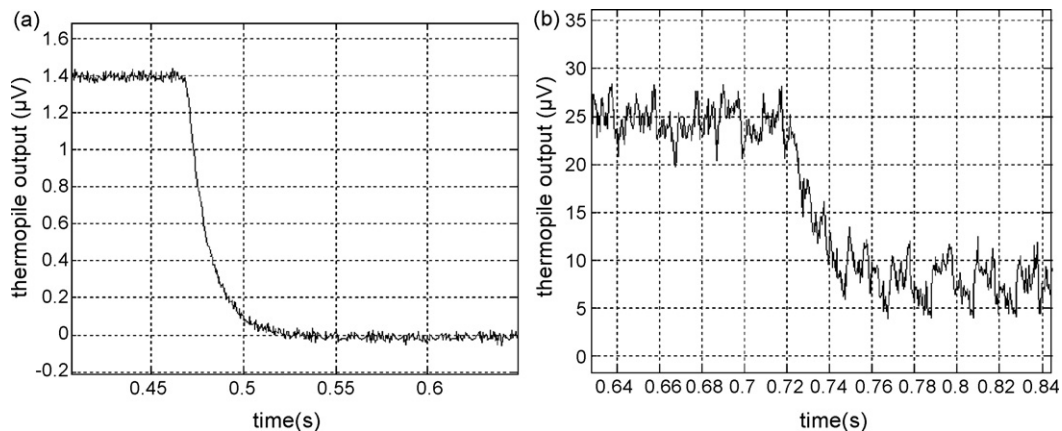

Fig. 7. Fall step for an element of a thermopile array in air without flip-chipped optical filters: (a) without any optical filter and (b) inserting a 3.95 μm CWL filter in front of the shutter.

Table 1
Rise and fall time, and signal level for a thermopile array in air without flip-chipped optical filters; without any optical filter and inserting a 3.95 μm CWL filter in front of the shutter.

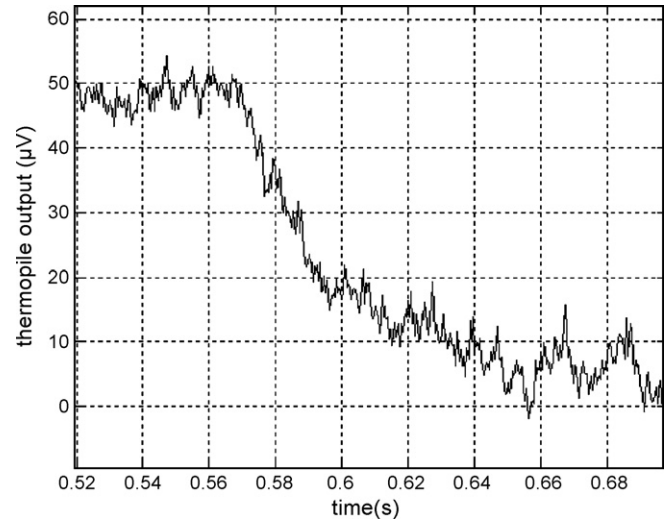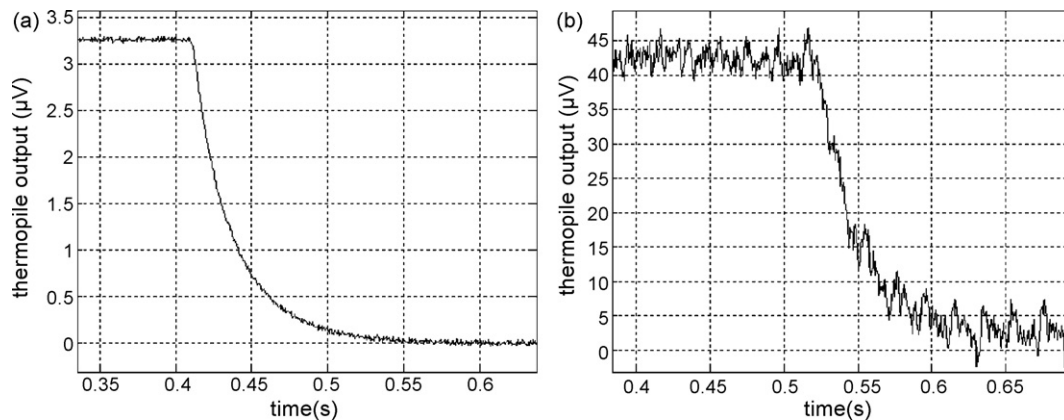| No optical filter			3.95 μm CWL filter in front of the shutter		
Signal level (mV)	τ rise (ms)	τ fall (ms)	Signal level (μV)	τ rise (ms)	τ fall (ms)
1.40 ± 0.02		13.3 ± 0.3	17 ± 2		14.5 ± 1.5
1.40 ± 0.02	13.6 ± 0.6		16 ± 2	16 ± 2	
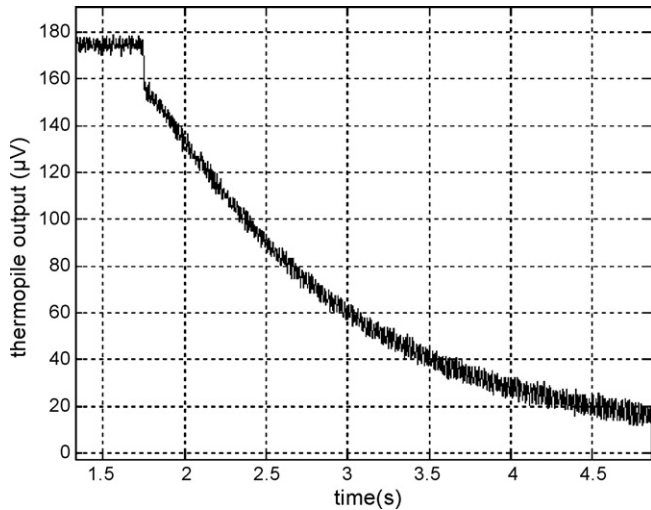
Fig. 8. Fall step for a thermopile array in air with flip-chipped optical filters on it.

Fig. 10. Fall step for a thermopile array with flip-chipped optical filters on it; in vacuum conditions.

Table 2
Rise and fall time, and signal level for a thermopile array in air with flip-chipped optical filters.

Flip-chipped optical filters		
Signal level (μV)	τ rise (ms)	τ fall (ms)
168 ± 2		1225 ± 15
168 ± 2	1300 ± 10	

This behavior can be explained by a thermal coupling between the detector and the filter. In order to test this possibility, the previous measurements have been repeated in vacuum conditions (Figs. 9 and 10, and Tables 3 and 4).

It can be observed from Tables 1 and 3 that inserting the optical filter far from the thermopile decreases the signal to the same 1.2% level, both in air or in vacuum, and that the time constant is not dramatically affected. Thermopile response remains slightly faster

Fig. 9. Fall step for a thermopile array without flip-chipped optical filters, in vacuum conditions: (a) without any optical filter and (b) inserting a 3.95 μm CWL filter in front of the shutter.

Table 3
Rise and fall time, and signal level for a thermopile array without flip-chipped optical filters; without any optical filter and inserting a 3.95 μm CWL filter in front of the shutter; in vacuum conditions.

No optical filter			3.95 μm CWL filter in front of the shutter		
Signal level (mV)	τ rise (ms)	τ fall (ms)	Signal level (μV)	τ rise (ms)	τ fall (ms)
3.26 ± 0.02		26.8 ± 0.1	40 ± 2		26.0 ± 0.5
3.28 ± 0.02	27.5 ± 0.1		42 ± 2	28.4 ± 0.4	

Table 4
Rise and fall time, and signal level for a thermopile array with flip-chipped optical filters; in vacuum conditions.

| Flip-chipped optical filters		
Signal level (μV)	τ rise (ms)	τ fall (ms)
47 ± 2		32 ± 5
46 ± 2	31 ± 3	

when operating in air, but output voltage is 2.3 times larger when the thermopile is operating in vacuum conditions.

However, the behavior in vacuum when the filter is flip-chipped on the thermopile drastically differs from its behavior in air. Both the signal level and the time response are similar to the case when the filter is placed far from the thermopile. That is, in vacuum, the presence of a closely located filter does not produce the same large amplitude, slow response that appears in air conditions. These results clearly support the hypothesis of the thermal coupling through the air as an underlying reason for the observed phenomena (Tables 2 and 4).

Moreover, the filter is probably slightly heated up by IR radiation absorption and a later heat transfer to the thermopile. Fig. 11 shows transmission and reflection spectrums of the optical filter, measured with a Fourier Transform spectrometer (Bomem, DA3).
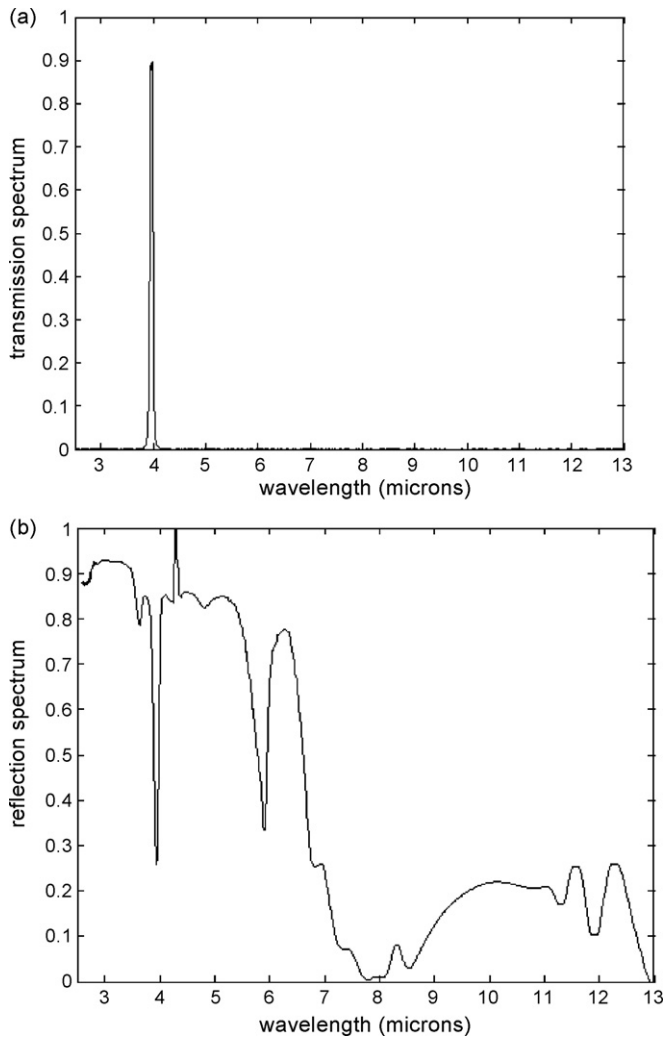
Fig. 11. Measured transmission (a) and reflection (b) spectrums for a 3.95 μm CWL optical filter, using a Fourier transform spectrometer.
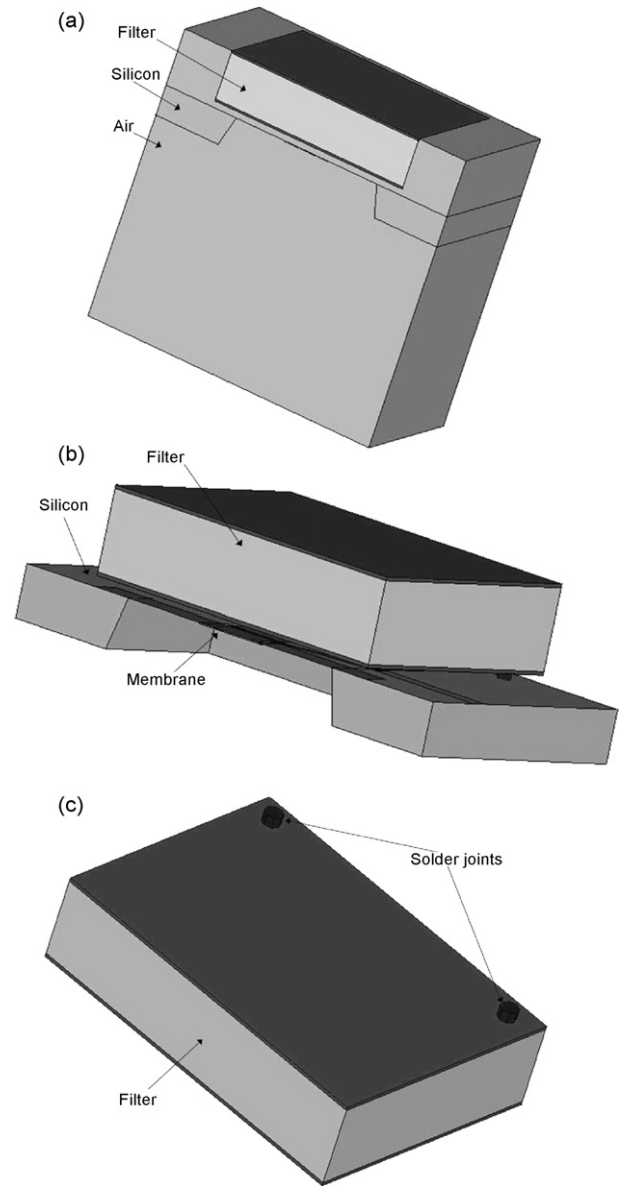
Fig. 12. (a) Half-symmetric model, (b) model view of solid component and (c) filter model view from the solder joints side.

Since the radiation which is neither transmitted nor reflected is absorbed, Fig. 11 shows that an important part of the radiation is absorbed.

4. Physical model

In order to confirm the interpretation of the empirical results and to study the detector's performance and obtain the influence of different design variables, a finite element model (FEM) has been created and implemented with ANSYS v.11 [15].

Fig. 12a shows a first view of the half-symmetric model where the air region and the silicon substrate can be observed. The extension of the bottom air region has been taken such that the heat flux through this region is no longer dependent on it. No air has been considered on top of the filter as the heat flux will always be preferably towards the filter. A second view of the model can be seen in Fig. 12b, where air has been eliminated in order to see more clearly the solid components.

Table 5
Material properties values at ambient temperature, used in the simulation model.

Material	K (W/(m K))	C_p (J/(kg K))	Density (kg/m³)
Silicon	150	700	2328
Si_3N_4	12	880	3180
SiO_2	1.4	780	2200
Al	180	900	2692
Poly-n⁺	30	754	2328
Ge	60.2	322	5350
Infrasil	1.38	772	2200
Air	0.026	1005	1.182
Solder	50	180	9290

The filter has been modelled as a sandwich structure made of the bulk material (which can be made of Infrasil or germanium) between two dielectric layers. The modelled solder joints between the filter and the silicon substrate are implemented as simple cylinders and can be seen in Fig. 12c.

The explanation of the model for the membrane and silicon substrate as well as the static results obtained for this component have been reported [16]. In summary, the membrane is modelled by 2D elements by using equivalent material properties over the different material regions. This is justified by the high aspect ratio of the membrane, being the heat flux principally in the membrane plane direction.

From the static model, it becomes clear that the only relevant heat transfer mechanism is conduction. Convection can be neglected compared to conduction as indicated by the low Rayleigh number [16], as well as radiation. These conclusions also hold for the dynamic model and specially for our device because the temperature is well below those of the referenced paper.

The bottom side of the silicon substrate is considered to be an ideal heat sink and, therefore, its temperature has been fixed at ambient temperature (T_{amb}). This boundary condition has been easily verified by a Thermal Infrared Camera (AM40, FLIR Systems). Two different heat loads have been considered: the power absorbed at the silicon absorber (P_{abs}) and the power dissipated at the filter bulk material (P_{filt}). P_{filt} has been applied uniformly over the filter volume.

Thermal conductivity of air has been considered temperature-dependent. Nevertheless, its heat capacity and density have been assumed constant since the temperature increases are very small. The material property values used in the model at ambient temperature are given in Table 5.
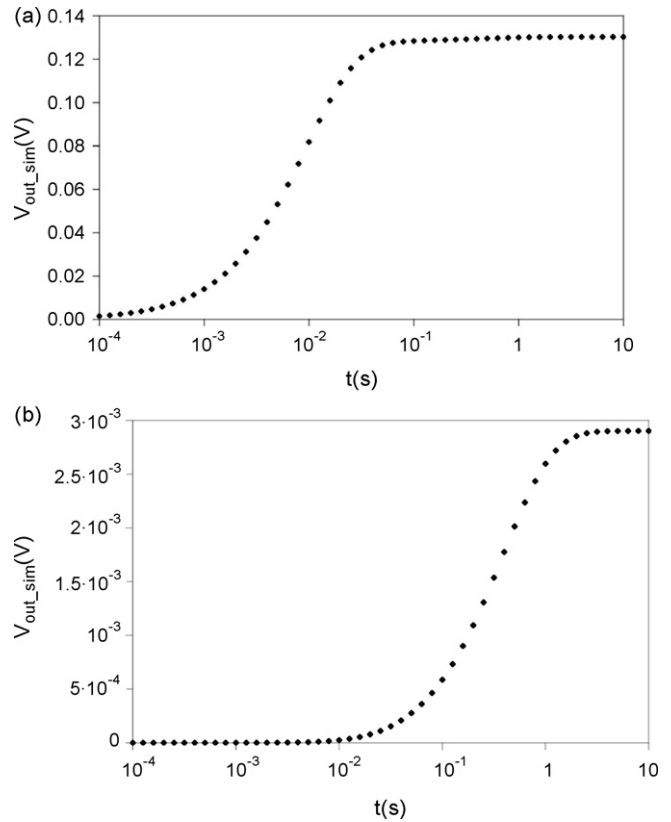
5. Simulation results

First of all, we have analyzed the output response (V_o) of the device for every load (P_{abs} and P_{filt}) separately. This response is shown in Fig. 13 for a Ge filter, when applying a total power of 10 mW.

It can be observed that for the same total power level, the output response is much larger when it is applied to the absorber, as it was expected. Nevertheless, the output produced by P_{filt} cannot be neglected as its actual relevance will be given by the ratio between both dissipated powers in real conditions. Another important point is that the response of the device is much faster when the power is only dissipated at the absorber than when it is only dissipated at the filter.

In order to have more realistic simulated power levels, they were obtained by comparison of the output steady state values in measurements and simulations. The chosen power values are P_{abs} = 1 mW and P_{filt} = 200 mW.

The two power dissipation locations can be the origin of the behaviors observed in the measurements. In order to clarify this


Fig. 13. V_o response for a Ge filter: (a) P_{abs} = 10 mW and (b) P_{filt} = 10 mW.

point and, at the same time, validate this model, the simulation results have been compared to measurements. First the comparison (scaling the amplitude of the measured values) of V_o obtained in vacuum conditions without the filter is shown in Fig. 14.

A very good agreement for the time constant can be observed. The slight differences can be perfectly due to discrepancies in the material properties values used in the simulation model.

The results of the thermopile with the flip-chipped filters in vacuum and air conditions have been also compared. These results are shown in Fig. 15. The simulation model also fits well the device behavior for those conditions. Although the noise level
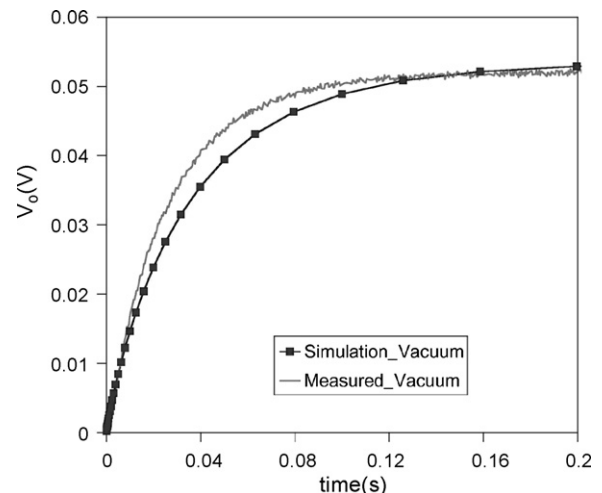
Fig. 14. Comparison of transient response between measurement (straight line) (with amplitude scaling) and simulation in vacuum conditions for thermopiles without filter.
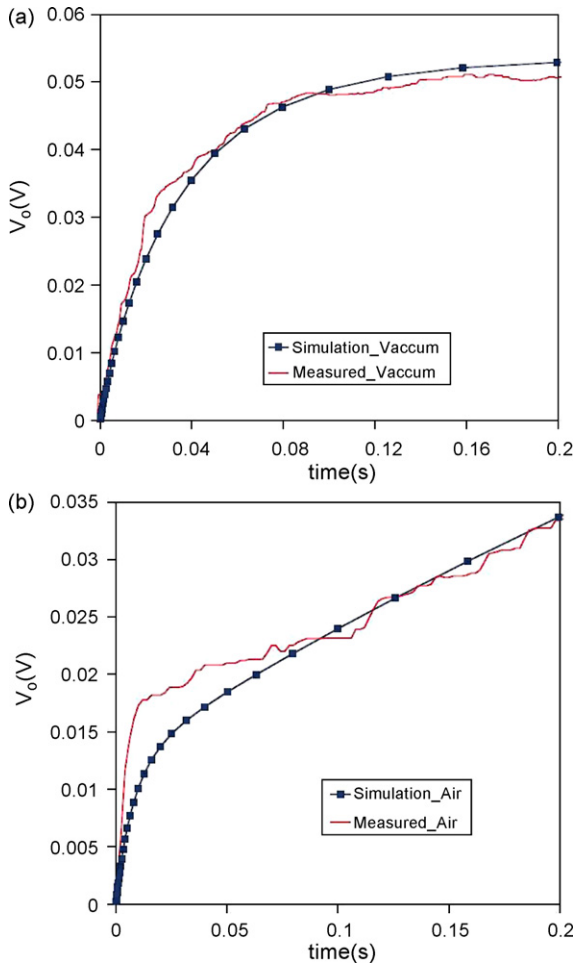
Fig. 15. Comparison of transient response between measurement and simulation for the thermopiles with the flip-chipped filters (a) in vacuum conditions and (b) in air.

Fig. 16. Thermopile response for $P_{abs} = 1$ mW and $P_{filt} = 200$ mW: (a) germanium substrate filter and (b) Infrasil substrate filter.
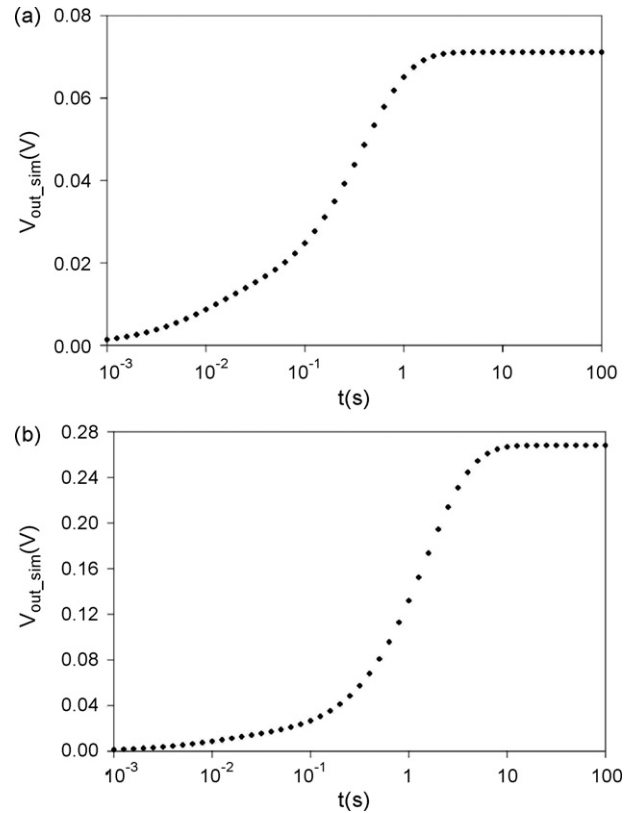
present is now higher, a good agreement is seen with regard to the appearance of two different time constants and the value of these time constants. Consequently, this model can be used for further analyzing its performance under different parameter variations.

The output responses for a Ge and an Infrasil substrates using both power dissipation locations (at absorber and filter) are shown in Fig. 16.

It is observed that the main component of V_o is the slow component, as a result of the high value of P_{filt}. This is an undesired effect which should be prevented. One possibility to avoid it is to ensure vacuum conditions between the membrane and the filter. In order to validate the filter power dissipation assumption, these conditions were also considered for measurement. By simulation, the expected response for vacuum conditions for the given power values are given in Fig. 17.

This response is independent of the filter substrate material. The steady state output value has been significantly increased and the response is much faster than in air. Nevertheless, vacuum conditions cannot be easily implemented for the packaged device and it would complicate the package conception.

A second option to avoid this effect has been investigated. It consists in increasing the solder joint height (h_{ball}) and, therefore, its width. Fig. 18 shows the effect of increasing the ball height (and width at the same time) for a germanium filter and for an Infrasil filter (with the same power values).

Two main points can be remarked. First, the output voltage value due to the power dissipated at the filter is reduced significantly as the parameter h_{ball} is increased. For a Ge filter, the effect becomes already small from a solder joint height of about 300 μm. And secondly, V_o due to power dissipated at the absorber is increased and the output response time becomes significantly faster. This fact can be better observed by plotting the response of the device by applying only P_{abs} as shown in Fig. 19.

It can be seen that the output response difference from h_{ball} values of 300–500 μm is already quite small for both filters. Nevertheless, there is still some influence of the power dissipated at the filter in both cases, and specially for the Infrasil filter, although it is small for larger solder joint sizes.

With the simulation model, we can estimate the effect of the temperature on the filter transmission characteristics. Simulation
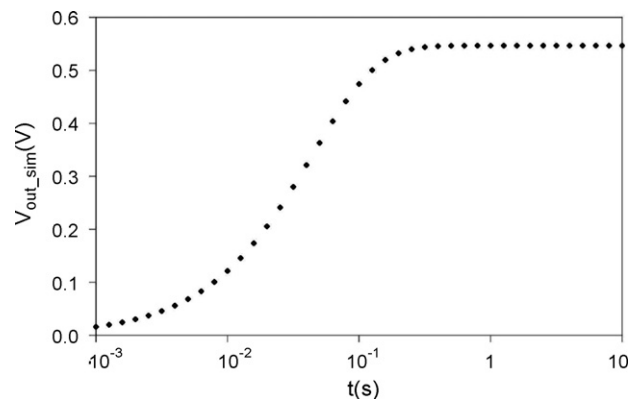
Fig. 17. Output response for total vacuum conditions (valid for both filter materials).
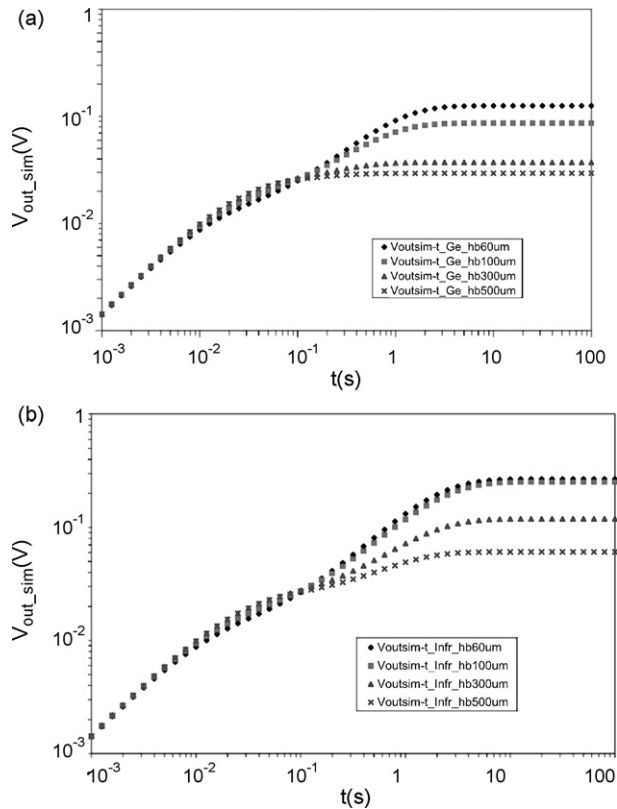
Fig. 18. V_o response for a filter flip-chipped onto the thermopiles with different h_{ball} values ($P_{abs} = 1$ mW and $P_{filt} = 200$ mW). In air conditions: (a) germanium substrate filter and (b) Infrasil substrate filter.

results provide filter temperature variations of 25 K and 5 K for a solder joint height of 60 μm and 500 μm, respectively. By taking an analytical expression of the refraction index as function of the temperature and wavelength [17], we obtain refraction index variations of 0.25% and 0.05% for the 25 K and 5 K of filter temperature increase, respectively. These slight variations are not expected to modify dramatically the bandpass filter spectrum and influence significantly the gas measurements of our application.

6. Discussion

A geometrical parametric analysis of an infrared detector has been done in order to optimize its performance. It has been possible due to the validation of a simulation model by comparing different experimental results with simulation results.

The ideal solution would be to have vacuum conditions inside the package. Nevertheless, this poses some issues. The packaging solution should be able to guarantee complete sealing conditions during the lifetime of the component. These conditions are not easily achieved. Therefore, another solution has been proposed. From the results presented, this solution is to increase the distance between the filter and the membrane. In this way two important improvements may be achieved: (i) the heat resistance from the filter to the membrane is increased, reducing in this way the heat flux that goes through the membrane to the substrate heat sink and (ii) the thermal coupling between the filter and the silicon rim in the thermopile chip is improved (as the solder joint width is also increased), reducing the thermal resistance in this thermal path, which does not contribute to output response, and helps decreasing filter temperature. These improvements are also achieved for both filter materials (Infrasil and germanium) and it appears to
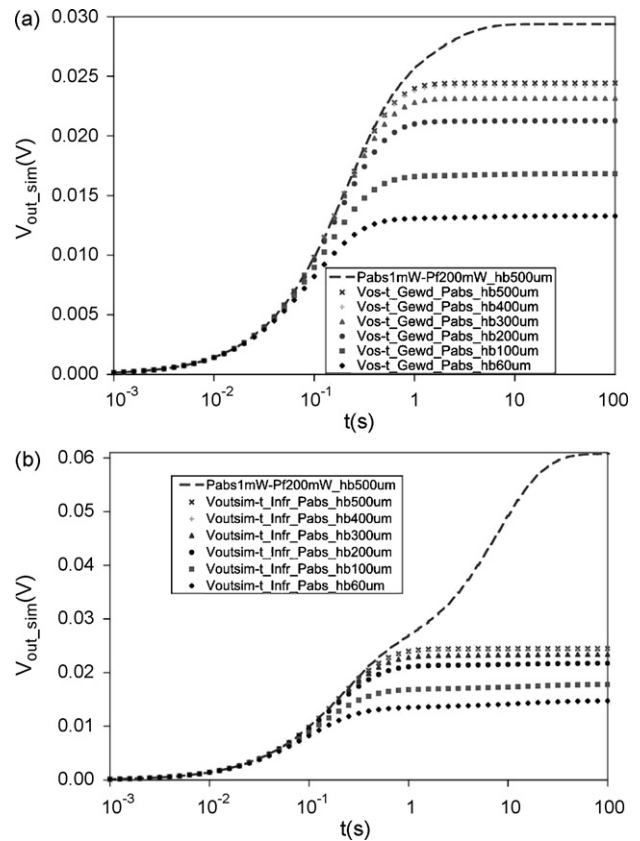
Fig. 19. V_o response with a flip-chipped filter for different h_{ball} (dotted lines) by applying just $P_{abs} = 1$ mW (also plotted (dashed line) the response applying both $P_{abs} = 1$ mW and $P_{filt} = 200$ mW for $h_{ball} = 500$ μm). In air conditions: (a) germanium substrate filter and (b) Infrasil substrate filter.

be good enough from a solder joint height of 300 μm for a Ge filter. For the Infrasil filter, it would be needed even taller and wider solder joints. Although this is a more feasible and easy solution to thermally uncouple the filter and the thermopile, it implies an increased height of the device itself and a larger non-active area occupied by the bump pads, which could represent a limitation depending on the available space for assembly for specific applications.

7. Conclusions

The presented analysis clearly shows that integration of filters (or lenses) too close to the infrared detector may produce unwanted effects. Infrared energy absorbed in the filter produces a slow temperature increase and, due to air thermal coupling, this results in an added thermal contribution producing an undesired response. This hypothesis has been corroborated by simulations and experimental results.

Different ways to optimize the performance of the detector have been evaluated by a validated simulation model. The main conclusion is that the thermopile substrate and the filter should be thermally uncoupled by vacuum conditions or by increasing the solder joints height. Simulation results allow us to quantify the needed separation to obtain a good thermal isolation. A large height would be needed if the filter material is made up of a thermally non-conductive material (like Infrasil). These options have been studied by simulations obtaining geometrical parameters values to be implemented in a further step. The specific solution should be considered depending on the application requirements.

Acknowledgments

References

[1] R.F. Wolffenbuttel, State-of-the-art in integrated optical microspectrometers, IEEE Trans. Instrum. Meas. 53 (2004) 197–202.

[2] S.S. Kim, C. Young, B. Mizaikoff, Miniaturized mid-infrared sensor technologies, Anal. Bioanal. Chem. 390 (2008) 231–237, doi:10.1007/s00216-007-1673-5.

[3] L. Dong, W. Yin, W. Ma, L. Zhang, S. Jia, High-sensitivity, large dynamic range, auto-calibration methane optical sensor using a short confocal Fabry–Perot cavity, Sens. Actuators B: Chem. 127 (2007) 350–357.

[4] T.A. Kwa, R.F. Wolffenbuttel, Integrated grating/detector array fabricated in silicon using micromachining techniques, Sens. Actuators A: Phys. 31 (1992) 259–266.

[5] G. Lammel, S. Schweizer, S. Schiesser, P. Renaud, Tunable optical filter of porous silicon as key component for a MEMS spectrometer, J. Microelectromech. Syst. 11 (2002) 815–828.

[6] H. Sagberg, M. Lacolle, I.R. Johansen, O. Lovhaugen, R. Belikov, O. Solgaard, A.S. Sudbo, Micromechanical gratings for visible and near-infrared spectroscopy, IEEE J. Selected Topics Quantum Electron. 10 (2004) 604–613.

[7] R.F. Wolffenbuttel, MEMS-based optical mini- and microspectrometers for the visible and infrared spectral range, J. Micromech. Microeng. 15 (2005) S145–S152 (special issue).

[8] D. Sander, J. Müller, Self-focusing phase transmission grating for an integrated optical spectrometer, Sens. Actuators A: Phys. 88 (2001) 1–9.

[9] D. Rossberg, Silicon micromachined infrared sensor with tunable wavelength selectivity for application in infrared spectroscopy, Sens. Actuators A: Phys. 46–47 (1995) 413–416.

[10] J. Muller, U. Dillner, Thermal microsensors: their bases, principles and applications, Sens. Mater. 8 (1996) U4–U6.

[11] J. Fonollosa, R. Rubio, S. Hartwig, S. Marco, J. Santander, L. Fonseca, J. Wollenstein, M. Moreno, Design and fabrication of silicon-based mid infrared multi-lenses for gas sensing applications, Sens. Actuators B: Chem. 132 (2008) 498–507.

[12] L. Fonseca, E. Cabruja, C. Calaza, R. Rubio, J. Santander, E. Figueras, I. Gracia, C. Cane, M. Moreno, S. Marco, Feasibility of a flip-chip approach to integrate an IR filter and an IR detector in a future gas detection cell, Microsyst. Technol. 10 (2004) 382–386.

[13] J. Schilz, Applications of thermoelectric infrared sensors (thermopiles): gas detection by infrared absorption; NDIR, Thermophysica Minima, Perking, Elmer Optoelectronics (2000).

[14] L. Fonseca, F. Perez-Murano, C. Calaza, R. Rubio, J. Santander, E. Figueras, I. Gracia, C. Cane, M. Moreno, S. Marco, AFM thermal imaging as an optimization tool for a bulk micromachined thermopile, Sens. Actuators A: Phys. 115 (2004) 440–446.

[15] www.ansys.com.

[16] S. Udina, M. Carmona, G. Carles, J. Santander, L. Fonseca, S. Marco, A micromachined thermoelectric sensor for natural gas analysis: thermal model and experimental results, Sens. Actuators B: Chem. 134 (2008) 551–558.

[17] N.P. Barnes, M.S. Piltch, Temperature-dependent Sellmeier coefficients and nonlinear optics average power limit for germanium, J. Opt. Soc. Am. 69 (1979) 178–180.

Biographies

Jordi Fonollosa was born in Barcelona, in 1980. He received his BS in physics and his BS in electronic engineering from the University of Barcelona in 2002 and 2007, respectively. He started his PhD studies in 2004 in the University of Barcelona. His main research areas are related to diffractive lenses design and synchronous detection for gas sensing applications.

Dr. Manuel Carmona obtained the PhD degree at the Universitat de Barcelona in 2000 in the field of modelling and simulation of MEMS. After that, he has worked at Infineon with thermo-mechanical issues of memory packages and at Seiko Epson with RF devices (resonators and microswitches). The main field of interest is the development of MEMS/NEMS, with strong focus on the use of modelling/simulation/test techniques.

Dr. J. Santander was born in Terrassa, Spain, in 1966. He received the BS and PhD degrees in physics from the Autonomous University of Barcelona, Spain, in 1989 and 1996, respectively. He is currently working at the Microelectronics National Center in Barcelona, as responsible for the electrical parametric characterization of different microelectronic technologies (CMOS, MCM, sensors, microsystems) using mainly test structures. His main research areas are related to microsystems, gas sensing applications and microfuel cells.

Dr. Luis Fonseca was born in Barcelona, Spain, in 1966. He received his BS and PhD degrees in physics from the Autonomous University of Barcelona in 1988 and 1992, respectively. In 1989, he joined the National Center of Microelectronics as a post-graduate student, working till 1992 on the growth and characterization of thin dielectric films for VLSI and ULSI applications. In 2001, he joined the Microsystems group as a full senior researcher being his actual research area focused on technological developments for gas sensing and more specifically on optical gas sensing.

Dr. Mauricio Moreno was born in Barcelona, Spain. He received the degree in physics in 1989 from the University of Barcelona (UB), and the PhD degree in sciences in 1995 from the Polytechnic University of Catalonia (UPC), Spain. He has been associate professor in the Electronics Department, UB, since 1997. He is involved in the design and test of microoptics devices in silicon technologies, and optical waveguide grating devices for biosensing applications. Other fields of interest include arrays of integrated photodetectors in CMOS technology for imaging.

Dr. Santiago Marco is associate professor at the Departament d'Electrònica of Universitat de Barcelona since 1995. He received the BS degree in physics from the Universitat de Barcelona in 1988, and in 1993 his PhD from the Departament de Física Aplicada i Electrònica, Universitat de Barcelona. His current research interests are the modelling, simulation and test of microsystems and the development of intelligent gas measurement instruments based on soft-computing techniques.

TECHNICAL PAPER

A compact optical multichannel system for ethylene monitoring

J. Hildenbrand · J. Wöllenstein · S. Hartwig · A. Eberhardt · B. Halford ·
M. Moreno · J. Fonollosa · L. Fonseca · J. Santander · R. Rubio ·
I. Gràcia · C. Cané

Abstract Precise and continuous ethylene detection is needed in various fruit ripening applications. The aim of this work is the development of a miniaturised mid-infrared filter spectrometer for ethylene detection at 10.6 µm wavelength. For this reason optical components and signal processing electronics were developed, tested and integrated in a compact measurement system. The main optical components, their integration of the optical system, as well as a description of the developed electronics and the first results of gas measurements are described in this paper. In fact the application conditions demand not a single channel system but a multichannel one. A silicon-based macroporous IR-emitter, a miniaturised absorption cell and a detector module for the simultaneous measurement with four channels including, ethylene, two interfering gases and the reference signal were integrated in the optical system. The new inner architecture of the detector module, consisted of optical filters which were directly attached by flip-chip technology onto the thermopile-arrays, allowing silicon-based Fresnel multilenses to be attached to the cap of the detector housing. Because of the high reflection losses at the silicon-air surface the Fresnel lenses were coated with zinc sulphide antireflection layers. For the signal processing electronics a preamplification stage and a DSP-based lock-in-amplifier has been developed. Although some of this work is still on-going, first ethylene measurements with the miniaturised gas cell, silicon-based IR-emitter, a commercial thermopile detector and the self-developed system electronics showed a detection limit better than 20 ppm.

1 Introduction

The on-line monitoring of ethylene plays a crucial role during the logistic chain of climacteric fruit such as pears and apples. In particular, at the earlier logistic stage, the long-term storage after harvest, low levels of ethylene have to be early detected since they are indicative of fruit ripening. Conversely, ethylene is actively added, when the ripeness of the fruit in storage is to be promoted, such as in the degreening process usual in citric fruit and bananas. In both cases, precise and continuous ethylene detection would be very advantageous. However, up to now no suitable and compact ethylene-monitoring systems are available on today's store-houses. For this reason a miniaturised filter spectrometer for ethylene monitoring in fruit applications has been developed. The aim is a small and low cost optical system for the ethylene detection in the mid-infrared at the wavelength 10.6 µm. For this application, a sensitivity of 20 ppm ethylene is required. In fruit storage applications other gases appear and can overlap the optical measurement of ethylene.

Numerous hydrocarbons in concentrations of ppb are negligible for the optical measurement, but ammonia, ethanol and acetaldehyde can occur in concentration ranges

J. Hildenbrand (✉) · J. Wöllenstein · S. Hartwig ·
A. Eberhardt · B. Halford
Fraunhofer Institute for Physical Measurement Techniques,
Heidenhofstr. 8, 79110 Freiburg, Germany
e-mail: juergen.hildenbrand@ipm.fraunhofer.de

M. Moreno · J. Fonollosa
Departament d'Electrònica. Facultat de Física,
Universitat de Barcelona, Martí i Franques, 1,
08028 Barcelona, Spain

L. Fonseca · J. Santander · R. Rubio · I. Gràcia · C. Cané
CNM-IMB (CSIC) Campus de la Universidad Autónoma de
Barcelona, 08193, Bellaterra, Barcelona, Spain

of several ppm, and thus have to be considered for cross sensitivity of the IR-measurement of ethylene. During long term fruit storage temperature is kept low (a few centigrade degrees), humidity is kept high (95%) and a special low oxygen preservation atmosphere is used, setting a environmental condition which is stressful for the fruit in the long run. Ethanol and acetaldehyde are the result of this fruit stress, whereas ammonia contamination may be caused by leakage of the cooling system. Therefore the absorption at other wavelengths has to be determined, i.e. a multi-spectral measurement has to be performed. The detection of these additional gases has not to be regarded as a penalty for precise ethylene monitoring because their detection is of interest in itself. The advantage of early detection of an ammonia leak is obvious, and the continuous monitoring of fruit stress could be used to actively tune the storage atmosphere by the accurate regulation of its content of oxygen and carbon dioxide, which results in the enhancement of the storage time and quality of the fruit (Veltman et al. 2003).

The principle of the optical (infrared) measurement system is shown in Fig. 1. The modulated radiation of a thermal emitter is coupled into a long-path gas cell and is detected by a multi-sensor array, preamplified and processed by lock-in technique. Non-dispersive infrared (NDIR) gas systems use one specific detector for each gas to measure. Therefore, a specific optical filter must be placed upon the IR detector to select the suitable wavelength for each gas. To increase the sensor signal lenses are usually include as well.

To reach the required selectivity and sensitivity of 20 ppm for ethylene, an IR-emitter, a compact long path absorption cell, the detection module and system electronics were developed and integrated in a compact system. In the subsequent sections the development of the component prototypes, the system integration and gas measurements with a first system set up are presented.

2 Optical components

2.1 Miniaturised White cell

Lambert–Beer law relates the infrared transmission loss through a sample to the gas absorption coefficient, gas concentration and to the optical path length. The detection of poorly absorbing species or at very low concentrations requires long optical paths. A miniaturised White cell has been developed in order to maintain small physical dimensions of the measurement system and fulfilling the minimum optical path length necessary for the detection of ethylene in the required concentrations. The principle of the White cell is based on multiple reflections between three spherical concave mirrors, which have all the same radius of curvature (White 1942). The optical set-up features a high light transmission where radiation losses are caused only by absorption and scattering on the reflecting surfaces. The optical path, i.e. the number of reflections is dependent on the adjustment of the mirrors, but limited by the diameter of the active area of the source. The

Fig. 1 Schematic set up of the measurement system consisting of a microstructured IR-emitter, a miniaturised multi-reflection cell, a thermopile-array with integrated optical filters and microstructured Fresnel lenses and signal processing electronics
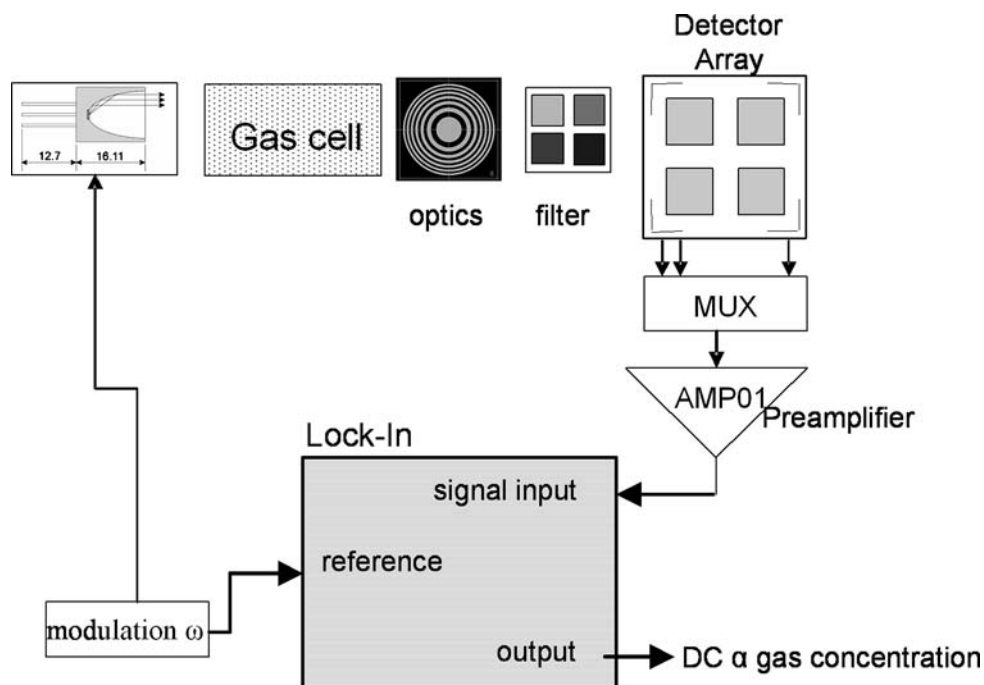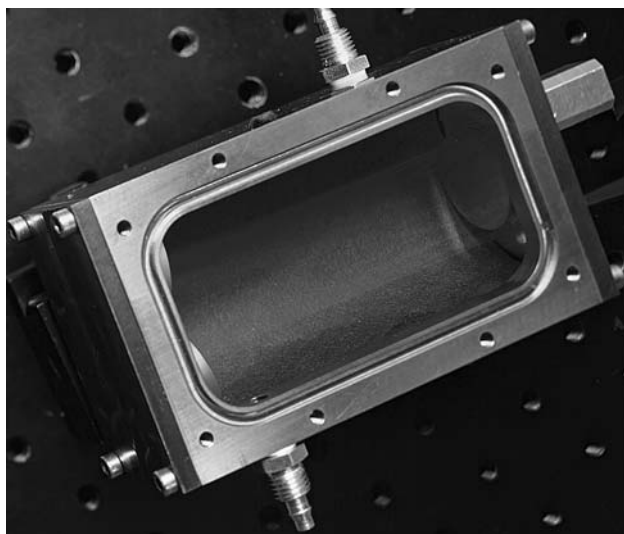
Fig. 2 Miniaturised White cell with 1.6 m optical path length. The light inlet and outlet ports are beside the single front mirror. The gas inlet and outlet are placed on the lateral walls

miniaturised White cell with front and rear field mirrors is shown in Fig. 2. Here an optical path length of 1.6 m after 20 reflections is achieved in a volume of $11 \times 5 \times 6$ cm^3. The body of the cell is machined in aluminium. The mirrors, gold-coated convex glass lenses are glued into the White cell.

The miniaturised White cell is a component of significant volume in terms of the whole instrument, and the degree of miniaturization achieved requires precision machining. For the rest of the elements of the optical instrument, namely, the emitter and the detector module, microsystem technologies have been employed in an attempt to obtaining a compact and cost-effective system. The multi-element nature of an optical system and its size could be regarded as a disadvantage of an optical approach when compared to other gas microsensor systems. Nevertheless, the inherent selectivity of the optical alternative and its unrivalled long term stability makes it the option of choice for the considered application in which, on the other

hand, the overall size of the instrument or its power consumption are not severe constraints.
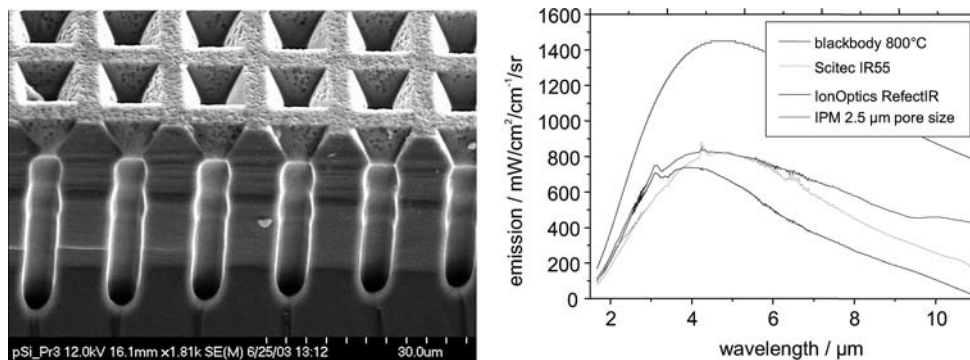
2.2 Micromachined IR-emitter

Commercially available emitters have a moderate emission compared with an ideal black body radiator, especially at longer wavelengths. For that reason, a novel type of micro machined thermal IR-emitter has been developed, see Fig. 3. It is based on micro structured silicon samples from Infineon Technologies. The main difference compared with common thermal micro emitters is the use of 3D structured bulk silicon. The regular ordered macro pores of the emitter are obtained by electrochemical etching of prepatterned silicon substrates (Lehmann 2002;Konz et al. 2005). Typical pore diameters of the fabricated photonic-crystal-like structures are in the range of 2.5–30 μm. The macroporous silicon shows a black-body-like emission profile for a wide wavelength range. The device is heated using a thin film Pt-heater structured onto the backside of the substrate and with a power of 2.5 W can be operated at 800°C with and advantageous emission in the 10 μm range.

2.3 Detector module

For multi-spectral measurements a thermopile-detector-array with integrated optical filters and microstructured Si-Fresnel lenses has been developed. The general architecture of the detection module is shown in Fig. 4 left. It consists of a substrate chip with an array of 2×2 thermopile-elements based on silicon-technology that is attached to the base of the package. For selection of the wavelengths the appropriate optical filters are placed onto them. Attached to the top of the package is a Fresnel multilens, intended to divide the total IR radiation transmitted by the absorption cell into four parts and focus each one of the parts into the corresponding absorber zone of the thermopiles.

Fig. 3 SEM-picture of the IR-emitter structure based on regular ordered macropore arrays (*left*). Comparison of the emission spectrum of the presented emitter compare to a black body and two commercially available ones (*right*)
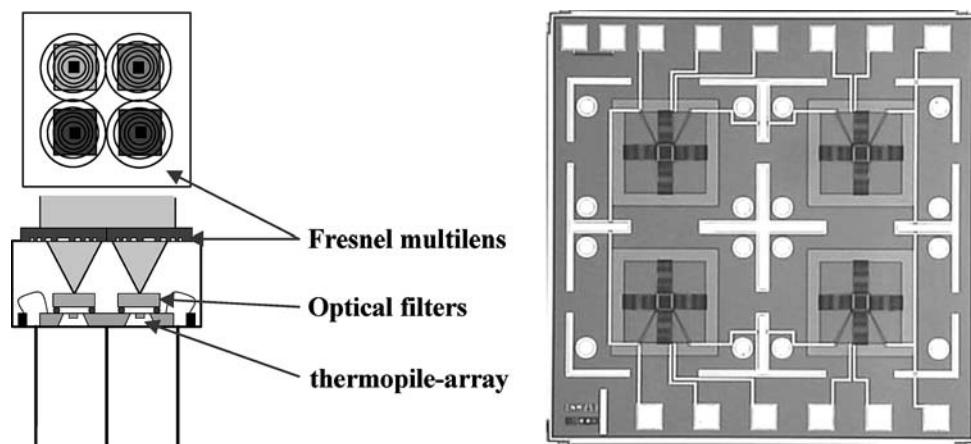
Thermopile detectors have been selected as infrared detector since they do not need power to be operated, offer a broadband response, can be fabricated in silicon technology, and an array of them can be easily integrated with a low foot-print in a single chip. In this case, a bulk micromachined fourfold thermopile-array, each one composed of 40 thermocouples, has been fabricated as shown in Fig. 4. A detailed description of the processing of the thermopiles can be found in Fonseca et al. (2004a, b), and their optical characterisation has been reported in Hartwig et al. (2005). The optical filters, providing the selectivity of each channel, are commercial narrow bandpass filters properly diced and conditioned to attach them onto the thermopile elements by flip-chip bonding. The required parameters of the optical filters were defined from the absorption spectra of the relevant gases, i.e. ethylene, ammonia, ethanol and acetaldehyde (Pouchert 1985). The gases show some interfering absorptions in the mid infrared, i.e. they can cause cross sensitivities during the IR-measurement of ethylene. Filter wavelengths for ethylene at 10.6 μm, ethanol at 3.46 μm, ammonia at 9.7 μm and a reference channel at 3.95 μm have been chosen for the 4-element thermopile-array (Fig. 5). The combined use of the three species oriented filters can elucidate the presence of any of these gases in a potential mixed sample.

### 2.4 Silicon-based Fresnel multilenses

In order to increase the irradiance on the thermopile elements silicon-based diffractive lenses, so called Fresnel lenses, are used as focusing elements, see Fig. 6 left. The advantages of diffractive lenses are less absorption and the possibility to fabricate micro lenses with microelectronic technology. A diffractive Fresnel lens is ideally shaped in such a way that all the points of the lens surface introduce a change of the optical path that produces a constructive interference at the lens focal point. Fabricated by planar silicon technology, the Fresnel lenses are staircase approximations to the original curved Fresnel profile. In the first steps single binary and 8-level lenses at different sizes and focal length for 4 and 10 μm wavelength, have been fabricated and optically characterised. Optical calculations showed that an 8-level staircase profile was a sufficient approximation to get good transmission values and the characterisation of the individual lenses fabricated for each wavelength showed sharp focussing properties. A detailed description of fabrication and characterisation of these lenses can be found in Fonollosa et al. (2006). In summary, the focal point was well defined along the optical axis of the lens and the measure spot size at the focal point was in the order of 100 μm, which is also the characteristic length of the thermopile absorber.

Fig. 5 Infrared spectra of ethylene, ammonia and ethanol and the four filter window selected for the proper optical discrimination of those substances
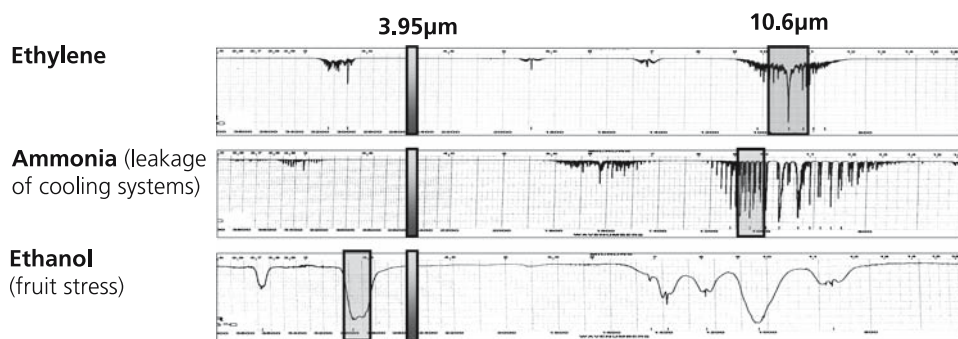
C.J. Pouchert: *The Aldrich Library of FT-IR Spectra, Vapor Phase*, Volume 3, Aldrich chemical company, Inc., 1985.

Fig. 6 SEM-picture of a 8-level micromachined silicon Fresnel lens (*left*) and photo of a Fresnel multilens with four sublenses (*right*)
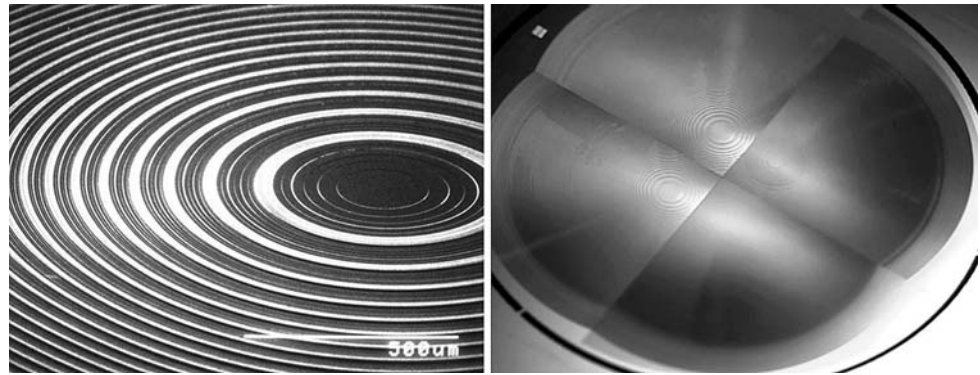
Subsequent Fresnel multilenses, as shown in Fig. 6 right, were designed consisting of four (fragmented) sublenses in a single chip. The topography of each sublens was adapted to the different target wavelengths, i.e. 3.5, 3.9, 9.7 and 10.6 μm. Some of the lens design parameters—namely ring diameter and groove depth—depend not only on the distance of the object and the image planes (focal length, centre position etc.) but also on the wavelength they are designed for. In order to fabricate the four lenses on the same substrate with a minimum number of photolithographical steps, a new design using a binary combination of four masks for all lenses is considered. This lead up to 16 level topography with a maximum accumulated etch depth of 3.75 μm. The four corresponding silicon etches were optimized for the longer wavelength sublens, 10.6 μm, and as many as possible of those fixed levels were used as the best approximation for the rest of sublenses. This approach provides at least 6–8 appropriated levels for the sublenses of the shorter wavelength assuring transmissions efficiencies over 85% in the worst case. A more detailed description of design and fabrication of the Fresnel multilenses is given in Fonollosa et al. (2007).

For the optical characterisation of the Fresnel multilenses their focal length were measured with the following set-up. An IR-emitter with an 1 mm pinhole in front has been mapped by the Fresnel lens on a liquid nitrogen cooled IR-detector (MCT-detector) with 1×1 mm^2 sensitive area. In front of the pinhole the corresponding optical filters for the target wavelengths 3.46, 3.95, 9.7 and 10.6 μm were used. All quadrants of the multilens—corresponding to the four wavelengths—were measured by covering the other three lens quadrants with an aperture. In the set-up the object distance D1 between IR-emitter (with pinhole) and the Fresnel lens was fixed. After adjusting the Fresnel lens in x- and y-direction and the image distance D2 to maximum signal, the focal length f was calculated from the measured object distance D1 and the image distance D2. The focal lengths measured in this way just showed a 5% deviation from the design value of 6.7 mm, so it is assumed that the fabricated multilenses are suitable for the proposed detector module.

### 2.5 Antireflection coating of Fresnel multilenses

The high index of refraction of silicon of $n = 3.42$ at 10 μm wavelength implies a significant loss of radiation by reflection. This can be estimated from the Fresnel formula of a silicon component (two interfaces) in air at 10 μm wavelength at about 51%. For this reason an antireflection-coating (AR-coating) has been used to obtain a higher transmission of the Fresnel lenses.

For the development of the AR-layer, simulations with the software TFCalc 3.5 have been performed calculating single layer AR-coatings based on a $\lambda/4$-layer. The geometrical thickness of the layer can be calculated by formula (1) where $n1$ is the refractive index of the material in front of the $\lambda/4$-layer, $n2$ the refractive index of the material behind the $\lambda/4$-layer and $n_{\lambda/4}$ the refractive index of the quarter-wave-layer. For complete AR behaviour it is an additional requirement, that the interfering waves have nearly the same amplitudes. This can be achieved by $n_{\lambda/4}$ as calculated by the formula (2).

$$d_{\lambda/4} = \frac{\lambda}{4} \cdot \frac{1}{n_{\lambda/4}} \tag{1}$$

$$n_{\lambda/4} = \sqrt{n_1 \cdot n_2} \tag{2}$$

For the interface air/silicon as well as for silicon/air the optimal refractive index of the $\lambda/4$-layer $n_{\lambda/4}$ is about 1.85. For this reason zinc sulphide (ZnS) with the refractive index 2.2 closest to the optimal refractive index has been chosen. Due to the high transmission of the used materials at the regarded wavelengths and the thin layers, the amount of absorption was neglected for the calculations. The simulated transmissions are for a silicon sample with an AR-coating on the front side and on the backside. Thus, the system has the form Air [AR]Si [AR]Air. Luckily enough, an AR-coating optimized for wavelengths in the vicinity of 10 μm has also a significant positive effect on wavelengths around 3.5 μm. In this way, the deposition of just one AR-coating is suitable for the four target wavelengths. In Fig. 7 the reflection losses of the silicon substrate – uncoated, with ZnS-AR-coating of thickness 1.193 nm on one side
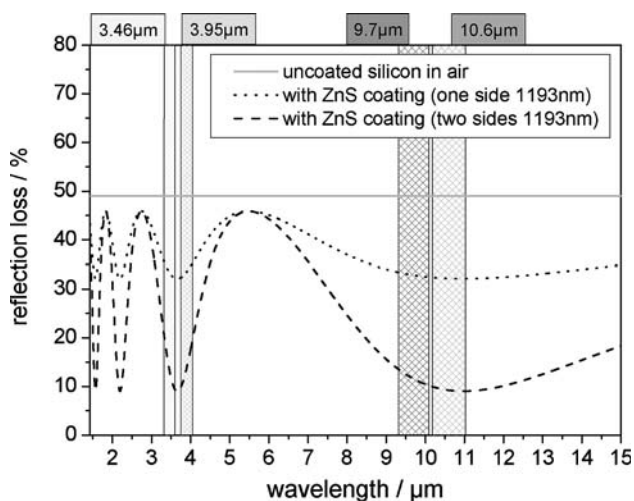
Fig. 7 Simulated reflection loss of silicon in air (two surfaces, *grey*) with ZnS-AR-coating on one (*dot*) and on both sides (*dash*) of the silicon

and on both sides are shown. With the AR-coating just on one side of the Fresnel lenses a value of reflectance of about 32–35% can be achieved, with the simulated ZnS-layer on both sides the reflection loss is decreased from 49 to 10% for all target wavelengths.

After tests with Si-samples and single Fresnel lenses, the multilenses, described previously, were coated with ZnS-AR-layers on both surfaces. There are small shifts between the focal lengths of uncoated and AR-coated multilenses. The difference in the focal lengths for the four wavelengths is about 0.25 mm. The transmitted signals could be increased for all target wavelengths by the ZnS-AR-coating. The corresponding enhancement factors of transmitted signals are given in Table 1.

Furthermore reflection measurements for the four quadrants of the multilens have been measured at a reflection angle of 30°. The measured and simulated reflectivity of the AR-coated surfaces for 10.6 μm wavelength is plotted in Fig. 7. Despite the influence of the backside of the lens, the measured minima of the reflectivity fit well to the simulated minima for 30° reflection angle. Therefore it can be assumed that the minima in reflectivity at reflection angle 0° fit well to the simulation at 0° and with this at the target wavelengths (vertical bars).

Table 1 Enhancement factors of transmitted signal after ZnS-AR-coating of the Fresnel multilens

Target wavelength/ μm	Signal uncoated/ mV	Signal AR-coated/ mV	Improvement factor
3.46	4.84	6.56	1.36
3.9	3.23	6.42	1.99
9.7	2.71	4.60	1.70
10.6	2.07	3.75	1.82

Fig. 8 Completed detectors with the AR coated silicon Fresnel lenses. The open package shows the thermopile array covered by the four narrow bandpass filters and the facing down Fresnel lenses attached to the package lid

A finished detector module following the proposed architecture of Fig. 4 can be seen in Fig. 8 featuring the different microcomponents described above.

3 System integration

The set-up of the optical system with miniaturised absorption cell, IR-emitter, optical chopper, coupling optics and detector module is shown in Fig. 9. The IR-emitter is mounted in a TO8-housing. For modulation of the radiation a motor driving a chopper blade as a light barrier is used. Different set-ups of coupling optics for the White cell have been tested. Spherical mirrors, a zinc selenide lens (ZnSe), parabolic mirrors and an ellipsoid mirror were compared. The ZnSe-lens showed the best results with regards to coupling efficiency and compactness and has been used in the final set-up. To avoid radiation losses at an additional window the ZnSe-lens is mounted in a tube and closes the White cell at the input focus. The distance between the output focus of the White cell and the detection module depends on the tolerances of focal length of Fresnel multilens and will be adjusted during the final system tests. The optical output port of the White-cell is sealed with a CaF_2-window.

4 System electronics

The fourfold thermopile array provides three information channels and one reference channel. To acquire the

Fig. 9 Optical system with miniaturised White cell, IR-source, optical chopper, ZnSe-lens and detector module
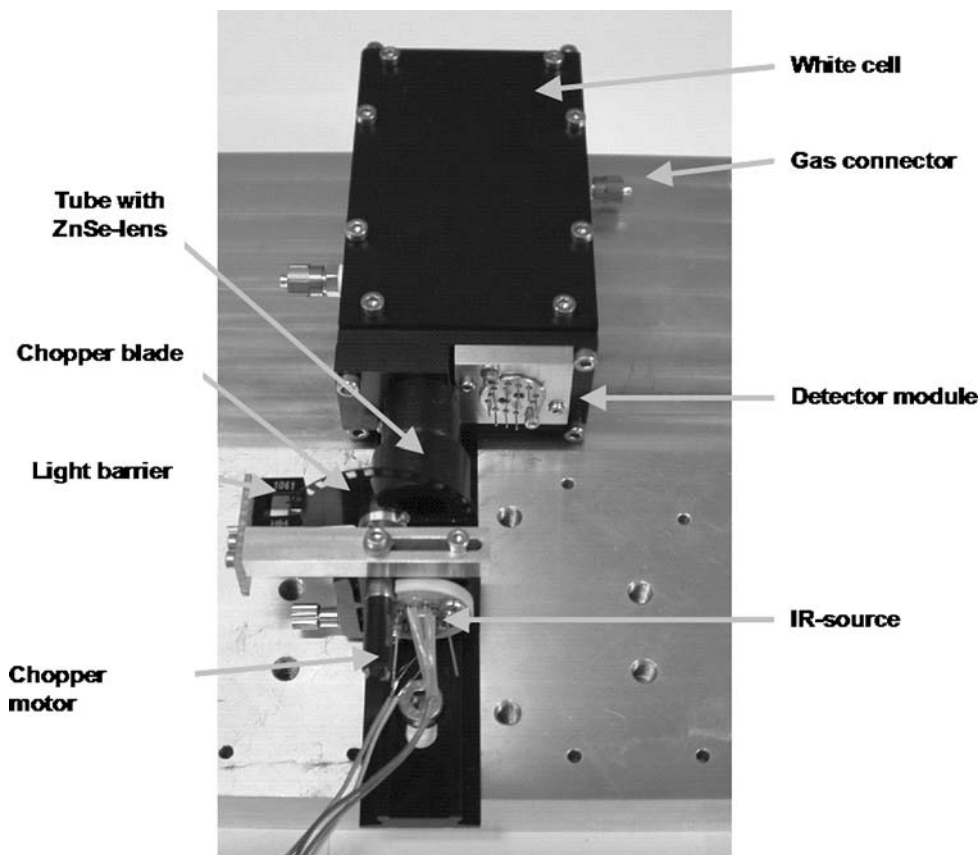
information from the three channels, a multiplexer is used. Following the preamplification stage, synchronous detection (lock-in-amplifier) is used to filter and measure the low level signal. The IR-emitter is stabilized to ensure a constant relative emission at all wavelengths of interest. An optical (mechanical) chopper modulates the emitter optical power at a frequency compatible with the optimum frequency response of the thermopiles. The modulation signal of the infrared source is also used as reference signal for the lock-in-amplifier. The lock-in amplifier has been designed and digitally implemented using a MSP430F4270 microcontroller (from Texas Instruments) and D4270 SoftBaugh PCB.
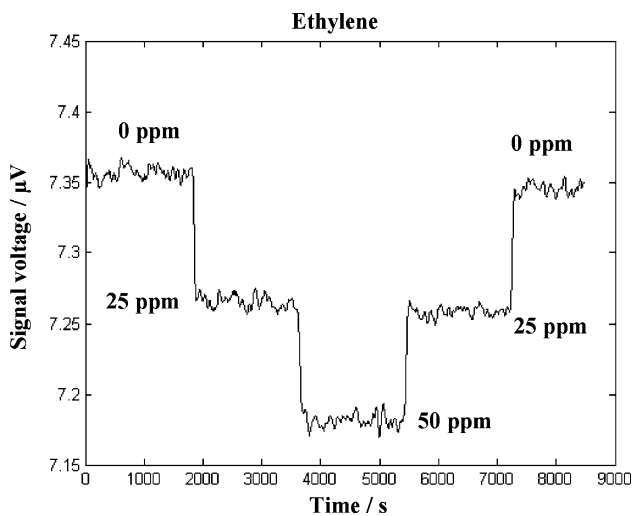
5 Measurements

The optical set-up and the pre-amplification board have been tested in different gas measurements with and without the pre-amplification board. In the set-up the 1.6 m White cell with the micromachined IR-emitter, a mechanical chopper at 8 Hz, a commercial thermopile from Heimann Sensor and a commercial lock-in has been used. Figure 10 shows the chopped signal without preamplification. For the tests, concentration sequences of ethylene of 0, 25, 50, 25 and 0 ppm with duration of 30 min for each step were

used. The detection limit of the optical set-up with and without preamplification board is below 20 ppm for a measurement time of 2 s. Similar measurements with the first generation of in-house thermopiles yielded a worse detection limit of 100 ppm, which is still valid for ethylene alarm management.

6 Conclusion and outlook

A miniaturised filter photometer for ethylene with an optical path of 1.6 m has been developed for fruit storage applications. In order to minimise cross-sensitivities to other expected gases (ammonia, ethanol) a multichannel system has been set up in what can be considered a multipurpose instrument for controlled atmosphere management. The IR-emitter, an optical chopper, a miniaturised cell and a detector module for the simultaneous measurement at four wavelengths have been integrated in the optical system. For the assembly of the detection unit optical filters were attached to fourfold thermopile-arrays by flip-chip-technology. As a focusing unit silicon-based Fresnel multilenses were processed. The fabricated Fresnel multilenses showed homogeneous focal lengths for the four target wavelengths. By coating the Fresnel multilenses with zinc sulphide antireflection layers the transmission of the

Fig. 10 Detector signal during measurement of different ethylene concentrations

lenses was increased by a factor of 1.4–2. For the signal processing electronics a preamplification stage and a Lock-in-board has been developed. First ethylene measurements with the optical system with miniaturised gas cell, silicon-based IR-emitter, a thermopile detector and the system electronics showed a detection limit better than 20 ppm, validating the overall approach. Currently newer, more sensitive thermopiles are processed, in the next step these thermopiles will be integrated together with the Fresnel multilens in one package. A significant signal to noise improvement is then expected.

References

Fonollosa J, Rubio R, Hildenbrand J, Moreno M, Marco S, Santander J, Fonseca L, Hartwing S, Woellenstein J (2006) Fresnel Lenses: study and fabrication in silicon technology for medium-IR applications. Proceedings SPIE 61860R-1:61860R–11

Fonollosa J, Rubio R, Hildenbrand J, Hartwig S, SantanderJ, Moreno M, Marco S, Fonseca L, Wöllenstein J (2007) Design and fabrication of micromachined silicon based mid infrared multilenses for gas sensing applications. Transducers 2007 Proceedings (in press)

Fonseca L, Cabruja E, Calaza C, Rubio R, Santander J, Figueras E, Gracia I, Cane C, Moreno M, Marco S (2004a) Feasibility of a flip-chip approach to integrate an IR filter and an IR detector in a future gas detection cell. Microsys Technol 10:382–386

Fonseca L, Perez-Murano F, Calaza C, Rubio R, Santander J, Figueras E, Gracia I, Cane C, Moreno M, Marco S (2004b) AFM thermal imaging as an optimization tool for a bulk microma-chined thermopile. Sens Actuators A Phys 115:440–446

Hartwig S, Hildenbrand J, Moreno M, Fonollosa J, Fonseca L, Santander J, Rubio R, Cané C, Lambrecht A, Wöllenstein J (2005) A highly sensitive IR-optical sensor for ethylene-monitoring. Proceedings SPIE 5836:452–460

Konz W, Hildenbrand J, Bauersfeld M, Hartwig S, Lehmann V, Wöllenstein J (2005) Micromachined IR-source with excellent blackbody like behaviour. Proceedings SPIE 5836:540–548

Lehmann V (2002) Electrochemistry of silicon. Wiley-Vch, Weinheim

Pouchert CJ (1985) The Aldrich library of FT-IR spectra, vapor phase, vol. 3. Aldrich chemical company, Inc

Veltman RH, Verschorr JA, Van Dugteren JH (2003) Dynamic control system (DCS) for apples (Malus domestica Borkh. cv "Elstar"): optimal quality through storage based on product response. Postharvest Biol Technol 27(1):79–86

White JU (1942) Long optical paths of large aperture. J Opt Soc Am 32:285–288
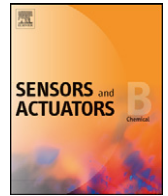
Ethylene optical spectrometer for apple ripening monitoring in controlled atmosphere store-houses

J. Fonollosa [a,d,*], B. Halford [b], L. Fonseca [c], J. Santander [c], S. Udina [a,d], M. Moreno [a], J. Hildenbrand [b], J. Wöllenstein [b], S. Marco [a,d]

[a] Departament d'Electrònica, Universitat de Barcelona, Martí i Franquès 1, 08028 Barcelona, Spain
[b] Fraunhofer Institute for Physical Measurement Techniques, Heidenhofstr. 8, 79110 Freiburg, Germany
[c] Centre Nacional de Microelectrònica, Campus UAB, 08193 Bellaterra, Spain
[d] Artificial Olfaction Lab, Institute of Bioengineering of Catalonia, Baldiri i Rexach 13, 08028 Barcelona, Spain

A B S T R A C T

In today's store-houses the ripening of fruit is controlled by managing the ethylene concentration in the ambient atmosphere. Precise and continuous ethylene monitoring is very advantageous since low ethylene concentrations are produced by the fruit itself and are indicative of its ripeness, and on other occasions, ethylene is externally added when ripeness or degreening of the product must be promoted. In this work, a multichannel mid-infrared spectrometer for ethylene measurement is built and characterized. The instrument contains additional channels to reject potential cross-interferences like ammonia and ethanol. Additionally, these channels are useful for monitoring a potential malfunction of the cooling system and possible fouling of the fruit, respectively. The complete spectrometer contains a silicon-based macroporous infrared (IR) emitter, a miniaturized long path cell (white cell), a four-channel detector module, low-noise analog amplification and filtering, and a microcontroller-based lock-in amplifier. The new inner architecture of the detector module features a fourfold thermopile array with narrow band optical filters attached by flip-chip technology, and a Fresnel lens array attached on the lid of the package. Laboratory tests show that the system is able to distinguish between ammonia and ethylene, featuring a detection limit of 30 ppm and 160 ppm (95% confidence) for ethylene and ammonia, respectively. Field tests show that the spectrometer is suitable as an ethylene alarm to detect fruit ripening and prevent fruit to decline into senescence. Simulation results show that system selectivity could be improved by setting ammonia channel to another absorption wavelength.

© 2008 Elsevier B.V. All rights reserved.

1. Introduction

At home most varieties of apple can be stored for approximately a couple of weeks. However, large-scale production of apples requires huge crop and fruit storing for several months, in such a way that the final fruit is in good organoleptic quality. With that aim, fruit is harvested before it is ripe enough to be consumed and is stored in controlled atmosphere chambers to delay ripening process. Harvesting mature unripe fruit increases shelf life, slows down degradation in firmness and acidity, and green ground-color becomes slower than in ripe fruit.

Nowadays apples can be stored in different conditions: cold storage (CS) which is the usual procedure during transport and at the retailer vending, low oxygen (LO), and ultra low oxygen (ULO) which

are the techniques applied for long duration fruit storage. Table 1 shows typical oxygen and carbon dioxide concentrations, relative humidity, and temperature for CS, LO, and ULO conditions. ULO storage rooms slow down ethylene synthesis and respiration process extending the storage period of 7–9 months [1], and have beneficial effects on fruit firmness, titratable acidity and color [2,3]. On the other hand, the use of unripe fruit and such storage conditions worsen apple's flavor since the production of volatile compounds responsible for the aroma is reduced [4,5] and fruit taste is strongly impaired [6].

Ethylene plays a twofold role in fruit development: it can be thought as an indicator that fruit is ripening (low ethylene concentrations are produced by the fruit itself), and also as a hormone that triggers the ripening process of fruit [7,8]. In some occasions ethylene is externally added when ripeness or degreening of the product must be promoted. In store-houses, ethylene concentration is below 1 ppm while fruit is unripe. Then, as fruit ripening begins, the production of ethylene increases dramatically and its concentration continuously rises to values higher than 100 ppm. Fruit

---

* Corresponding autor at: Departament d'Electrònica, Universitat de Barcelona, Martí i Franquès 1, 08028 Barcelona, Spain.
E-mail address: jfonollosa@el.ub.es (J. Fonollosa).

Table 1
Environment for different storage conditions.

	Oxygen concentration	Carbon dioxide concentration	Humidity	Temperature
CS	21%	200 ppm	(90%, 96%)	0 °C
LO	(2%, 3%)	(2%, 5%)	(90%, 96%)	(−1 °C, +1 °C)
ULO	(1%, 1.5%)	(1%, 1.5%)	(93%, 95%)	(0.3 °C, 0.5 °C)

senescence starts typically 15 days after ethylene burst [9]. Therefore, ethylene can be used to establish the ripening of fruits [6]. Since ethylene accumulation in conservation or transport chambers threatens the conservation process and may lead to important losses, precise and continuous ethylene detection is very advantageous to assess fruit ripening and prevent the fruit to decline into senescence.

Nowadays, most of the apple store-houses only monitor continuously oxygen and carbon dioxide concentrations, which do not provide any fruit status information. While ethylene can be controlled by gas chromatography–mass spectrometry, this technique is expensive, typically off-line, and requires periodic air samples extracted from the chambers, at a frequency (e.g. weekly) that may be too low to address conservation requirements in an efficient way. Commercial systems based on chemiluminescent reaction of ethylene (Portable ethylene monitor, Geo-centers INC, USA) or on electrochemical sensors (Polytron 3000, Dräger, Germany) are available. However ozone is needed as a reagent in the first case, and electrochemical cells have a limited lifetime and show a gradual decrease of sensitivity that renders calibration obsolete rapidly [10], making them unpractical for long-term fruit monitoring. Metal oxide sensors have also been proposed for monitoring ethylene but they exhibit strong cross-interferences, humidity sensitivity, and stability problems [11].

Infrared (IR) optical gas analyzers are selective and stable instruments based on the attenuation of the incident radiation at specific absorption bands. They can be configured for the measurement of several species by using different selective filters and they are rather immune to false alarms and poisoning since the detectors are not in direct contact with the gas. In addition, long-term stability can be improved by the use of a reference band without absorptions [12]. Although the relationship between the optical absorption and the gas concentration shows a non-linear behavior (Lambert–Beer law), optical measurements are considered, in general, to be more reliable than solid-state gas sensors [10].

Exposing apples to low oxygen conditions consistently enhances acetaldehyde and ethanol concentrations, which can greatly exceed concentrations of several hundred of ppm. However, when the atmosphere is set to air conditions, ethanol and acetaldehyde concentrations decrease to initial values [13,14]. On the other hand, ammonia is increasingly the coolant of choice for food cooling systems instead of substances with high ozone layer endangering potential. When an ammonia leakage occurs, its concentration can easily reach 200–1000 ppm and safety regulations make some reaction obligatory [15]. Unfortunately, ethanol, acetaldehyde and ammonia all absorb at 10.6 μm, which is the strongest absorption region for ethylene. Therefore, these gases must be considered for cross-sensitivity of the IR optical measurement of ethylene and a multichannel spectrometer is a must. Additionally, typical flavor compounds of apples are produced when ripening is initiated. Over 300 volatile compounds have been identified in the aroma profile of apples [13], but they are of a very low concentration and it can be assumed that they do not interfere to ethylene measurement.

Several unspecific infrared spectrometers based on non-specific filters have already been presented [16,17]. However, since target gases are well-defined for the application of apple ripening

detection the authors already introduced a specifically oriented multichannel optical miniaturized spectrometer [18].

In this work we present for the first time a fully calibrated spectrometer for ethylene and ammonia with the aim to show that the system is suitable for ethylene monitoring in the store-houses and is able to detect the ethylene burst that indicates that fruit is ripening. The presented spectrometer features significant differences in comparison with already presented previous versions [18] such as it is calibrated for both ethylene and ammonia, a new assembly of the optical components is presented, it features a pre-amplification stage based on an instrumentation amplifier and a specifically developed digital lock-in amplifier, and a multi-variable regression model is built for the gas calibrations.

The spectrometer is presented in Section 2, giving details regarding signal recovery. Laboratory tests and the calibration system are presented in Section 3. Section 4 introduces an output space data-processing method to reduce measurement errors, where it is assumed that only one of the species is in a high concentration. Field tests are presented in Section 5. Finally, in Section 6 we suggest new filter selection for improved system selectivity.

2. IR spectrometer description

Optical gas sensors usually consist of an IR emitter, an absorption cell that contains the gas to be measured, and an IR detector where the transmitted radiation is collected. Lambert–Beer law relates the radiation loss through the gas sample to the optical path length, the gas concentration, and to the gas absorption coefficient.

Non-dispersive infrared (NDIR) gas sensors use one specific detector for each gas to measure. Therefore, a four-channel optical spectrometer is presented to measure ethylene, ammonia, and ethanol concentrations, plus a reference channel. The developed spectrometer features an analog pre-amplification stage, and a digital lock-in amplifier as a signal recovery system. Therefore, the IR radiation must be modulated. A mechanical chopper is used with that purpose.

In this section the main components of the developed spectrometer are presented. Fig. 1 shows its block diagram.

2.1. IR emitter

A novel type of micromachined thermal IR emitter has been developed [19] with increased IR emission efficiency. The use of 3D structured macroporous silicon gives a higher black-body-like emission compared to the commercially available emitters at longer mid-infrared wavelengths. The device is heated using a thin film Pt-heater structured onto the backside of the substrate consuming 2.5 W of power at a maximum operating temperature at 800 °C, with an advantageous emission in the interesting 10 μm band.

2.2. Miniaturized white cell

The Lambert–Beer equation relates the optical path length to the transmittance. The detection of poorly absorbing species or at very low concentrations requires long optical paths. One possibility to increase the optical path length yet maintain the small physical dimensions of the gas sample chamber is the use of a white cell; the principle of which is based on multiple reflections between mirrors [20].

The white cell developed here employs three concave mirrors achieving an optical path length of 1.6 m after 19 reflections within a volume of 11 cm × 5 cm × 6 cm [21]. The body of the white cell is machined in aluminum and the mirrors are suitable gold-coated plan-concave glass lenses.
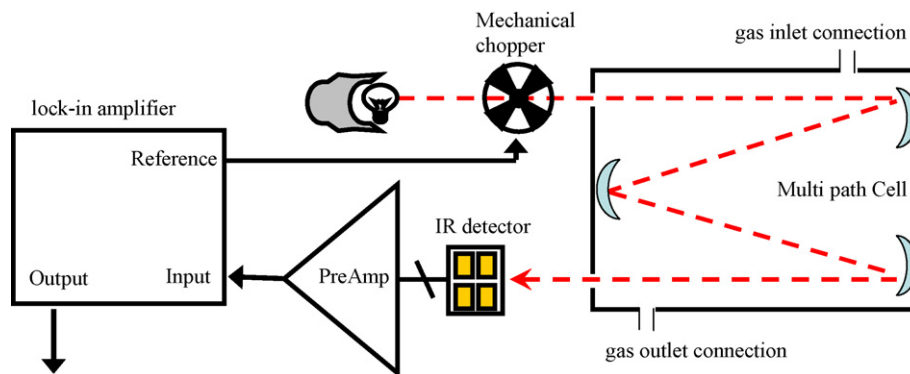
Fig. 1. Optical system, with miniaturized white Cell, IR emitter, detector module, and optical chopper.

2.3. Detector module

A novel highly integrated compact detection module comprising thermopiles, optical filters, and focusing elements is used to measure the remaining radiation after gas absorption [22]. IR detectors consist of a substrate chip with a 2×2 array of thermopile-elements that is attached to the base of a TO-8 package. For wavelength selection the appropriate optical filters are flip-chipped onto the thermopile-elements. A multi-Fresnel lens array is assembled in the lid of the package to optimize the device detectivity.

Micromachined thermopiles based on CMOS processing and bulk micromachining are chosen as infrared detectors since they exhibit good performance in terms of reproducibility, accuracy, low cost, sensitivity and rapid response [23]. Additionally, thermopiles do not need power to be operated, offer a wide spectral response, can be fabricated in silicon technology, and an array of them can be easily integrated with a low foot-print in a single chip [18]. Substrate chips ($6.1\,mm \times 6.1\,mm$ size) with four micromachined thermopiles in a 2×2 arrays, featuring a size compatible with a TO-8 package, have been fabricated [24]. Each thermopile features 32 thermocouples and absorber and membrane sizes are $350\,\mu m \times 350\,\mu m$ and $1300\,\mu m \times 1300\,\mu m$, respectively.

Optical filters, which provide the selectivity of each channel, are commercial narrow bandpass filters (supplied by Filtrop AG, Liechtenstein; and by LOT-Oriel, Germany) properly diced and conditioned to be attached to the thermopile substrate by flip-chip techniques [23]. Filter selection was made considering the most prominent absorption bands for the target gases: $3.4\,\mu m$ central wavelength (CWL) and 4% bandwidth (BW) for ethanol; $9.7\,\mu m$ CWL and 4% BW for ammonia, $3.9\,\mu m$ CWL and 2% for reference band, and $10.6\,\mu m$ CWL and 4% for ethylene.

The purpose of the lens array is to collect as much radiation as possible from the absorption cell and to divide the total IR radiation transmitted into four parts and focus each one of them into the corresponding absorber element of the four thermopile array. Diffractive Fresnel lenses are chosen as focusing element since they are compatible with the planar nature of silicon microtechnology and silicon is transparent in the IR range of interest. The advantages of diffractive lenses are less absorption, and the typical advantages of silicon technology such as reliability, mass production, and cost issues [22,25].

A Fresnel lens consists of a series of concentric rings with a given tapered shape, whose width decreases with the distance to the centre. Each ring is ideally shaped in such a way that produces a constructive interference at the lens focal point. However, planar silicon technology leads Fresnel lenses design to follow a staircase approximation of the original curved profile. Lens efficiency calculations show that an approach based on the use of four photolithographic masks to design a four lens array in a single chip is a cost effective alternative and assures optical transmission efficiencies over 85% in the worst case. To prevent reflection losses at the lens surfaces, zinc sulphide antireflection $\lambda/4$ layers were deposited. A specific four $6.7\,mm$ focal length lens array for the required system application was fabricated [22].

2.4. Signal recovery system

Lock-in amplifiers are widely used as signal recovery systems since they are characterized by a wide dynamic range which gives the ability to measure signals accompanied by relatively high levels of noise and interference. A lock-in amplifier behaves like a band-pass filter centred on a reference frequency. Signal modulation (at reference frequency) is convenient to shift the signal to a lower noise band. In practice, the modulation frequency is usually made as high as possible to facilitate separation of the chopped output voltage from noise components [26].

The signal recovery system is composed of an analog pre-amplification stage with pre-filters and a digital lock-in amplifier based on a MSP430F4270 microcontroller (Texas Instruments, USA). The aim of the pre-amplification stage is to expand the low thermopile voltage range to the 0–0.6 V programmed analog-digital converter input range. Instrumentation amplifier configuration is particularly advantageous if the amplifier is positioned some distance away from the signal source, in order to cancel common mode disturbances at the input terminals. An AMP01 (Analog Devices) low-noise instrumentation amplifier was chosen for this task.

The IR radiation, which will be later partially absorbed by the gas, must be modulated since the designed signal recovery system is a lock-in amplifier. In some cases, IR radiation may be directly modulated by switching the IR emitter. But in our case, the large thermal capacity of the IR emitter and the corresponding large time constant (up to 5 s) limit the modulation frequency. For this reason the IR emitter operates in continuous mode, and an optical chopper modulates the emitted radiation at 1 Hz, which is the optimum frequency compatible with the time response of the detector.

Since the detector unit is a four-channel device, the pre-amplification stage is fourfold. Each pre-amplification stage features one AMP01 instrumentation amplifier and a follow up filter stage to reduce the noise and avoid aliasing before the lock-in routine. Instrumentation amplifiers are designed with the required gain to expand the voltage to 0–0.6 V (10^4 V/V for reference and ethylene channels, and 6×10^3 V/V for ethanol and ammonia channels). The pre-filter stage features a 4th order unity gain low-pass filter, implemented using Sallen-Key architecture, and with a cut-off frequency of 2.5 Hz.

The advantages of digital lock-in are the implementation of the carrier frequency range to arbitrarily low values, implementa-
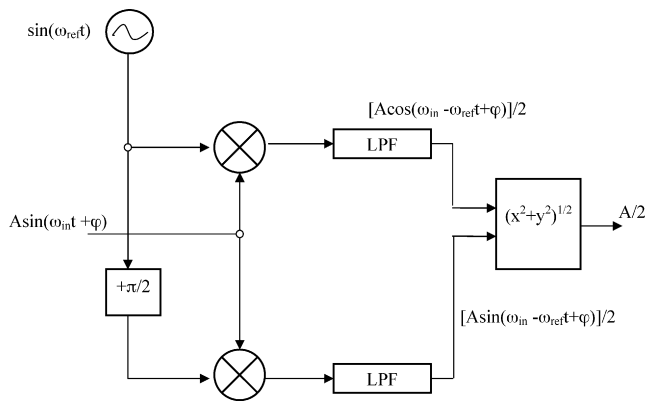
Fig. 2. Block diagram of a dual-phase lock-in amplifier. Two internal reference sine waves in quadrature, with the same ω_{ref} frequency are synthesized by the microcontroller. Assuming that the input signal is a sine wave with ω_{in} frequency, the multiplication stage outputs are composed by a low frequency component at $\omega_{ref} - \omega_{in}$ and a high frequency component at $\omega_{ref} + \omega_{in}$. The low-pass filter attenuates the AC signals and the lock-in output is null when ω_{ref} and ω_{in} are different. Finally, to remove the phase sensitivity, the magnitude of the vector is computed.

Fig. 3. Simulated (full line) and measured (circles) lock-in amplifier frequency responses.

tion of the low-pass digital filter cut-off frequency to both shorter and longer values, rejection of unwanted DC components, and reduced drift [27]. Additionally, higher order digital filter may be more easily implemented since it depends solely on the processor computing power, in comparison to analog filters which require more hardware components (and board space) as the filter order increases.

The improvement factor obtained by the use of demodulation techniques depends on the bandwidth of the low-pass filter B_O. Eq. (1) gives the theoretical improvement factor (assuming ideal filter behavior)

$$\text{improvement factor} = \frac{\text{SNR}_O}{\text{SNR}_I} = \frac{B_I}{B_O} \tag{1}$$

where SNR_I and SNR_O are the input and output signal-to-noise ratios, respectively. The input signal noise is assumed to white noise with bandwidth B_I [26].

The selected lock-in architecture is a dual-phase lock-in amplifier. This architecture incorporates a pair of phase-sensitive detectors operated with quadrature reference waveforms. Therefore, it is not sensitive to phase shifts between the reference and input signal. The implemented dual-phase lock-in block diagram is presented in Fig. 2.

A trade-off between sampling frequency and digital filter order is faced. Usually sample frequency is set to high values to reject aliasing effects, but it entails less available computation time for the microcontroller and in consequence less digital filter complexity. Additionally, since a dual-phase lock-in amplifier is used, this requires the implementation of two digital filters per channel. In order to increase the available computation time and optimize the lock-in routine, one lock-in is fully devoted for a channel at a time. Optimized dual-phase lock-in routine with input signal multiplexing capability has been implemented in two microcontrollers. The resulting architecture features one lock-in which alternates reference/ammonia channels and a second lock-in which alternates ethylene/ethanol channels. Input signals are multiplexed every 15 min, which is considered to be a short time compared to the expected concentration variations in the fruit store-houses.

Although interfering power line interference (50 Hz) is theoretically reduced 104 dB by the previous analog low-pass filter, it can still be picked up on the signal path between the analog filter output to the digital lock-in input. Therefore, the main components to be reduced by the digital lock-in amplifier are thermal noise,
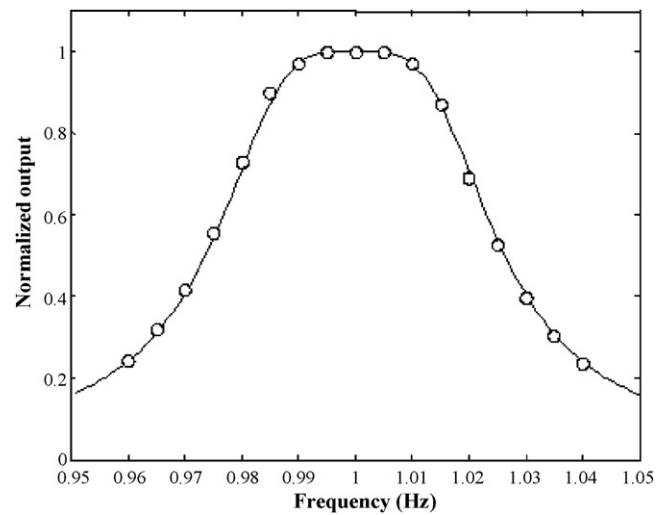
interfering power line noise, and thermopile and preamplifier offsets. A solution to attenuate power line noise and thermopiles offset is to design the lock-in required low-pass filter with one specific notch filter for the specific frequencies to be rejected. The complete routine is computationally equivalent to a 6th order filter when low-pass stage and both notch stages are second-order filters. For MSP430F4270 microcontroller, the fastest sampling frequency, which can support real time 6th order filter operation, is 8 Hz.

Complete lock-in simulations have been performed to optimize the digital filter in terms of noise reduction. A lock-in featuring 0.02 Hz cut-off frequency second-order low-pass filter, together with second-order notch filters for power line noise (50 Hz) and offset component have been simulated; and compared to a simple 6th order low-pass filter (Table 2) and to an ideal filter. Digital filters featuring notch filters show better performance for offset and power line noise reduction and still good performance for white noise attenuation.

Therefore, a lock-in amplifier is programmed with a sample frequency of 8 Hz and with a reference frequency of 1 Hz, which is used for IR emitter modulation. The low-pass digital filter is implemented using direct form II and is composed by a 0.02 Hz cut-off frequency second-order Butterworth filter because of its maximally flat bandpass, and by specific second-order notch filters to reject offset component and power line noise (50 Hz). The lock-in frequency response has been measured and compared to simulated response. Fig. 3 shows measured and simulated curves and exhibits typical bandpass filter lock-in behavior.

3. Laboratory test and spectrometer calibration

Spectrometer components presented in Section 2 have been extensively tested [18]. A main outcome from this test (reported elsewhere [28]) shows that the integration of narrow optical filters too close to the thermopiles leads to thermal coupling, caused by radiation absorption in the filter and a later heat transfer to the thermopile. Such detrimental effects dramatically worsen the required selectivity of a NDIR system when the filters are flip-chipped on the thermopiles and possible solutions are proposed. In the meanwhile, a four-channel commercial thermopile from Heimann Sensor (HTS-Q21), with similar optical filters on the package lid, but no Fresnel lenses, is used to overcome the problem and test the system selectivity.

Table 2
Comparison between different filter implementations.

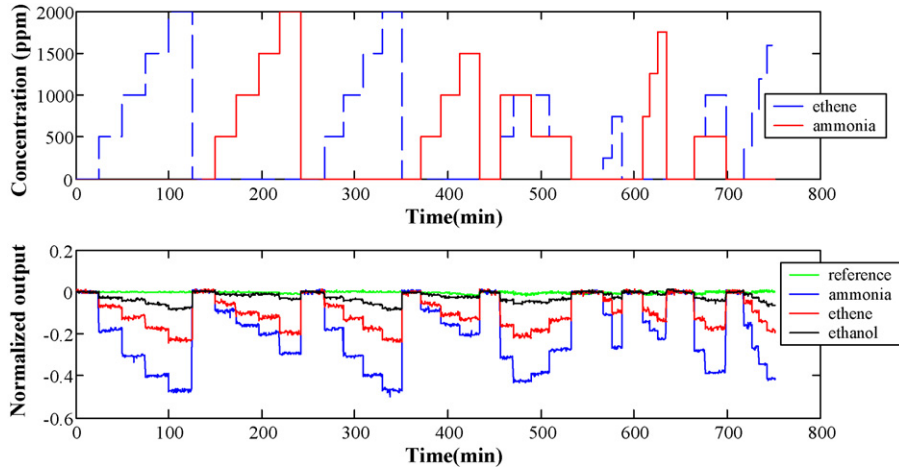| Attenuation (dB)	Second-order low-pass filter + second-order notch filter (DC) + second-order notch filter (power line)	Sixth-order low-pass filter	Ideal filter
DC component	392	204	Inf
Power line (50 Hz)	407	260	Inf
Thermal white noise	37	38	46

Fig. 4. Concentration gas profile (above) and corresponding system response (below).

Spectrometer calibration to ethylene and ammonia concentrations, including their mixtures, has been performed in laboratory conditions. A multimeter sampling at 1.2 Hz (HP34970A, Agilent, USA) was used to measure the voltage output of the lock-in, and mass flow controllers (Brooks 5850, USA) for gas mixing. Low ethylene and ammonia concentrations (in the range of 250–2000 ppm for ethylene and 500–2000 ppm for ammonia) are achieved by mixing 1% purity dilutions in synthetic air, and while maintaining a constant flow of 500 ml/min.

Eq. (2) shows the resulting gas concentration as a function of ethylene or ammonia gas flows (f_{gas}), synthetic air flow (f_{air}), and gas bottle concentration (c_{bottle}). Gas mixing station concentration error (Eq. (3)) is given by mass flow control errors (1% of the full range, that is $\delta f_{ethylene}$ = 1 ml/min, δf_{air} = $\delta f_{ammonia}$ = 10 ml/min), the gas flows to set the desired concentrations, and gas concentration bottles $c_{ethylene}$ = $c_{ammonia}$ = 1%, which are considered with no significant error. The maximum gas mixing concentration error corresponds to the maximum gas flow, and leads to an error of 43 ppm

for ethylene and 165 ppm for ammonia

$$C_{gas} = \frac{f_{gas}c_{bottle}}{f_{air} + f_{gas}} \tag{2}$$

$$\delta C_{gas}^2 = \left[\frac{f_{air}c_{bottle}}{(f_{air} + f_{gas})^2} \right]^2 \delta f_{gas}^2 + \left[\frac{f_{gas}c_{bottle}}{(f_{air} + f_{gas})^2} \right]^2 \delta f_{air}^2 \tag{3}$$

The duration of each concentration step is 15 min or 1 h, which is long enough to fill the white cell (250 ml) with a total flow of 500 ml/min. Data sets from each channel were normalized as shown in Eq. (4), where $v(c)$ is the acquired data, and $\overline{v(c = 0)}$ is the mean value of the system response when the white cell is 100% filled with synthetic air. Fig. 4 shows normalized system response (below) next to the complete gases concentration profile (above)

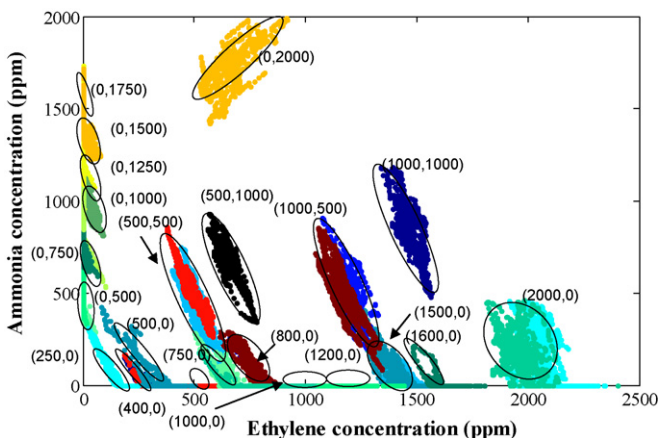$$v(c)^{normalized} = \frac{v(c) - \overline{v(c = 0)}}{\overline{v(c = 0)}} \tag{4}$$

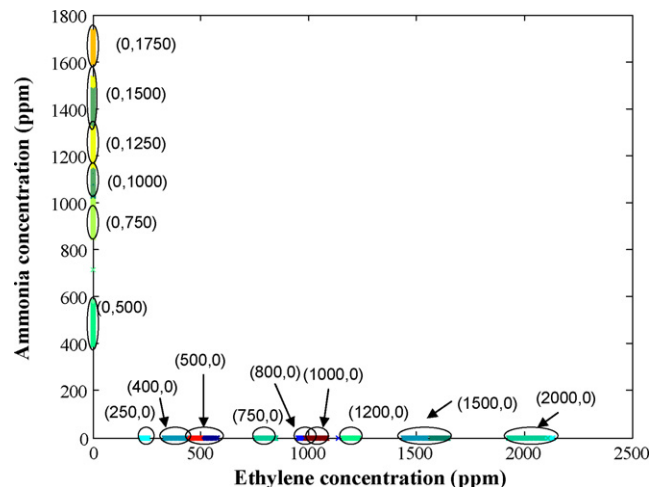**Fig. 5.** Processed data for ethylene and ammonia prediction.

Fig. 6. Processed data for ethylene and ammonia prediction, after projection.
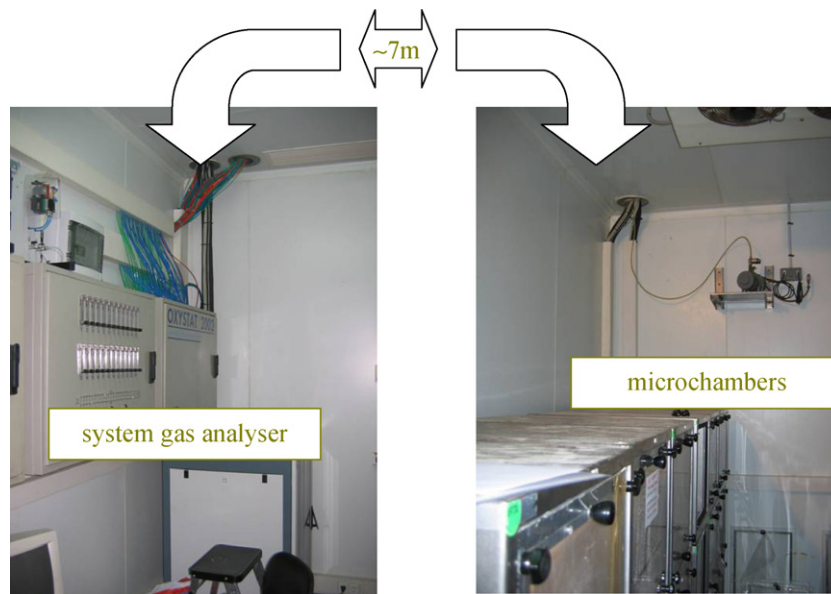
Fig. 7. System gas control (Oxystat 2002, David Bishop Instruments Ltd., UK) (left) that pumps gas out of the microchamber (right).

Obtained results clearly show that, interfering absorptions lead to cross-sensitivities among ethylene and ammonia channels: both channels present a significant sensitivity to both ethylene and ammonia presence. Due to the cross-sensitivities between the different channels, univariate calibration has been discarded. Therefore, a multivariate system calibration has been performed using the data presented in Fig. 4.

Usually, some measurements are not used to build the calibration model and are kept for a later validation technique and assess the calibration model quality. However, in our case, only 21 different concentration profiles are measured, and a data set reduction for a later validation may shorten critically the calibration set and worsen significantly the calibration model. Therefore, Leave-one-concentration step-out method has been used.

Partial Least Squares (PLS) regression [29] has been used to build calibration models for both ethylene and ammonia. The root mean square error of the distance of the validation data to the corresponding predicted model output was used as an indicator to choose the best model. For ammonia prediction, the best model found is a PLS using three latent variables. Due to the intrinsic linearity of PLS technique it does not provide good calibration models for ethylene, the data of which still exhibits significant non-linearity in the PLS predictions. However, adding an inner polynomial correction before PLS (poly PLS) the non-linearity in ethylene can be correctly modeled [30,31]. The best model for ethylene prediction is a poly PLS, with three latent variables and a third-order polynomial inner relation.

Fig. 5 shows the model predictions. The resulting root mean square error for ethylene and ammonia prediction is 95 ppm and 120 ppm, respectively. After the proposed data processing, pure species appear close to the corresponding axis, and ethylene–ammonia gas mixtures appear in the central zone.

4. Predicted gas variance reduction

Predicted model outputs present a clear principal direction for the variance in output space (Fig. 5), which represents the main error for the prediction model. This feature opens the possibility to reduce the calibration error using a later algorithmic correction if both gases are not present simultaneously. In fact, in real working conditions, ammonia alarm level will be produced by a cooling system leakage and ethylene alarm level will indicate fruit degradation. Therefore, it can be safely assumed that both alarms will not take place at the same time and that they are independent.

A new calibration model can be proposed assuming that only one of the species is in a high concentration level and the other gases are in residual concentration levels which do not affect spectrometer measurements. Therefore, gas mixtures measurements are not considered to build this new calibration model. Additionally, since the experiment corresponding to 2000 ppm of ammonia (Fig. 5) clearly differs from the rest of the experiments after data processing, it was considered as an outlier and not included for new data processing.

In summary, independent PLS models for ammonia and ethylene are built. Then a simple classifier detects which gas is in a high concentration (the one predicted with the highest concentration). Under the hypothesis of pure gases, the other gas concentration is automatically zeroed. Moreover, to improve the prediction accuracy for the selected gas, the data is later transformed using a linear operator in the direction of maximum variance towards the
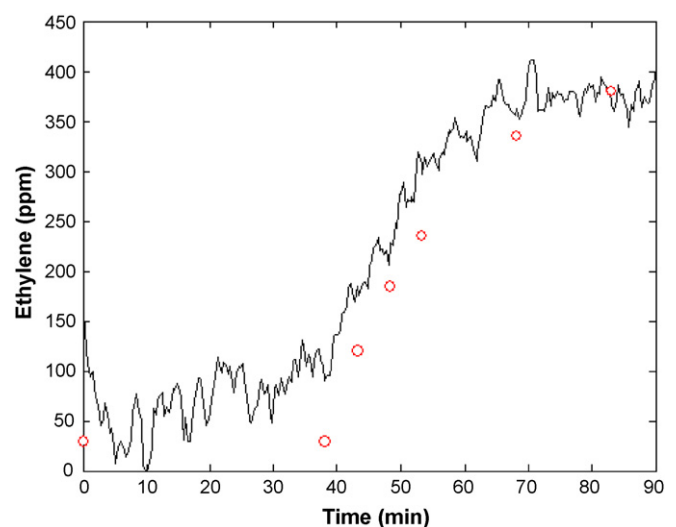

Fig. 8. Normalized IR spectrometer voltage output (full line) and gas concentration reference measured with gas chromatograph (circles).

corresponding gas axis (in prediction space). By doing so, the transformed clusters have their variance greatly reduced. After this data processing, prediction errors become much smaller reaching a root mean square error of 15 ppm for ethylene and 80 ppm for ammonia. Fig. 6 shows the data projected to the axis.

With the new calibration model, it can be said that the detection limit is 30 ppm of ethylene and 160 ppm of ammonia, with a confidence interval of 95%. In consequence, the fabricated spectrometer is able to detect the fruit ethylene burst which indicates that the fruit is ripe at least 1 week before it declines to senescence. Additionally, the instrument detects ammonia leakage before the 200 ppm, which obliges to switch on the ventilation and set a pre-alarm [15]. It is remarkable that experimental gas detection limits for the designed spectrometer are close to the gas mixing station errors. Therefore, the obtained gas detection limits represent upper limit values, and a better spectrometer performance may be found when using a gas mixing station featuring better accuracy. However, obtained results show that the designed IR spectrometer is suitable for ethylene and ammonia alarm system.

5. Field tests

Laboratory tests give promising results concerning ethylene and ammonia detection. However, in order to assess the spectrometer performance in real storage conditions, field test were carried out in IRTA-Lleida, Spain, where usually ripening tests of fruit in typical fruit storage conditions are performed. Microstorage chambers, with a volume of 140 l and featuring gas connections to an ethylene gas line, were used to simulate real fruit storage conditions.

The IR spectrometer, which is at room temperature outside the fruit conservation room, is connected in series with the system gas analyzer (Fruit Store Analyzer 770, David Bishop Instruments Ltd., UK) that pumps gas out of the microchamber through a silica gel drying column and a 7 m long pipe (Fig. 7). The composition of the atmosphere can be controlled by adding oxygen, carbon dioxide, ethylene, and nitrogen to the microchamber. Gas control was achieved using an Oxystat 2002 system (David Bishop Instruments Ltd., UK). In our case, the microchamber is filled with nitrogen, simulating ULO conditions while the storage temperature is set to 2 °C and 90% humidity. Apple's ethylene burst is simulated by increasing ethylene concentration in the microstorage chambers. With that aim, a 400 ppm ethylene gas flow (10 l/min) is injected into the microstorage chamber.

In order to have a reference gas concentration, gas samples were taken directly from the microstorage chamber gas outlet at specified times, and the corresponding concentration measured with a HP 6890GC gas chromatograph (Agilent, USA). Fig. 8 shows that in field conditions, 400 ppm ethylene introduction is clearly observed by the IR spectrometer.

6. Optimization of the optical window selection

Fig. 4 shows that ethylene and ammonia channels behave similarly to ethylene and ammonia presence. Additionally, ethanol and reference channels are also slightly sensitive to these gases. Channels behavior leads to hard gas prediction distinction (shown in Figs. 4–6), which mainly comes from ethanol channel and its slightly higher sensitivity in ammonia than in ethylene. This problem arises from the interfering absorptions in the selected absorption window for each channel, and the corresponding cross-sensitivities. Filter window selection was made in terms of maximum absorbance for each gas, but complete IR spectrums (Fig. 9) show important interfering absorptions in the selected windows.
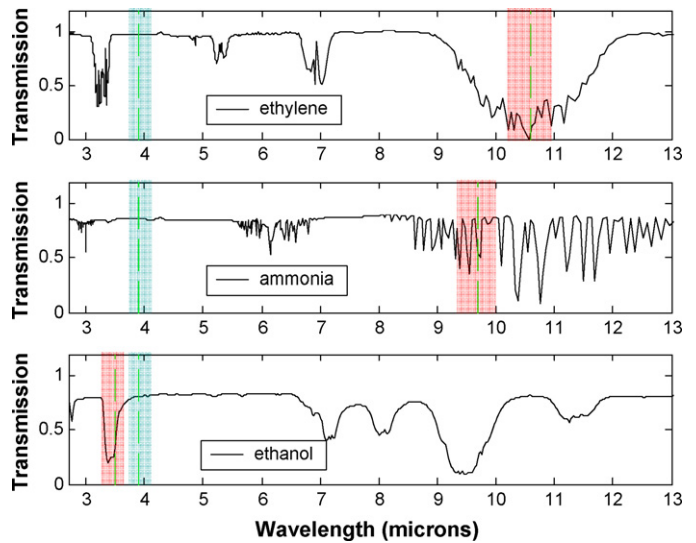

Fig. 9. Ethylene (above), ammonia (middle) and ethanol (lower) transmission spectrums, with the corresponding selected windows, and the reference window [32].

A trade-off between maximum sensitivity and gas selectivity is faced. A detailed optical spectrum analysis has been carried out to find new regions with less interfering absorptions between ethylene and ammonia and increase system selectivity, but still featuring high sensitivity for both gases.

With that aim, a simulation of the IR transmission of two optical windows (0.4 μm bandwidth) in the 2.5–13 μm wavelength range was performed. For each window position, both ethylene and ammonia transmission were simulated. Eq. (5) shows the two-component vector built for each gas, where $T^{ethylene}$ and $T^{ammonia}$ are ethylene and ammonia transmission spectrums, respectively, λ_1 and λ_2 are the position of each window, and $\Delta\lambda$ is the filter bandwidth

$$\vec{v}_{\lambda_1\lambda_2}^{ethylene} = \left(\int_{\lambda_1}^{\lambda_1+\Delta\lambda} T^{ethylene}(\lambda)d\lambda, \quad \int_{\lambda_2}^{\lambda_2+\Delta\lambda} T^{ethylene}(\lambda)d\lambda \right)$$

$$\vec{v}_{\lambda_1\lambda_2}^{ammonia} = \left(\int_{\lambda_1}^{\lambda_1+\Delta\lambda} T^{ammonia}(\lambda)d\lambda, \quad \int_{\lambda_2}^{\lambda_2+\Delta\lambda} T^{ammonia}(\lambda)d\lambda \right) \tag{5}$$

More selective spectrometers will come from window selections that make ethylene and ammonia feature vectors orthogonal. Therefore, the angle between vectors can be used to identify the window selection that makes the system maximally selective and it has been calculated as is indicated in Eq. (6). Fig. 10 shows the sinus of the angle between ethylene and ammonia vectors and it represents the system selectivity as a function of the position of the windows

$$\cos(\theta) = \frac{\vec{v}_{\lambda_1\lambda_2}^{ethylene} \cdot \vec{v}_{\lambda_1\lambda_2}^{ammonia}}{||\vec{v}_{\lambda_1\lambda_2}^{ethylene}|| \; ||\vec{v}_{\lambda_1\lambda_2}^{ammonia}||} \tag{6}$$

Fig. 10 shows that spectrometer window selection 9.7 μm and 10.6 μm ($\theta = 0.14\pi$ rad) is not in the most selective region to distinguish between ethylene and ammonia, and it is close to a region where any tolerance in the central wavelength of the optical filter may render to an almost non-selective spectrometer. The window selection with the highest channel selectivity is 10.1 μm and 12.4 μm ($\theta = 0.21\pi$ rad). Therefore, spectrometer selectivity could be improved by selecting ethylene and ammonia windows at 10.1 μm and 12.4 μm, respectively, without worsening the system sensitivity.
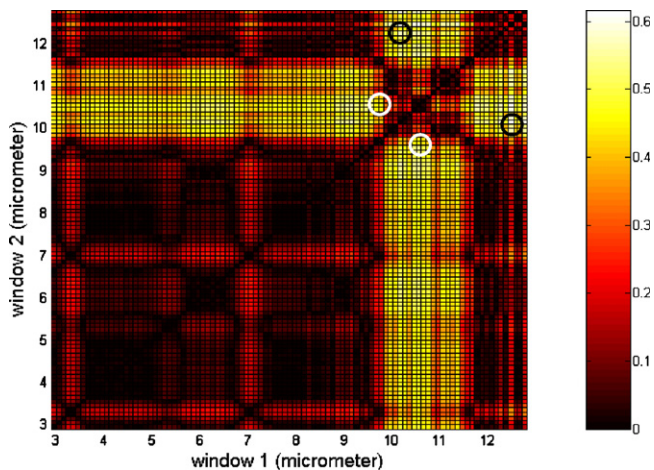
Fig. 10. Sinus of the angle between ethylene and ammonia vectors, for all the windows positions. The highest the angle, the more selectivity between ammonia and ethylene features the spectrometer. Showing the implemented filter selection (9.7 μm and 10.6 μm, white circle) and the maximum selectivity selection (10.1 μm and 12.4 μm, black circle).

7. Conclusions

A compact miniaturized IR spectrometer for ethylene and interfering gases such as ammonia and ethanol has been developed for fruit storage applications. A silicon-based macroporous IR emitter, a miniaturized absorption cell, a four-channel detector module, and a microcontroller-based lock-in amplifier have been assembled in the optical system for simultaneous measurements. A lock-in has been designed and implemented in a low-cost microcontroller as a signal recovery system, improving spectrometer features such as signal-to-noise ratio. The complete system can be considered as a multipurpose instrument for controlled atmosphere management.

A new algorithm for error reduction in PLS output space has been proposed for error reduction, assuming that both gases may not appear simultaneously. Ethylene detection limit (30 ppm) is suitable for detecting that fruit is ripe and preventing it to decline to senescence (typically when ethylene concentration is over 100 ppm). Additionally, the spectrometer is also able to detect ammonia over 160 ppm if a leakage from the cooling system occurs. System detection limits are close to gas mixing station errors, which may point to the idea that the spectrometer is measuring gas station variance in fact. To assess real spectrometer detection limits it would be desirable to perform new gas measurements in a more accurate gas station. Field tests show that designed spectrometer is suitable as gas alarm for the proposed application.

Further improvements are envisaged. At this point standard commercial detectors are used in the system because of problems of thermal coupling between optical filters and thermopiles of our initial detector design. However, once these problems are solved the performance of the original detector looks promising since it features the integration of Fresnel lenses for improved optical throughput.

Additionally, simulation results show that system selectivity can be improved by new optical spectral window selections.

References

[1] M.H. Jijakli, P. Lepoivre, State of the art and challenges of post-harvest disease management in apples, Fruit and Vegetable Diseases 1 (2004) 59–94.
[2] M.L. Lopez, M.T. Lavilla, I. Recasens, J. Graell, M. Vendrell, Changes in aroma quality of 'Golden Delicious' apples after storage at different oxygen and carbon dioxide concentrations, Journal of the Science of Food and Agriculture 80 (2000) 311–324.
[3] A. Brackmann, J. Streif, F. Bangerth, Relationship between a reduced aroma production and lipid-metabolism of apples after long-term controlled-atmosphere storage, Journal of the American Society for Horticultural Science 118 (1993) 243–247.
[4] A. Brackmann, J. Streif, F. Bangerth, Influence of CA and ULO storageconditions on quality parameters and ripening of preclimacteric and climacteric harvested apple fruits.2. Effect on ethylene, CO2, aroma, and fatty-acid production, Gartenbauwissenschaft 60 (1995) 1–6.
[5] G.A. Willaert, P.J. Dirinck, H.L. Depooter, N.N. Schamp, Objective measurement of aroma quality of golden delicious apples as a function of controlled-atmosphere storage time, Journal of Agricultural and Food Chemistry 31 (1983) 809–813.
[6] J. Song, F. Bangerth, The effect of harvest date on aroma compound production from 'Golden Delicious' apple fruit and relationship to respiration and ethylene production, Postharvest Biology and Technology 8 (1996) 259–269.
[7] J.H. Oetiker, S.F. Yang, in: H. Hyodo, A.E. Watada (Eds.), The role of ethylene in fruit ripening, Postharvest Physiology of Fruits (1995) 167–178.
[8] M.J.C. Rhodes, The climacteric and ripening of fruits, in: A.C. Hulme (Ed.), Food Science and Technology, a Series of Monographs. The Biochemistry of Fruits and their Products, vol. 1 Xviii + 620p, Illus. Academic Press Inc. (Ltd.), London, England/New York, NY, U.S.A., 1970, pp. 521–533.
[9] E. Kupferman, The role of ethylene in determining apple harvest and storage life, Postharvest Pomology Newsletter 4 (1986) No1.
[10] SiraTechnology, Gas Detector Selection and Calibration Guide, Withrebys Publishing, 2005.
[11] A. Giberti, M.C. Carotta, V. Guidi, C. Malagù, G. Martinelli, M. Piga, B. Vendemiati, Monitoring of ethylene for agro-alimentary applications and compensation of humidity effects, Sensors and Actuators B: Chemical 103 (2004) 272–276.
[12] R. Rubio, J. Santander, J. Fonollosa, L. Fonseca, I. Gracia, C. Cane, M. Moreno, S. Marco, Exploration of the metrological performance of a gas detector based on an array of unspecific infrared filters, Sensors and Actuators B: Chemical 116 (2006) 183–191.
[13] J. Dixon, E.W. Hewett, Factors affecting apple aroma/flavour volatile concentration: a review, New Zealand Journal of Crop and Horticultural Science 28 (2000) 155–173.
[14] M. Knee, S.G.S. Hatfield, The metabolism of alcohols by apple fruit tissue, Journal of the Science of Food and Agriculture 32 (1981) 593–600.
[15] A. Jerger, H. Kohler, F. Becker, H.B. Keller, R. Seifert, New applications of tin oxide gas sensors II. Intelligent sensor system for reliable monitoring of ammonia leakages, Sensors and Actuators B: Chemical 81 (2002) 301–307.
[16] R. Rubio, J. Santander, L. Fonseca, N. Sabate, I. Gracia, C. Cane, S. Udina, S. Marco, Non-selective NDIR array for gas detection, Sensors and Actuators B: Chemical 127 (2007) 69–73.
[17] F.G. Nogueira, D. Felps, R. Gutierrez-Osuna, Development of an infrared absorption spectroscope based on linear variable filters, IEEE Sensors Journal 7 (2007) 1183–1190.
[18] J. Hildenbrand, J. Wollenstein, S. Hartwig, A. Eberhardt, B. Halford, M. Moreno, J. Fonollosa, L. Fonseca, J. Santander, R. Rubio, I. Gracia, C. Cane, A compact optical multichannel system for ethylene monitoring, Microsystem Technologies-Micro- and Nanosystems-Information Storage and Processing Systems 14 (2008) 637–644.
[19] W. Konz, J. Hildenbrand, M. Bauersfeld, S. Hartwig, A. Lambrecht, V. Lehmann, J. Wollenstein, Micromachined IR-source with excellent blackbody like behaviour, Smart Sensors, Actuators, and Mems Ii 5836 (2005) 540–548.
[20] J. White, Long optical paths of large aperture, Journal of the Optical Society of America 32 (1942) 4.
[21] S. Hartwig, J. Hildenbrand, M. Moreno, J. Fonollosa, L. Fonseca, J. Santander, R. Rubio, C. Cane, A. Lambrecht, J. Wollenstein, A highly sensitive IR-optical sensor for ethylene-monitoring, Smart Sensors, Actuators, and Mems Ii 5836 (2005) 452–460.
[22] J. Fonollosa, R. Rubio, S. Hartwig, S. Marco, J. Santander, L. Fonseca, J. Wöllenstein, M. Moreno, Design and fabrication of silicon-based mid infrared multi-lenses for gas sensing applications, Sensors and Actuators B: Chemical 132 (2008) 498–507.
[23] L. Fonseca, E. Cabruja, C. Calaza, R. Rubio, J. Santander, E. Figueras, I. Gracia, C. Cane, M. Moreno, S. Marco, Feasibility of a flip-chip approach to integrate an IR filter and an IR detector in a future gas detection cell, Microsystem Technologies-Micro- and Nanosystems-Information Storage and Processing Systems 10 (2004) 382–386.
[24] L. Fonseca, F. Perez-Murano, C. Calaza, R. Rubio, J. Santander, E. Figueras, I. Gracia, C. Cane, M. Moreno, S. Marco, AFM thermal imaging as an optimization tool for a bulk micromachined thermopile, Sensors and Actuators A: Physical 115 (2004) 440–446.

[25] J. Fonollosa, R. Rubio, J. Hildenbrand, M. Moreno, S. Marco, J. Santander, L. Fonseca, S. Hartwig, J. Wollenstein, Fresnel lenses: study and fabrication in silicon technology for medium-IR applications—art no. 61860R, Mems, Moems, and Micromachining Ii 6186 (2006) R1860–R11860.

[26] M.L. Meade, Lock-in Amplifiers: Principles and Applications, Peter Peregrinus Ltd., London, 1983.

[27] L.A. Barragan, J.I. Artigas, R. Alonso, F. Villuendas, A modular, low-cost, digital signal processor-based lock-in card for measuring optical attenuation, Review of Scientific Instruments 72 (2001) 247–251.

[28] J. Fonollosa, M. Carmona, J. Santander, L. Fonseca, M. Moreno, S. Marco, Limits to the integration of filters and lenses on thermoelectric IR detectors by flip-chip techniques, Sensors and Actuators A: Physical 149 (2009) 65–73.

[29] S. Wold, M. Sjöström, L. Eriksson, PLS-regression: a basic tool of chemometrics, Chemometrics and Intelligent Laboratory Systems 58 (2001) 109–130.

[30] S. Wold, N. Kettanehwold, B. Skagerberg, Nonlinear PLS modeling, Chemometrics and Intelligent Laboratory Systems 7 (1989) 53–65.

[31] C. Calaza, E. Meca, S. Marco, M. Moreno, J. Samitier, L. Fonseca, I. Gracia, C. Cane, Assessment of the final metrological characteristics of a MOEMS-based NDIR spectrometer through system modeling and data processing, IEEE Sensors Journal 3 (2003) 587–594.

[32] N. I. o. S. a. T. (NIST), The NIST Chemistry WebBook, 2005.

Biographies

Jordi Fonollosa was born in Barcelona, on December 26, 1980. He received his B.S. in Physics in 2002, and his B.S. and the master of science degree in Electronic Engineering in 2007, from the University of Barcelona, where he started his Ph.D. studies in 2004. His main research areas are related to infrared sensing technologies, including optical components design, and both analog and digital signal recovery systems.

Bernard Halford received his B.S. in Electronic Engineering from the Bolton Institute of Technology in 1976. In 1982 he joined Fraunhofer IPM, where his work experience has been mainly focussed on the development and implementation of components related to opto-electronic applications in optical spectroscopy, including the design of low-noise front-end amplifiers and system calibration with optical sources. Most recent projects include work on the development of a FTIR spectrometer, a rotating filter spectrometer and electronics used in digital imaging processing. Further experience includes work in the field of design, fabrication and testing of mid-IR detectors for spectroscopic applications.

Luis Fonseca was born in Barcelona, Spain, on February 17, 1966. He received his B.S. and Ph.D. degrees in physics from the Autonomous University of Barcelona in 1988 and 1992, respectively. In 2001 he joined the CNM Microsystems group as a full senior researcher being his actual research focused on technological developments for gas sensing and more specifically on optical gas sensing. He has been involved in more than 30 Spanish and European projects, the last one being the FP6 Integrated Project GoodFood (Food Safety and Quality with Microsystems) which he helped to coordinate.

Joaquín Santander was born in Terrassa, Spain, in 1966. He received the B.S. and Ph.D. degrees in physics from the Autonomous University of Barcelona, Spain, in 1989 and 1996, respectively. He is currently working at the Microelectronics National Center in Barcelona, as responsible for the electrical parametric characterization of different microelectronic technologies (CMOS, MCM, sensors, microsystems) using mainly test structures. His main research areas are related to microsystems, gas sensing applications and micro-fuel cells.

Sergi Udina began his degree in physics in 1995 and obtained the degree in electronic engineering by the Universitat de Barcelona in 2004, and the Master of Science degree in electronic engineering in 2007. His current investigation work is related to chemical and thermal sensors, multivariate calibration, signal processing and standard sensor interfacing basically including IEEE1451. Other strong interests include audio signal processing and engineering, power electronics, DLP, and 6 DOF real-time positioning. He is currently pursuing his Ph.D. degree at the *Departament d'Electronica* of the *Universitat de Barcelona*.

Mauricio Moreno was born in Barcelona, Spain. He received the degree in physics in 1989 from the University of Barcelona (UB), and the Ph.D. degree in sciences in 1995 from the Polytechnic University of Catalonia (UPC), Spain. He has been Associate Professor in the Electronics Department, UB, since 1997. He is involved in the design and test of microoptics devices in silicon technologies, and optical waveguide grating devices for biosensing applications. Other fields of interest include arrays of integrated photodetectors in CMOS technology for imaging.

Jürgen Hildenbrand, scientist, received his degree in Microsystems Engineering from the University of Freiburg in 2003. After 1-year collaboration work between Fraunhofer IPM and the simulation group of the Institute of Microsytems Technology, he started his Ph.D. on MEMS based thermal emitters at Fraunhofer IPM. Beside the thermal emitter research he works in the field of mid-infrared spectroscopic system development. This includes NDIR-systems as well as quantum cascade based laser spectrometers. Here, his main interests are optical simulation and system integration.

Jürgen Wöllenstein received his diploma in electrical engineering from the University of Kassel, Germany in 1994. In 2003 he finished his Ph.D.-thesis at the same university. In 1994 he joined the Fraunhofer Institute of Physical Measurement, Freiburg, Germany, where he is engaged in development of optical and semiconductor based microsystems for gas analysis.

Santiago Marco completed his university degree (Licenciado) in Applied Physics in 1988 and received a Ph.D. in Microsystem Technology from the University of Barcelona in 1993. He is associate Professor (Profesor Titular) at the Departament d'Electronica of Universitat de Barcelona since 1995. He has recently been appointed leader of the Artificial Olfaction Lab at the Institute of Bioengineering of Catalonia. His research concerns the development of signal/data processing algorithmic solutions for smart chemical sensing based in sensor arrays or microspectrometers integrated typically using Microsystem Technologies (more at http://www.ibecbarcelona.eu and http://isp.el.ub.es).

7.- CONCLUSIONS:

A multichannel mid-infrared spectrometer for ethylene measurement in today's apple store-houses is built and characterized in this Thesis. The performed laboratory and field tests validate the proposed instrument architecture to continuously monitor ethylene concentration in the store-houses atmosphere and prevent the fruit to decay into senescence. Additionally, the instrument is able to detect ammonia if a leakage from the cooling system occurs and keep the fruit from quality degradation.

The complete spectrometer contains a silicon-based macroporous infrared (IR) emitter, a miniaturized long path cell, a novel compact four-channel detector module, low-noise analog amplification and filtering, and a microcontroller-based lock-in amplifier.

A novel highly-integrated compact detection module to measure the remaining radiation after gas absorption has been presented, designed, fabricated, and characterized. In the trend towards miniaturization, the new inner architecture of the detector features a fourfold thermopile array with narrow band optical filters attached by flip-chip technology for wavelength selection, and an optical focusing unit on the lid of the package to optimize the device detectivity.

Diffractive Fresnel lens approach is chosen as a focusing element since they are compatible with silicon microtechnology. The four Fresnel lenses are fabricated on the same silicon substrate in a combined multi-lens array. In order to reduce the number of photolithographic steps, a new design based on four photolithographic masks and sharing up to sixteen quantization steps by the four lenses is done. Lens efficiency calculations show that the proposed approach is a cost effective alternative and assures optical transmission efficiencies over 85%. The focal length measurement of the fabricated device has an error smaller than 5%, and the measured spot size at the focal plane is smaller than the typical thermopile absorber size.

To prevent reflection losses at the lens surfaces, antireflection layers are post-processed on both sides of some multi-lens arrays. A gain of 140 is expected on the developed detector signal by introducing the fabricated Fresnel lens array with the proper antireflection coating. The coated FL is optically tested and exhibit better efficiency compared to uncoated lenses and only small shifts in the focal length are observed. Additionally, alignment fixtures are fabricated to assemble the Fresnel lenses chip on the detector lid in the correct orientation. Therefore, the fabricated lens array is suitable to be integrated in the detection module.

It has been found that integration of filters too close to the IR detector leads to degraded performance due to thermal coupling. Infrared energy absorbed in the filter produces a slow temperature increase and, due to air thermal coupling, this results in an added thermal

contribution producing an undesired response. To avoid such detrimental effects the thermopile substrate and the filter should be thermally uncoupled. This hypothesis has been corroborated by simulations and experimental results and leads to degraded performance of the detector module. Different alternatives are proposed to thermally uncouple the thermopile and the filter.

A possibility is to set the device in vacuum conditions, obtaining an improved output response and avoiding the influence of the filters. Another alternative is to increase the solder joint height. Beyond a certain height, the filter is considered to be isolated from the thermopile. These options have been studied by simulations obtaining geometrical parameters values to be implemented in a further step. The specific solution should be considered depending on the application requirements.

The signal recovery system is based on a digital lock-in amplifier to take advantage of the great capabilities to measure signals accompanied by relatively high levels of noise and interferences of this architecture. The lock-in amplifier is implemented on a general purpose microprocessor, which also controls the mechanical chopper required to modulate the emitted radiation. The developed lock-in amplifier shifts the signal to a lower noise band (modulation at 1Hz frequency) and features notch filters to reject power line interference and offset components.

In practice, the modulation frequency is usually made as high as possible to facilitate separation of the chopped output voltage from noise components. However, the integration of the optical filters too close to the thermopiles increases the output time response of the IR detector and limits the modulation frequency. Otherwise, the modulation frequency could be set to higher values and improve the noise rejection.

In the meanwhile, a four-channel commercial with similar optical filters on the package lid, but with no optical module, is used to overcome the thermal coupling problem and to perform gas measurements. Laboratory tests and system calibration based on a multi-variant data model show that the system is able to distinguish between ammonia and ethylene, featuring a detection limit of 30ppm and 160ppm (95% confidence) for ethylene and ammonia, respectively. In consequence, the fabricated spectrometer is able to detect the fruit ethylene burst which indicates that the fruit is ripe at least one week before it declines to senescence and it can detect ammonia leakages that threatens fruit quality.

Although it is proved that the spectrometer is suitable for the proposed application, some further work can still improve the components for a better system performance.

It would be desirable to reduce the thermal mass of the IR emitter, in order to avoid the external modulation based on a mechanical chopper. A direct modulation of the emitter does not require external mechanical parts and the typical problems related to mechanical parts such as piece aging and replacement could be avoided.

Several points are still open for a better optical performance of the spectrometer. The mirrors of the White Cell are gold-coated lenses, which exhibit good reflection performance when the IR beam is reflected on them. However, the radiation loss after 19 reflections can be significant. Assuming an efficiency of 99% for each beam reflection, the final efficiency decreases to 83%. Additionally, the White cell was designed assuming a small active area of the IR source, which is not the case for a thermal emitter. Therefore, new simulations including the real IR emitter should be performed in order to assess the part of the incoming beam which covers the designed path of 1.6m.

The required antireflection layer has been post-processed on both sides of some multi-lens arrays. However, the ZnS layer exhibits adherence problems on the non-structured side of the lenses chip and it starts peeling off after some time. Additionally, the thickness of the antireflection coating is very critical for the shorter wavelengths. Two different methods have been proposed to overcome the adherence problems. On one hand, patterning a periodic subwavelength structure acting as antireflection layer on the non-structured side of the lens is suggested. This alternative avoids depositing a ZnS layer on that side, but requires the use of a technological technique able to define submicron features. On the other hand, structuring the rear side of the FL chip with some stripes has been proposed as well to solve the adherence problems.

Additionally, it would be desirable to perform ethanol measurements and test ethanol channel and its cross-sensitivity to ethylene and ammonia channels. Other interfering gases such as acetaldehyde could be tested as well in order to test the cross-sensitivity strongly.

Finally, a real long-term measurement in an ongoing store-house with fruit would be desirable to assess the fabricated spectrometer performance in terms of drift, cross-sensitivities, temperature and humidity changes, and capability of ethylene burst detection in real working conditions.

However, obtained results show that the fabricated IR spectrometer is suitable for ethylene monitoring and ammonia leakage detection in the today's fruit store-houses. Therefore, the proposed spectrometer architecture with the novel IR detector is useful to prevent the fruit to decline to senescence in the today's fruit store-houses, avoid post-harvest diseases, optimize storage conditions, and obtain a final fruit with a better organoleptic quality that meets consumer expectations.

8.- RESUM EN CLAR I CATALÀ:

Índex:

8.1.- Resum:

Avui en dia, el control i monitoratge de la concentració d'etilè a les càmeres d'emmagatzematge de fruita pot proporcionar informació de gran interès sobre el seu estat. Per una banda, la fruita mateixa emet petites concentracions d'etilè que n'indiquen l'estat de maduració, i per l'altra banda, la concentració d'etilè es pot augmentar externament per accelerar el procés de maduració quan convingui.

En aquesta Tesi, s'ha desenvolupat un espectròmetre òptic multicanal per mesurar de forma contínua la concentració d'etilè a les càmeres frigorífiques d'emmagatzematge. S'han dissenyat i fabricat els components òptics i la corresponent electrònica d'amplificació i de processament de senyal. El resultat és un espectròmetre de gasos basat en una arquitectura tipus Non-Dispersive Infrared (NDIR).

Seguint la constant tendència tecnològica de la miniaturització, en aquesta Tesi s'ha desenvolupat un detector d'infraroig per actuar al sistema NDIR. El detector consta d'una matriu 2x2 de termopiles amb els filtres òptics corresponents per seleccionar les bandes d'absorció dels gasos i una matriu de lents de Fresnel per augmentar la sensitivitat del sistema. L'etapa electrònica es compon d'una primera part d'amplificació analògica i d'una segona de digital basada en un lock-in per recuperar el senyal.

S'han realitzat diferents tests de l'espectròmetre complet en el laboratori i a les càmeres de conservació de fruita i s'ha calibrat el sistema. El resultat és que l'aparell pot detectar fins a 30ppm d'etilè, que és una concentració prou baixa per evitar que la fruita envelleixi dins de les càmeres, i 160ppm d'amoníac, que pot ser útil per detectar una possible fuita del sistema de refrigeració.

8.2.- Sistemes NDIR: estat de l'art:

Miniaturització

"Més petit, més ràpid i més barat" és una constant d'evolució tecnològica, que pren especial rellevància en el camp de l'electrònica. A la dècada dels 1950 es van realitzar els primers estudis per miniaturitzar equips electrònics i incloure-hi funcions més complexes en un espai més reduït. Des de la invenció dels circuits integrats al 1959, la miniaturització és una constant en el desenvolupament de tecnologia electrònica.

La indústria del semiconductor ha augmentat la seva productivitat de circuits integrats segons la llei de Moore, qui al 1965 va preveure que el nombre de transistors per centímetre quadrat es doblaria cada 12 mesos. Tot i que actualment el ritme d'integració ja no és el proposat per Moore, tecnològicament es poden arribar a fabricar detalls d'una dimensió de fins a 45nm.

En la cursa vers la integració, va néixer un nou camp on es combinen micro-dispositius mecànics i electrònics MEMS (Micro-Electrical-Mechanical Systems). Els MEMS es caracteritzen per la integració en un substrat de silici de parts mecàniques, sensors, actuadors i electrònica aprofitant la tecnologia desenvolupada per l'electrònica de silici. Aquesta integració permet aprofitar els avantatges clàssics d'aquesta tecnologia com els alts nivells de funcionalitat assolits, fidelitat, sofisticació i baix cost, a banda de la gran varietat d'equips disponibles, l'ampli suport tècnic i operar a baix voltatge.

Els dispositius MEMS han revolucionat pràcticament tots els productes electrònics i han permès la fabricació de sistemes complets en un mateix xip i desenvolupar instruments amb capacitat de control. El mercat actual dels MEMS (que va arribar a 7.000 milions de dòlars l'any 2007) evidencia la importància dels MEMS avui en dia. Paral·lelament, a la dècada dels 1990, la integració dels MEMS amb dispositius òptics va donar lloc als MOEMS (Micro-Optical-Electrical-Mechanical Systems). Aquests dispositius també s'estan obrint lloc al mercat ja que tenen els mateixos avantatges que els MEMS i a més tenen dispositius òptics com guies d'ona, miralls mòbils i xarxes de difracció. Aplicacions típiques dels MOEMS són interruptors, filtres, interferòmetres i lents.

En particular, els MOEMS han trobat un camp d'aplicació important en l'espectroscòpia d'infraroig (IR) ja que permeten optimitzar el banc òptic i l'aparell final és més compacte i petit.

Tècniques de detecció de gasos

A banda de l'espectroscopia d'infraroig, diverses tècniques per la mesura de gasos també són populars actualment, cadascuna d'elles amb uns avantatges i inconvenients i adequades per un tipus d'aplicació o una altra.

Els sensors d'òxid de metall (MOX) són una de les opcions més populars gràcies a la seva sensibilitat i solidesa. Es basen en la variació de la conductivitat del sensor quan els gasos són adsorbits a la superfície del semiconductor. Aquest tipus de sensors presenten problemes d'estabilitat a llarg termini i, a causa de la seva baixa especificitat i repetibilitat, la seva principal aplicació és d'alarma o detecció de fuites.

Les cel·les electroquímiques són similars a una bateria, que produeix un corrent elèctric proporcional a la concentració de gas present. Aquest tipus de sensor encara presenten una sensibilitat creuada alta i s'utilitzen principalment per aplicacions de seguretat i detecció de gasos tòxics i oxigen.

Els sensors catalítics (o pelistors) associen la temperatura d'una flama amb la concentració del gas present. Actualment són utilitzats per la detecció de gasos inflamables, però poden ser greument afectats per certs components químics que poden desactivar el principi del sensor.

Els detectors d'infraroig es basen en l'absorció de radiació a determinades regions de l'espectre i que són específiques del gas a mesurar. La llei de Lambert-Beer (Eq. 1) relaciona la radiació transmesa (T) amb la longitud del camí òptic (L), la concentració de gas (c) i el coeficient d'absorció (α), que és funció de la longitud d'ona (λ).

$$T(\lambda) = \exp\left[-\alpha(\lambda).c.L\right] \qquad \text{Eq.1}$$

Els analitzadors de gas òptics són instruments selectius, estables i molt immunes a efectes d'enverinament ja que el gas no es troba en contacte directe amb l'element sensor. Per aquests motius, habitualment són l'opció escollida en aplicacions que requereixen una mesura estable i contínua en el temps i un manteniment senzill.

La majoria dels espectròmetres d'infraroig comercials dissenyats per control de processos o per monitoratge continu estan basats en una arquitectura NDIR. Aquesta es basa en aïllar les bandes d'absorció específiques dels gasos mitjançant filtres òptics estrets.

Des d'un punt de vista experimental, la concentració de gas es pot predir mesurant la radiació absorbida quan aquesta passa a través del medi. La Figura 1 mostra l'esquema típic d'un espectròmetre d'infraroig, amb l'emissor, la cel·la de gas, el filtre òptic per seleccionar la banda d'absorció del gas a mesurar i el detector.

Tot i que normalment els instruments comercials tenen unes mides relativament grans, també hi ha sistemes NDIR miniaturitzats. Tot i això, la miniaturització és un repte pels espectròmetres d'infraroig ja que la seva sensibilitat depèn de la llargada del camí òptic. Per aquest motiu, els sistemes NDIR comercials més petits estan dissenyats per mesurar gasos amb una gran absorbància, com el diòxid de carboni, i només mesuren concentracions de gas relativament altes.
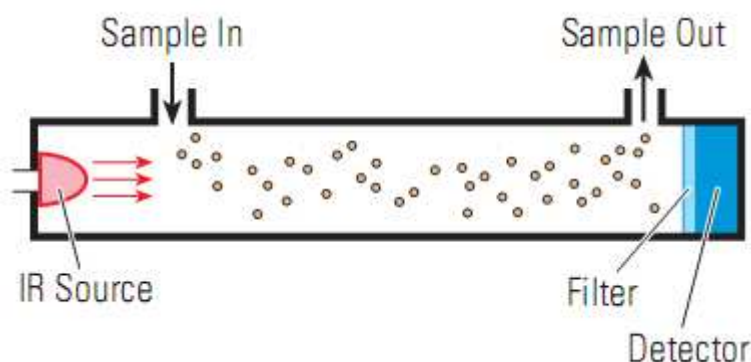

Figura 1: Esquema bàsic d'un espectròmetre d'infraroig

8.3.- Control atmosfèric per l'emmagatzemament de fruita:

Motivació

La clau per mantenir una bona salut és combinar certa activitat física amb una dieta equilibrada. Per tal que d'aconseguir-ho, es suggereix menjar diàriament almenys dues racions de fruita. Entre la fruita que es consumeix a Europa, la poma n'és una de les més populars.

El període de collita de les pomes depèn de diversos factors, com ara la varietat, però als països mediterranis normalment comença l'agost i acaba a finals d'octubre. En canvi, tot i que la majoria de pomes només es poden guardar a les cases algunes setmanes, la demanda de pomes és alta durant tot l'any.

Malgrat les tècniques desenvolupades per allargar el temps de mercat de les pomes, la pèrdua de qualitat durant l'emmagatzemament causa importants pèrdues a la indústria agrícola. Amb l'objectiu de reduir la pèrdua de qualitat de les pomes durant aquesta etapa i que la fruita resultant satisfaci el consumidor final s'han estudiat les tècniques de conservació i la maduració de les pomes.

Maduració de la fruita i tècniques de conservació

La fruita es pot dividir en dos grans grups en funció de la presència d'etilè. Els fruits no climatèrics com la taronja, les maduixes, les cireres i la pinya que es caracteritzen per un procés de maduració independent de l'etilè, i els fruits climatèrics com la poma, el tomàquet, el meló, la pera i el préssec que mostren un gran augment de la concentració d'etilè quan la maduració de la fruita s'inicia.

En les càmeres de conservació de fruita climatèrica la concentració d'etilè es pot trobar per sota de 1ppm mentre la fruita està verda, però tan bon punt comença la maduració la seva concentració augmenta fins assolir valors superiors als 100ppm. Típicament, la fruita envelleix al cap de 15 dies de la ràfega d'etilè. La Figura 2 mostra la concentració d'etilè en funció de l'estat de les pomes. D'altra banda, l'etilè també juga un altre rol ja que pot ser afegit externament per accelerar la maduració. Per aquest motiu, la concentració d'etilè és un bon indicador per saber l'estat de maduració de la fruita.
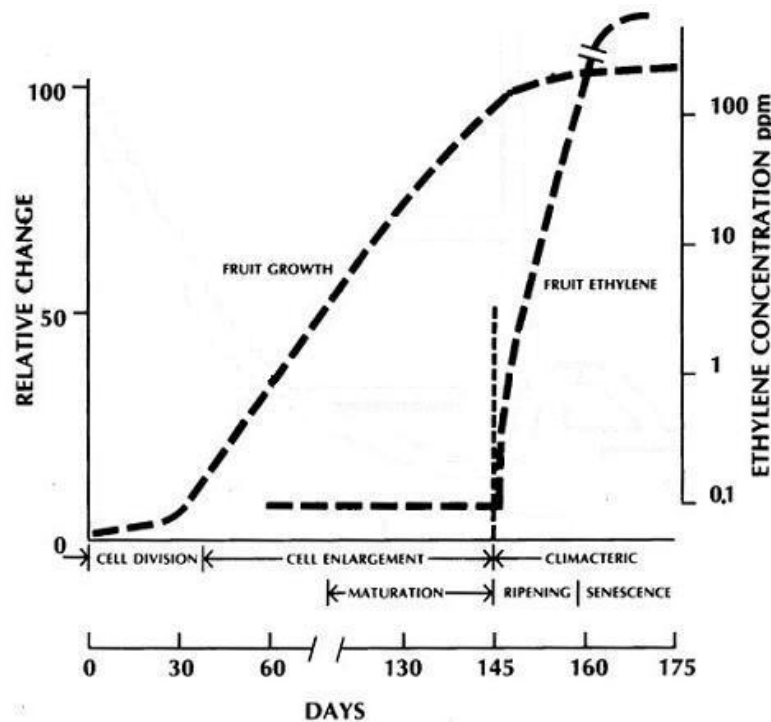

Figura 2: Estat de la poma en funció de la concentració d'etilè.

Per tal d'allargar la vida de la fruita, aquesta es conserva en càmeres d'atmosfera modificada (MA) o d'atmosfera controlada (CA). MA fa referència a atmosferes amb composicions diferents a la normal, i CA a més demana un estricte control de les variables d'aquesta. Actualment, MA i CA impliquen atmosferes amb baixa concentració d'oxigen i/o una elevada concentració de diòxid de carboni. D'aquesta manera, conjuntament amb un control de temperatura acurat, la respiració de la fruita es redueix i aquesta es pot emmagatzemar durant més temps.

Tècniques per avaluar l'estat de la fruita

Malgrat que una acumulació d'etilè a les càmeres de conservació o transport pot amenaçar el procés de conservació de la fruita, actualment no es mesura de forma contínua l'etilè. En la majoria de càmeres es mesura només de forma contínua l'oxigen i el diòxid de carboni, però aquests no aporten informació directa sobre l'estat de la fruita.

Per conèixer l'estat de la fruita, es mesura l'etilè externament mitjançant instruments portàtils. Hi ha instruments basats en cel·les electroquímiques, però presenten sensibilitat creuada a altres gasos i fàcil pèrdua de calibratge. Altres es basen en una reacció luminescent de l'etilè, però fan ús d'ozó, cosa que fa prendre unes precaucions especials de seguretat i necessita una càmera especial de baixa pressió per crear-lo. Això fa que no sigui una solució ni pràctica ni còmoda per ser instal·lada a les càmeres actuals ja que requereix un espai considerable.

Altres tècniques com la cromatografia de gasos s'utilitzen per controlar la concentració d'etilè. Encara que aquesta tècnica és off-line i la freqüència amb la qual s'extreu la mostra pot ser massa baixa per perfilar l'estat de la fruita de forma eficient. Sensors semiconductors també s'han proposat, però aquests es veuen afectats per les variacions d'oxigen, humitat i temperatura, cosa per la qual no són desitjables per la mesura a llarg terme d'etilè.

Un instrument basat en la detecció òptica NDIR s'ha desenvolupat al llarg d'aquesta Tesi per aprofitar les bones característiques d'aquesta arquitectura en les mesures contínues al llarg de tot el procés d'emmagatzematge de les pomes.

8.4.- Objectius de la Tesi

Aquesta Tesi està emmarcada en el Projecte GoodFood (508774-IP), que pretén desenvolupar eines basades en sistemes miniaturitzats per assegurar la qualitat dels productes al llarg de tota la cadena alimentaria. En particular, l'objectiu principal d'aquesta Tesi inclou el desenvolupament d'un espectròmetre òptic per una mesura estable, precisa i contínua d'etilè útil per monitorar l'estat de les pomes a les càmeres de conserva actuals.

El desenvolupament d'aquest instrument i dels seus components és l'objectiu principal d'aquesta Tesi. En particular, una nova arquitectura pel detector d'infraroig que comprèn els filtres òptics i un sistema d'amplificació òptica, la miniaturització de la cel·la de gasos sense perdre camí òptic, l'amplificació de senyal elèctric i la reducció de soroll, i l'anàlisi dels experiments per un calibratge òptim de l'espectròmetre.

8.5.- Espectròmetre d'infraroig

En aquest capítol es presenta l'espectròmetre desenvolupat per tal de per mesurar de forma contínua la concentració d'etilè a les càmeres frigorífiques d'emmagatzematge i evitar que la fruita envelleixi prematurament. D'aquesta manera es pot allargar el temps de conserva i obtenir una fruita final de major qualitat i més valorada.

El sistema presentat es basa en un espectròmetre d'infraroig per aprofitar el seu excepcional comportament en termes de selectivitat, estabilitat i immunitat a falses alarmes i enverinament respecte altres alternatives.

Descripció del sistema complet

Els analitzadors de gas òptics es basen en l'atenuació de radiació en certes bandes d'absorció dels gasos. La quantitat de llum absorbida determina la concentració de gas. Per tal d'optimitzar la detecció d'etilè, la selecció de la corresponent banda d'absorció ha estat feta en termes de la màxima absorbància d'aquest gas, resultant ser a les 10.6μm.

Tot i que s'han detectat més de 300 altres gasos en l'aroma de les pomes, es pot considerar que es troben en unes concentracions prou baixes com per no afectar la mesura d'etilè. D'altra banda, altres gasos com l'etanol i l'acetaldehid (apareixen quan s'exposa a baix oxigen la fruita) o l'amoníac (pot provenir d'alguna fuita del sistema de refrigeració) poden ser presents a les càmeres de conservació i afectar la mesura d'etilè. En aquestes condicions cal tenir present la possible sensibilitat creuada i dissenyar un sistema multi-canal.

S'ha desenvolupat un espectròmetre NDIR de quatre canals per mesurar etilè, i afegint canals per l'amoníac (9.7μm) i l'etanol (3.4μm) per reduir la sensibilitat creuada d'aquests gasos i un canal de referència (3.9μm) per augmentar l'estabilitat a llarg termini del sistema. La Figura 3 mostra els espectres dels gasos, amb les corresponents bandes d'absorció seleccionades.

El sistema ha de ser capaç de detectar l'augment de la concentració d'etilè quan la fruita comença a madurar. D'altra banda, el canal d'amoníac pot aportar informació addicional ja que aquest gas pot enverinar la fruita i cal activar un sistema de ventilació si la concentració sobre passa certs nivells. Així, els límits de detecció per l'etilè i l'amoníac han de ser de 100pmm i 200ppm respectivament per tal d'assegurar un funcionament correcte de l'espectròmetre.

L'espectròmetre està format per un emissor d'infraroig, una cel·la de gas, un detector d'infraroig, una etapa d'amplificació analògica i una de digital que fa d'amplificador lock-in. La Figura 4 mostra un diagrama de blocs del sistema.
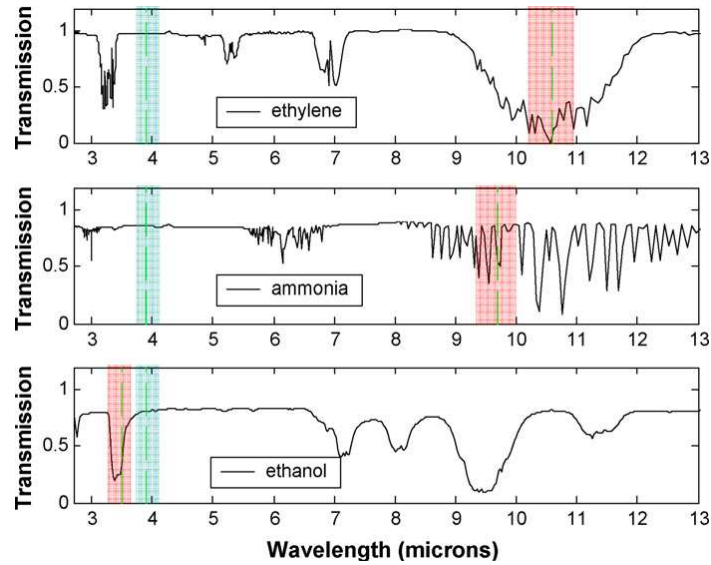
Figura 3: Espectres de l'etilè (dalt), amoníac (mig) i etanol (baix); i bandes d'absorció seleccionades pels gasos i pel canal de referència.
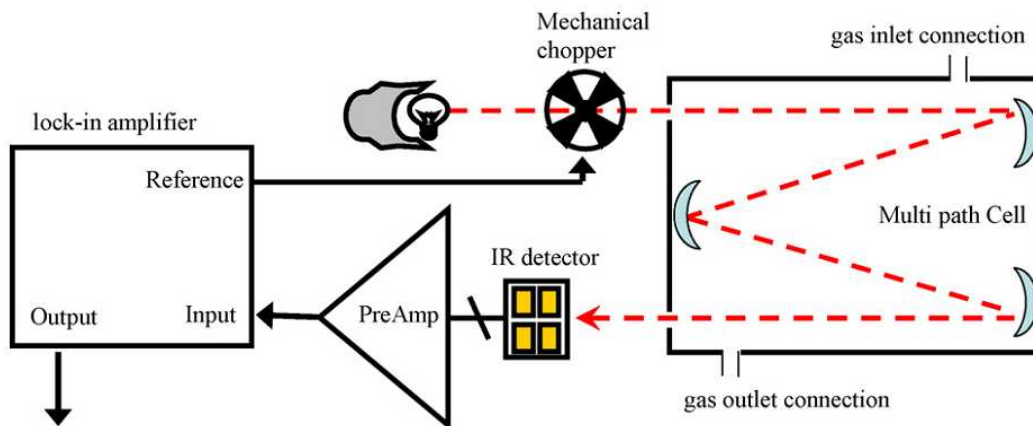

Figura 4: Diagrama de blocs de l'espectròmetre, amb l'emissor IR, la cel·la de gasos, el detector IR, la pre-amplificació analògica i l'amplificador lock-in digital.

Descripció dels components

a) Emissor IR

L'emissor IR s'ha desenvolupat amb la col·laboració del Fraunhofer Institute for Physical Measurement Techniques de Freiburg, i presenta una emissió major a les longituds d'ona altes (entorn de les 10μm) comparat amb els disponibles comercialment.

El disseny de l'emissor inclou elements òptics addicionals per augmentar la radiació què es focalitza a la cel·la de gasos i per reduir la mida del focus a la seva sortida. Amb aquest

objectiu s'interposa una lent que permet augmentar l'angle capturat per l'entrada de la cel·la de gasos de 7º a 18.4º.

El sistema de recuperació de senyal és un amplificador lock-in. Per la qual cosa, cal modular la radiació incident. La constant de temps observada per l'emissor desenvolupat no permet una modulació directa, cosa per la qual cal interposar-hi un chopper extern controlat pel microcontrolador que sincronitza el senyal de referència amb el senyal a recuperar.

b) Cel·la de gasos

Per tal de reduir les dimensions de la cel·la de gasos però mantenint la llargària del camí òptic s'ha desenvolupat un cel·la de gasos tipus White cell basada en múltiples reflexions. S'ha assolit un camí òptic de 1.6m després de 19 reflexions en un volum de $11x5x6cm^3$. Una imatge de la cel·la de gasos desenvolupada es presenta a la Figura 5.
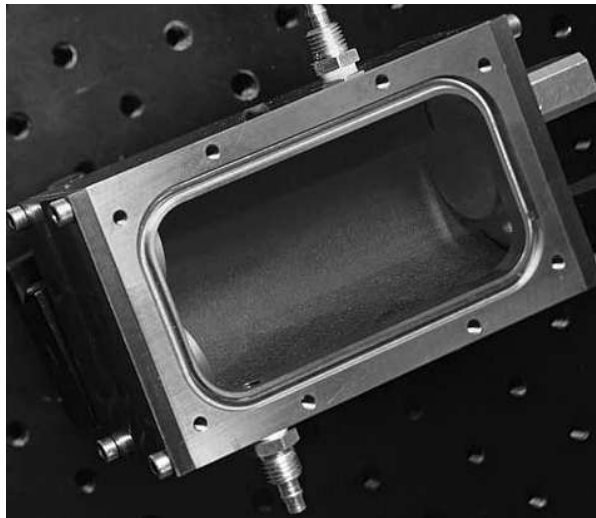

Figura 5: Cel·la de White, amb un camí òptic de 1.6m després de 19 reflexions en un volum de $11x5x6cm^3$

c) Detector d'infraroig

S'ha dissenyat i fabricat un innovador detector d'infraroig que inclou termopiles com a element sensor, filtres òptics per seleccionar les bandes d'absorció i una matriu de lents de Fresnel per focalitzar la radiació i augmentar l'efectivitat del detector. El diagrama de blocs del detector, conjuntament amb una foto del dispositiu final es presenta a la Figura 6.

Com a element sensor s'han escollit termopiles micromecanitzades en silici ja que aquesta alternativa presenta bones característiques en termes de reproducibilitat, exactitud, cost, sensibilitat i temps de resposta i poden ser fabricades en un mateix xip que actua de substrat. S'han fabricat quatre termopiles en forma de matriu 2x2 en un mateix xip de silici de

6.1x6.1mm^2, mida compatible amb una posterior integració en un encapsulat TO8. Cada termopila consta de 32 termoparells i les mides de l'absorbidor i de la membrana són 350x350µm^2 i 1300x1300µm^2 respectivament. La fabricació s'ha dut a terme al Centre Nacional de Microelectrònica (IMB-CNM-CSIC, Barcelona).
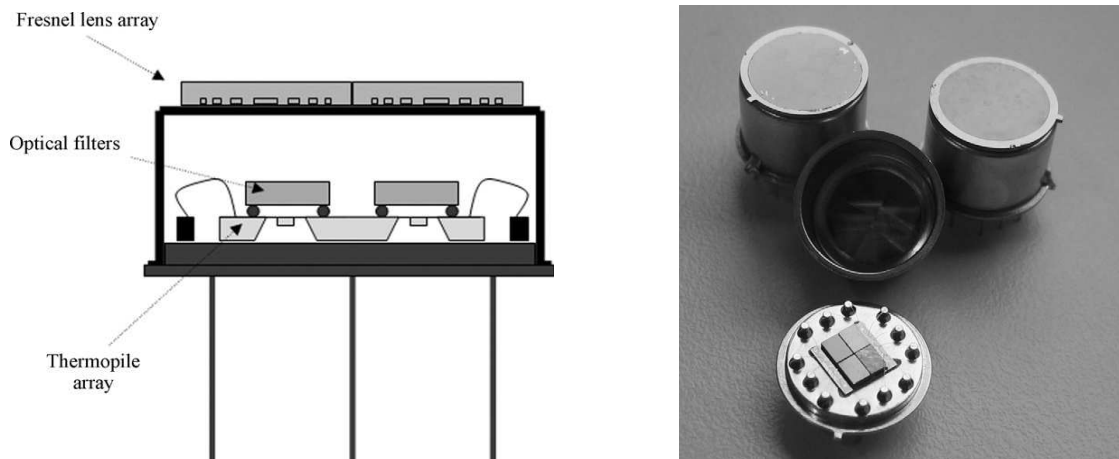

Figura 6: Diagrama de blocs del detector d'infraroig (esquerra) i imatge del dispositiu final

Els filtres òptics proporcionen la selectivitat de cada canal, i un cop tallats i condicionats, han estat integrats mitjançant tècniques flip-chip damunt del xip on s'han fabricat les termopiles al Centre Nacional de Microelectrònica.

El disseny i fabricació de la matriu de lents i la seva integració amb el detector és una de les tasquest importants d'aquesta Tesi. L'objectiu d'aquests elements òptics és recollir el màxim de radiació possible i dividir-la en quatre parts i focalitzar cadascuna d'elles damunt del corresponent absorbidor de les termopiles.

S'ha escollit una alternativa basada en lents difractives de Fresnel ja que aquestes són compatibles amb l'ús del silici com a substrat i amb la tecnologia de silici. D'aquesta manera es poden aprofitar els avantatges habituals que comporta aquesta tecnologia. D'altra banda, degut a les limitacions de la tecnologia de silici planar, cal reproduir el perfil de la lent amb un nombre discret d'esglaons plans.

A nivell de test s'han fabricat lents binàries i lents de vuit nivells (per tal d'augmentar l'eficiència òptica) de diferents diàmetres i distàncies focals. Les lents binàries reprodueixen el perfil amb un sol nivell i requereixen només d'una màscara fotolitogràfica i les lents de vuit nivells s'han dissenyat aprofitant la combinació de tres màscares. S'ha mesurat la distància focal, la mida del focus, i el patró de radiació i els resultats validen l'alternativa de disseny per integrar aquests dispositius al detector IR.

Per la integració final al detector es necessiten quatre lents diferents operant a longituds d'ona diferents. El dispositiu proposat consta de quatre sectors amb la lent centrada en la corresponent longitud d'ona en cadascun. Seguint el model de fabricació de les lents de vuit nivells, caldrien 3 màscares per cada sublent, i 12 màscares en total. Tanmateix, un nou disseny basat en 4 màscares repartides per les 4 lents és una alternativa de menor cost i permet assolir fins a 16 nivells. A més, simulacions mostren que l'eficiència és per les quatre sublents major al 85%.

Per tal de reduir les pèrdues per reflexió a les superfícies, una capa de sulfur de zinc de 1193nm s'ha dipositat a les dues cares de la matriu de lents. S'ha mesurat de nou la distància focal del dispositiu i s'ha pogut comprovar que aquesta no varia i que la transmissió augmenta. D'aquesta manera, es pot considerar vàlid el dispositiu per augmentar la sensibilitat del detector. El màxim guany esperat pel fet d'interposar la matriu de lents és el quocient entre l'àrea de l'absorbidor i l'àrea de les lents. En el cas del dispositiu desenvolupat assoleix un guany màxim de 140. La Figura 7 mostra la matriu 2x2 de lents fabricada amb 4 màscares.
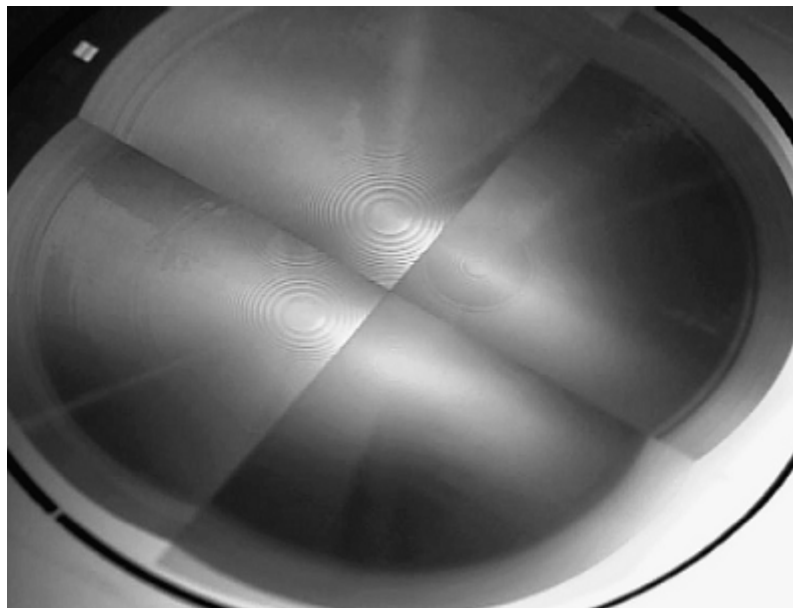

Figura 7: Matriu 2x2 de lents difractives de 16 nivells, assolits amb 4 màscares fotolitogràfiques.

Malauradament, s'ha trobat que la integració dels filtres massa prop de les termopiles condueix a un acoblament tèrmic entre les dues parts i causa un rendiment menor del detector en conjunt. Per evitar aquest efecte, que empitjora dràsticament la selectivitat necessària d'un sistema NDIR, s'han proposat dues alternatives. Operar al buit o bé augmentar les dimensions de les boles de soldadura flip-chip. Mentre s'estudien aquestes alternatives, per tal de sobreposar-se a aquest impediment, s'ha utilitzat una termopila comercial de quatre canals amb uns filtres òptics semblants (HTS-Q21, Heimann Sensor GmbH, Alemanya) per integrar-la a l'espectròmetre i poder realitzar mesures de gas.

d) Etapa d'amplificació analògica

L'objectiu de l'etapa d'amplificació analògica és expandir el senyal de les termopiles, que és d'unes desenes de microvolts, al rang d'entrada del convertidor analògic digital, que és de 0-0.6V. El detector consta de quatre canals, per tant, l'electrònica també s'ha duplicat quatre vegades.

Com que cal una gran amplificació, aquesta s'ha de dissenyar amb especial cura. Després d'una selecció d'amplificadors, s'ha escollit el AMP01 (Analog Devices) per les seves bones prestacions a nivell soroll, per la baixa freqüència de colze i per la seva arquitectura d'amplificador d'instrumentació que permet cancel·lar les interferències en mode comú.

A continuació de l'etapa de guany basada en el AMP01, se li afegeix un filtre per reduir l'aliasing. El filtre dissenyat té una arquitectura de Sallen-Key d'ordre 4, guany unitari i freqüència de tall de 2.5Hz.

e) Lock-in digital

El sistema de recuperació de senyal utilitzat és tipus lock-in perquè permeten traslladar el senyal a una banda de menor soroll. Per aquest motiu, cal una modulació del senyal a una freqüència de referència, que pel sistema desenvolupat és de 1Hz.

El lock-in s'ha implementat de manera digital en el microcontrolador de propòsit general MSP430F4270 (Texas Instruments). El filtre passa-baixos corresponent està dissenyat amb l'arquitectura de Butterworth en forma directa II, amb una freqüència de tall de 0.02Hz i filtres específics per atenuar la component de 50Hz i l'offset.

Resultats

El calibratge de l'instrument s'ha realitzat en el laboratori aplicant 21 perfils diferents de concentració d'etilè i amoníac, però emprant el detector d'infraroig comercial. La Figura 8 mostra les concentracions d'etilè i amoníac i la corresponent resposta del sistema.

Assumint que només un gas es troba en concentracions altes i que la resta no afecten a la mesura del sistema, l'error quadràtic mig per la predicció d'etilè és de 15ppm i de 80pmm per l'amoníac. També s'han realitzat mesures en condicions reals a les sales de conserva del IRTA-Lleida utilitzant microcàmeres de 140 litres, on s'ha simulat l'evolució de la fruita canviant la concentració d'etilè. La Figura 9 mostra la sortida de l'espectròmetre quan es canvia la concentració d'etilè a 10 litres/min fins els 400ppm. Per tal disposar de referències dels nivells

de concentració s'han pres mostres i s'han mesurat mitjançant cromatografia de gasos. Aquests resultats mostren que l'espectròmetre desenvolupat és adequat per detectar si la fruita està madura i evitar que aquesta envelleixi i per detectar concentracions altes d'amoníac que posen en perill la qualitat final de la fruita.
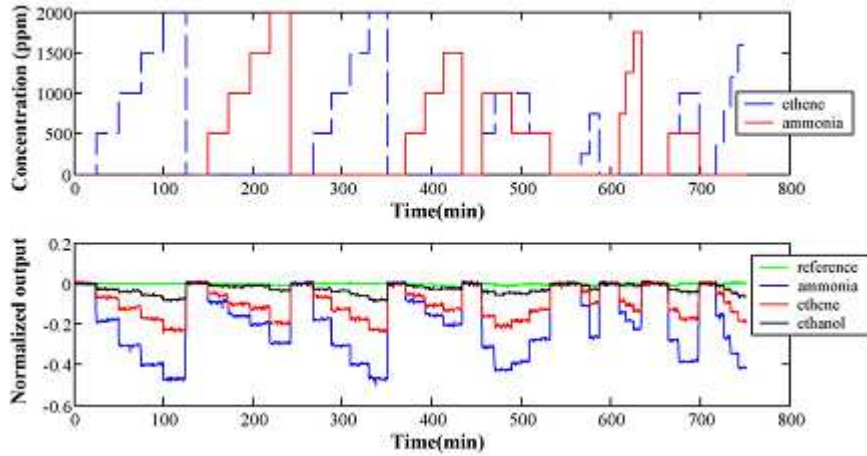

Figura 8: Perfil de concentracions per calibrar l'espectròmetre (dalt) i resposta dels quatre canals de l'instrument (baix)
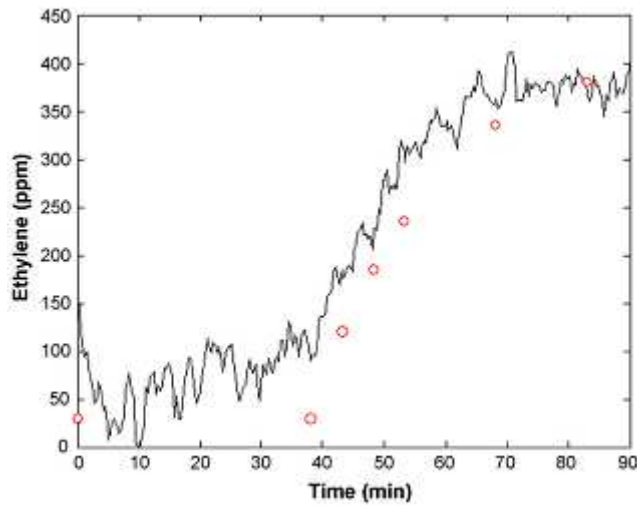

Figura 9: Resposta normalitzada de l'espectròmetre en funció de la concentració d'etilè a la microcàmera i la corresponent referència mesurada amb el HP6890GC (Agilent)

8.6.- Conclusions

S'ha desenvolupat un espectròmetre multi-canal per mesurar la concentració d'etilè a les càmeres d'emmagatzematge de fruita actuals. Els tests de laboratori i les proves de camp validen l'arquitectura proposada i confirmen que l'instrument és capaç de monitorar de forma contínua la concentració d'etilè per avaluar l'estat de maduració de la fruita i detectar una possible fuita d'amoníac del sistema de refrigeració que n'amenaci la qualitat.

El sistema complet està format per un emissor d'infraroig, una cel·la de gasos miniaturitzada, un nou i compacte detector multi-canal, una etapa d'amplificació analògica i un lock-in digital implementat en un microcontrolador.

El mòdul detector està basat en una nova arquitectura que consta de quatre termopiles amb els filtres òptics integrats mitjançant tècniques flip-chip i un mòdul òptic que optimitza la detectivitat del detector. Com a mòdul òptic s'ha escollit una alternativa basada en lents difractives de Fresnel ja que aquesta és compatible amb la tecnologia de silici. S'han fabricat quatre lents de Fresnel en un mateix substrat de silici mitjançant un nou disseny que combina quatre màscares fotolitogràfiques per obtenir 16 nivells que reprodueixen el perfil ideal de les lents. Posteriorment, per evitar les pèrdues per reflexió, s'ha recobert el dispositiu d'una capa antireflectant. El test dels dispositius òptics finals valida l'alternativa i confirma que amb el seu ús es pot assolir un guany màxim de 140 en la detectivitat del detector.

S'ha trobat que la integració dels filtres òptics massa prop de les termopiles causa un acoblament òptic que limita l'ús del detector. Per tal de reduir aquest efecte es proposa augmentar la mida de les boles de flip-chip o bé treballar al buit.

El sistema de recuperació de senyal consta d'una etapa analògica i d'una de digital. L'analògica està basada en un amplificador d'instrumentació de baix soroll que permet cancel·lar les interferències en mode comú. L'etapa digital està implementada en un microcontrolador que actua com a lock-in i controla el chopper que modula la radiació a la freqüència de referència. El lock-in trasllada el senyal a un rang de menor soroll i permet atenuar el soroll de 50Hz i d'offset ja que té filtres dissenyats especialment per aquestes components.

Mentre l'acoblament tèrmic entre les termopiles i els filtres òptics no estigui solucionat, s'ha utilitzat un detector comercial amb uns filtres òptics semblants per integrar-lo al sistema. Les mesures de laboratori i el posterior calibratge del sistema mostren que l'instrument té un límit de detecció de 30ppm i 160ppm per l'etilè i l'amoníac (95% de confiança) respectivament. Per tant, l'espectròmetre desenvolupat és vàlid per detectar l'augment de concentració d'etilè que indica que la fruita està madura almenys una setmana abans que aquesta envelleixi i per detectar una possible fuita d'amoníac que amenaci la qualitat final de la fruita.

9.- PUBLICATION LIST:

9.1.- Journal Papers:

[1]   **J. Fonollosa**, B. Halford, L. Fonseca, J. Santander, S. Udina, M. Moreno, J. Hildenbrand, J. Wollenstein, and S. Marco, "Ethylene optical spectrometer for apple ripening monitoring in controlled atmosphere store-houses," Sensors and Actuators B-Chemical, vol. 136, (no. 2), pp. 546-554, 2009.

[2]   **J. Fonollosa**, M. Carmona, J. Santander, L. Fonseca, M. Moreno, and S. Marco, "Limits to the integration of filters and lenses on thermoelectric IR detectors by flip-chip techniques," Sensors and Actuators A-Physical, vol. 149, (no. 1), pp. 65-73, 2009.

[3]   J. Hildenbrand, J. Wollenstein, S. Hartwig, A. Eberhardt, B. Halford, M. Moreno, **J. Fonollosa**, L. Fonseca, J. Santander, R. Rubio, I. Gracia, and C. Cane, "A compact optical multichannel system for ethylene monitoring," Microsystem Technologies-Micro-and Nanosystems-Information Storage and Processing Systems, vol. 14, (no. 4-5), pp. 637-644, 2008.

[4]   **J. Fonollosa**, R. Rubio, S. Hartwig, S. Marco, J. Santander, L. Fonseca, J. Wöllenstein, and M. Moreno, "Design and fabrication of silicon-based mid infrared multi-lenses for gas sensing applications," Sensors and Actuators B: Chemical, vol. 132, (no. 2), pp. 498-507, 2008.

[5]   R. Rubio, J. Santander, **J. Fonollosa**, L. Fonseca, I. Gracia, C. Cane, M. Moreno, and S. Marco, "Exploration of the metrological performance of a gas detector based on an array of unspecific infrared filters," Sensors and Actuators B-Chemical, vol. 116, (no. 1-2), pp. 183-191, 2006.

[6]   K. Hedsten, **J.Fonollosa**, P. Enoksson, P. Modh, J. Bengtsson, D. Sutherland, and A. Dmitriev, "Downscaling Biosensing Nanoplasmonic System," Submitted to Analytical Chemestry.

9.2.- Participation in Congresses:

[1]   **J. Fonollosa**, R. Rubio, J.Hildenbrand, S.Hartwing, J. Santander, M. Moreno, S. Marco, L. Fonseca , J. Woellenstein, "Design and fabrication of micromachined silicon based mid infrared multilenses for gas sensing applications" Digest of Technical Papers Vol.: 2. pàg.: 2565-2568
Transducers '07 & Eurosensors XXI. Lyon 2007

[2]   J. Wöllenstein, S. Hartwig, J. Hildenbrand, A. Eberhardt, M. Moreno, J. Santander, R. Rubio, **J. Fonollosa**, L. Fonseca, "A Compact optical ethylene monitoring system" Smart Sensors, Actuators, and MEMS II. Proceedings of the society of photo-optical instrumentation engineers (SPIE) Vol.:6589. pàg 6589-07.
SPIE Europe International Symposium: Microtechnologies for the New Millennium. Gran Canaria 2007

[3]   **J.Fonollosa**, R.Rubio, M.Moreno, J.Santander, S.Marco, L.Fonseca, "Diseño y fabricación de lentes de Fresnel en silicio para aplicaciones de sensores ópticos de gas en el infrarojo" Libro de actas pàg. 537-542.
Quinta Reunión Española de Optoelectrónica Bilbao 2007

[4]   **J.Fonollosa**, R.Rubio, J.Hildenbrand, M.Moreno, S.Marco, L.Fonseca, J.Santander, S.Hartwing, J. Woellenstein, "Fresnel Lenses: study and fabrication in silicon technology for medium-IR applications" MEMS, MOEMS, and Micromachining II, Proceedings of SPIE--the international society for optical engineering. Vol.:6186. pàg.:61860R1-61860R11
Photonics Europe. Strasbourg 2006

[5]   J. Wöllenstein, S. Hartwig, J. Hildenbrand, M. Moreno, **J. Fonollosa**, J. Santander, R. Rubio, L. Fonseca, C. Cané. "Compact Filter Photometer for Ethylene Monitoring"
The 11th International Meeting on Chemical Sensors. Brescia 2006

[6]   J. Hildenbrand, S. Hartwig, M. Moreno, **J. Fonollosa**, R. Rubio, J. Santander, L. Fonseca, V. Lehmann, W. Riedel, J. Wöllenstein, "Ethylene monitoring in the "Fingerprint" Region using a mini white-cell and a micromachined ir-emitter".
Eurosensors XIX. Barcelona. 2005

[7]   R. Rubio, J. Santander, S.Marco, L. Fonseca, **J. Fonollosa**, M. Moreno; "Simulation of an infrared detector array for gas detection"
International Symposium on Olfaction and Electronic Nose. Barcelona 2005

[8] R. Rubio, J. Santander, S. Marco, L. Fonseca ,**J. Fonollosa**, M. Moreno, "Non-selective NDIR array for gas detection" Smart Sensors, Actuators, and MEMS II. Proceedings of the society of photo-optical instrumentation engineers (SPIE) Vol.:5836. pàg 239-246.
SPIE Europe International Symposium: Microtechnologies for the New Millennium. Sevilla 2005

[9] S. Hartwig, J. Hildenbrand, M. Moreno, **J. Fonollosa**, L. Fonseca, J. Santander, R. Rubio, C. Cané, A. Lambrecht, and J. Wöllenstein, "A higly sensitive IR-optical sensor for ethylene monitoring" Smart Sensors, Actuators, and MEMS II. Proceedings of the society of photo-optical instrumentation engineers (SPIE) Vol.:5836. pàg 452-460.
SPIE Europe International Symposium: Microtechnologies for the New Millennium. Sevilla 2005

[10] **J.Fonollosa**, R.Rubio, M.Moreno, S.Marco, L.Fonseca, J.Santander, S.Hartwing, J. Woellenstein, "Estudio y fabricación de Lentes de Fresnel, en tecnología de silicio, para aplicaciones de infrarojo medio" Libro de actas pàg. 297-302.
Cuarta Reunión Española de Optoelectrónica. Elx 2005